University of Minnesota
St. Anthony Falls Hydraulic Laboratory

Project Report No. 332

Hydraulic Transient Modeling of TARP Systems

by

Charles C. S. Song

Wenchin Lin, and

Cuiling Gong

Prepared for

METROPOLITAN WATER PRECLAMATION DISTRICT
OF GREATER CHICAGO
Chicago, Illinois 60611

August 1992

TABLE OF CONTENTS

LIST OF FIGURES

Figure No.

Figure No.

Figure No.

I. INTRODUCTION

The Mainstream System excluding North Branch and the Calumet System excluding Indiana Avenue tunnel of Greater Chicago were studied in 1988. The solutions based on these systems were suggested in a project report [1][1] in 1988. Since then a new North Branch tunnel is being planned to join the original Mainstream System, and the Indiana Avenue tunnel to be added to the Calumet System, it therefore becomes necessary to reevaluate the previously suggested operational plans. A new computer simulation and solution alternatives for these expanded systems are described in this report. The North Branch System has also been studied separately and reported herein.

The fully dynamic transient mixed flow mathematical model (MXTRANS) developed at the University of Minnesota was used for this study. In order to study the performance of the Mainstream System, including North Branch, under different operating concepts, four sets of system configurations are being considered and are shown on Table 1:

System M–I Four branch system including North Branch, Chicago River, South Fork and 73rd St. without reservoir at downstream end.

System M–II Four branch system including North Branch, Chicago River, South Fork and 73rd St. with reservoir at downstream end.

System M–III Seven branch system including North Branch, Lawrence Avenue tunnel, Chicago River, South Fork, Nashville Ave, 13A tunnel and 73rd St. without reservoir at downstream end.

System M–IV Seven branch system including North Branch, Lawrence Avenue tunnel, Chicago River, South Fork, Nashville Ave, 13A tunnel and 73rd St. with reservoir at downstream end.

Table 1. Systems Modeled for Mainstream System

	Reservoir	Branches
System M–I	without	4
System M–II	with	4
System M–III	without	7
System M–IV	with	7

[1] Number refers to the references listed on page 22.

For each system listed above, two inflow hydrographs were used for the purpose of simulation. One is the design inflow and the other is the simulated inflow of the storm on Oct.18, 1985. For the design inflow, inflow rate was assumed to increase to maximum from zero within two hours, and thereafter the inflow rate was kept constant. The inflow due to the storm of October 18, 1985, was the simulated inflow furnished by Clint J. Keifer in 1987.

Various short–term and long–term solution alternatives for all four sets of systems were studied, and the results are described in section IV. Short–term solutions are based mainly on inflow controls using the structures that exist at the present time along with Song et al.'s [1] proposed orifice controls. Long–term solutions are based on the simulated conditions found after the planned storage reservoirs at the downstream ends of the Mainstream and Calumet Systems have been completed. Long–term solutions may include inflow control and structural modifications. Tables 3 and 4 are overlooks of work done on the Mainstream System for both design inflow and the October 18, 1985, storm. The configurations of the Mainstream System with four and seven branches are plotted on Figs. M–1 and M–2.

The expanded Calumet system was also modeled under four different conditions, depending on the existence or nonexistence of a reservoir and whether the roller gate at St. 3+90 on the 73–287–2H tunnel was opened or closed. The four systems modeled are shown on Table 2 below:

System C–I No reservoir at the downstream end and the roller gate is at fully open condition.

System C–II With reservoir at the downstream end the roller gate is at fully open condition.

System C–III No reservoir at the downstream end and the roller gate is closed. In this case the Calumet tunnels are divided into two independent systems.

System C–IV With reservoir at the downstream end and the roller gate is closed.

Table 2. Systems Modeled for Calumet System

	Reservoir	Roller Gate
System C–I	without	open
System C–II	with	open
System C–III	without	closed
System C–IV	with	closed

All four systems need the design storm inflow data as the input. Solution alternatives are suggested for all four systems.

Table 3. Overlook of work done on Mainstream System for Design Inflow

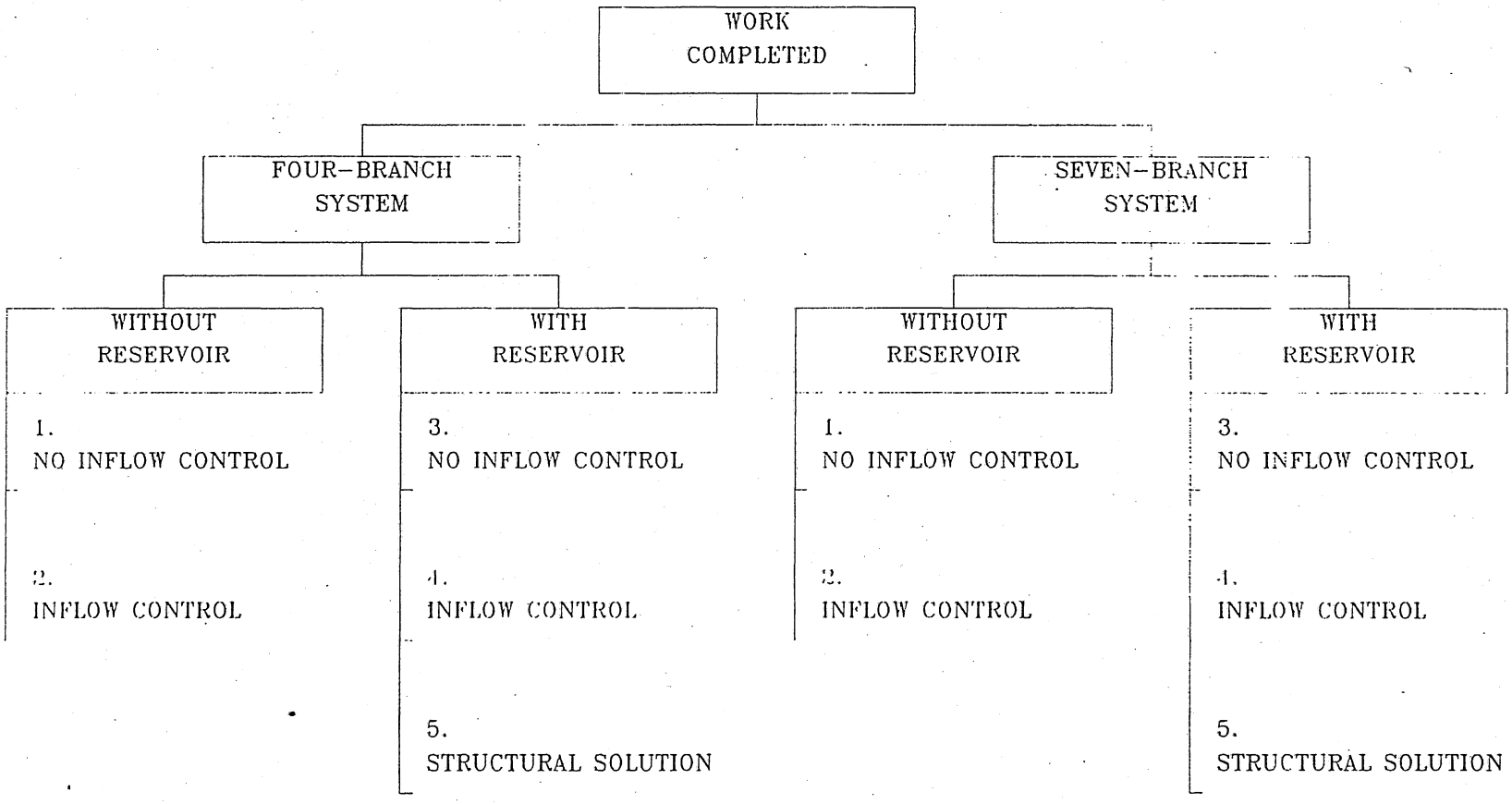

Table 4. Overlook of work done on Mainstream System for Storm Oct 18, 1992

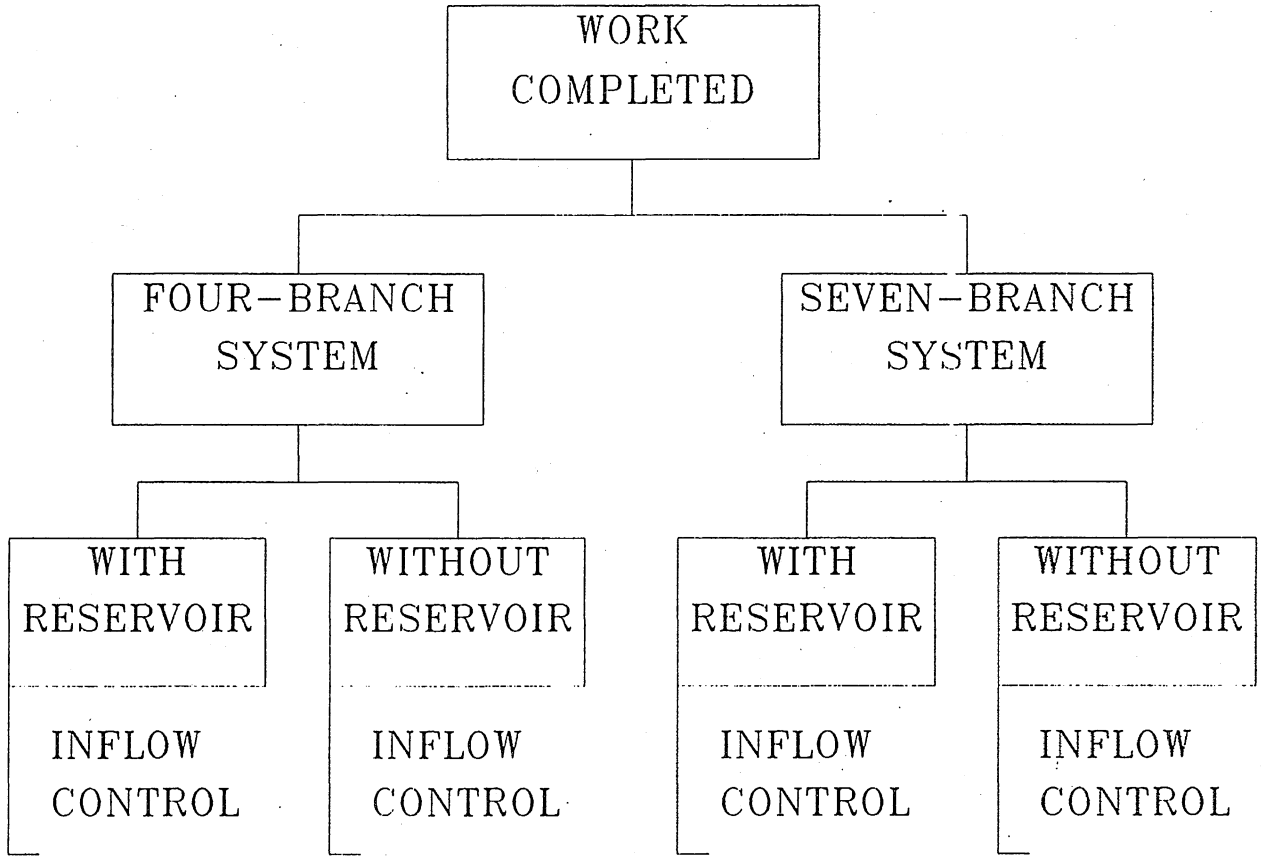

II. THE MIXED TRANSIENT FLOW MODEL

The flow to be simulated is very unsteady and contains highly dynamic phenomena such as pressurization surge. The model used, then, must be able to simultaneously calculate unsteady open channel flows and unsteady pressurized flows, including the abrupt change that occurs at the shock or the surge front.

The well–known St. Venant equations:

$$\frac{\partial y}{\partial t} + V \frac{\partial y}{\partial x} + \frac{c^2}{g} \frac{\partial v}{\partial x} = 0 \tag{1}$$

$$g \frac{\partial y}{\partial x} + \frac{\partial v}{\partial t} + v \frac{\partial v}{\partial x} + g(S_f - S_o) = 0 \tag{2}$$

are used to represent the unsteady open channel flow. In the above equations, y is the flow depth, v is the flow velocity, c is the gravity wave speed, S_o is the channel slope, S_f is the energy slope, and g is the acceleration due to gravity.

The corresponding equations for unsteady pressurized flow are:

$$\frac{\partial y}{\partial t} + V \frac{\partial y}{\partial x} + \frac{a^2}{g} \frac{\partial v}{\partial x} = 0 \tag{3}$$

$$g \frac{\partial y}{\partial x} + \frac{\partial v}{\partial t} + v \frac{\partial v}{\partial x} + g(S_f - S_o) = 0 \tag{4}$$

in which a is the pressure wave speed, while y takes the meaning of piezometric head measured from the tunnel invert. The systems of equations (1) ~ (4) are solved by the methods of characteristics [3].

Because the transition from the open channel flow condition to pressurized flow condition must be abrupt, as in the case of a hydraulic jump, the special shock boundary conditions must be applied. It was shown by Cardle and Song [2], for a pressurization surge or a positive surge, that three characteristic equations plus two shock boundary conditions can be used to calculate five unknowns at the interface. These five unknowns are v and y on both sides of the interface and the speed of the interface movement. The model can also simulate the negative surge which occurs during the depressurization process.

A number of other boundary conditions representing junctions, dropshafts, upstream end, downstream end, reservoirs, and other accessories are also provided in the model. Inflow hydrographs, outflow conditions, and other active or passive flow control methods can also be included in the input data file. Velocity depth, discharge, and other variables at any location and any time may be specified as outputs.

III. GENERAL TRANSIENT CHARACTERISTICS FOR MAINSTREAM SYSTEM

A. Mainstream System without Reservoir

System M–III is used for illustration for this case. Inflow comes from the October 18, 1985, storm. The system configuration is shown in Fig. M–2. The results along the main tunnel as in Fig. M–3 are discussed here. The downstream end is first pressurized at t=5.3 minutes. As the tunnel continues to be filled and the pressurized portion expands, surge develops at the interface between the pressurized zone and the free surface zone. The magnitude of the surge increases as the inflow rate increases. This situation is illustrated by the four instantaneous hydraulic gradelines shown in Fig. M–30. The station number shown in Fig. M–30 refers to that of Fig. M–3.

Water flows in the opposite direction across the surge front. Water flows towards the downstream direction in front of the surge while it flows towards the upstream direction behind the surge. The water surface is far from level, and water rushes towards the upstream end. When the surge front first arrives at the upstream end, at t=221.9 min. as shown in Fig. M–24, a large amount of backflow causes water to be squeezed into the dropshaft so that water level rises rapidly inside the dropshaft. The smaller the diameter of the shaft, the higher the water level rise due to this first surge. The high head generated at the upstream end now travels downstream as a reflected surge, causing head in the tunnel to surge up once again. When the reflected surge arrives at the downstream end, it is reflected again and starts to move upstream. Instantaneous hydraulic gradelines after this time are shown in Fig. M–31.

When the first pressurization surge arrives at a junction, it may break up into two surges; one continues to move along the main tunnel and the other moves along the branch tunnel. Due to the same mechanism just described for the main tunnel, the upstream end of the branch channel may also reflect the surge. Thus, each branch also contributes to surging and rocking of certain characteristic periods. Since the Chicago River branch pressurizes first, any station downstream experiences first pressure peak due to the pressurization of this branch.

B. Mainstream System with Reservoir

A reservoir having the total storage capacity of 32,000 acre–feet and the depth of 196 feet is assumed to exist at the downstream end of the system. Surge conditions still exist in midstream and upstream portions of the tunnel because of insufficient conveyance capacity caused by the backwater effect.

For this case, system M–IV and design inflow are used for illustration. When the reservoir is initially empty and inflow is large, then pressurization may initiate somewhere in the midstream of the tunnel due to inadequate conveyance. Two pressurization surges, one moving upstream and the other moving downstream, are generated. The surge that moves upstream will collide with the upstream end and cause a rapid head increase there at t= 87.3 minute. The surge that moves downstream behaves quite differently because of the existence of the reservoir. When the positive surge first arrives at the downstream end, it is immediately eliminated, and the head is reduced to that of the reservoir. At this time, the reservoir reflects a negative surge which will travel upstream. This negative surge cannot travel very far upstream before it changes direction and becomes a positive surge because of the large pressure gradient. The reservoir will eliminate the second positive surge and reflect another negative surge. The process repeats itself until pressurization is thus completed. Instantaneous hydraulic gradelines are shown in Figs. M–27 and M–28.

C. Storage Volume – Stage Relationship

Inflow control is a possible means of preventing surge related problems. Since the surge intensity is strongly related to the total inflow rate during the final stage of the filling process, it is necessary to limit the inflow rate as the tunnel approaches the full condition. The real time information on the amount of water stored in the system is needed to operate the inflow control gates. At the present time the volume of water stored is calculated from the water level data taken at the downstream end of the Mainstream System in conjunction with several other stations over the entire system.

Under a dynamic condition the water surface profile in an open channel flow portion is not level and actual volume may be quite different from that estimated by the depth data at the downstream end alone. The correlations between the storage volume and the water depth at the downstream end under two different conditions for the Mainstream System are shown in Fig. M–4.

According to Fig. M–4, a static approach for the Mainstream System utilizing only the downstream reading may overpredict the storage by as much as 20 percent.

Real time depth data at more than one station along the main tunnel are, therefore, clearly required for accurate storage estimation. It is not known what accuracy the multiple station calculation currently utilized affords. However, according to the previous numerical experimentations, depth data at two stations, one at the downstream end and one near the upstream end, would be sufficient to make very accurate storage volume calculations. The basic form of the equation needed is given as follows.

$$\hat{V} = \hat{V}_0(y_1) + \hat{V}_1(y_1, y_2) \tag{5}$$

in which

$\hat{v}$ = estimated dynamic storage

$\hat{v}_o(y_1)$ = static storage volume

$\hat{v}_1(y_1,y_2)$ = correction due to dynamic effect

The correction term in Eq. 5 for design inflow of the Mainstream system is given by

$$\hat{V}_1(y_1,y_2) = -16{,}000\ y_2\sqrt{|14.6 + y_2 - y_1|},\ \text{if } y_2 \leq D_2 \qquad (6)$$

$$\hat{V}_1(y_1,y_2) = -16{,}000\ D_2\sqrt{|14.6 + y_2 - y_1|},\ \text{if } y_2 > D_2 \qquad (7)$$

In the above equations, y_1 is the measured water depth or piezometric head at the downstream end of each system, and y_2 is the measured water depth or piezometric head at the Roosevelt Road construction shaft of the Mainstream System. D_2 is the diameter of the tunnel at the location where y_2 is being measured. It should be noted that Eqs. 6 and 7 are applicable to the design inflow of the Mainstream System without reservoir.

IV. SOLUTION ALTERNATIVES FOR MAINSTREAM SYSTEM

Table 5 and Table 6 are the solution overlook of Mainstream System. A sketch of the Dropshaft–Drift Tube System for geyser analysis is given in Fig. M–5.

A. Short Term Solutions for Design Flow

(1) System M–I

The modeling results indicate that the existing control gates are not sufficient to prevent geysering. It is possible to mitigate the surge problem by applying fixed orifices to all ungated dropshafts, thereby adding two additional control gates, one at each site DS–1 and DS–114.

The gates at dropshafts Nos. 27, 28, and 29 (Racine Ave. pumping station) should start to close when the tunnel is 30 percent full. All other control gates should be closed at 40 percent full. All the gates should be closed completely within 10 minutes. This solution is essentially the same as the corresponding case without the North Branch System analysed previously. The effects of increased inflow and storage volume due to the addition of the North Branch System apparently will cancel each other out.

A total inflow hydrograph for this case is plotted in Fig. M–8. The time variation of water depth at the downstream and upstream ends and DS–53 are plotted in Fig. M–9. For comparing, total inflow hydrographs and time variation of water depth using the same three stations are given in Figs. M–6 and M–7 respectively.

(2) System M–III

Using the same procedures as for the four branch system, we have not been able to find a complete solution. The main problems are DS–2 in the 73rd Avenue and the DS–53 in the main tunnel.

The apparent reason is that the 13A and Nashville branches are at higher elevation so that they increase the inflow to the main tunnel but provide little additional storage during the critical period. Substantial improvements may be obtained when these two branches are disconnected. Total inflow hydrograph and time variation of water depth at three stations under no inflow control conditions are given in Figs. M–13 and M–14 respectively.

Table 5. Solution of Mainstream System for Design Inflow

	Inflow Control Current storage (percentage of total storage in tunnel) when the gates start to close			Structural Solution
	gates at DS-27,28,29	other gates	inflow allowed*	
System I	30%	40%	0%	-----
System II	50%	70%	20%	Diameter of USBC** Main Tunnel: 40ft North Branch: 20ft CS-2 at North Branch: 100ft
System IV	50%	70%	20%	-----

Table 6. Solution of Mainstream System for Storm on Oct 18, 1985

	Inflow Control Current storage (percentage of total storage in tunnel) when the gates start to close		
	gates at DS-27,28,29	other gates	inflow allowed*
System I	50%	65%	20%
System II	70%	90%	20%
System III	20%	40%	20%
System IV	70%	90%	20%

* Numbers below means percentage of inflow hydrograph allowed after the gates are partially closed.

** USBC means Upstream Stream Boundary Condition

B. Short Term Solution for October, 18, 1985, Storm

(1) System M–I

Since the total inflow for this case is about one–half of the design inflow, the magnitude of the surge is reduced sufficiently, thereby making it possible to avoid geysering by using the existing gates. The gates at dropshaft Nos. 27, 28, and 29 should start to close when the tunnel is 50 percent full and all other control gates start to close when the tunnel is 65 percent full. All gates are not closed completely, but rather are left partially open to allow 20 percent of the hydrograph to enter the tunnel at the end of closing.

For the purpose of analysis, the gate closing process was assumed to be completed in 10 minutes.

The total inflow hydrograph for this operation is plotted in Fig. M–18. The time variation of water depth at the upstream end, downstream end, and DS–53 are plotted in Fig. M–19. This figure clearly shows the existence of surges as the system is being filled. For comparing, total inflow hydrograph without inflow control is given in Fig. M–17.

(2) System M–III

The gates at dropshaft Nos. 27, 28, and 29 should start to close when the tunnel is 20 percent full. All other gates should start to close at 40 percent full. After 10 minutes, all gates are partially closed to allow 20 percent of the inflow hydrographs to enter the tunnel.

The total inflow hydrograph for this operation is plotted in Fig. M–23. The variation of water depth at three key stations are plotted in Fig. M–24. For comparing, total inflow hydrograph without inflow control is given in Fig. M–22. Instantaneous hydraulic gradelines are given in Figs. M–30 and M–31.

C. Long–Term Solution for Design Inflow

The planned reservoir increases the storage capacity and reduces flooding problems. Because of the conveyance limitation, however, the surge and geyser problems cannot be completely eliminated without further controls for both the design inflow and the inflow of the October 18, 1992, storm.

(1) System M–II

For the reservoir system at the downstream end, there are two options to mitigate the surge problem. One is inflow control; the other is a structural solution.

In the case of inflow control, the gates at dropshaft Nos. 27, 28, and 29 should start to close when the tunnel is 50 percent full. All other control gates should start to close at 70 percent full. All gates are to be partially closed to allow 20 percent of the hydrograph to enter the tunnel.

For the purpose of analysis, each gate is assumed to take 10 minutes to complete its operation.

Total inflow hydrograph for this case is plotted in Fig. M–10. The time variation of water depth at three key stations are plotted in Fig. M–11.

As far as the structural solution is concerned, the shaft diameter at the upstream end of the main tunnel should be enlarged to 40 feet. The upstream end of North Branch is also needed to increase to 20 feet, and the diameter of the construction shaft should be 100 feet in order to keep the system free from the geyser problem. This analysis is based on the assumption that the resonance condition at DS–53 has already been removed.

The time variation of water depth at three key stations for a structural solution is plotted in Fig. M–12.

(2) System M–IV

Two options are also considered to avoid geyser problems for the seven branch system with a reservoir at the downstream end.

The inflow control solution is: the gates at dropshaft Nos. 27, 28, 29 should start to close when the tunnel is 50 percent full. All other control gates should be closed at 70 percent full. After 10 minutes of closing operation, 20 percent of inflow hydrographs are allowed to enter the tunnel. Instantaneous hydraulic gradelines are given in Fig. M–29. For comparing, instantaneous hydraulic gradelines without inflow control are plotted in Figs. M–27 and M–28.

The total inflow hydrograph for this operation is given in Fig. M–15. The variation of water depth at three key stations is given in Fig. M–16.

No satisfactory structural solution has been found for this case. After

increasing the dropshaft diameter at the upstream end of the main tunnel to 50 feet, North Branch to 60 feet, Lawrence Ave to 20 feet, construction shaft (CS–2) to 100 feet, the condition improves substantially, but some problems remain at North Branch: DS–10A, DS–7; Lawrence Branch: L09 and L10; Main tunnel, DS–53.

D. Long Term Solution for the October 18, 1985, Storm

Only the inflow control solution is considered in this case.

(1) System M–II

The gates at dropshaft Nos. 27, 28, and 29 should start to close when the tunnel is 70 percent full. All other control gates should start to close when the tunnel is 90 percent full. All gates are partially closed to allow 20 percent of the inflow hydrograph to enter after 10 minutes of closing.

The total inflow hydrograph for this operation is given in Fig. M–20. The variation of water depth at three key stations is given in Fig. M–21.

(2) System M–IV

The gates at dropshafts Nos. 27, 28, and 29 should start to close when the tunnel is 70 percent full. All other control gates should start to close when the tunnel is 90 percent full. All gates are partially closed to allow 20 percent of the inflow hydrograph to enter the gated dropshaft after 10 minutes of closing.

The total inflow hydrograph for this operation is given in Fig. M–25. The variation of water depth at three key stations is given in Fig. M–26. Instantaneous hydraulic gradelines are given in Figs. M–32 and M–33.

V. SOLUTION FOR INDEPENDENT NORTH BRANCH TUNNEL

The North Branch tunnel was considered to be independent in this case. This study was conducted earlier to assist the preliminary design of the North Branch.

The object of studying the North Branch tunnel was to determine the optimum elevation at which the drift tunnel from dropshaft DS–N20 should enter the construction shaft at the north end of the North Branch tunnel if the diameter of this drift tunnel is 10 feet rather than 20 feet as the rest of the tunnel. Also to be explained was whether the diameter of DS–N20 should be increased from 7'–2", which is the requirement when DS–N20 is considered to be normal dropshaft size.

Based on the drawings furnished by Joseph R. Pivnicka, a preliminary flow filling model for the North Branch tunnel was prepared. The water depth at the downstream end of North Branch was given as input, which came from the previous calculation in 1988 of the Main Stream System.

It turned out that the geysering at dropshaft DS–N20 depends not only on the elevation of the drift tunnel, but also on the sizes of the dropshaft, the size of the drift tunnel, and the intensity of surges in the Mainstream tunnel.

After a number of trial runs, some conclusions are drawn corresponding to two different surge conditions in main tunnel. One is the worst surge condition and the other is modest surge condition.

The configuration for modeling purposes is shown in Fig. M–34.

A. The Worst Surge Condition (uncontrolled inflow to Mainstream tunnel)

Under this severe surge condition the proposed 10 ft drift tunnel and 7'–2" dropshaft will produce geysering at any height. To avoid geysering, it is necessary to reduce the drift tunnel size and/or increase the dropshaft size. If the 8 ft drift tunnel is used, then the relationship between the dropshaft size and the minimum height of the drift tube above the invert of the North Branch tunnel is as follows.

Dropshaft diameter	Minimum height
9 ft	100 ft
10 ft	80 ft

A larger dropshaft size is needed if smaller height is desirable. If a 10 ft diameter drift tunnel is to be retained, then an even larger dropshaft size will be needed.

Time variation of water surface elevation at the downstream end of the North Branch tunnel for this case is given in Fig. M–35. The time variations of water depth at the upstream end and construction shaft for the above two solutions are given in Figs. M–36 and M–37.

B. Modest Surge Condition (Controlled Inflow to Mainstream Tunnel)

Under this mild surge condition, the minimum height needed for the proposed drift tunnel size of 10 ft and dropshaft size of 7'–2" is 20 ft. If an 8 ft drift tunnel and 9 ft dropshaft are used then there is no limitation for the drift tube elevation.

The time variation of water depth at the downstream end for this case is given in Fig. M–38. The time variations of water depth at the upstream end and construction shaft for this case is given in Fig. M–39.

It is also interesting to note that, if a 20 ft drift tunnel is used, the drift tunnel becomes part of the North Branch tunnel and requires a very large dropshaft. In this case the construction shaft loses much of its surge relief characteristics.

VI. TRANSIENT CHARACTERISTICS OF CALUMET SYSTEM

The simplified configuration for modeling purposes of the Calumet TARP tunnel system is shown in Fig. C–1. By adding approximately 11.5 miles of tunnels and a number of dropshafts, the system includes the main tunnel and six branches. The entire system is divided into 323 finite segments of 500 feet each. For system C–I, the tunnel near the pumping station pressurized first and a moving hydraulic jump formed at the downstream end which gradually moved upstream as the system filled.

Five selected instantaneous hydraulic gradelines are shown in Fig. C–2. When the surge moves to the junction between the existing tunnel and the proposed Indiana Avenue tunnel, the surge breaks into two surges—one moving into the Indiana Avenue tunnel and the other moving along the existing tunnel. The surges move along five branches, as shown in Figs. C–3 to C–7.

When a surge reaches an upstream end, the pressure head rises rapidly unless a large diameter surge relief structure is provided there. It can be observed in Fig. C–8 that the water depth at station 1 rises by more than 200 feet in about one minute as the result of the pressurization surge. The surges moving along six branches arriving at the upstream end of these branches also produce a rapid water depth increase. The time variations of water depths at the upstream ends are plotted in Fig. C–8 to Fig. C–10. Guo and Song [4] showed that the flow in a dropshaft–drift tube system may become unstable if the head in the main tunnel increases too rapidly.

The dropshaft analysis recommended by Guo and Song [4] was applied at these dropshafts. The results show that the potential geyser problem may occur at the upstream end of Mt. Greenwood #1, Mt. Greenwood #2, Sag Relief Sewer, Markham Avenue, and 140th Avenue. The time variations of water depth at the junctions are plotted in Figs. C–11 and C–12. According to Fig. C–11, the water depth rise at station 205, which is at the connection of existing tunnel and the proposed Indiana Avenue tunnel, is rather slow and should not cause geysering.

Instantaneous hydraulic gradelines in the main tunnel and five branches are plotted in Figs. C–13 ~ C–18 for system C–II. The time variations of water depths at the upstream ends are plotted in Figs. C–19 to C–21. The water depth variations at the junctions are plotted in Figs. C–22 and C–23. As can be observed from these figures, the proposed future reservoir slows down the water depth rise substantially. For example, the water depth at station 1 rose about 170 feet in about 1.5 minutes. This rise in speed is not large enough to cause geysering. Therefore, no inflow gate control is needed for this case.

In case of system C–III, the roller gate effectively divides the Calumet System into two parts. The simulated hydraulic gradelines and water depth variations upstream of the roller gate are plotted in Figs. C–24 to C–27. Since the inflow rate in this part is small and the roller gate prevents the surge from the downstream side to enter, geyser problems are not likely in this part.

The simulated instantaneous hydraulic gradelines and time variation of water depth downstream of the roller gate in system C–III are plotted in Figs. C–28 to C–36. The dynamic analysis of dropshaft–drift tube at upstream end dropshafts shows that the potential geyser problem may occur at the upstream end of 19R–1, Indiana Avenue, and Markham.

For system C–IV, the modeling results at the downstream side of the roller gate are plotted in Figs. C–37 to C–44. The dynamic analysis of dropshaft–drift tube shows that a potential geyser problem may occur at the upstream end of 19R–1 branch. The condition upstream of the roller gate in this case is identical to that of system C–III.

Under a dynamic condition, the actual volume of the Calumet System may be quite different from that estimated by the depth data at the downstream end alone. The correlations between the storage volume and the water depth at the downstream end for the Calumet System are shown in Fig. C–76. Similar plots for the Calumet System at the downstream side of the roller gate are shown in Fig. C–77.

The correction term of dynamic effect in Eq. 5 for the entire Calumet System is given by

$$\hat{V}_1(y_1,y_2) = -25{,}000\ y_2\sqrt{|100 + y_2 - y_1|},\ \text{if } y_2 \le D_2 \tag{8}$$

$$\hat{V}_1(y_1,y_2) = -25{,}000\ D_2\sqrt{|100 + y_2 - y_1|},\ \text{if } y_2 > D_2 \tag{9}$$

The corresponding equations for the Calumet System at the downstream side of the roller gate is given by

$$\hat{V}_1(y_1,y_2) = -298{,}000\ y_2\sqrt{|100 + y_2 - y_1|},\ \text{if } y_2 \le D_2 \tag{10}$$

$$\hat{V}_1(y_1,y_2) = -298{,}000\ D_2\sqrt{|100 + y_2 - y_1|},\ \text{if } y_2 > D_2 \tag{11}$$

In the above equations, y1 is the measured water depth or piezometric head at the downstream end of the Calumet System, and y_2 is the measured water depth or piezometric head at the st. 3+90. D2 is the diameter of the tunnel at the location where y_2 is being measured.

VII. SOLUTION ALTERNATIVES FOR CALUMET SYSTEM

Limiting inflow by using the existing gate can mitigate the geyser problem. The gates at the Calumet tunnel, Indiana Avenue, Markham Avenue, and 140th Avenue can be closed at different conditions for different cases. With respect to sluice gate closures, except for CDS–13, all gates can be treated equally. There are no potential geyser problems in system C–II and in the upstream side of the roller gate of system C–III and system C–IV. Therefore, no inflow gate control is necessary in these cases. The inflow controls necessary to mitigate hydraulic transient problem are described as follows.

A. System C–I

When the system is 50 percents full, the control gate at dropshaft CDS–13 should be closed to allow a 10 percent inflow rate within 10 minutes. All other control gates are closed to a 10 percent inflow rate within 5 minutes when the system is 60 percent full. The total inflow hydrograph for this operation is plotted in Fig. C–45. Instantaneous hydraulic gradelines in the main tunnel and five branches at different times are plotted in Figs. C–46 to C–51. The variation of water depth at the upstream ends, junctions, and downstream end are plotted in Figs. C–52 to C–56.

B. System C–III

In this case, all control gates downstream of the roller gate, including the dropshaft CDS–13, should start to reduce the inflow to 40 percent of the original inflow within 10 minutes when the system is 80 percent full. The total inflow hydrograph for this gate control operation is plotted in Fig. C–57. Instantaneous hydraulic gradelines in the main tunnel and four branches at different times are plotted in Figs. C–58 to C–62. The variation of water depth at upstream ends, junctions, and downstream end are plotted in Figs. C–63 to C–66.

C. System C–IV

In this case, all control gates downstream of the roller gate, except dropshaft CDS–13, should be closed to 80 percent of gate opening within 10 minutes when the system is 80 percent full. The total inflow hydrograph for this gate control operation is plotted in Fig. C–67. Instantaneous hydraulic gradelines in the main tunnel and four branches at different times are plotted in Figs. C–68 to C–72. The variation of water depth at upstream ends, junctions, and downstream end are plotted in Figs. C–73 to C–75.

VIII. CONCLUSIONS AND OBSERVATIONS

Following is a list of some conclusions drawn from the results of computer simulations:

1. The transient problems can be controlled with proper inflow control. Satisfactory control procedures have been identified and described in this report. These control procedures are not necessarily optimum because optimum conditions depend on multiple objectives and require considerable search efforts.

2. Inflow control or another surge mitigating device is necessary for the Main Stream System, even after the construction of the planned reservoir at the downstream end. This is due to insufficient conveyance.

3. There is a choice between construction of small surge mitigating reservoirs at the upstream end of the main tunnel and at a constructural shaft in the North Branch and the use of inflow control when the planned reservoir for the Main Stream System are in place.

4. For North Branch, it is possible to avoid geysering by reducing the drift tunnel size, or by increasing the dropshaft size at the upstream end, or by increasing the height of the drift tube that connects the upstream end dropshaft with the constructural shaft above the invert of the tunnel.

5. The solution for the Calumet System is quite different from that of the Main Stream System. It has sufficient conveyance so that the presence of the planned reservoir can prevent the surge problem if the roller gate has an open condition. Some inflow reduction is needed downstream of the roller gate if the gate is closed.

Some recommendations:

1. All the solution procedures described in this report are satisfactory from the transient point of view, but not necessarily optimum from operational or other possible viewpoints. Therefore, either the procedures should be further refined by analysis or field trials before being regarded as final.

2. Control procedures described in this report are based on specific inflow hydrographs. In actual conditions, the inflow rate is not known, and any control procedure based on storage volume alone has specific inherent drawbacks. If the operating procedure based on large storms is adopted, then the risk is underutilization of the tunnel. On the other hand, if the operating procedure is based on small storm, the risk is geysering and safety.

3. The long–term solutions for Main Stream and Calumet System are based on the assumption that the tunnels are connected to the reservoirs at all times and there is no gate or valve to impede the flow. Further analysis is needed if the flow between the tunnel and reservoir is to be disrupted for draining or other reasons.

REFERENCES

1. Song, C.C.S., Guo, Q., and Zheng, Y., "Hydraulic Transient Modeling of TARP Systems," St. Anthony Falls Hydraulic Laboratory, Project report No. 270, March 1988.

2. Cardle, J. A. and Song, C.C.S., "Mathematical Modeling of Unsteady Flow in Storm Sewers." *International Journal of Engineering Fluid Mechanics*, Vol. 1, No. 4, 1988.

3. Guo, Q. and Song, C.C.S., "Surging in Urban Storm Drainage Systems," ASCE, *Journal of Hydraulic Engineering*, Vol. 116, No. 12, June, 1989.

4. Guo, Q. and Song, C.C.S., "Dropshaft Hydrodynamics Under Transient Conditions," ASCE, *Journal of Hydraulic Engineering*, Vol. 117, No. 8. Aug. 1991.

APPENDIX

Figures M-1 through M-39
Figure C-1 through C-77

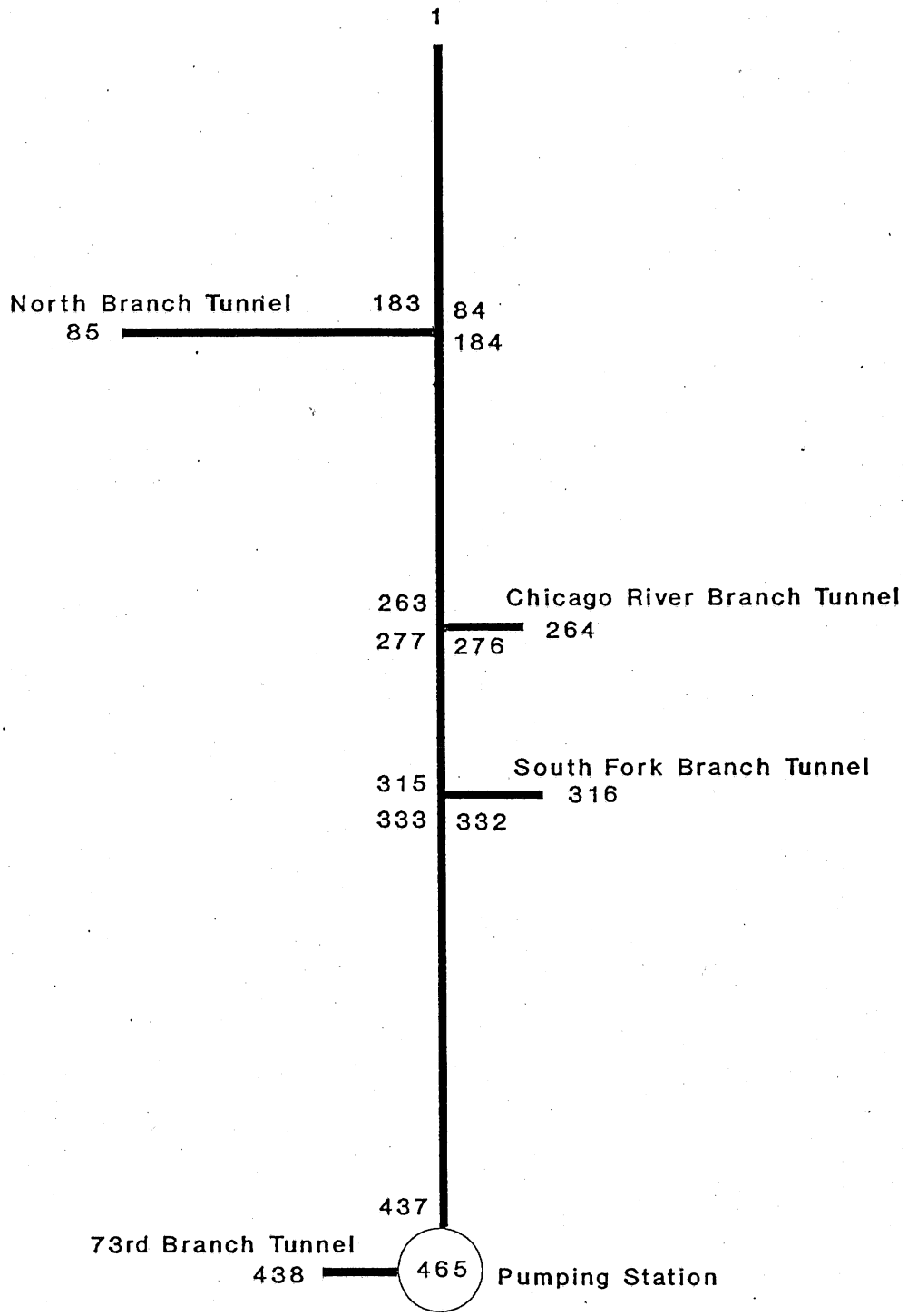

Fig.M-1 Mainstream system configuration (four branches) for modeling purposes

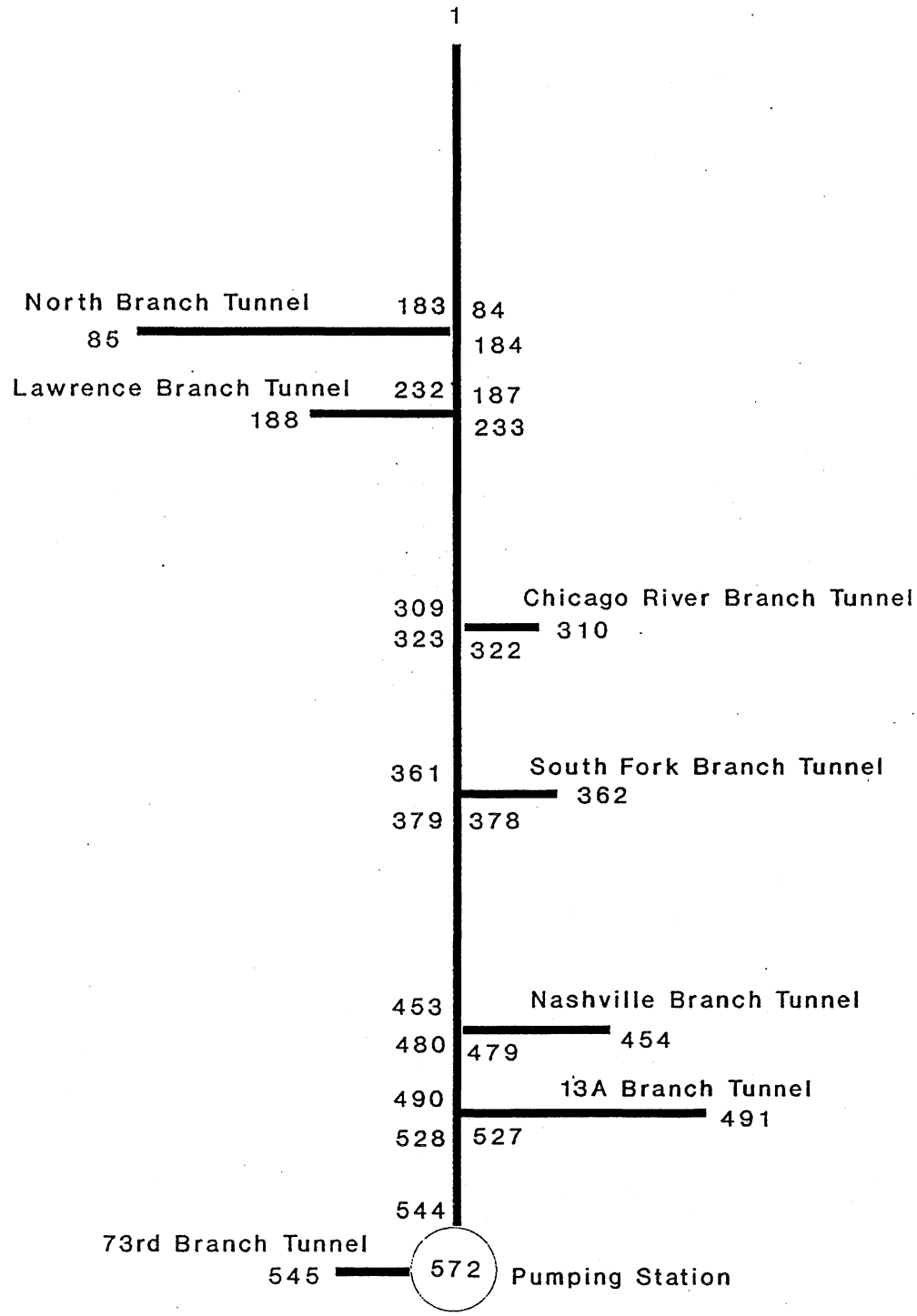

Fig.M-2 Mainstream system configuration (seven branches) for modeling purpose

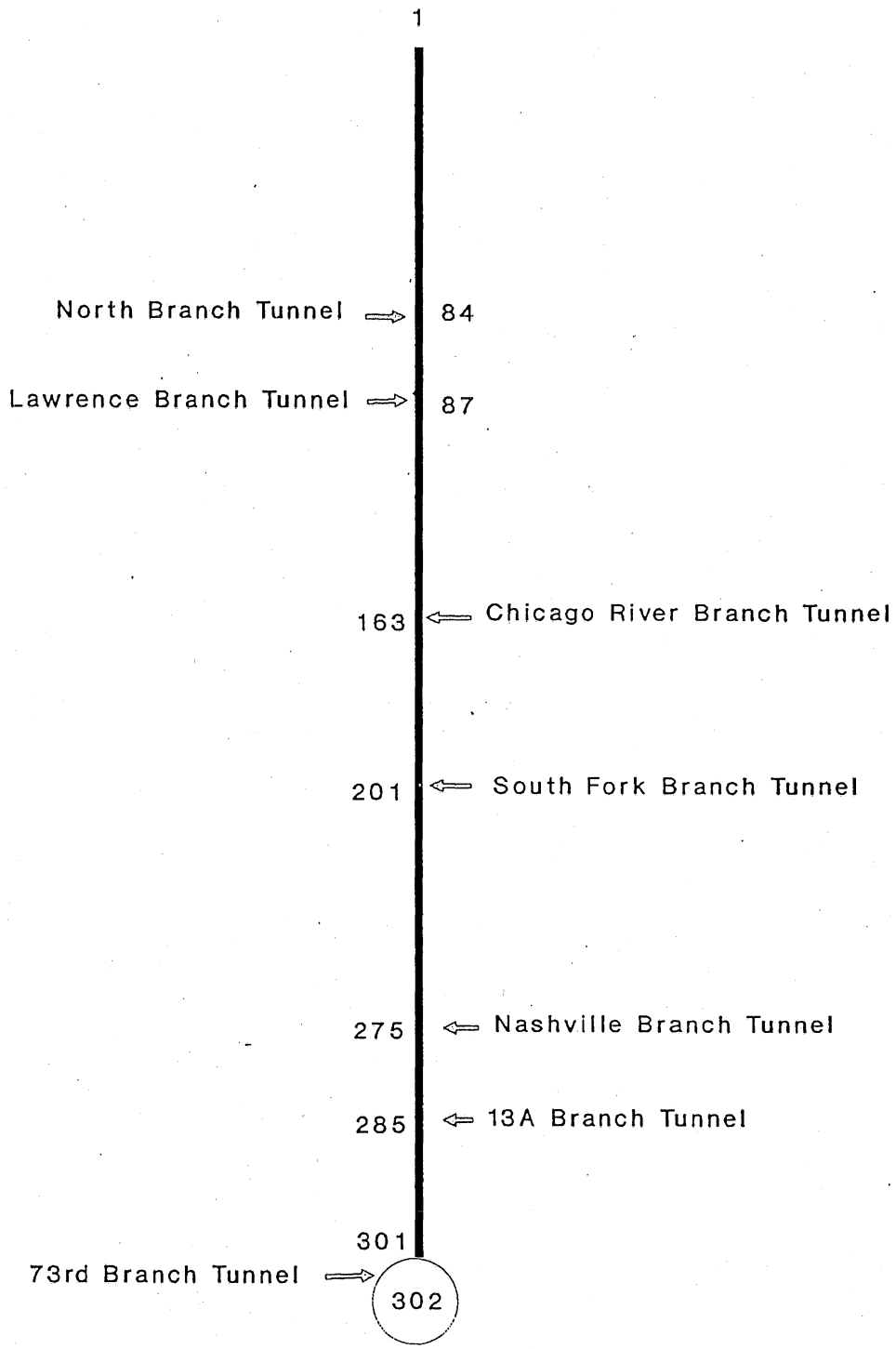

Fig.M-3 Stationing of mainstream system excluding all branch tunnels

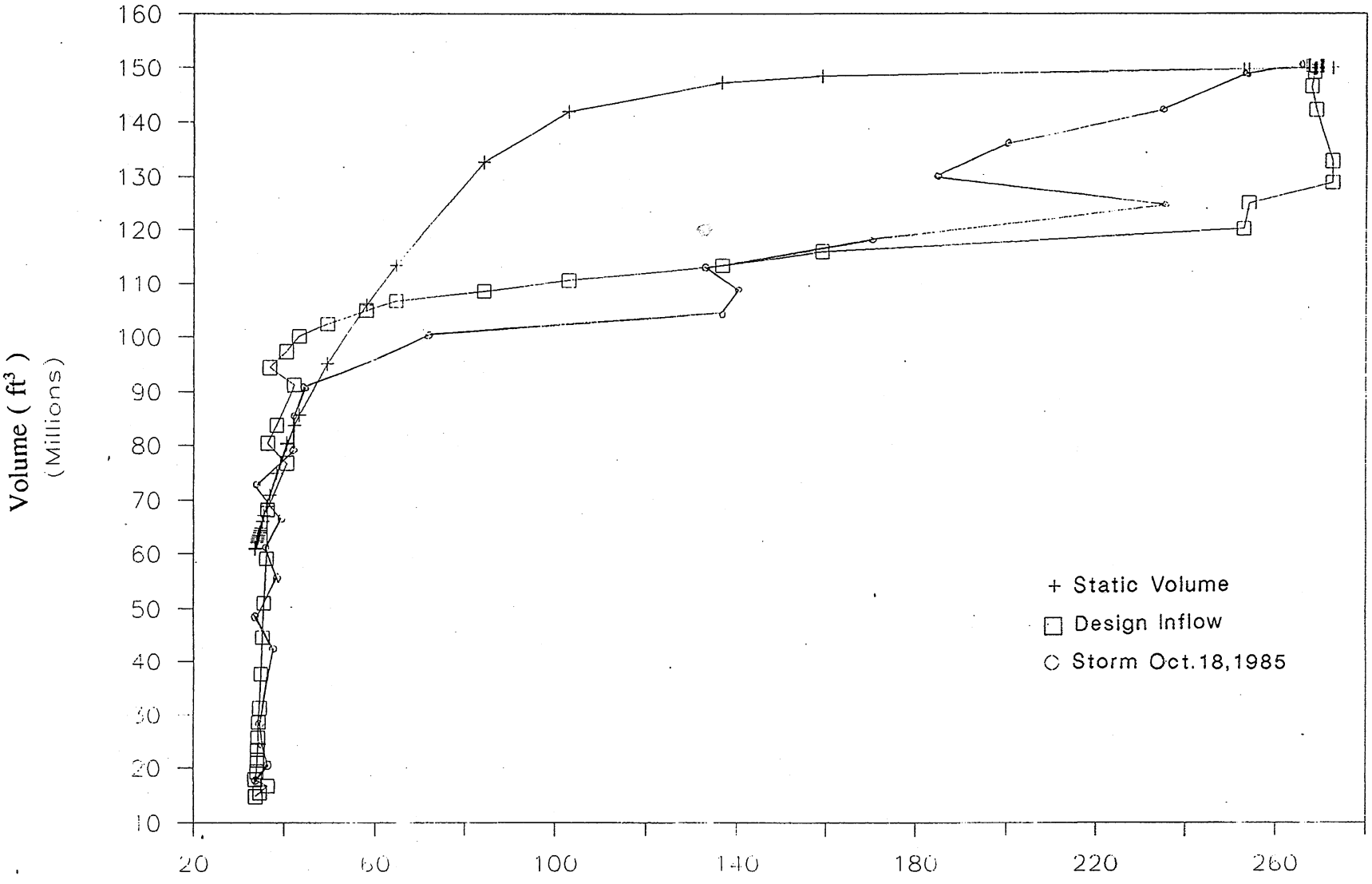

Fig.M-4 Statically and dynamically determined correlation between volume and depth at downstream end, Mainstream System

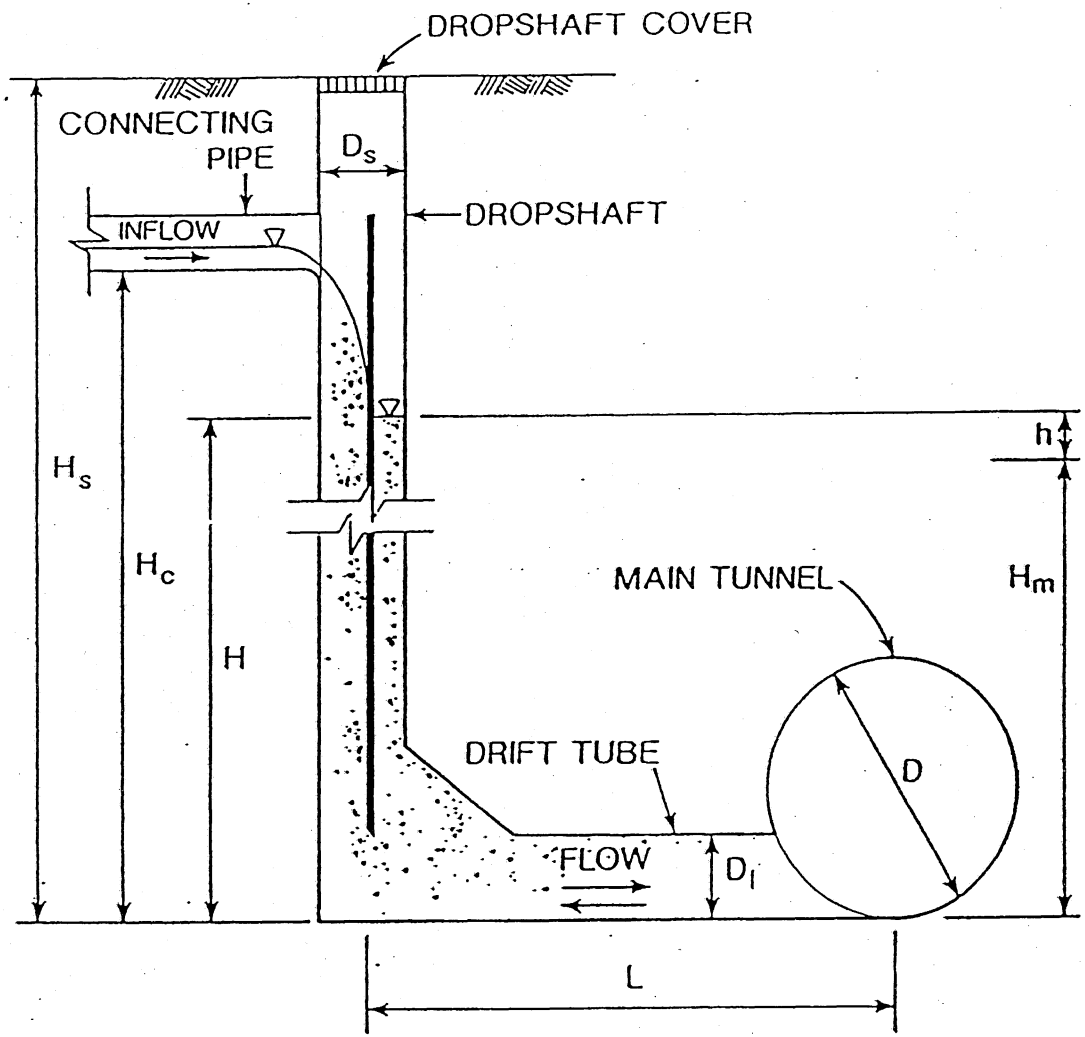

Fig.M-5 A sketch of dropshaft-drift tube system for geyser analysis

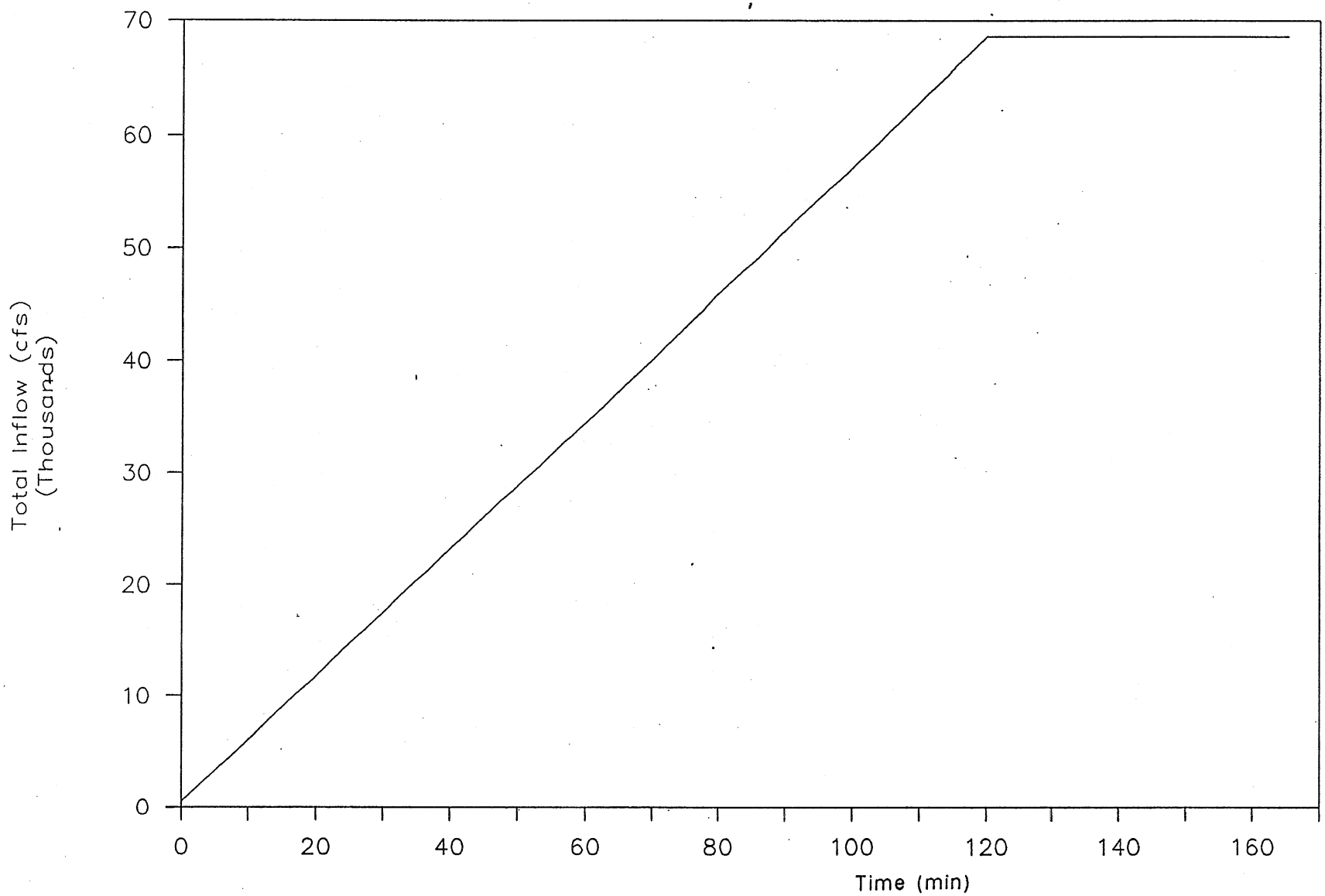

Fig.M-6 Total inflow hydrograph of four branch system (design inflow - no inflow control)

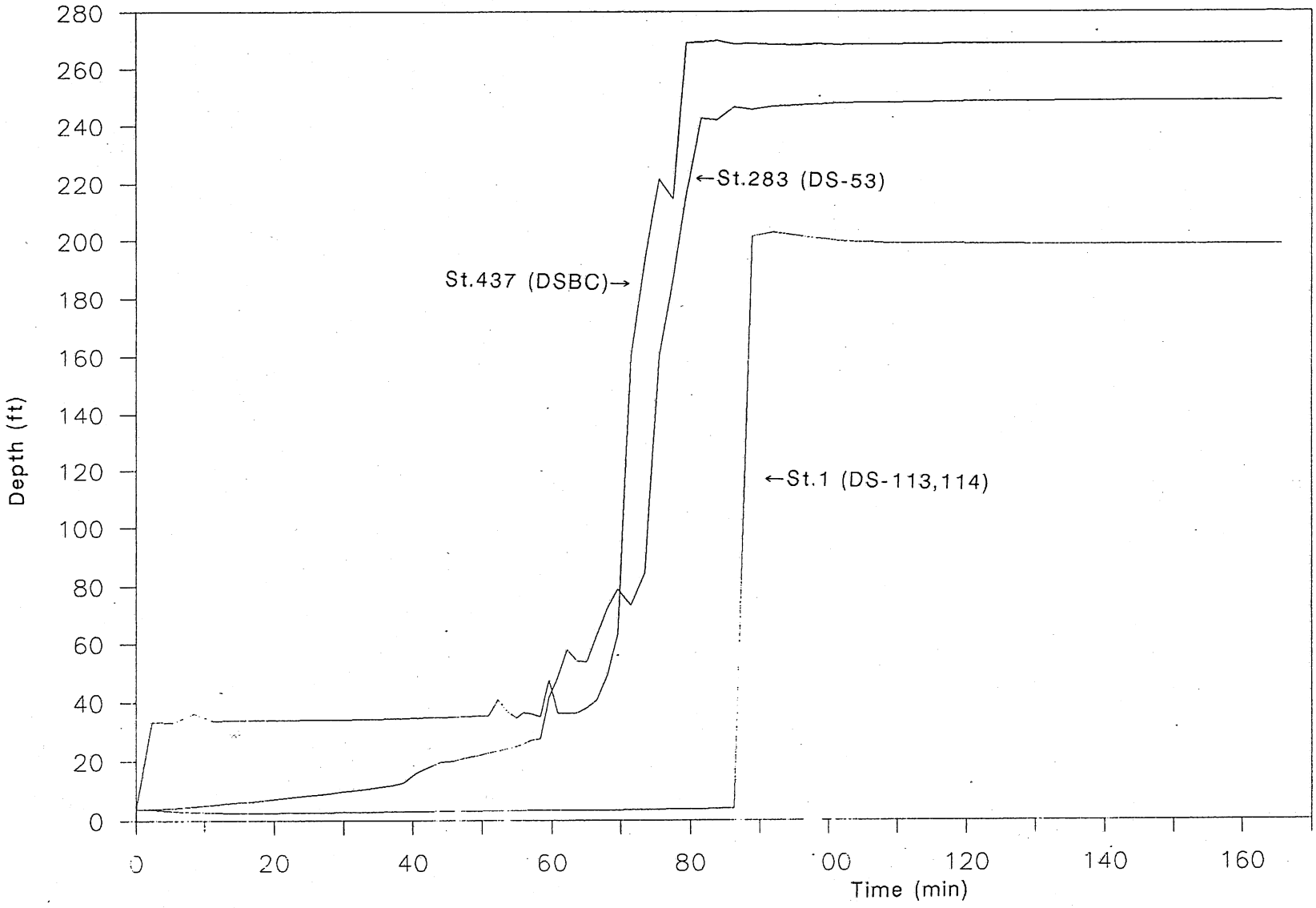

Fig.M-7 Time variation of water depth at three key stations (four branch system without reservoir, design inflow without inflow control)

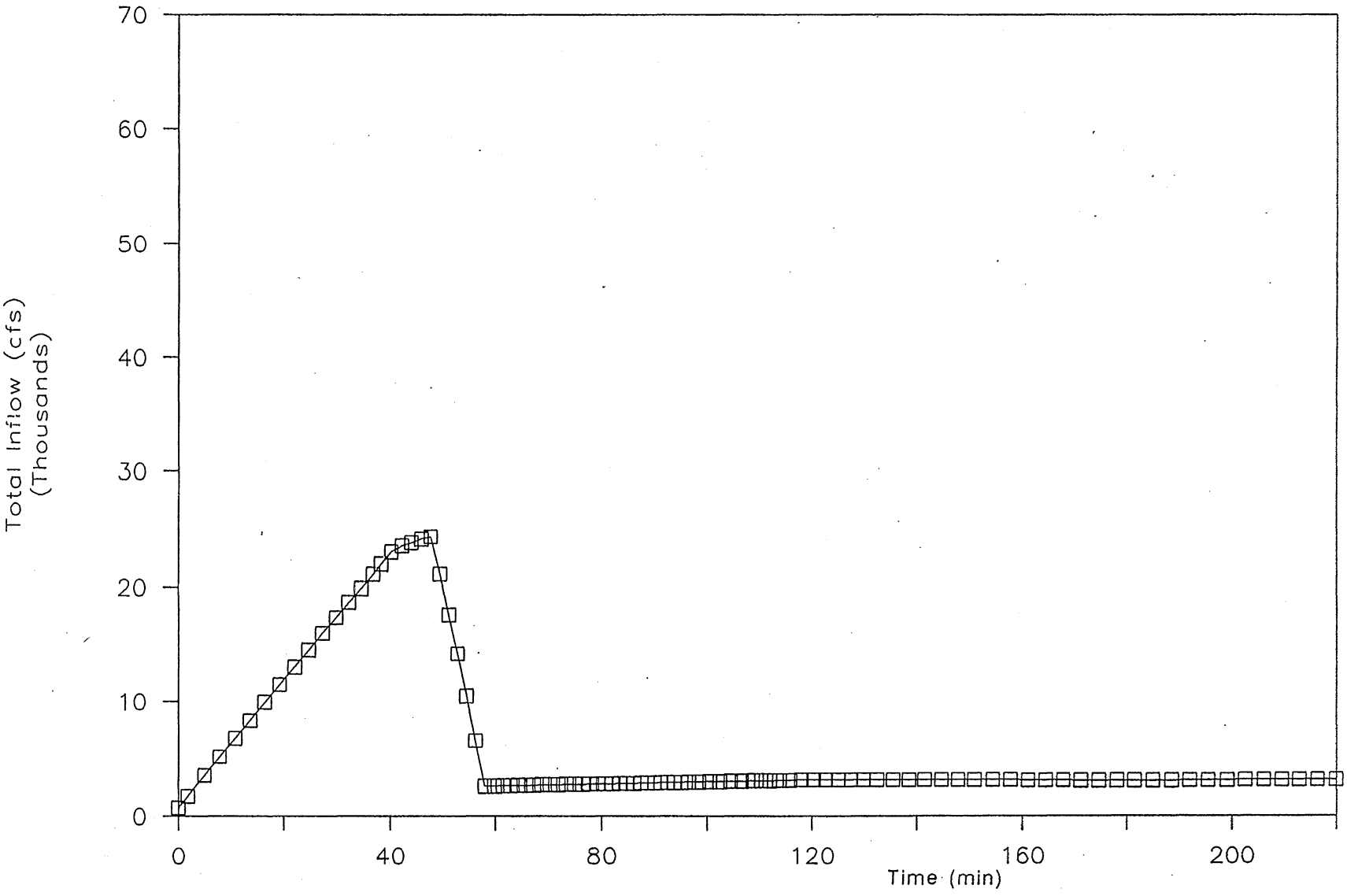

Fig.M-8 Total inflow hydrograph of four branch system, without reservoir (design inflow - inflow control)

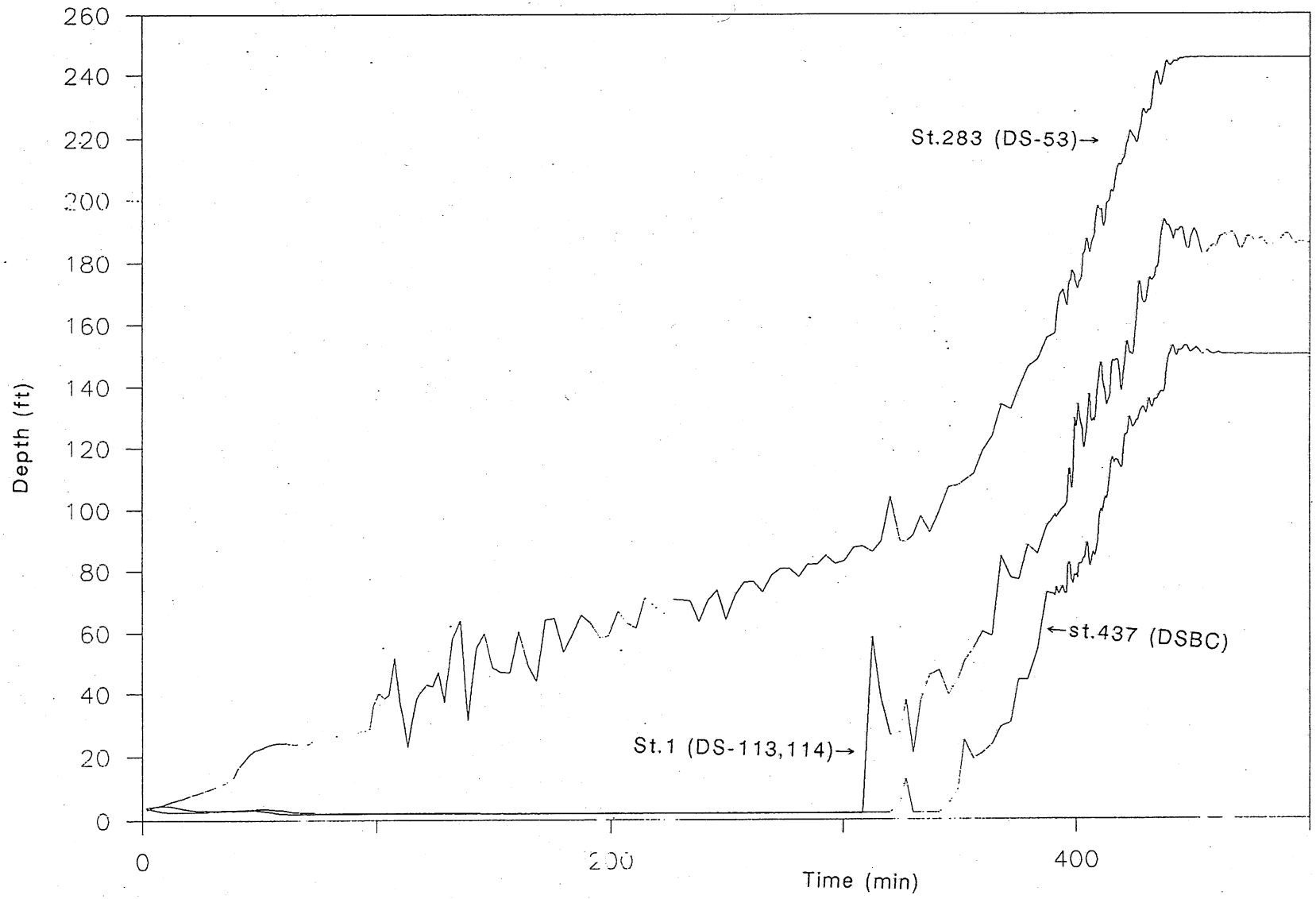

Fig.M-9 Time variation of water depth at three key stations (four branch system without reservoir, design inflow with inflow control)

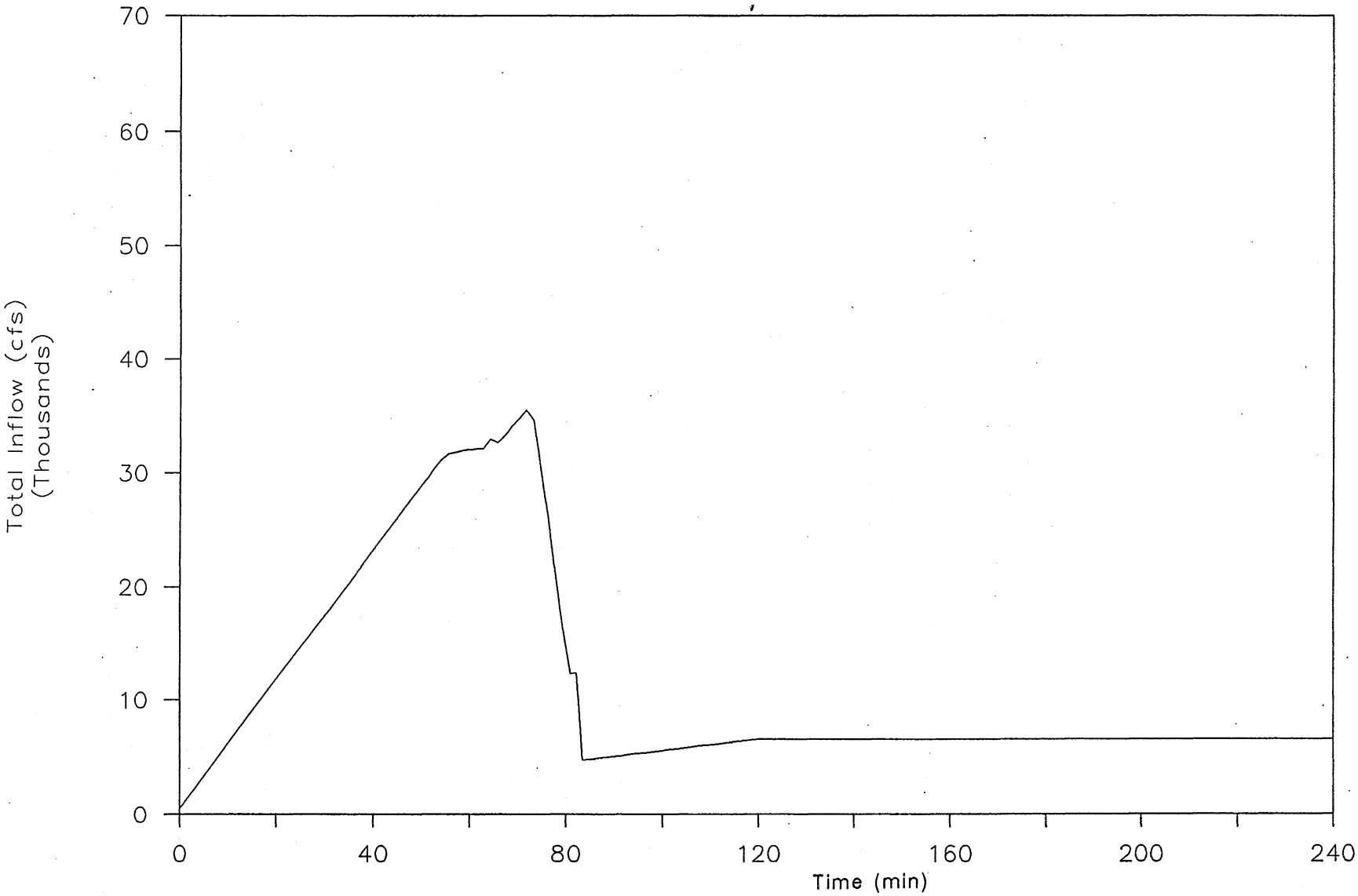

Fig.M-10 Total inflow hydrograph of four branch system, with reservoir (design inflow - inflow control)

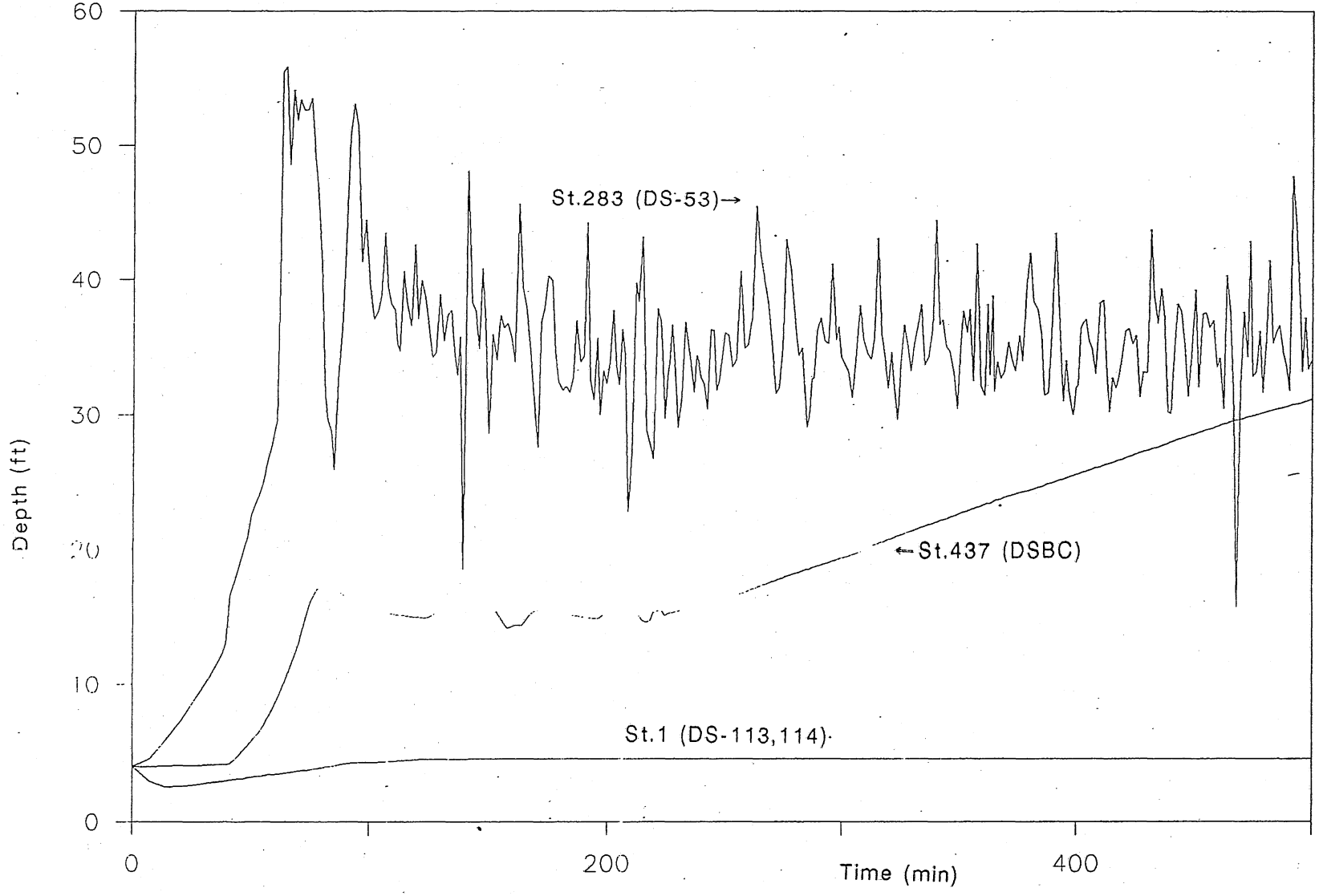

Fig.M-11 Time variation of water depth at three key stations (four branch system with reservoir, design inflow with inflow control)

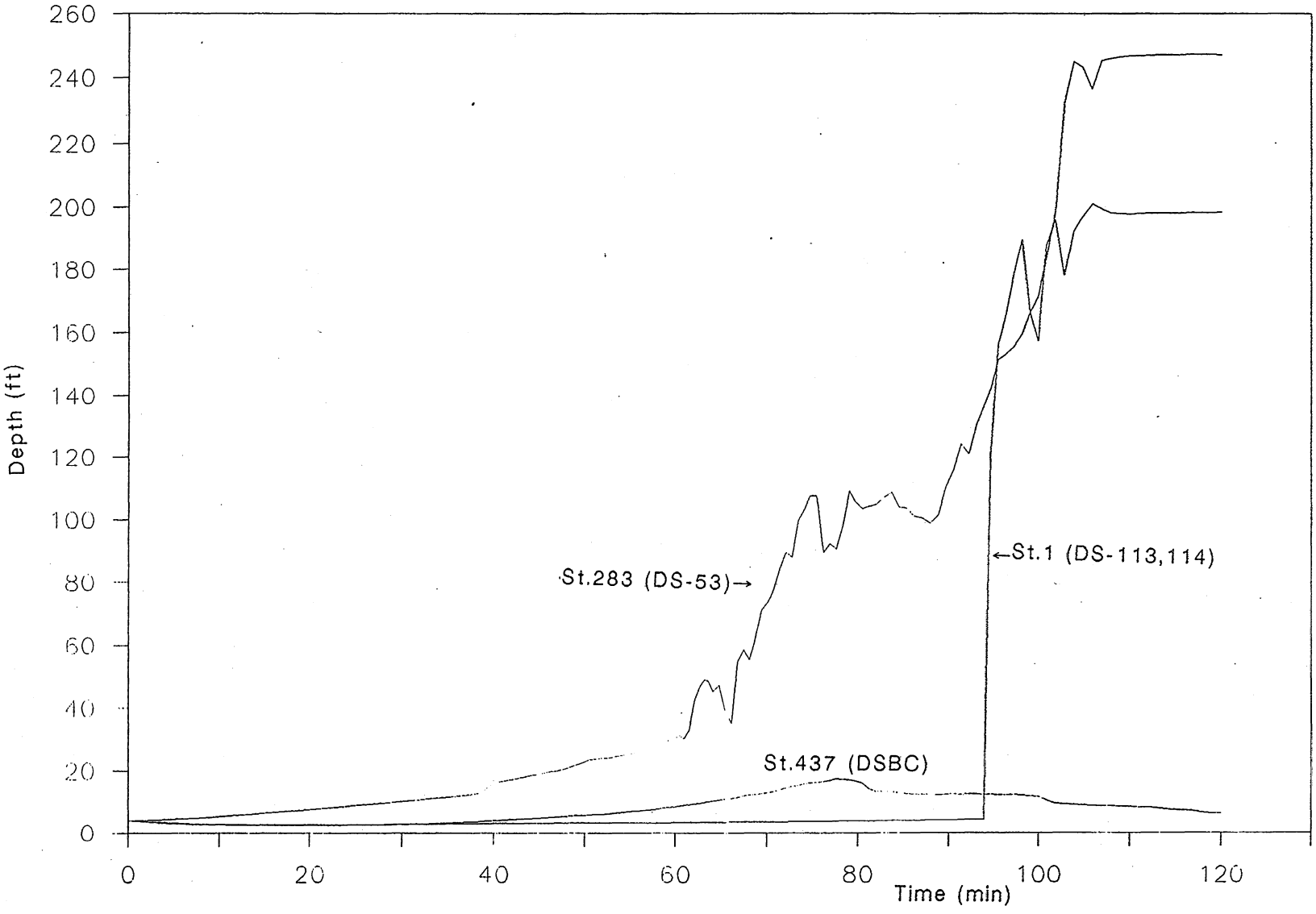

Fig.M-12 Time variation of water depth at three key stations (four branch system with reservoir, design inflow with structural solution)

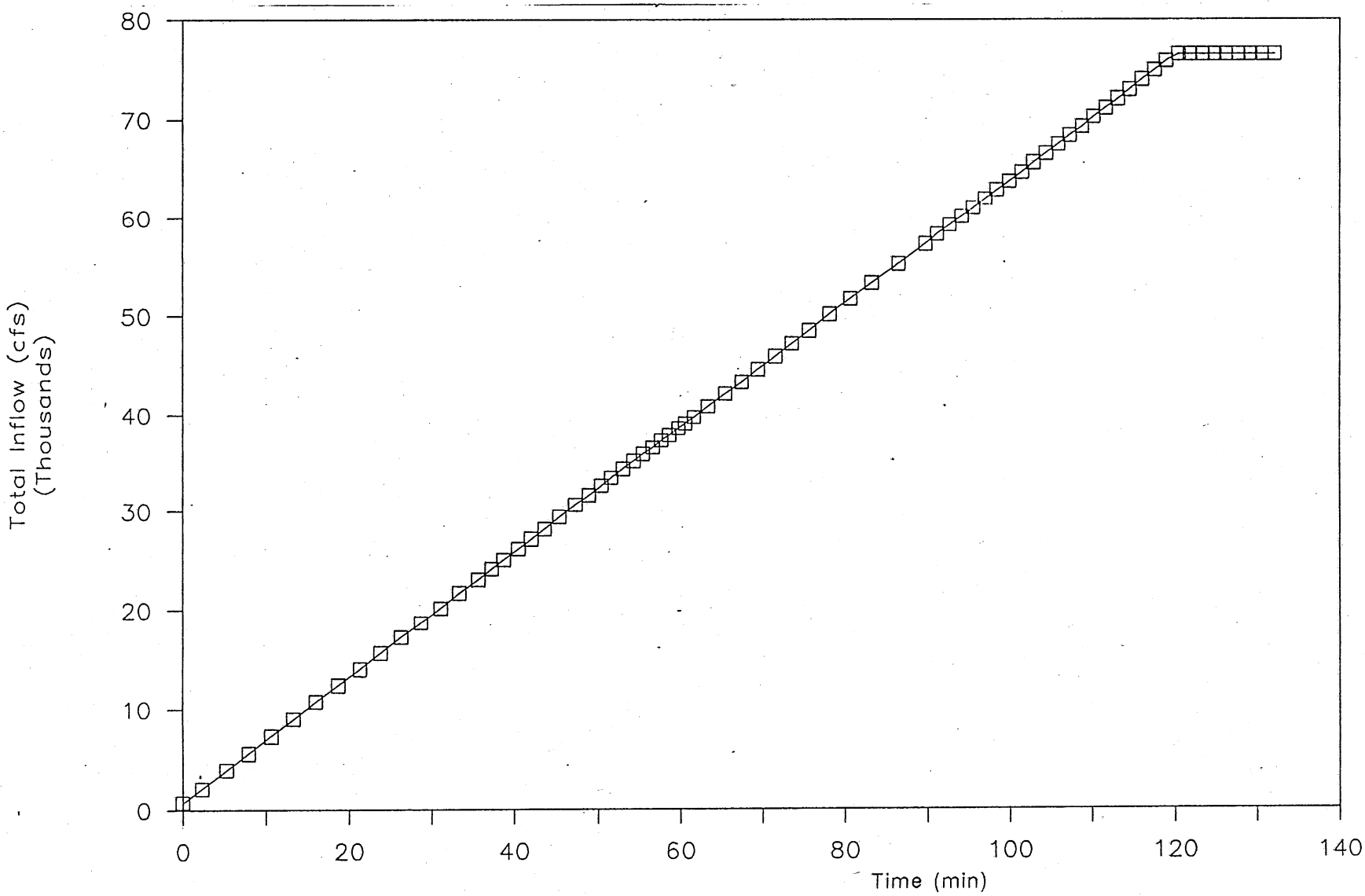

Fig.M-13 Total inflow hydrograph of seven branch system (design inflow - no inflow control)

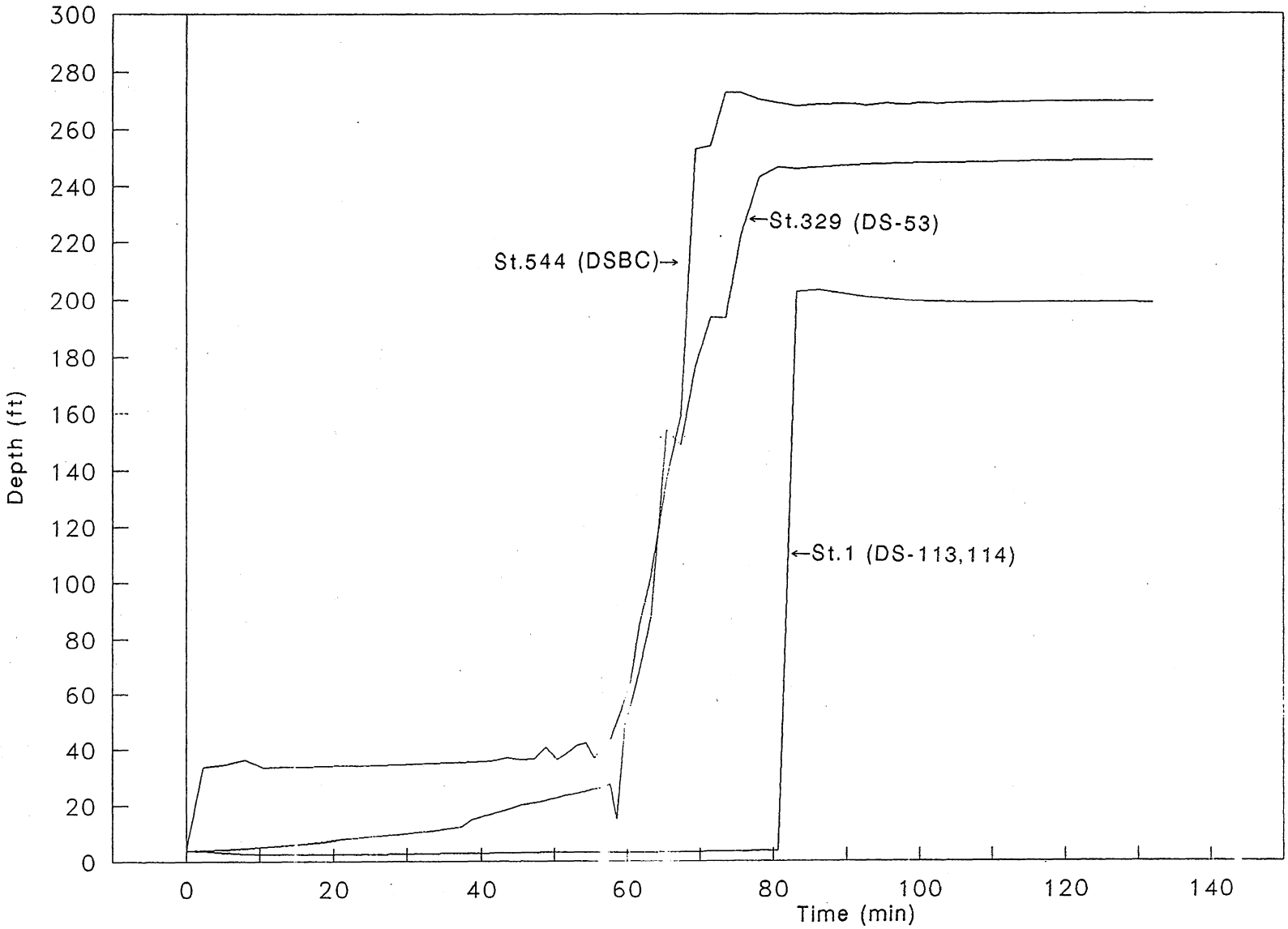

Fig.M-14 Time variation of water depth at three key stations (seven branch system without reservoir, design inflow without inflow control)

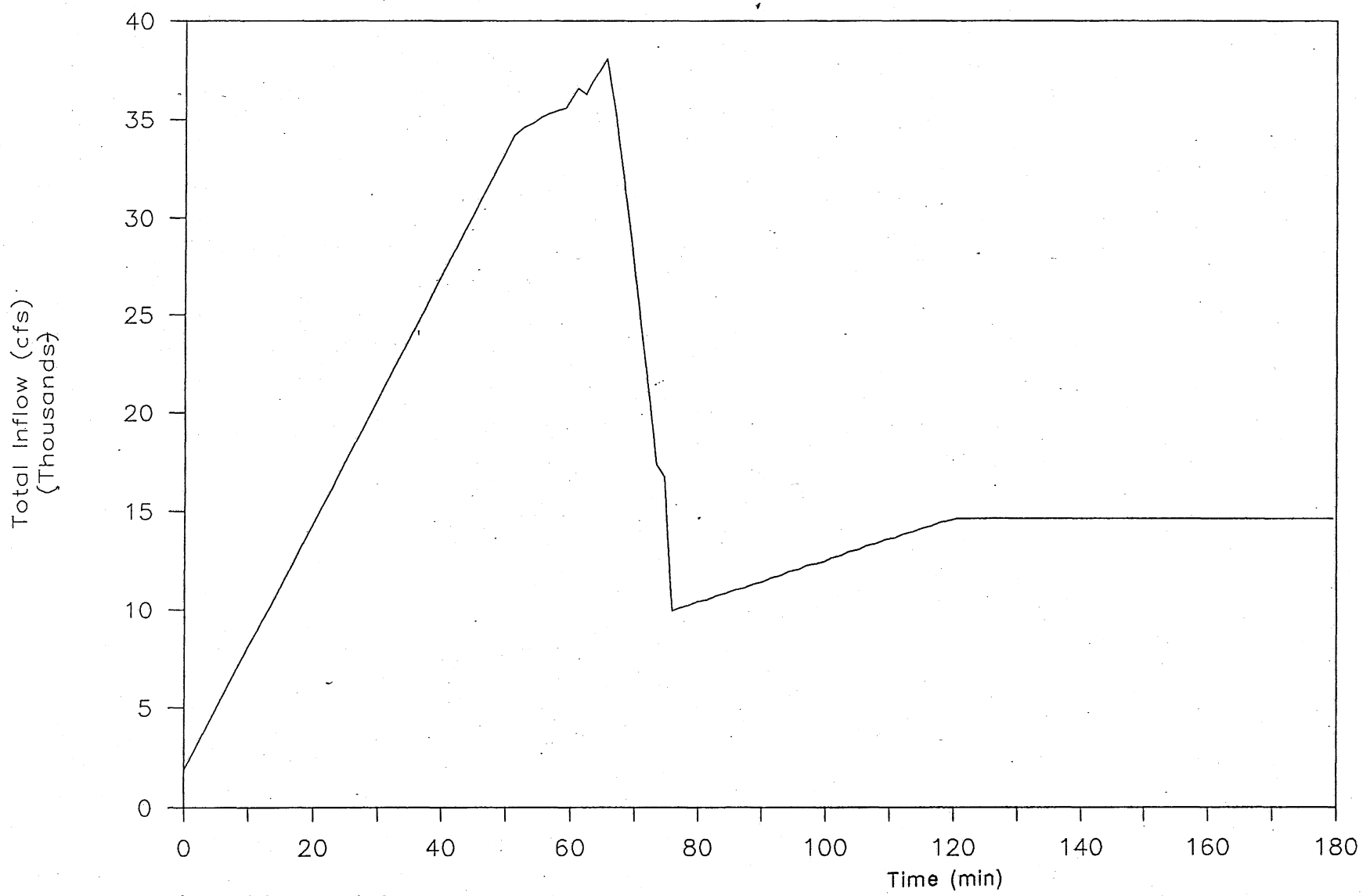

Fig.M-15 Total inflow hydrograph of seven branch system, with reservoir (design inflow - inflow control)

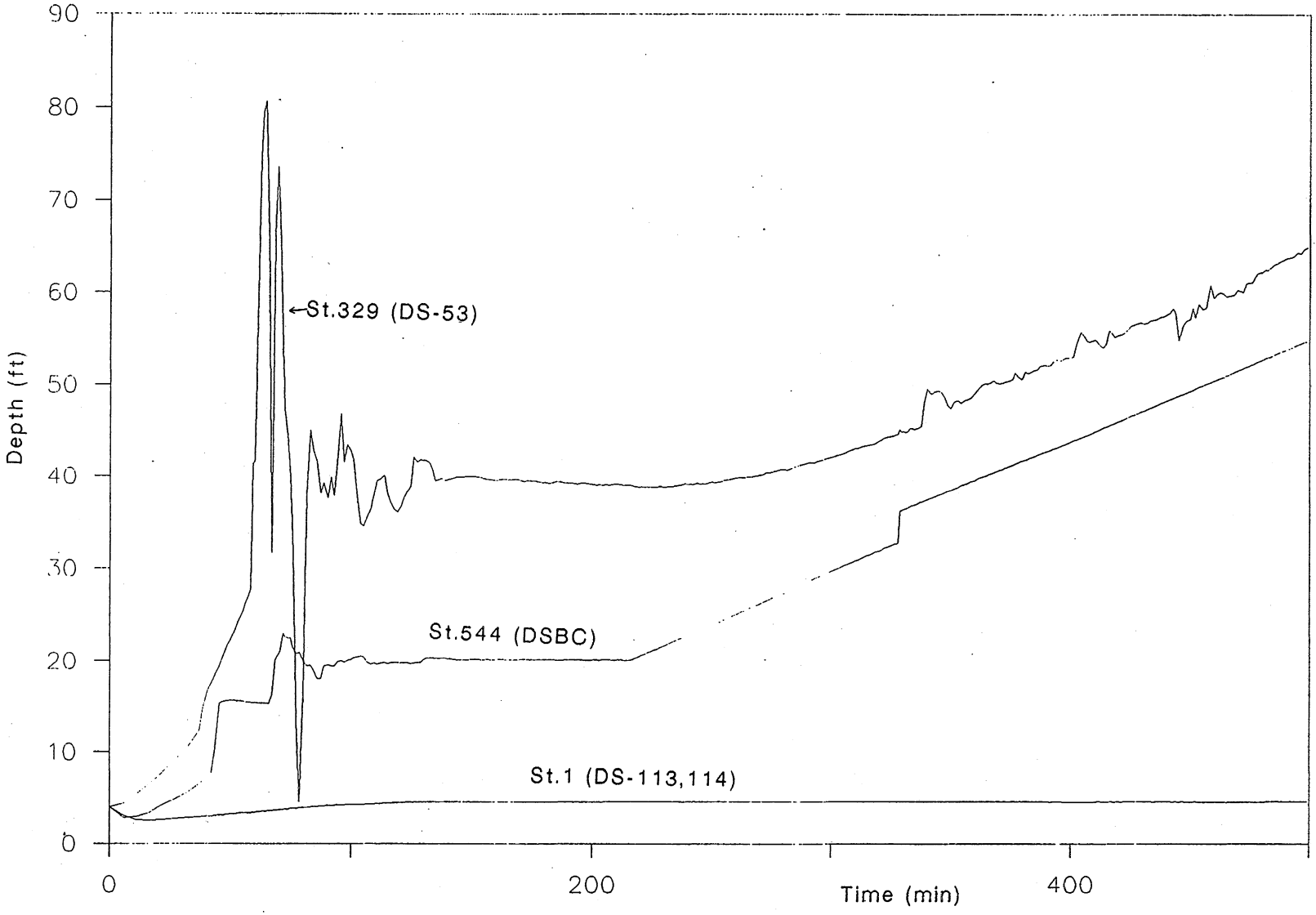

Fig.M-16 Time variation of water depth at three key stations (seven branch system with reservoir, design inflow with inflow control)

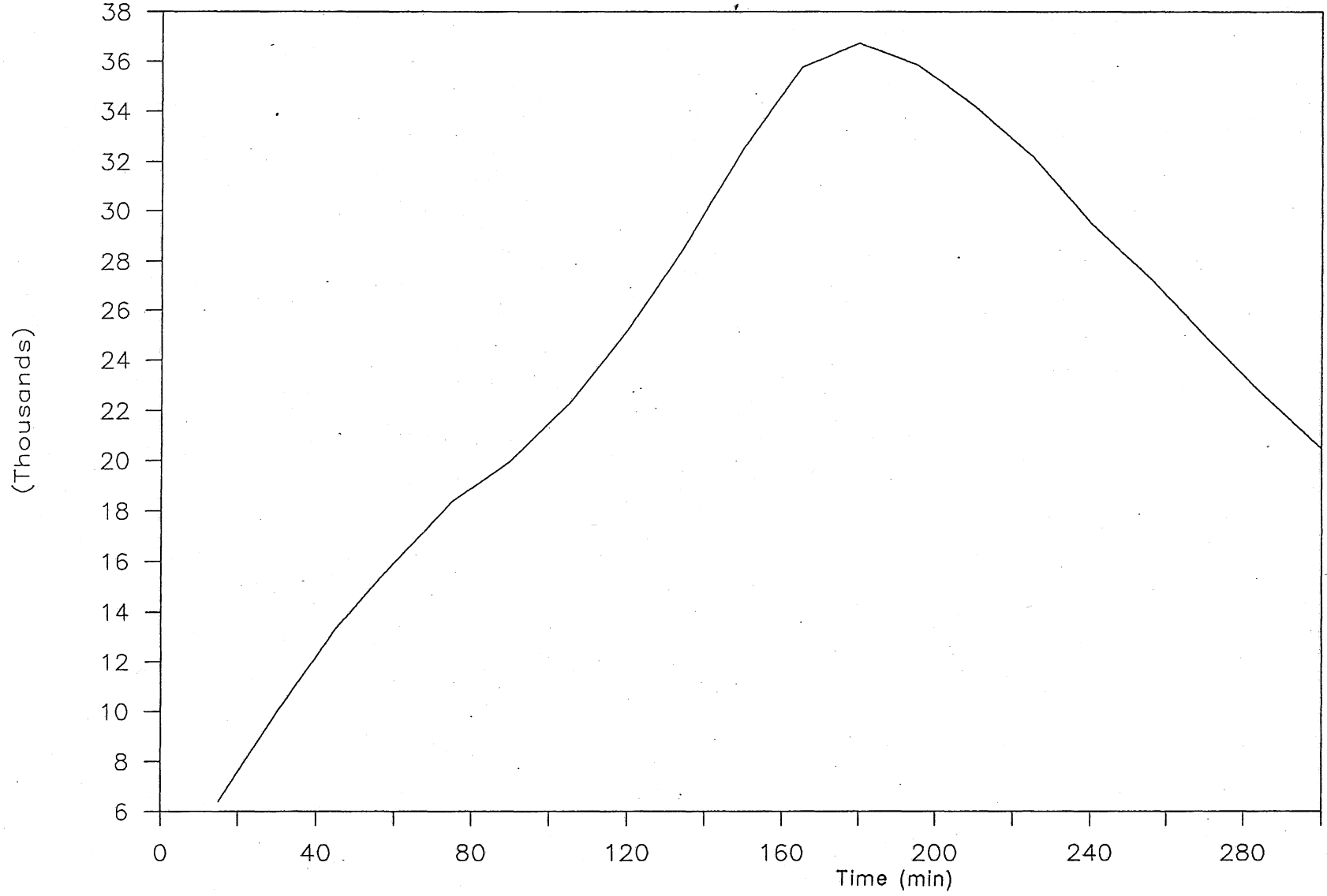

Fig. M-17 Total inflow hydrograph of four branch system (Storm Oct.18,1985 - no inflow control)

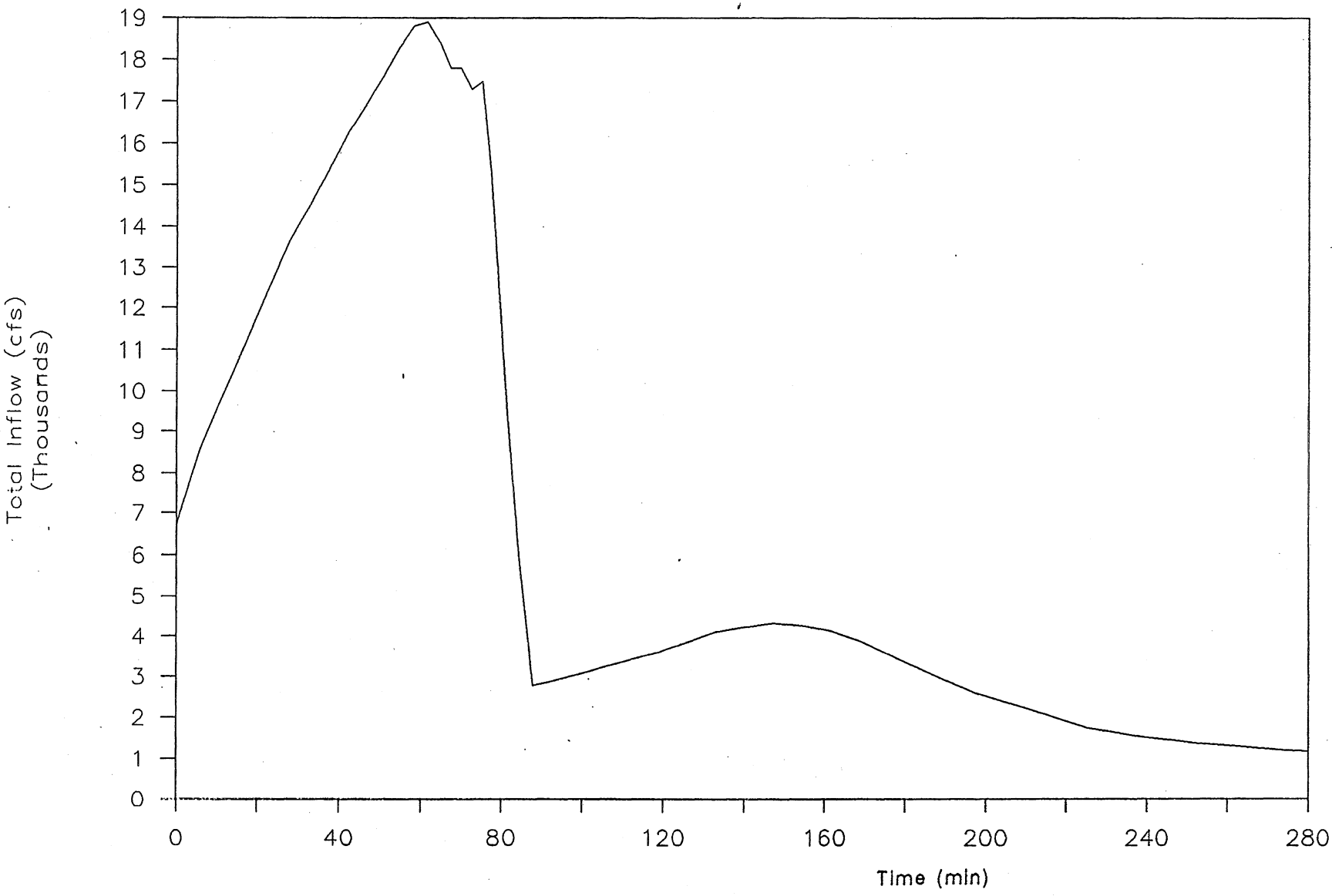

Fig.M-18 Total inflow hydrograph of four branch system, without reservoir (Storm Oct.18,1985 - inflow control)

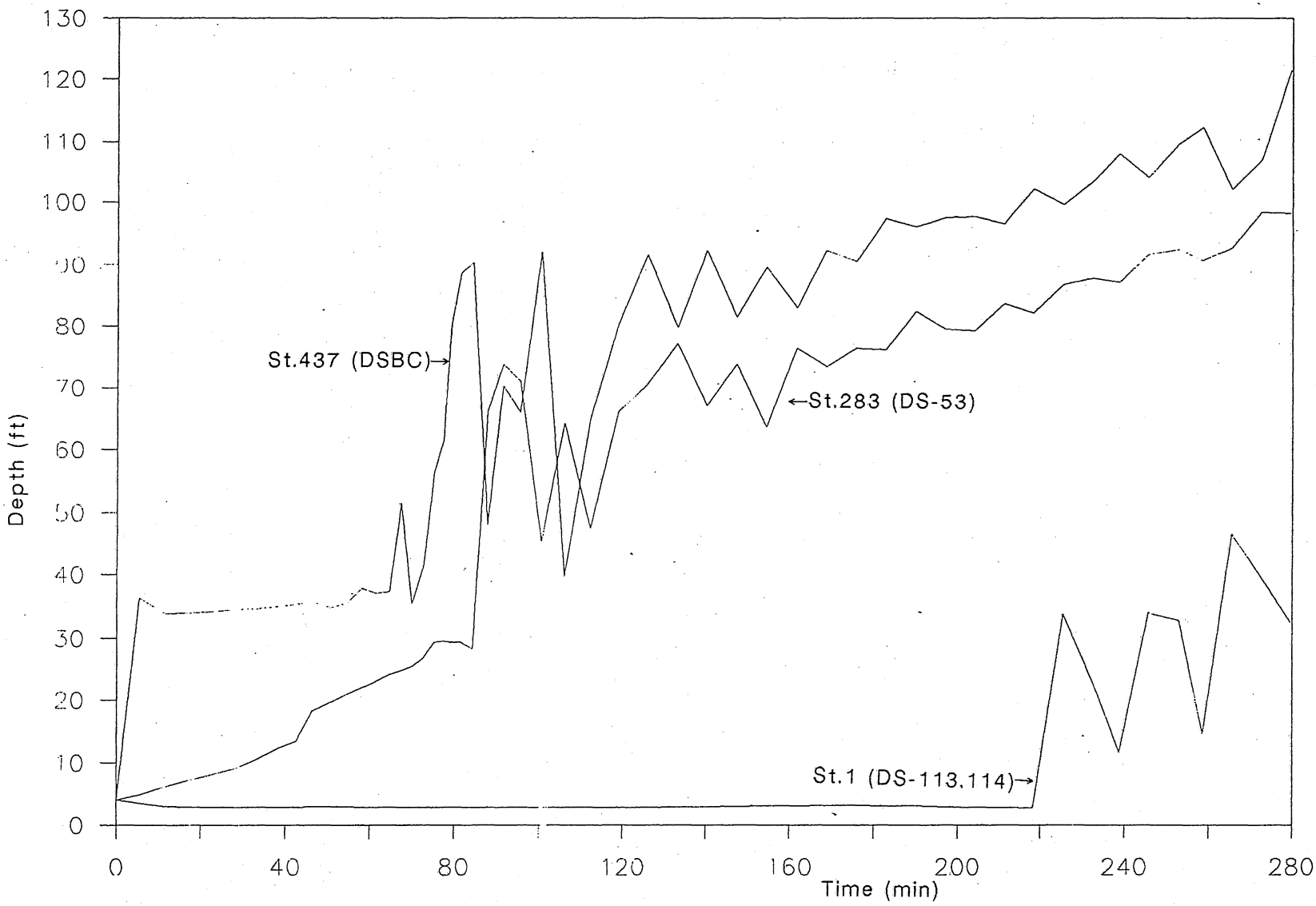

Fig.M-19 Time variation of water depth at three key stations (four branch system without reservoir, storm Oct.18,1985 with inflow control)

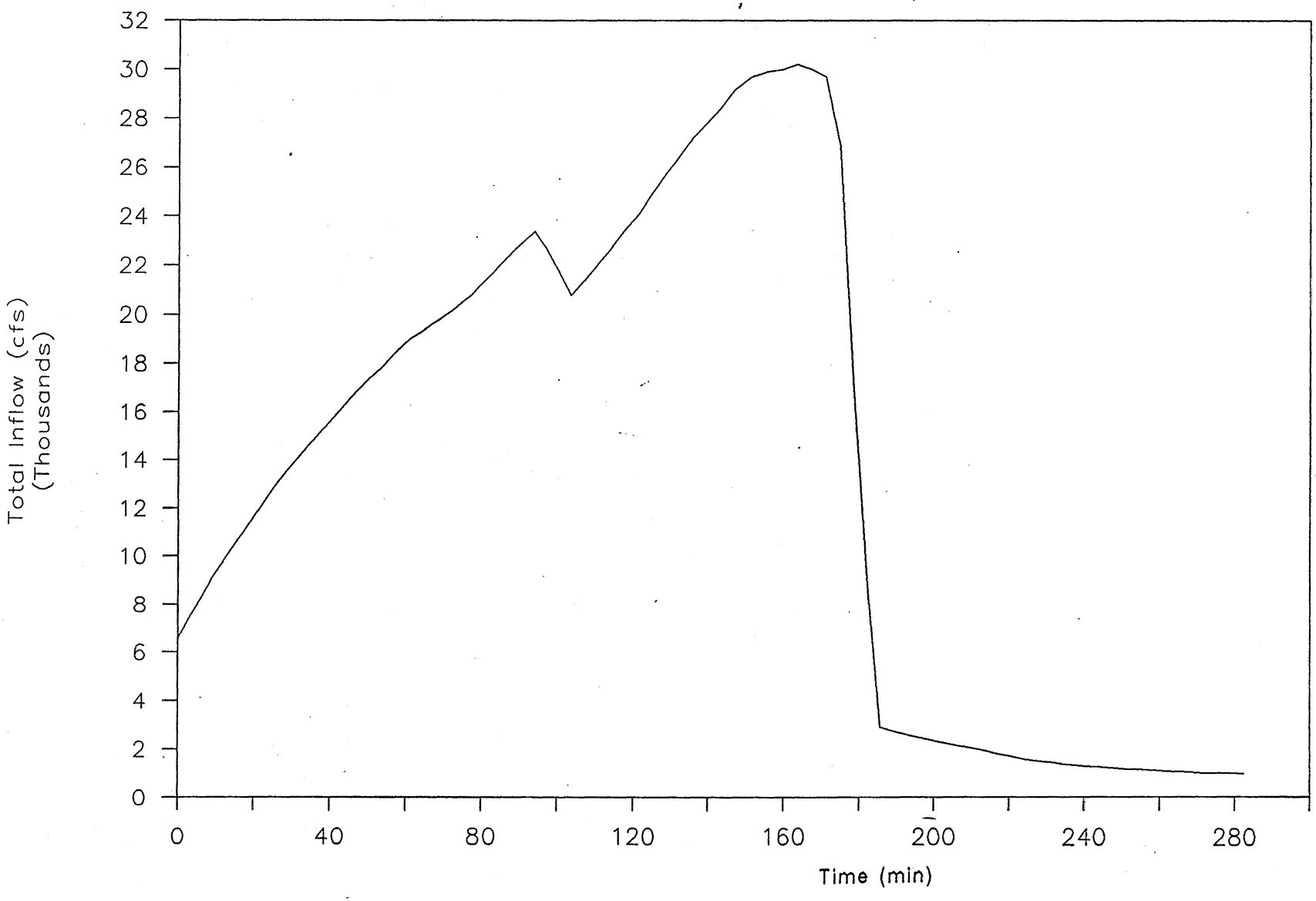

Fig.M-20 Total inflow hydrograph of four branch system, with reservoir (Storm Oct.18,1985 - inflow control)

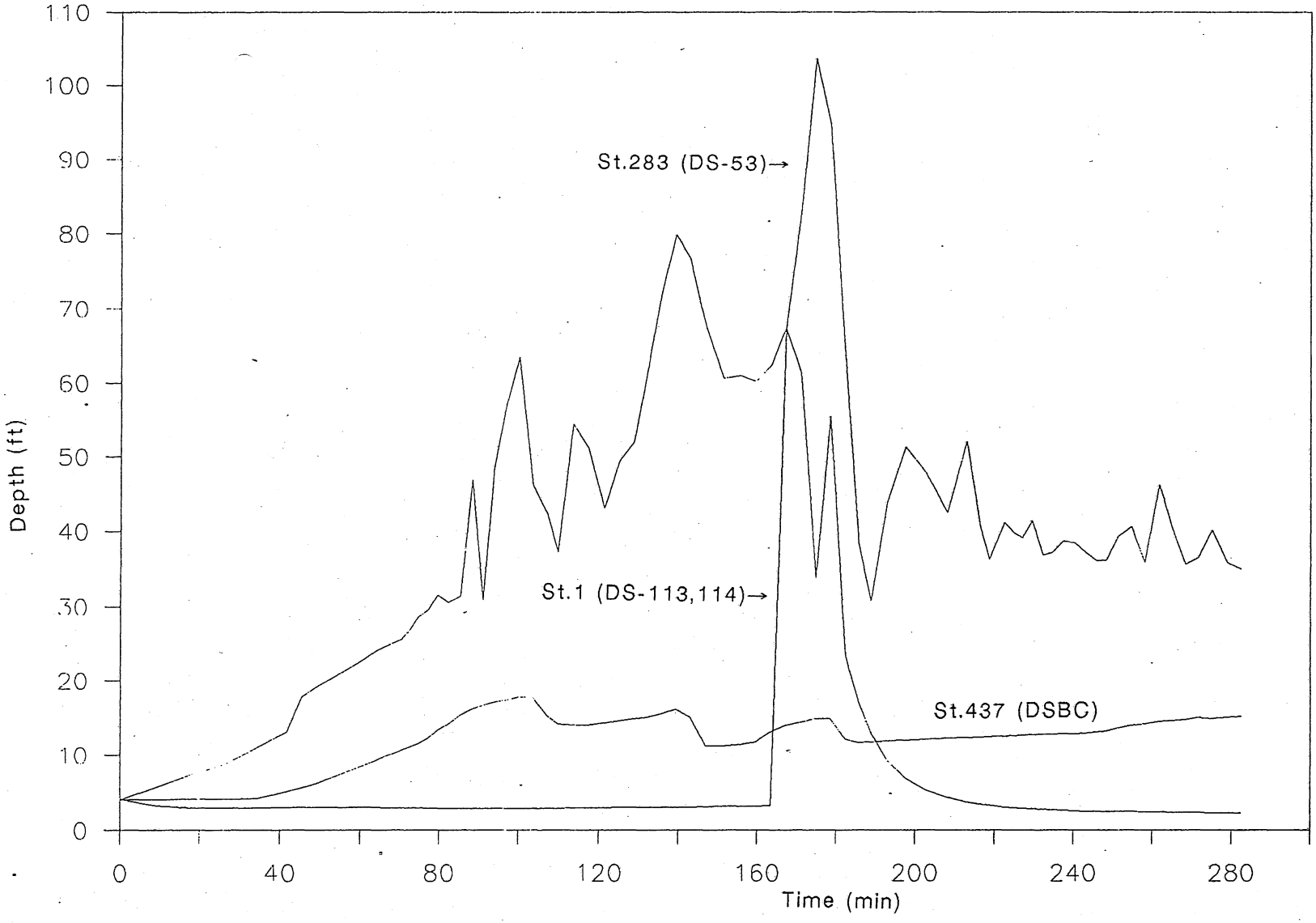

Fig.M-21 Time variation of water depth at three key stations (four branch system with reservoir, storm Oct.18,1985 with inflow control)

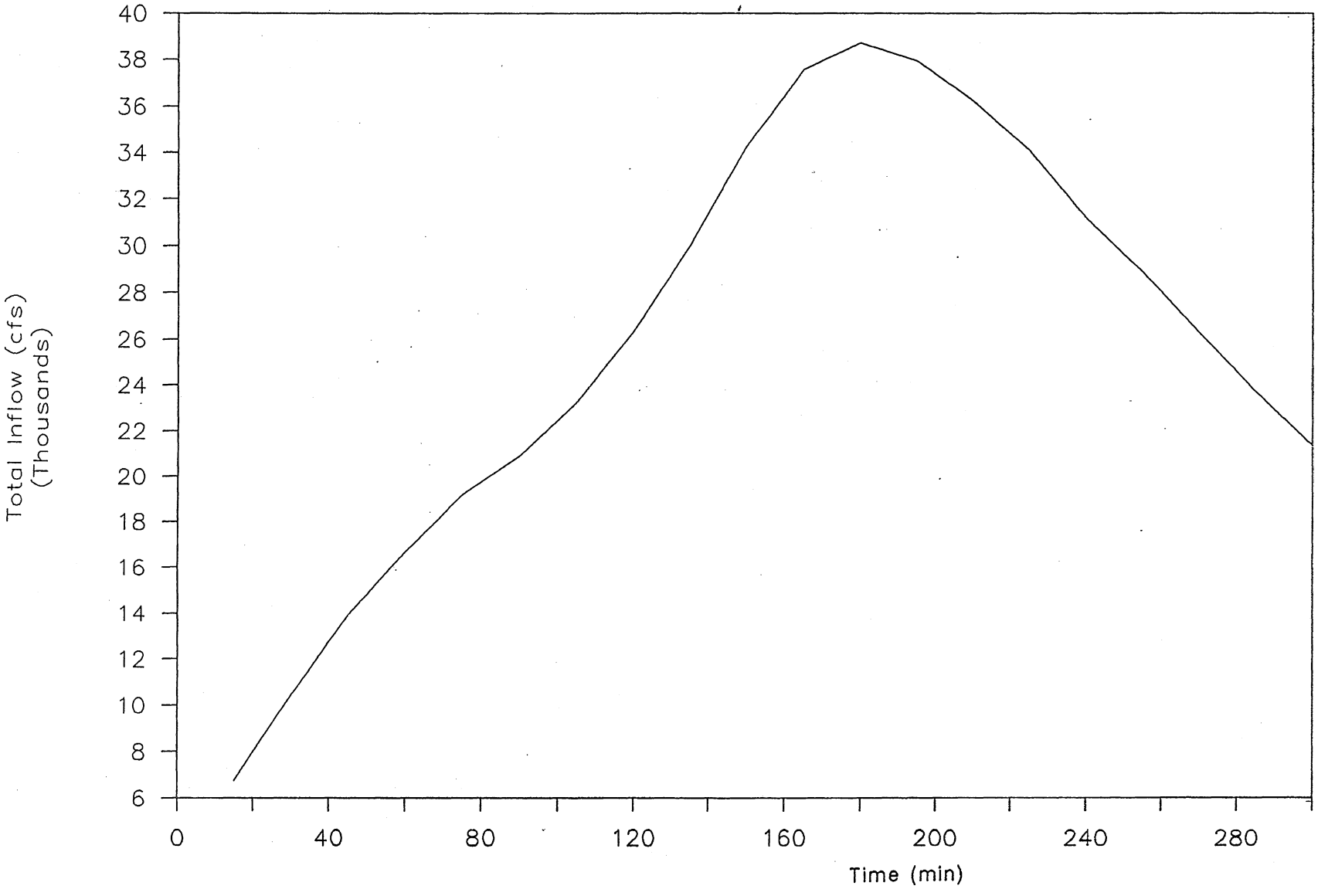

Fig.M-22 Total inflow hydrograph of seven branch system (Storm Oct.18,1985 - no inflow control)

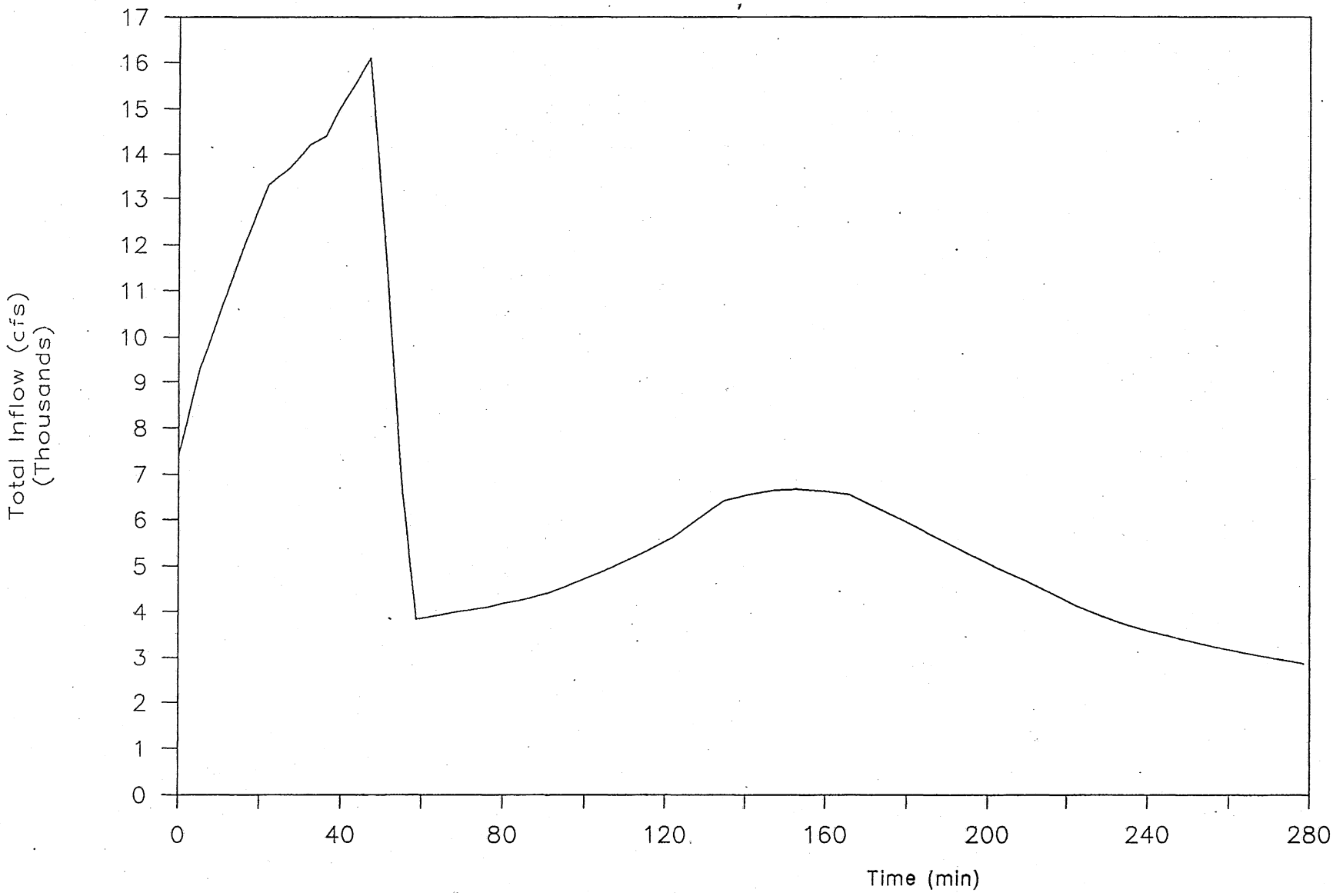

Fig.M-23 Total inflow hydrograph of seven branch system, without reservoir (Storm Oct.18,1985 - inflow control)

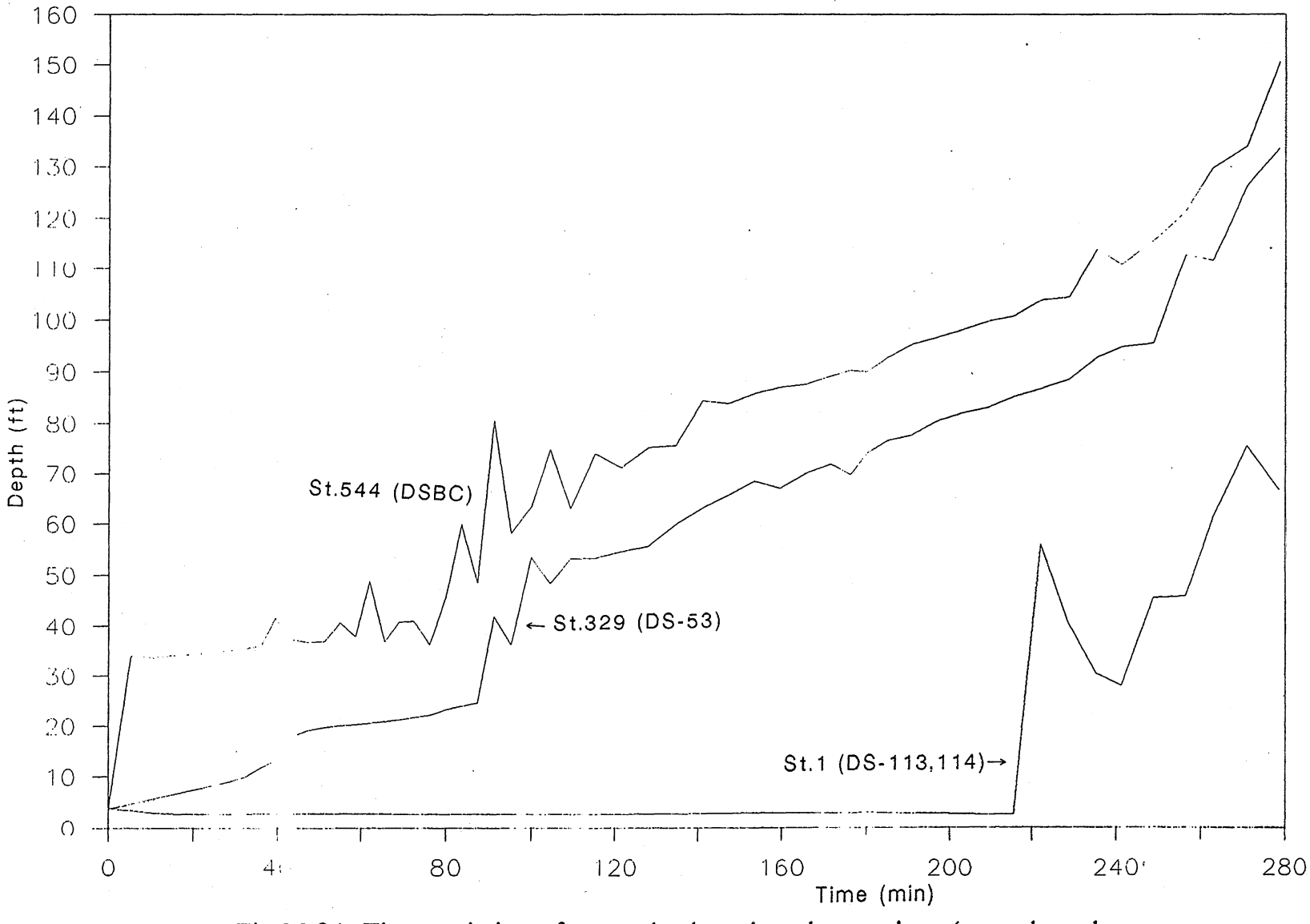

Fig.M-24 Time variation of water depth at three key stations (seven branch system without reservoir, storm Oct.18,1985 with inflow control)

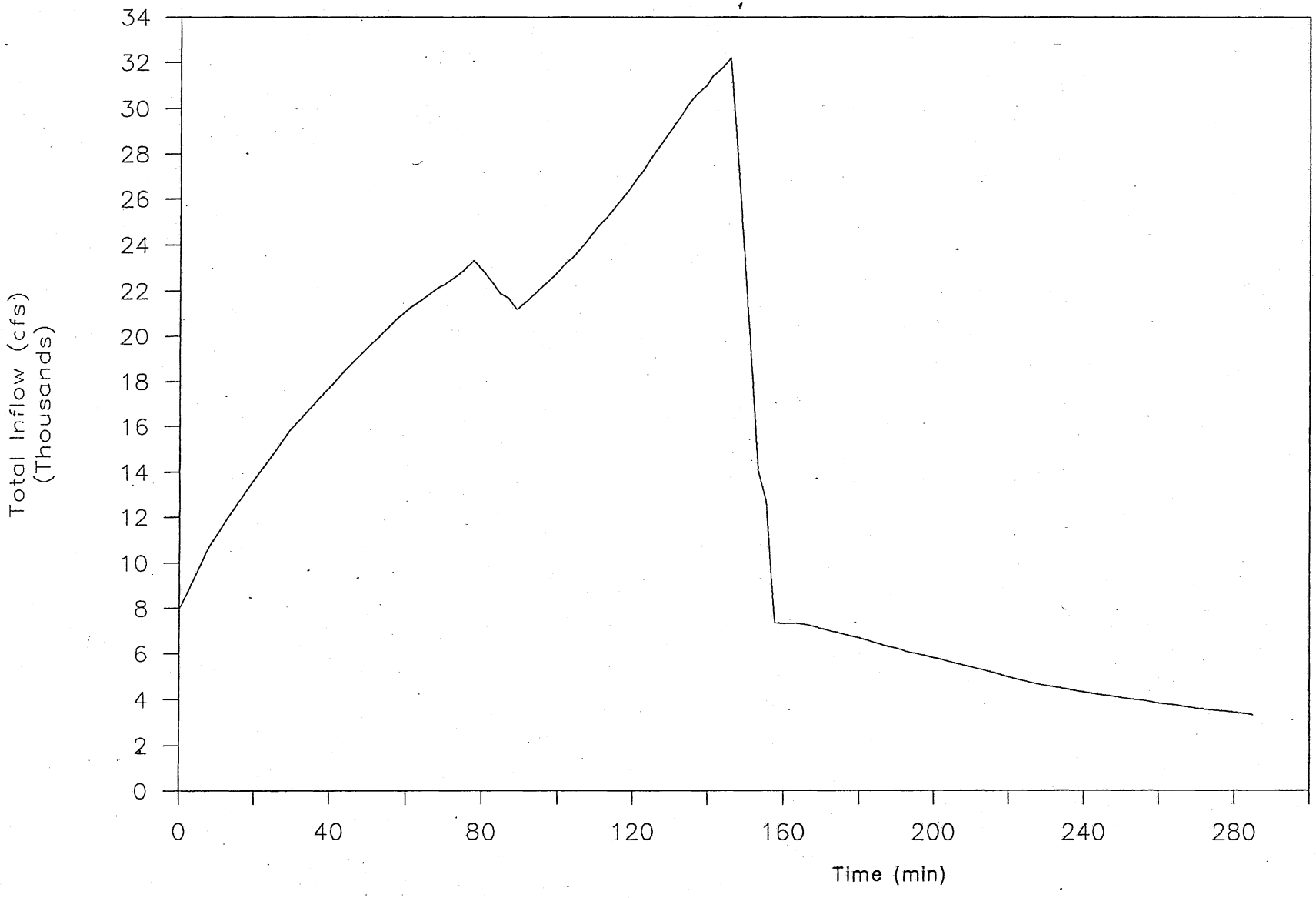

Fig.M-25 Total inflow hydrograph of seven branch system, with reservoir (Storm Oct.18,1985 - inflow control)

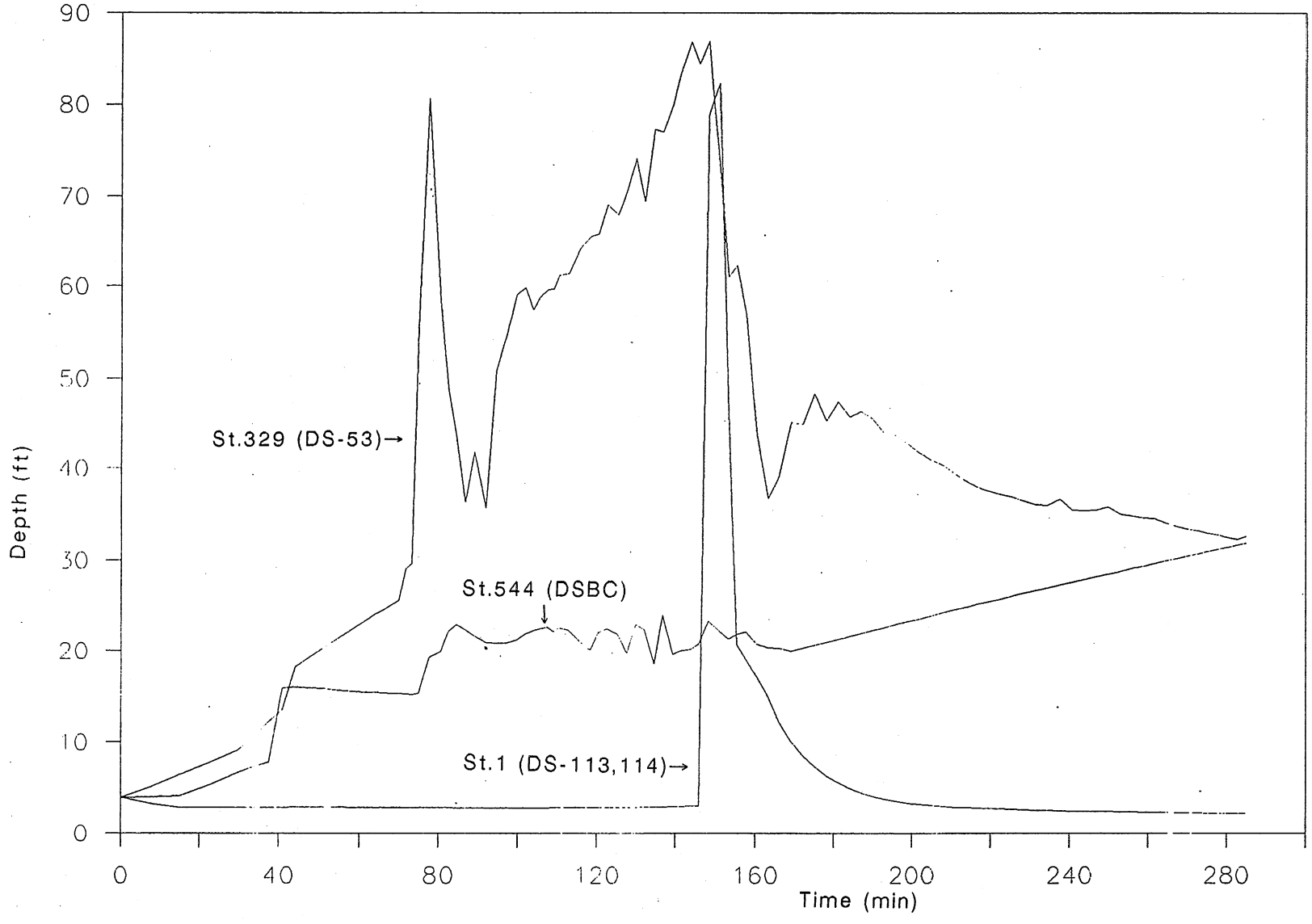

Fig.M-26 Time variation of water depth at three key stations (seven branch system with reservoir, storm Oct.18,1985 with inflow control)

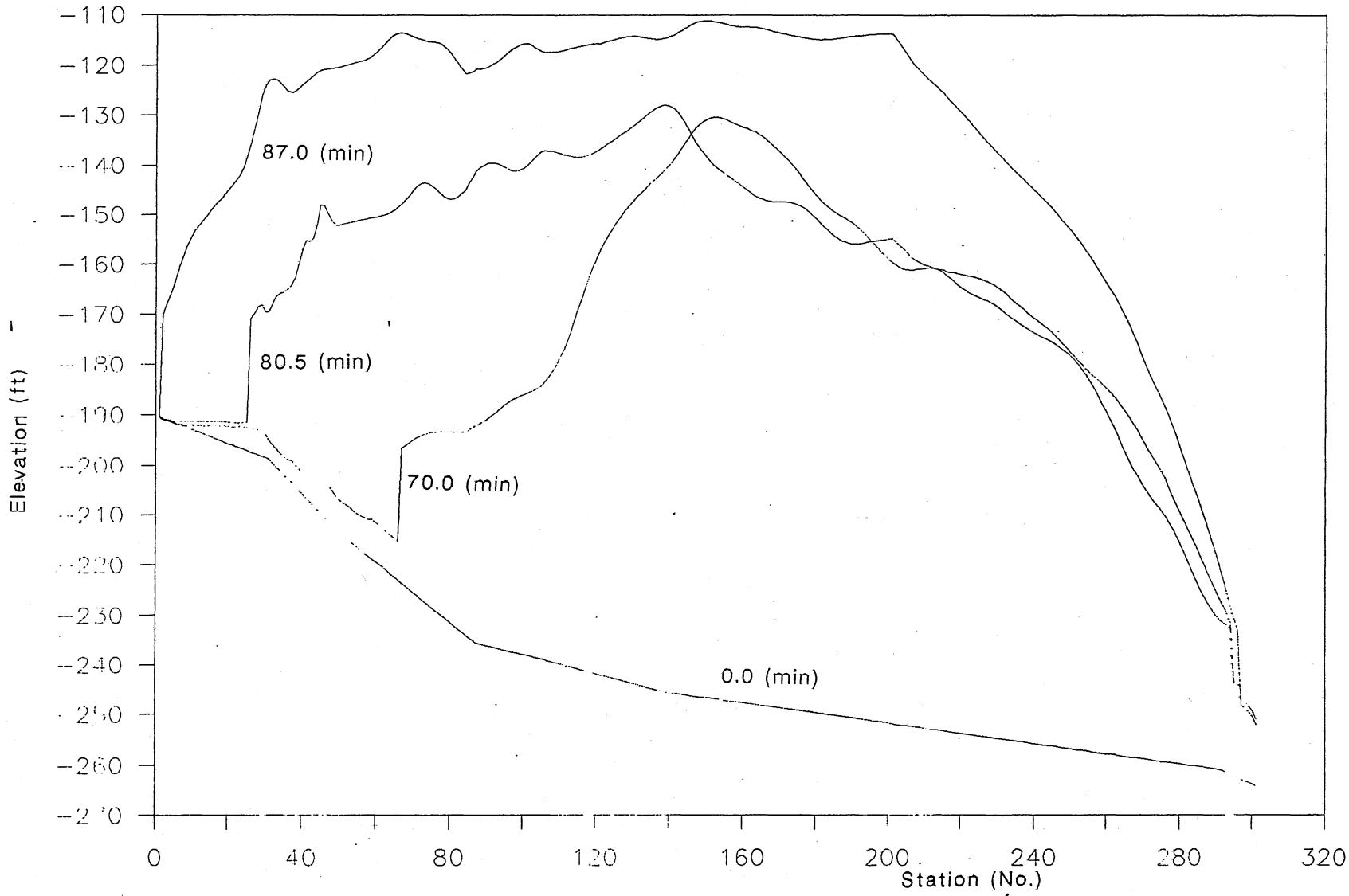

Fig.M-27, Instantaneous hydraulic gradelines (seven branch system
28 with reservoir, no inflow control,-- design inflow)

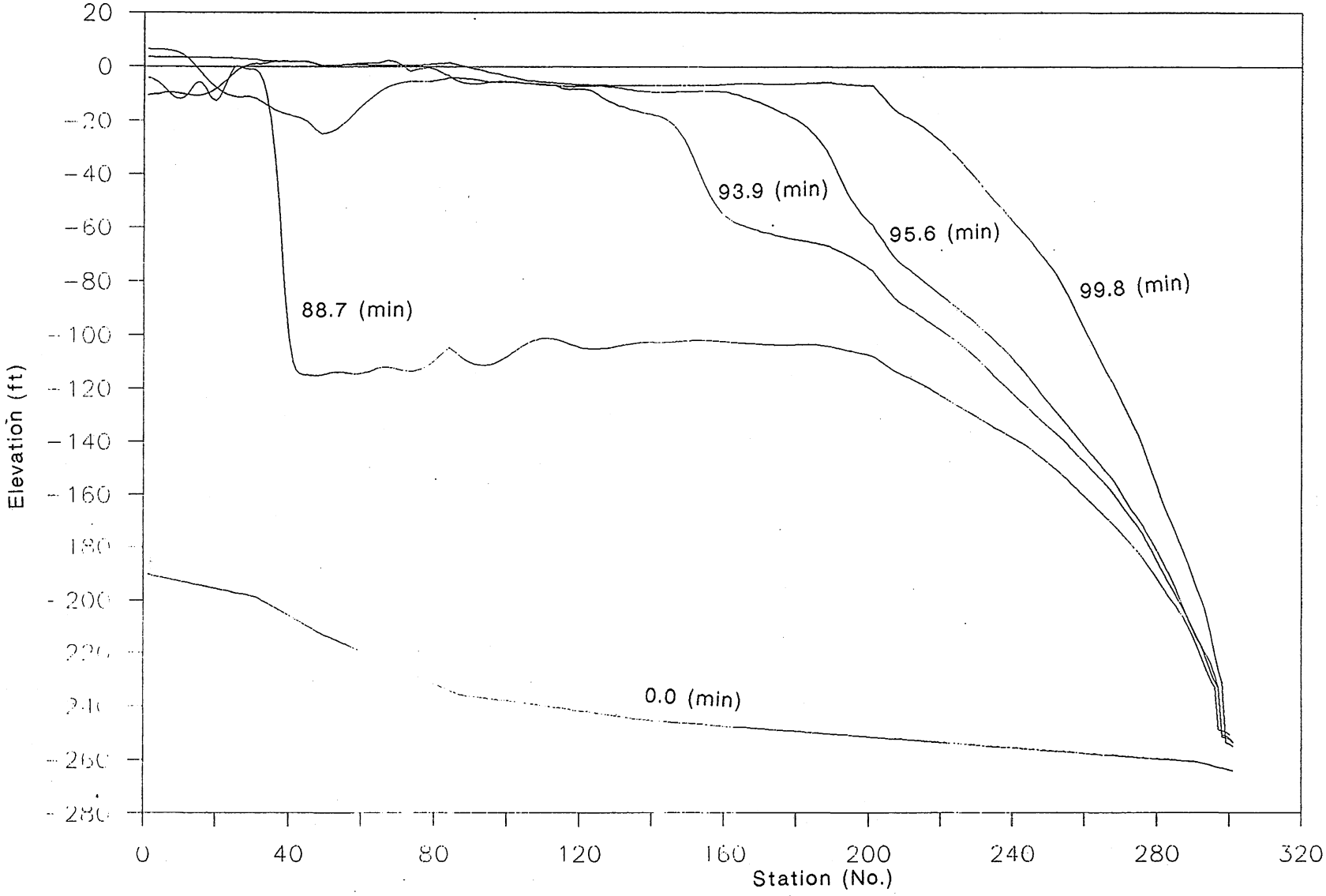

Fig.M-27, Instantaneous hydraulic gradelines (seven branch system
28 with reservoir, no inflow control,-- design inflow)

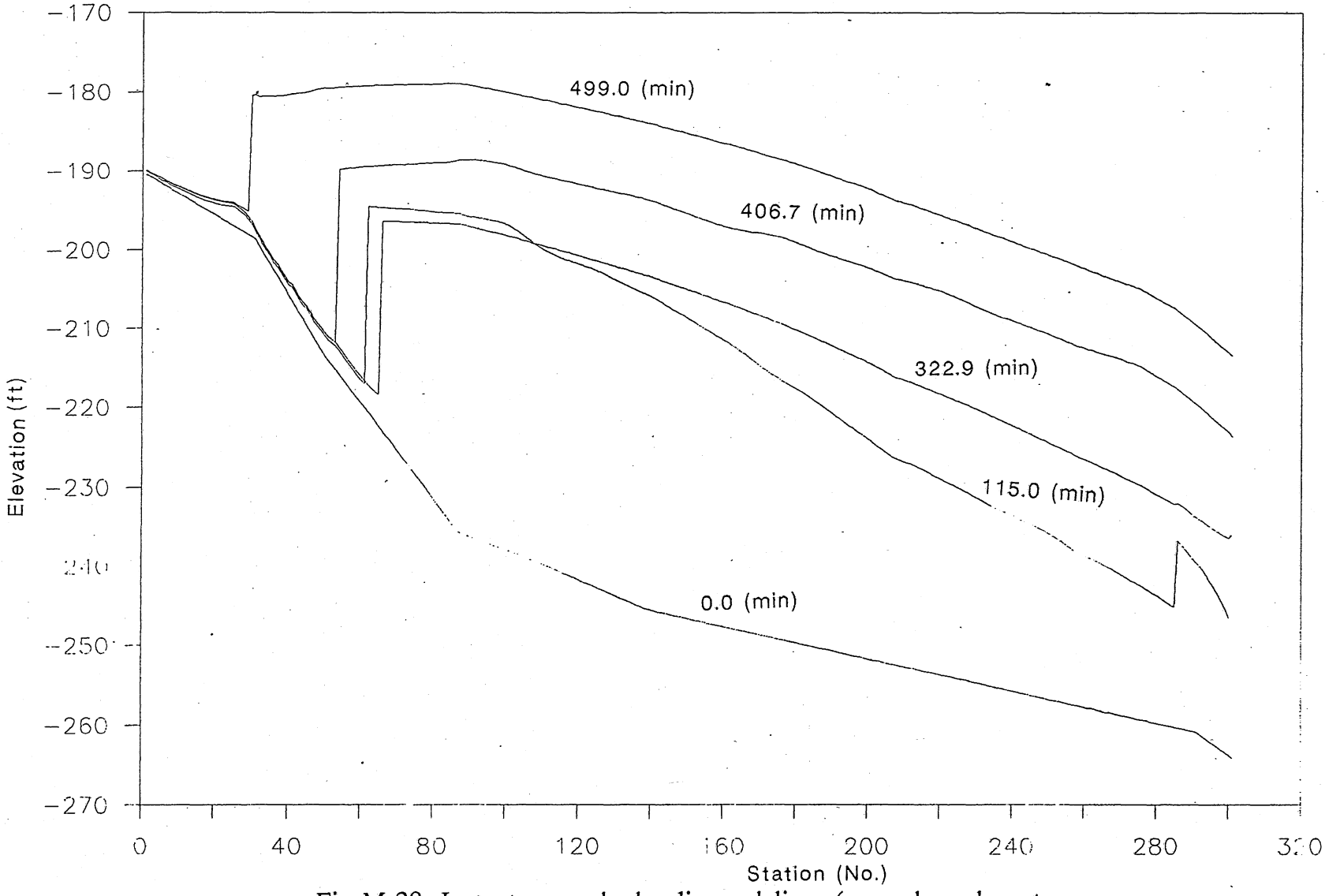

Fig.M-29 Instantaneous hydraulic gradelines (seven branch system with reservoir, inflow control,-- design inflow)

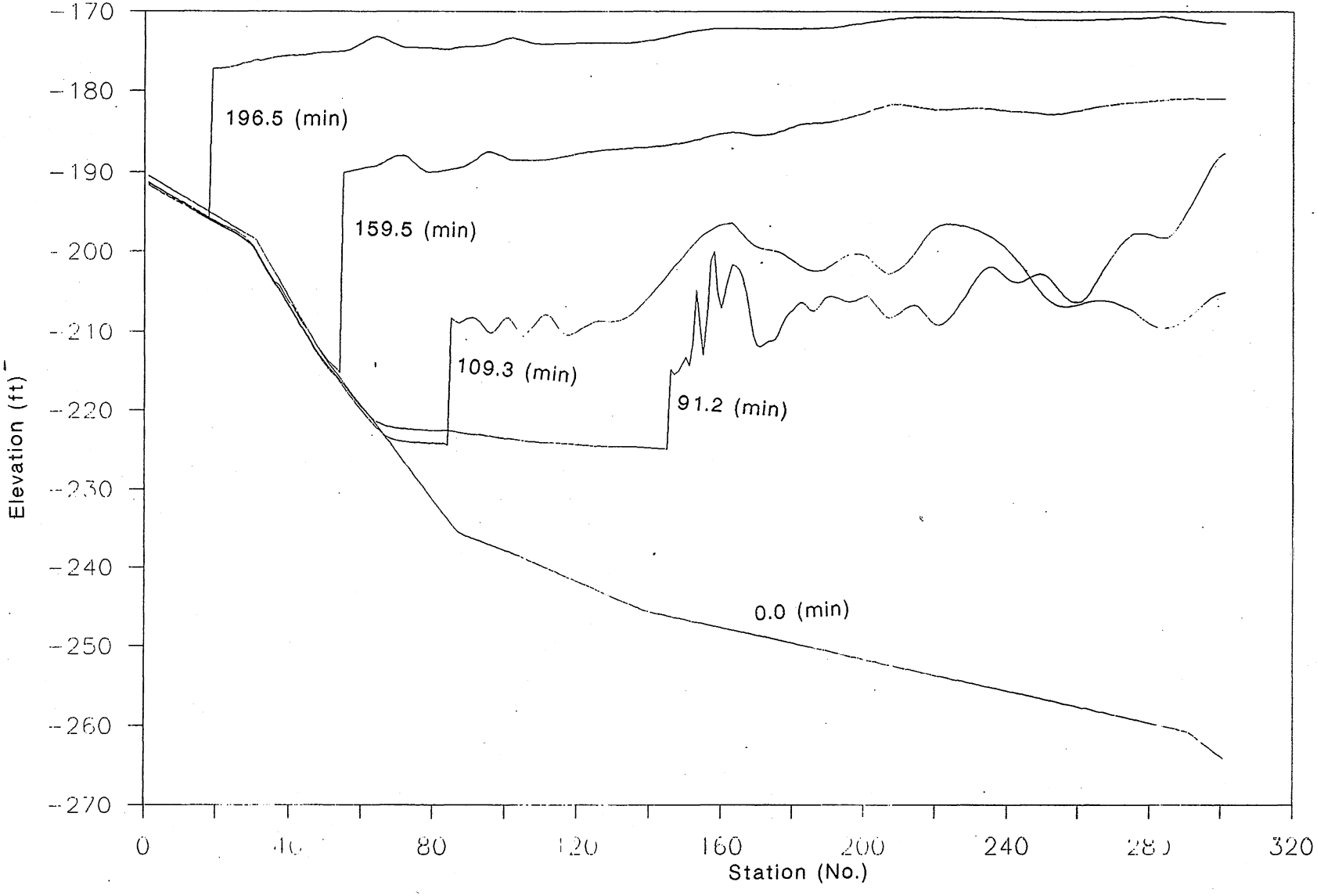

Fig.M-30, 31 Instantaneous hydraulic gradelines (seven branch system without reservoir, inflow control,-- Storm Oct.18,1985)

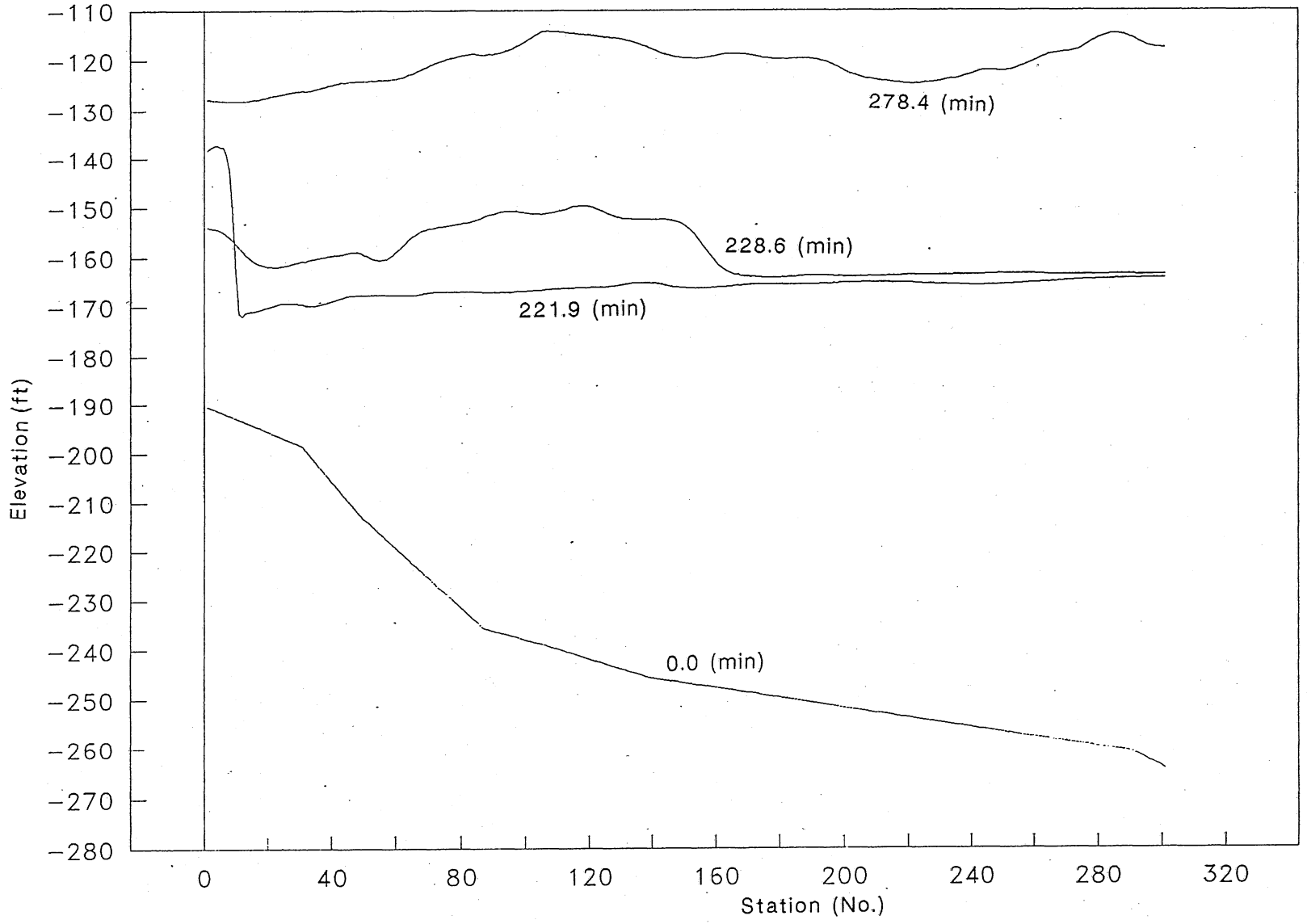

Fig.M-30, Instantaneous hydraulic gradelines (seven branch system
31 without reservoir, inflow control,-- Storm Oct.18,1985)

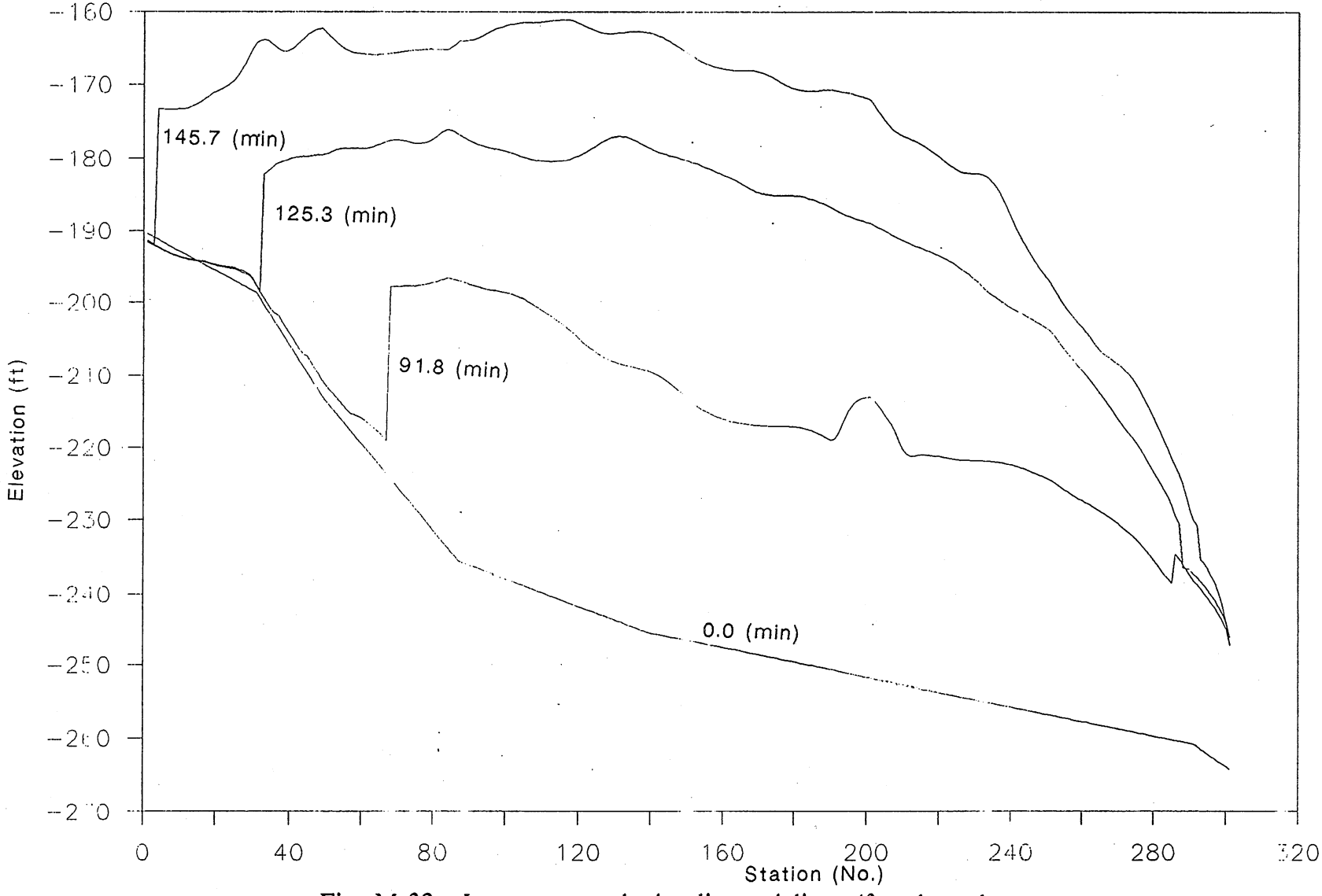

Fig. M-32, Instantaneous hydraulic gradelines (four branch system
33 with reservoir, inflow control,--storm Oct.18,1985)

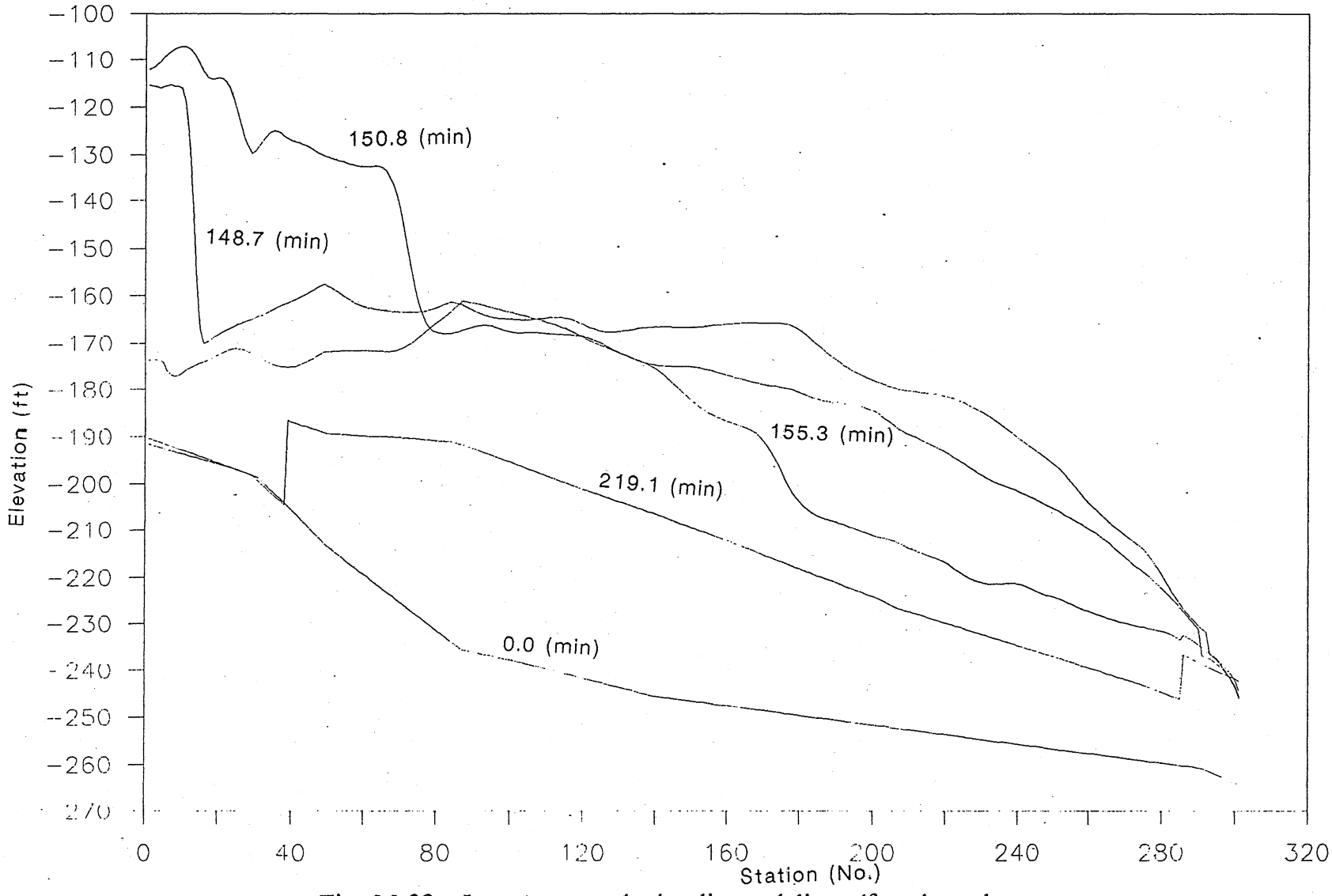

Fig. M-32, Instantaneous hydraulic gradelines (four branch system
33 with reservoir, inflow control,--storm Oct.18,1985)

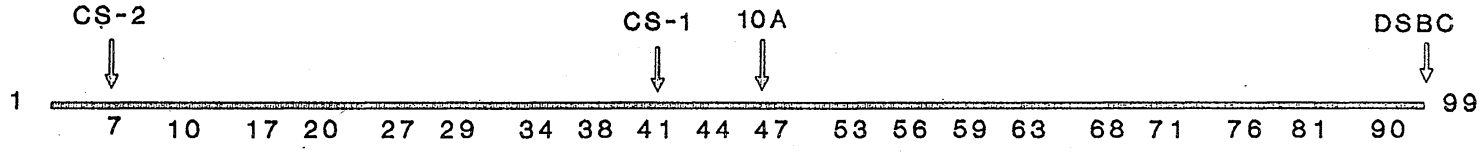

Fig.M-34 North Branch model system configuration

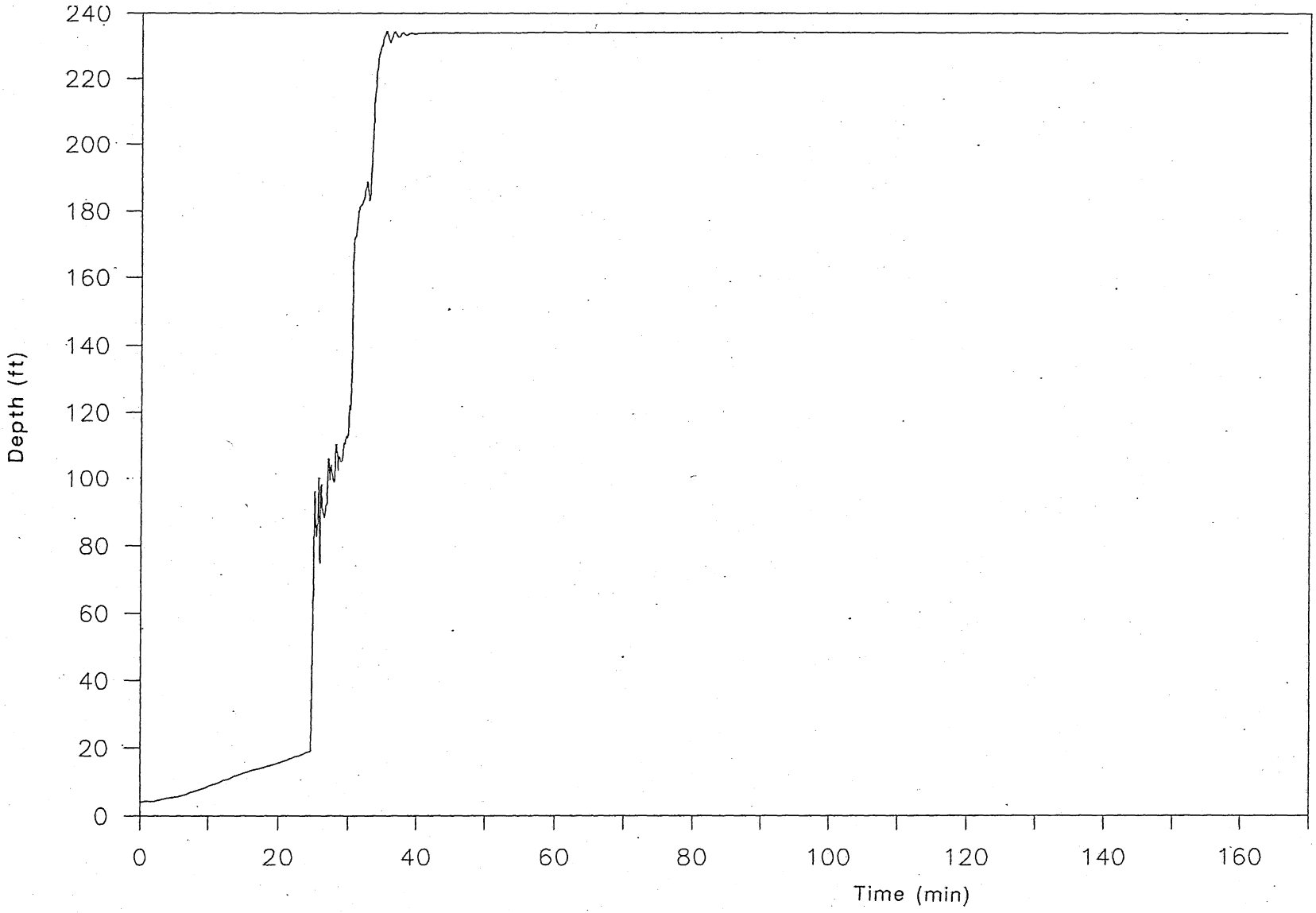

Fig.M-35 Time variation of water surface elevation at downstream end for sever surge problem in main tunnel

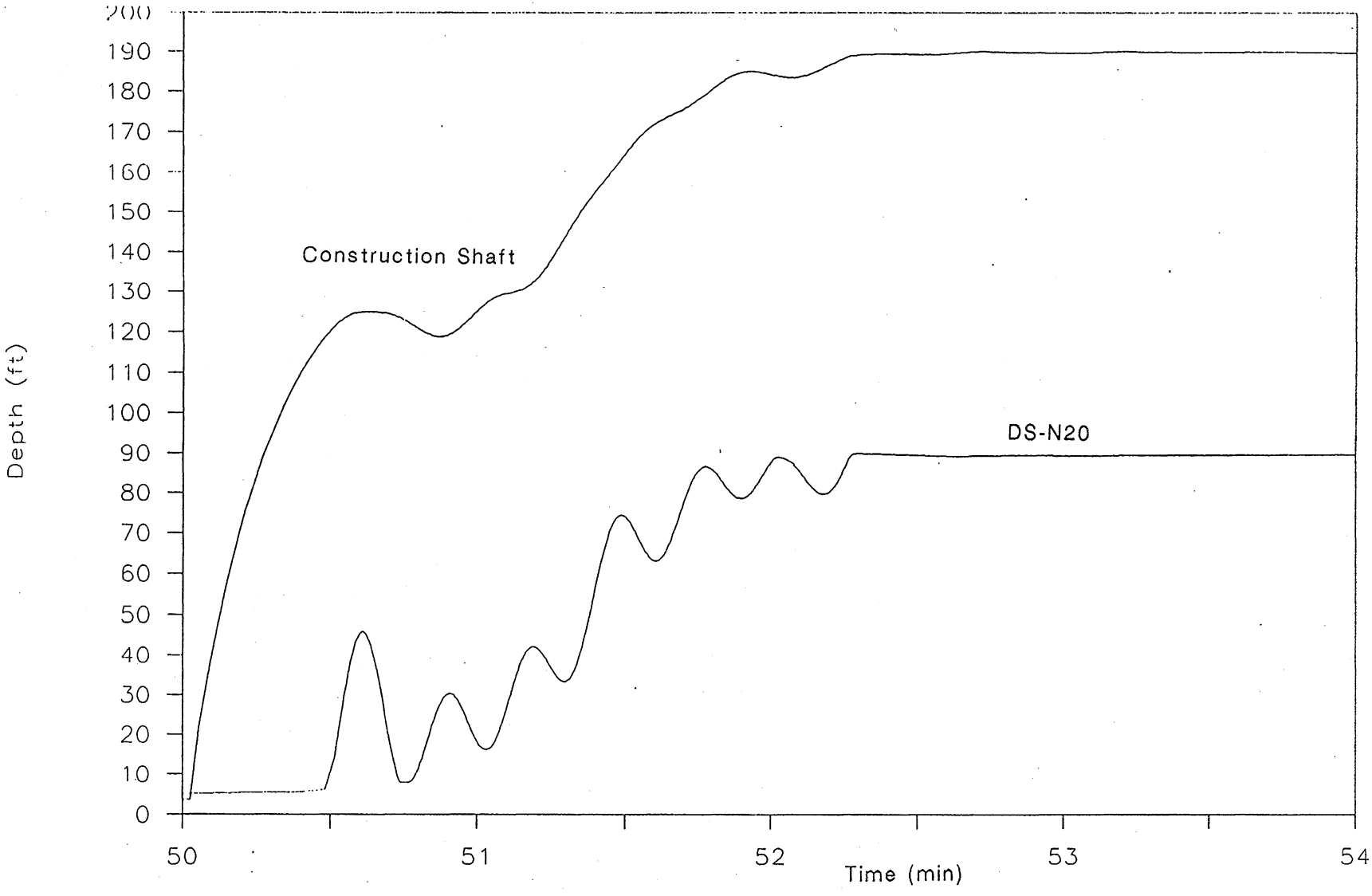

Fig.M-36 Time variation of water surface elevation at upstream and construction shaft for sever surge problem in main tunnel (Diameter of drift tube: 8 ft. Diameter of DS-N20: 9 ft height of the drift tube above the invert of tunnel:100ft)

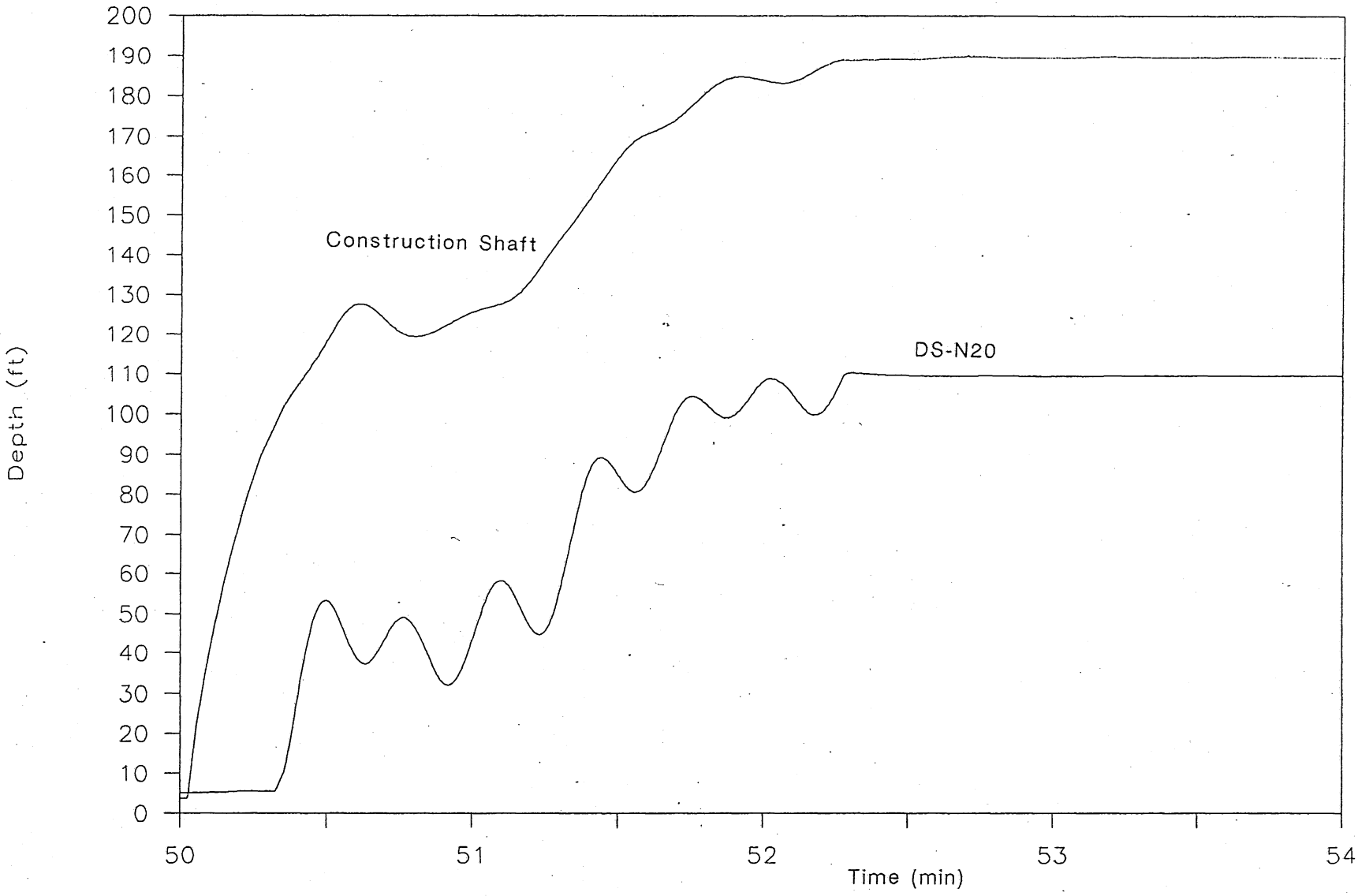

Fig.M-37 Time variation of water surface elevation at upstream and construction shaft for sever surge problem in main tunnel (Diameter of drift tube: 8 ft. Diameter of DS-N20: 10 ft. height of the drift tube above the invert of tunnel:80ft)

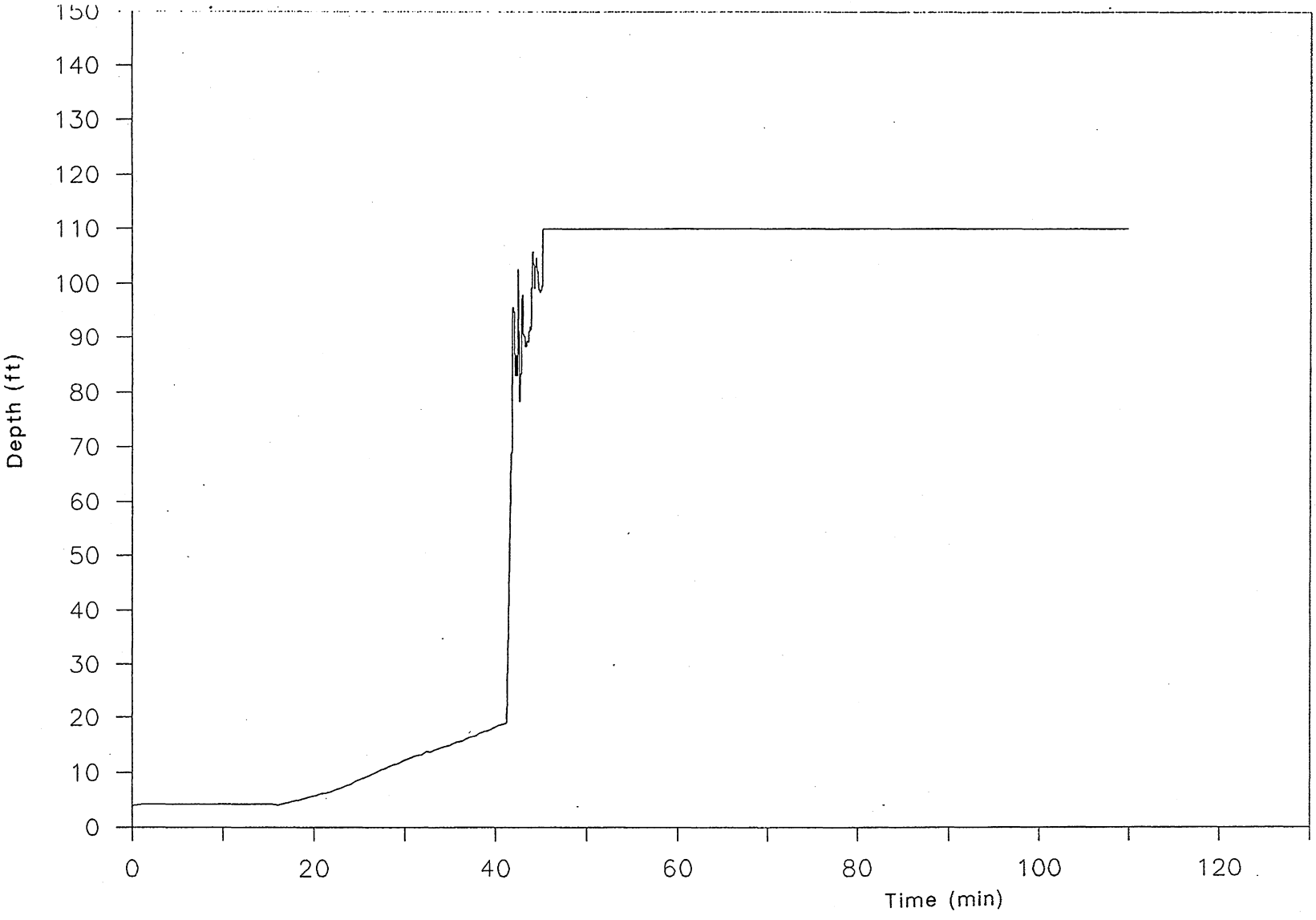

Fig.M-38 Time variation of water surface elevation at downstream end for modest surge condition in main tunnel

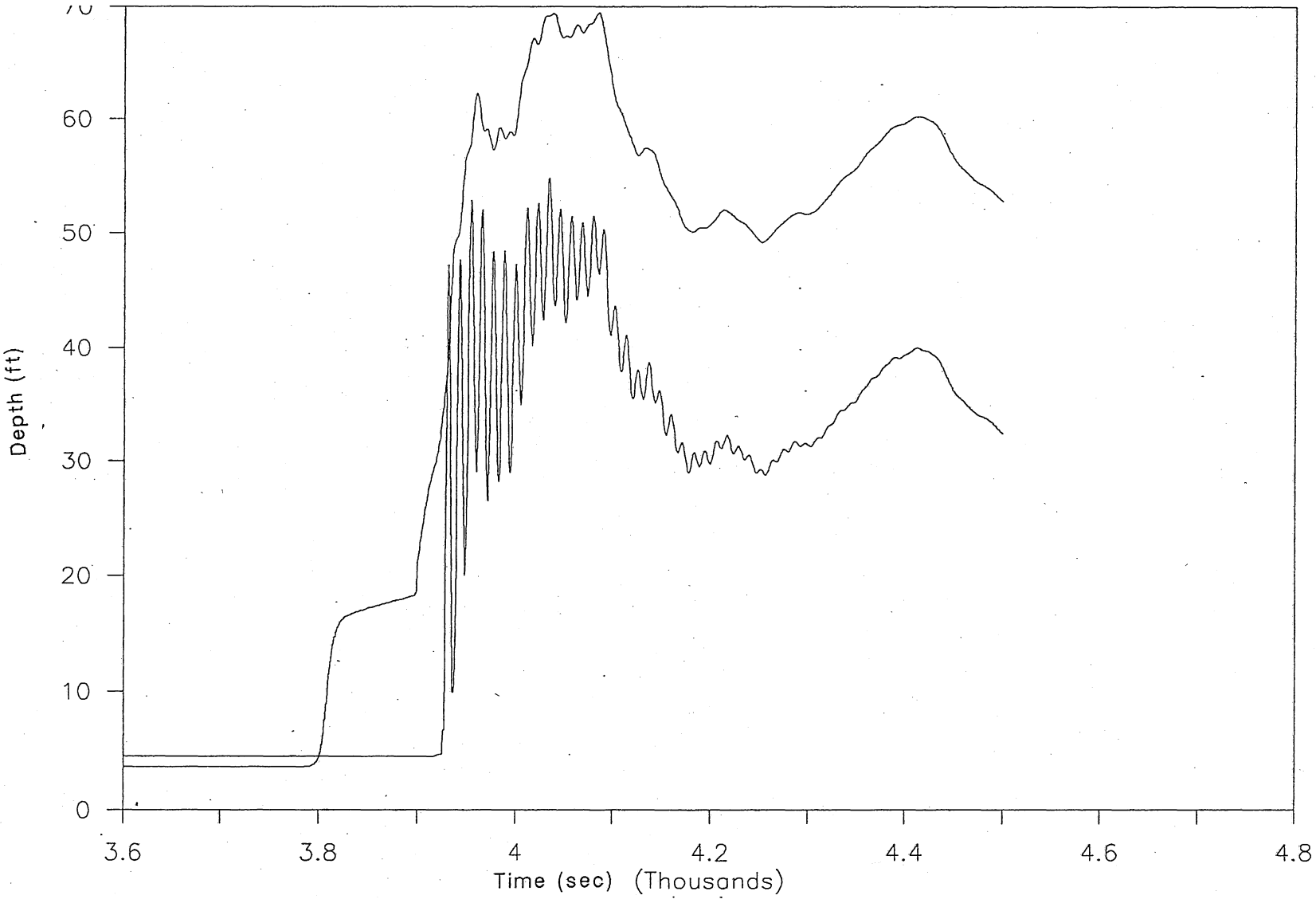

Fig.M-39 Time variation of water surface elevation at upstream and construction shaft for modest surge problem in main tunnel (Diameter of drift tube: 10 ft. Diameter of DS-N20: 7'-2" height of the drift tube above the invert of tunnel: 20ft)

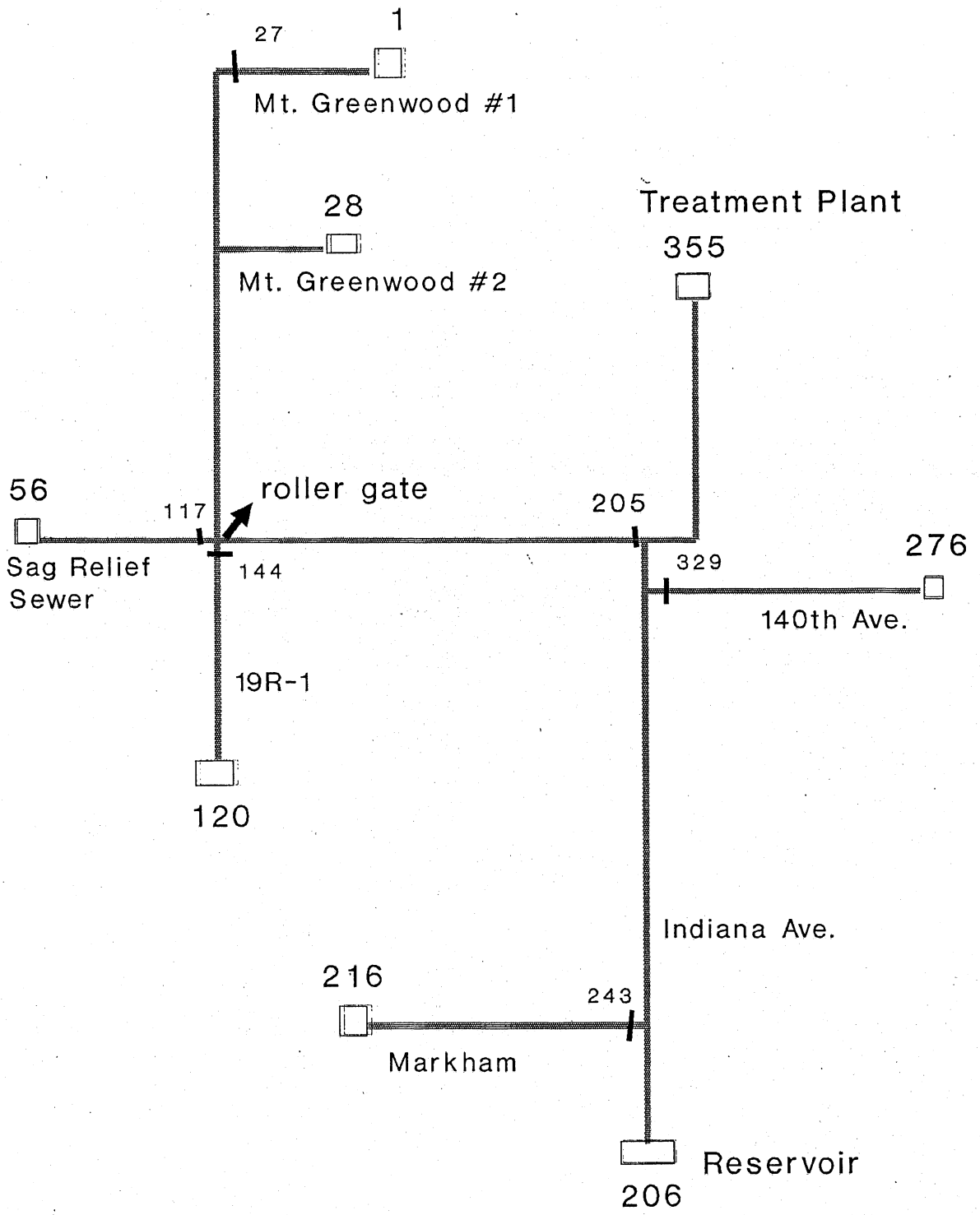

Fig. C-1, Calumet Tunnel System's Configulation for modeling purpose

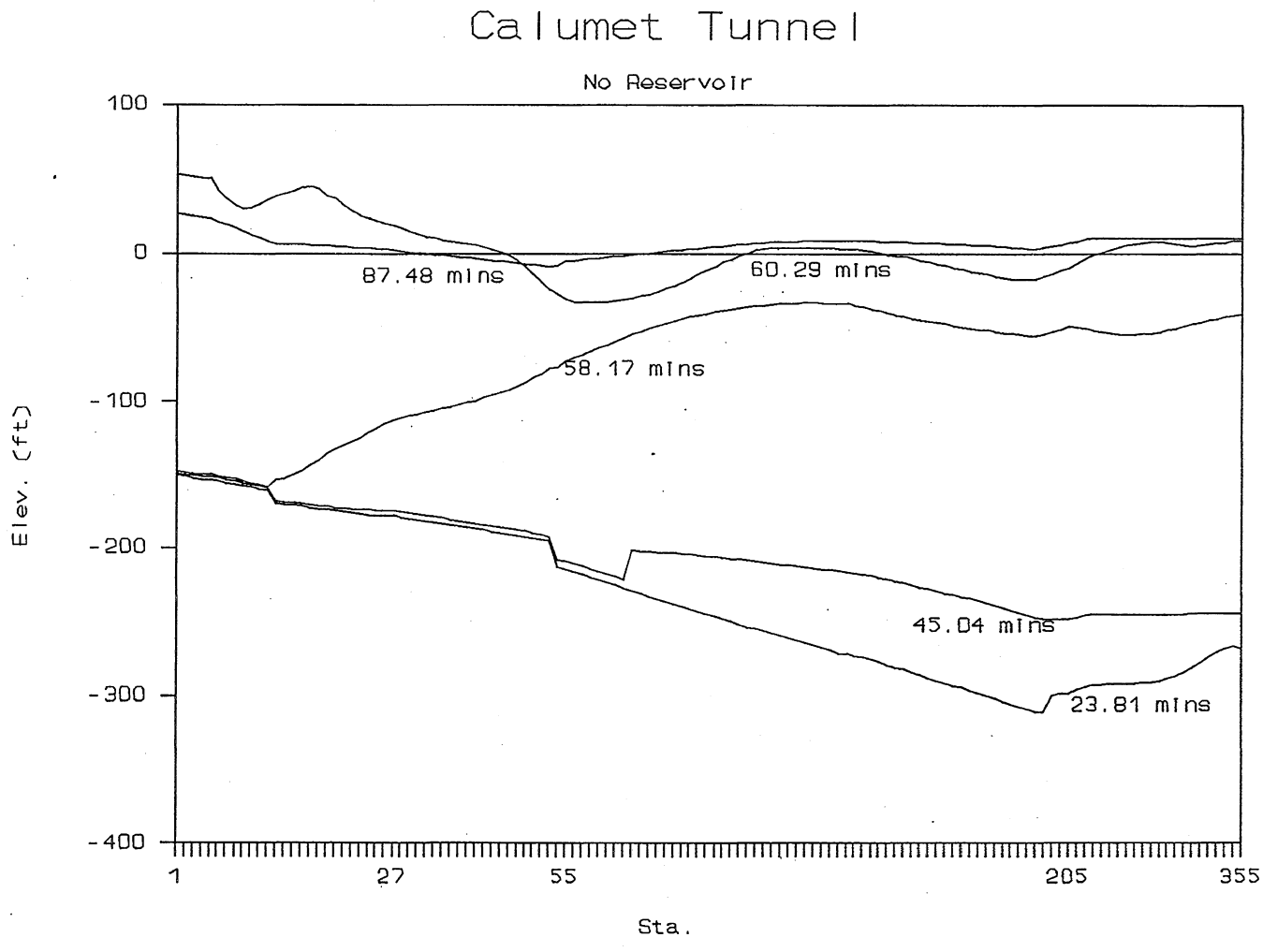

Fig. C-2, Hydraulic gradelines during the filling period in main tunnel of system C-I.

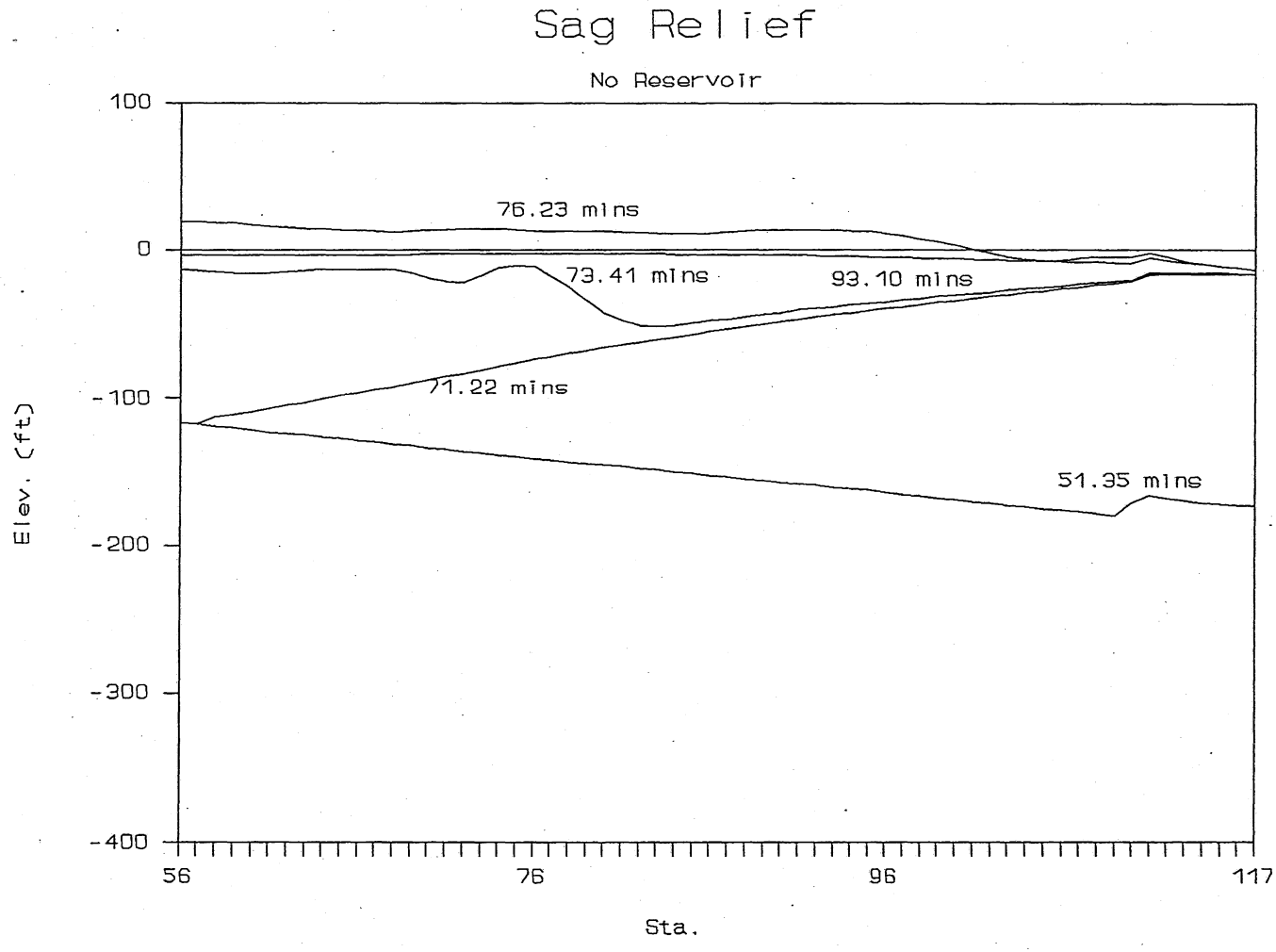

Fig. C-3, Hydraulic gradelines during the filling period in Sag Relief tunnel of System C-I.

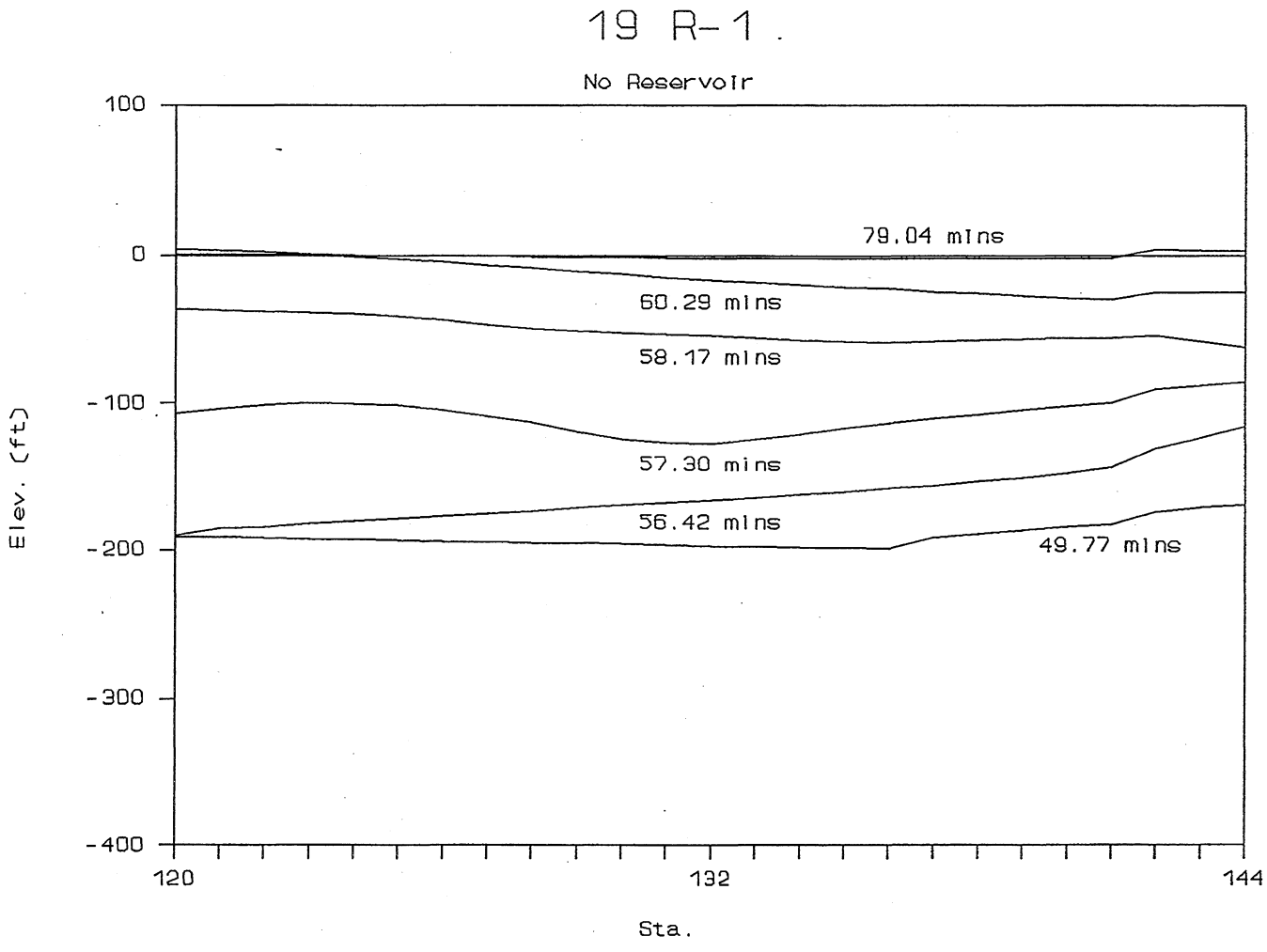

Fig. C-4, Hydraulic gradelines during the filling period in 19R-1 tunnel of System C-I.

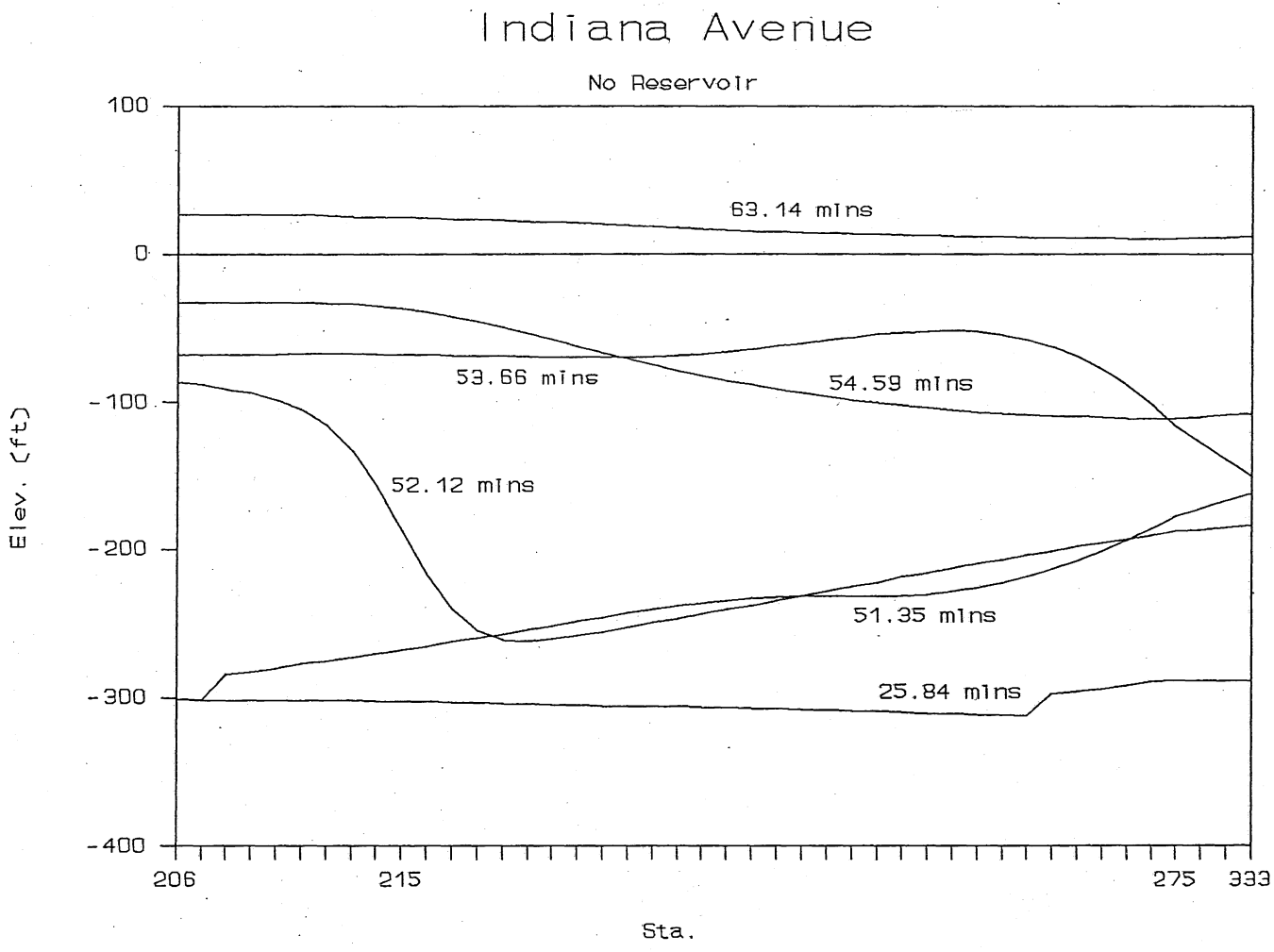

Fig. C-5, Hydraulic gradelines during the filling period in Indiana Avenue tunnel of System C-I.

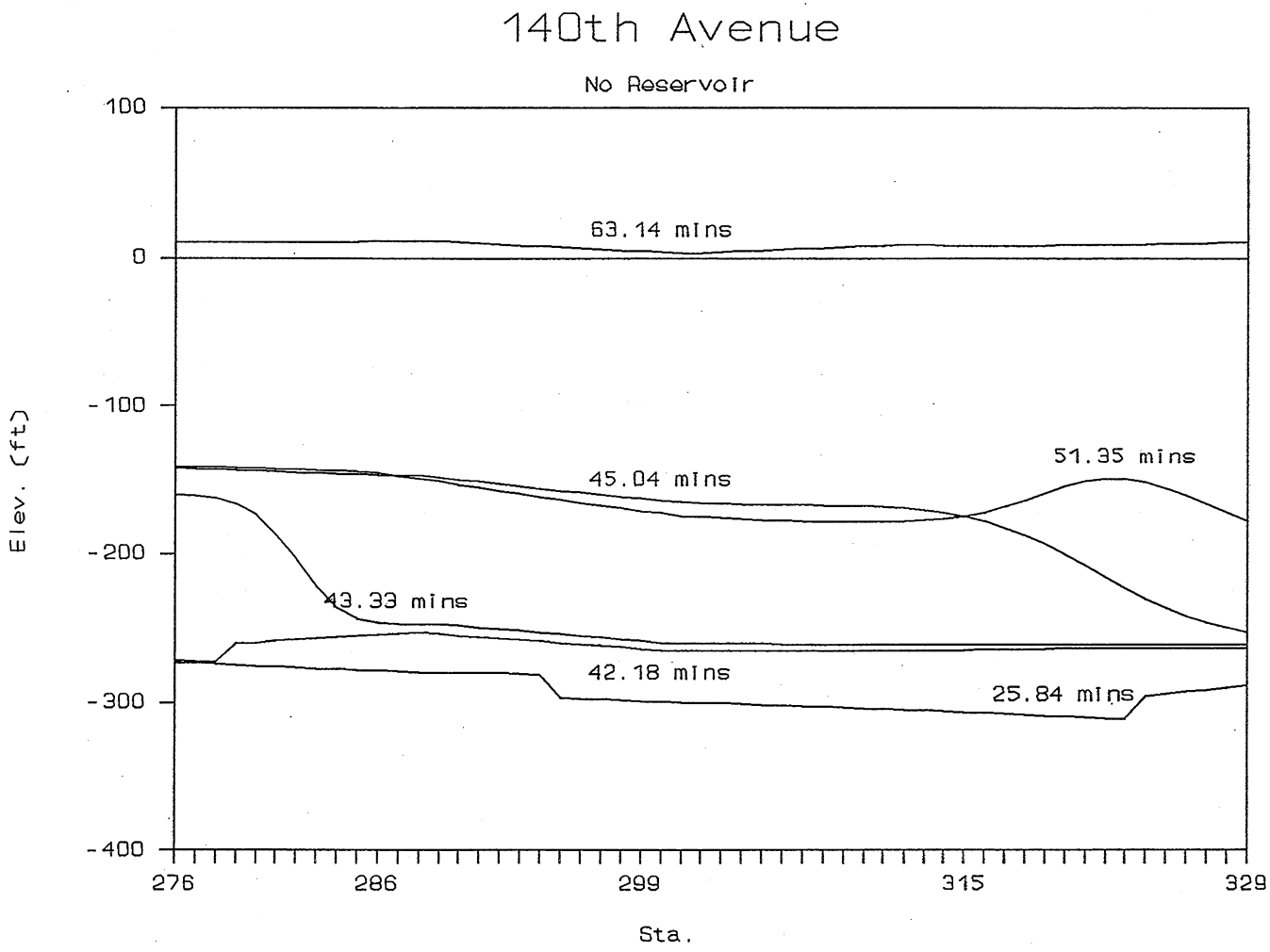

Fig. C-6, Hydraulic gradelines during the filling period in 140th Avenue tunnel of System C-I.

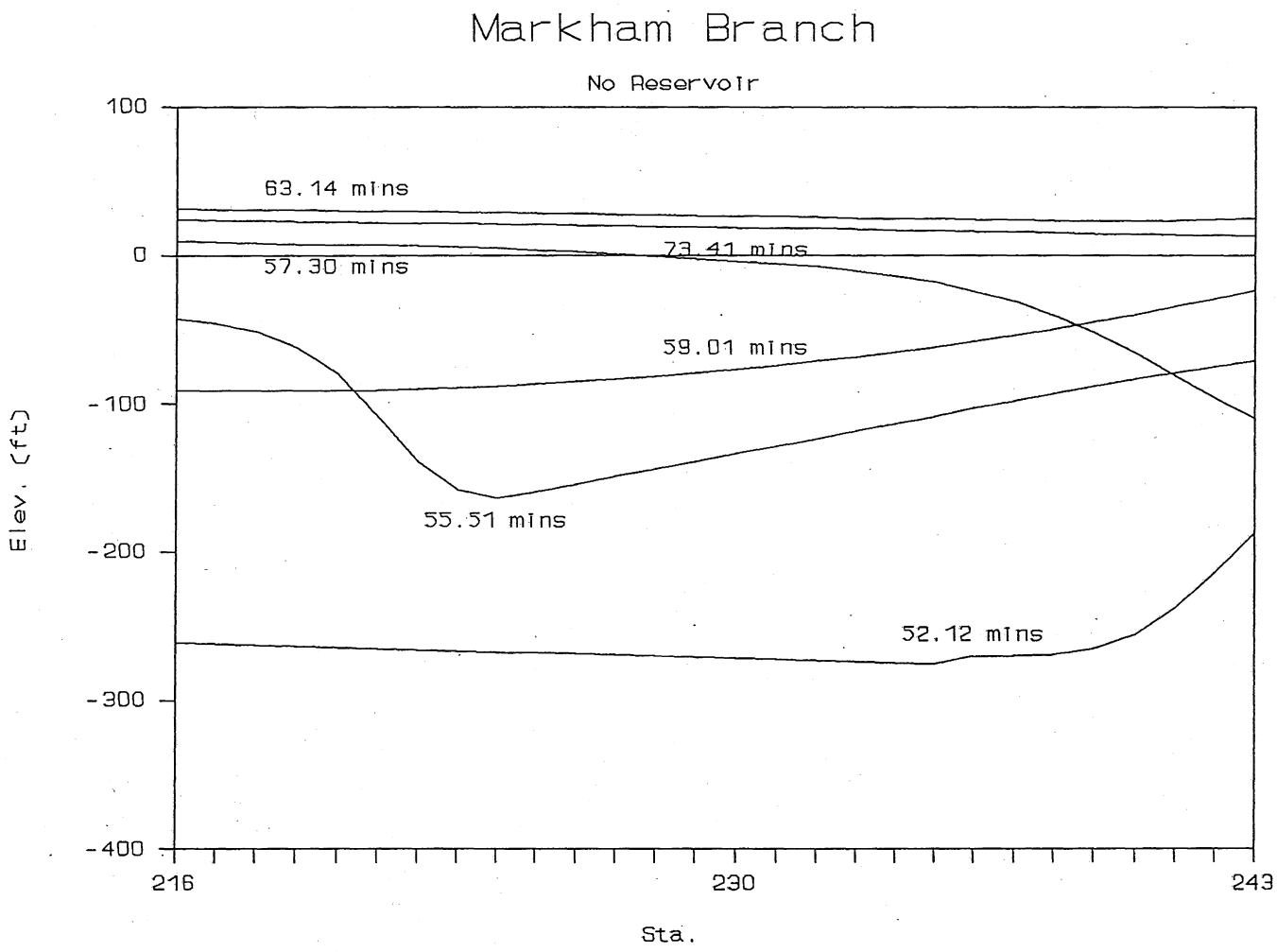

Fig. C-7, Hydraulic gradelines during the filling period in Markham tunnel of System C-I.

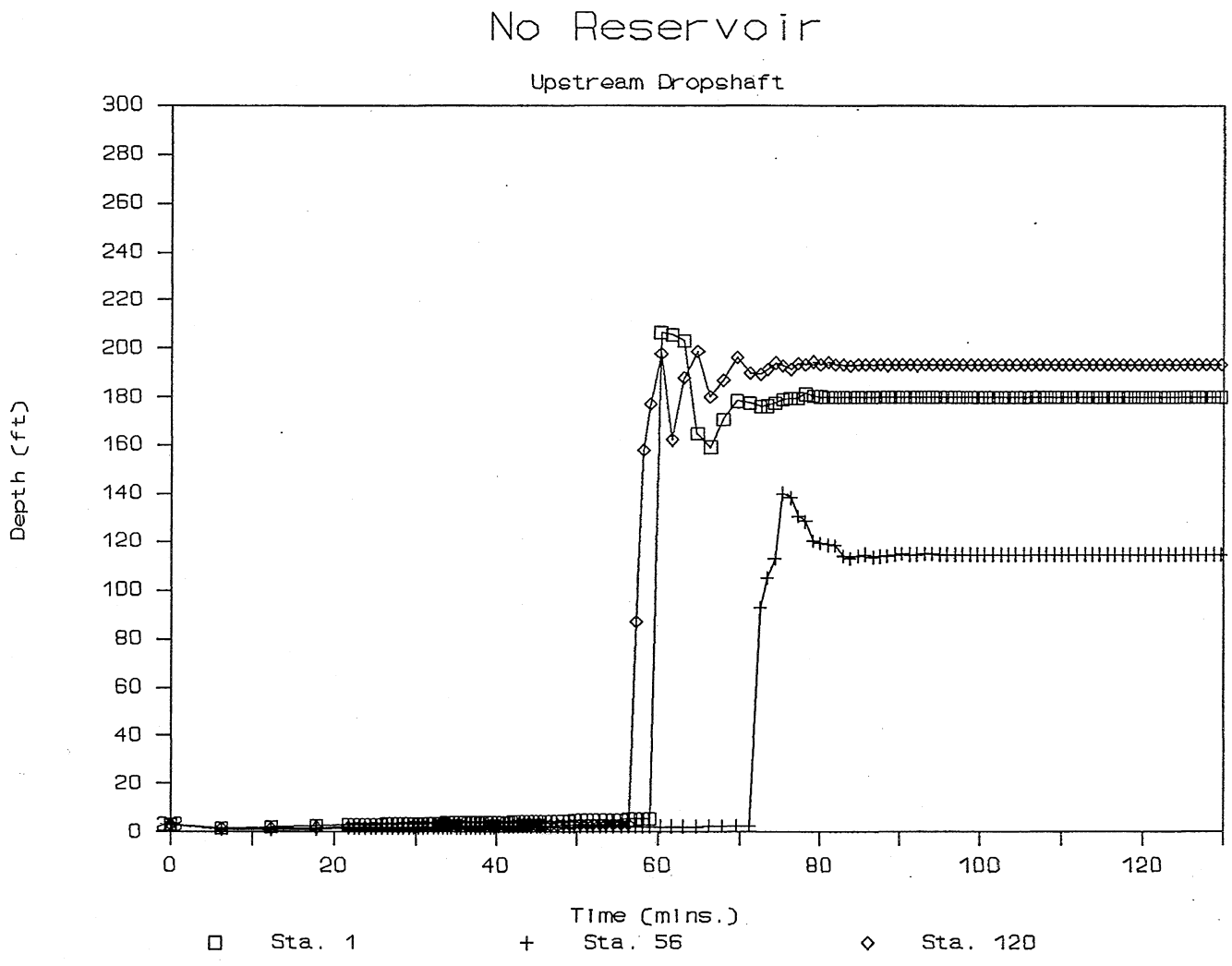

Fig. C-8, Time variation of water depth at 3 upstream ends, System C-I (Sta. 1, 56, 120).

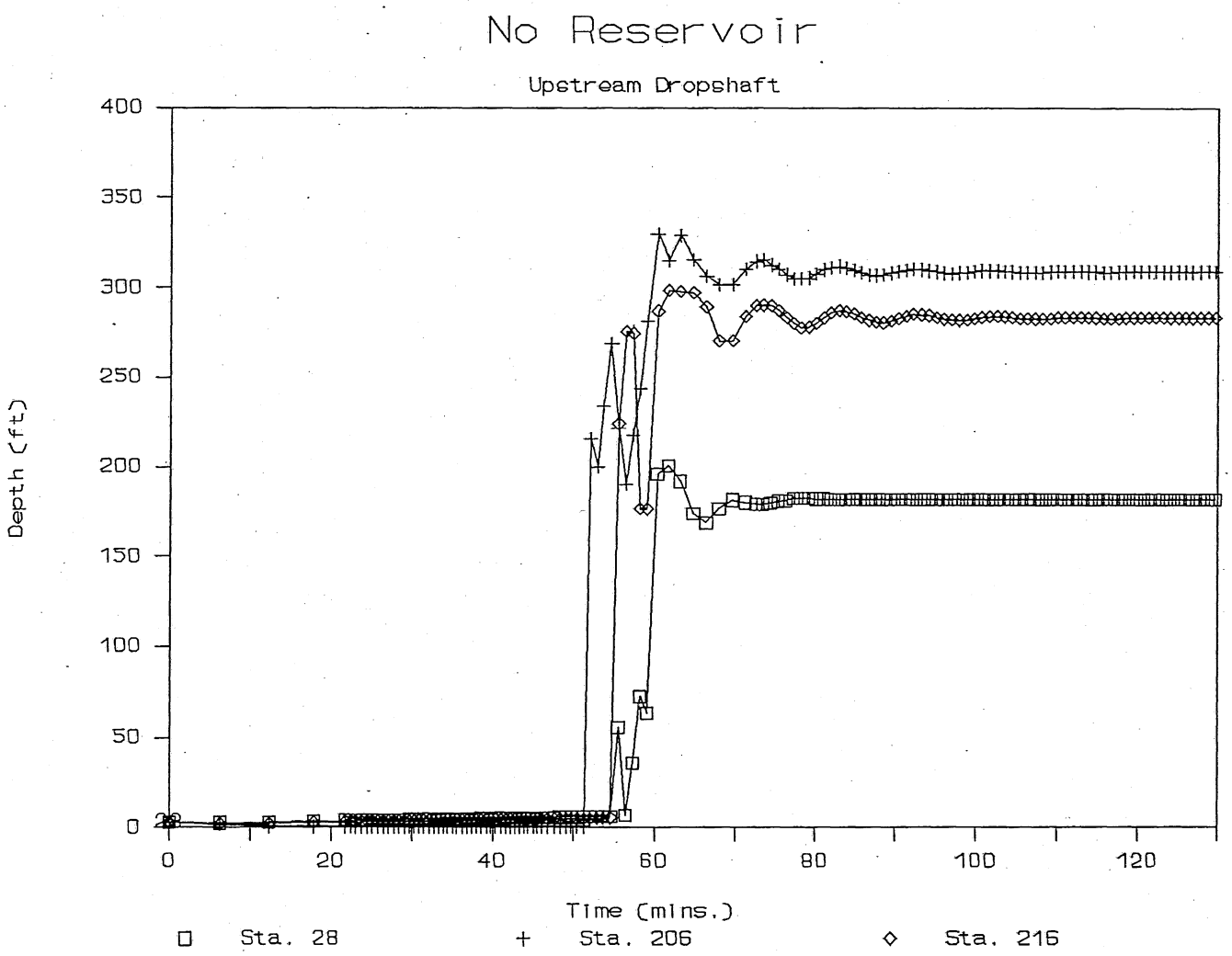

Fig. C-9, Time variation of water depth at 3 upstream ends, System C-I (Sta. 28, 206, 216).

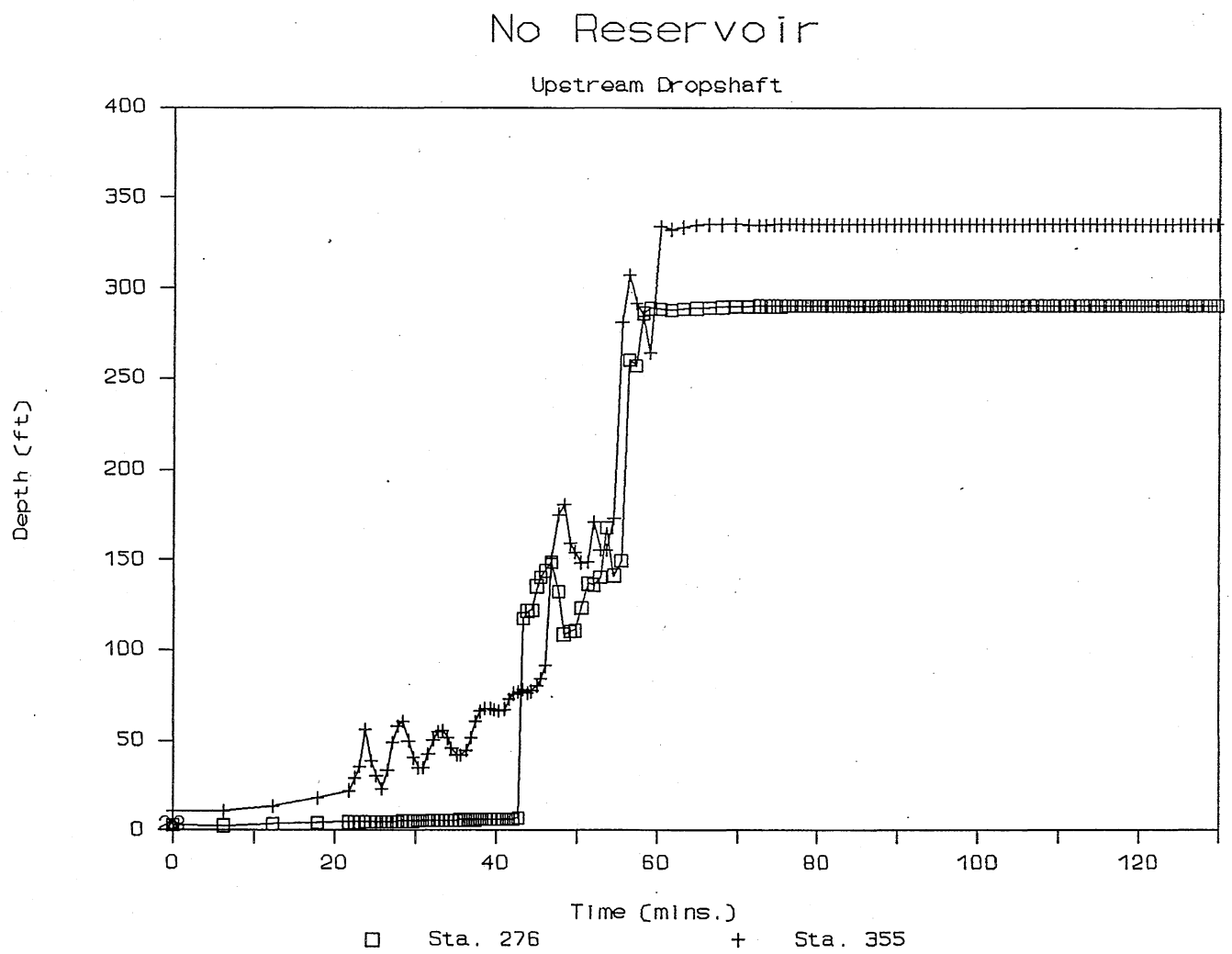

Fig. C-10, Time variation of water depth at 2 upstream ends, System C-I (Sta. 276, 355).

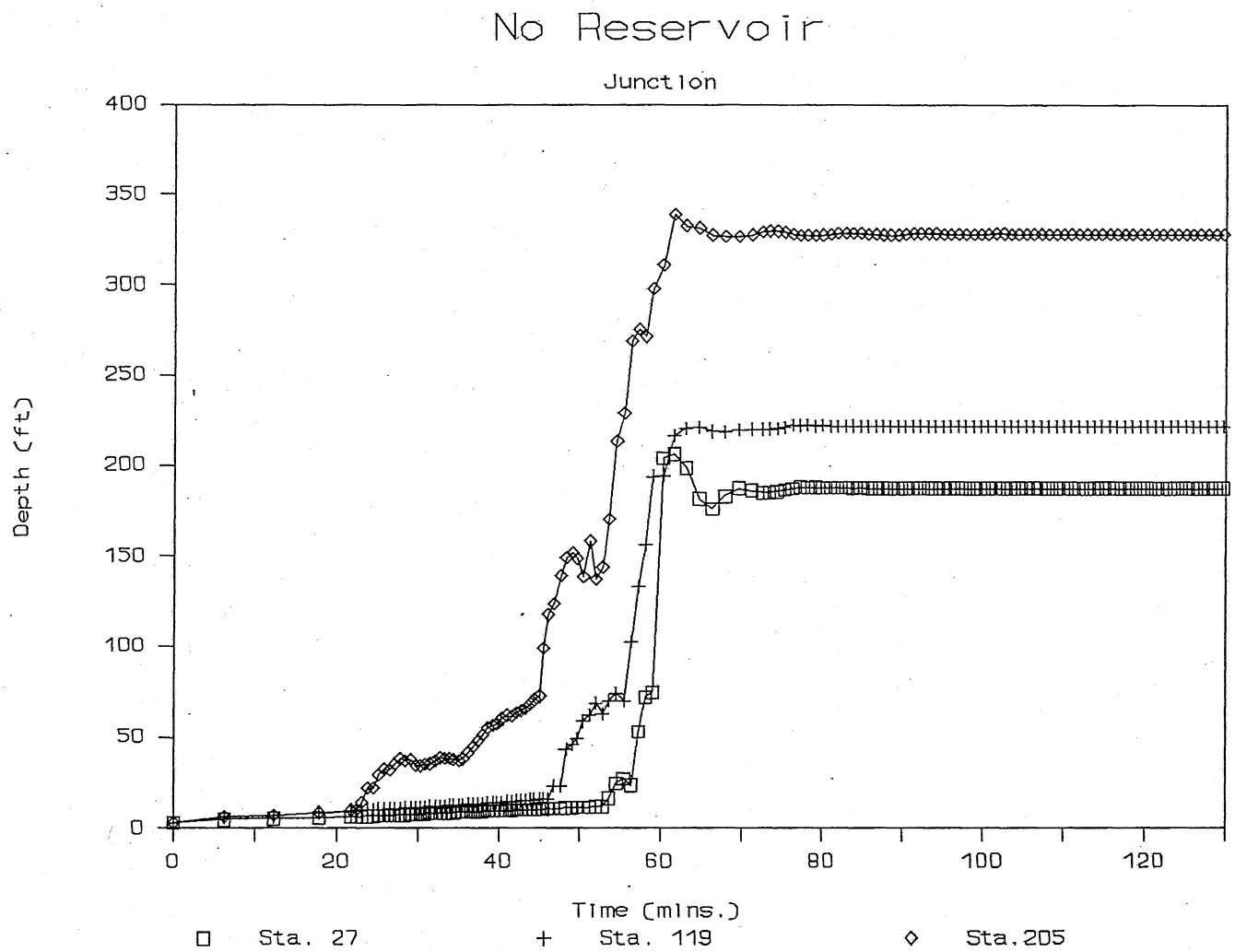

Fig. C-11, Time variation of water depth at 3 junction points, System C-I (Sta. 27, 119, 205).

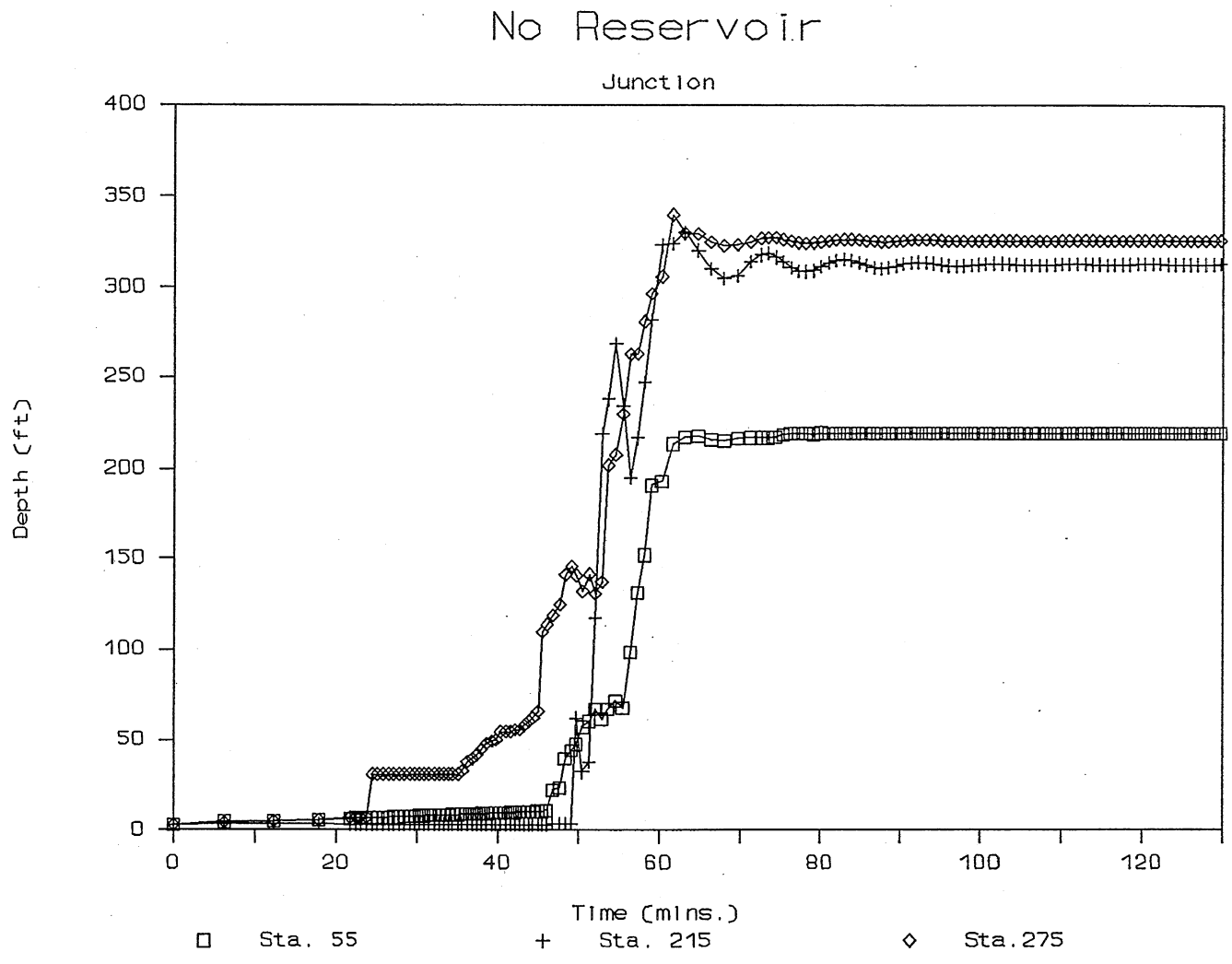

Fig. C-12, Time variation of water depth at 3 junction points, System C-I(Sta. 55, 215, 275).

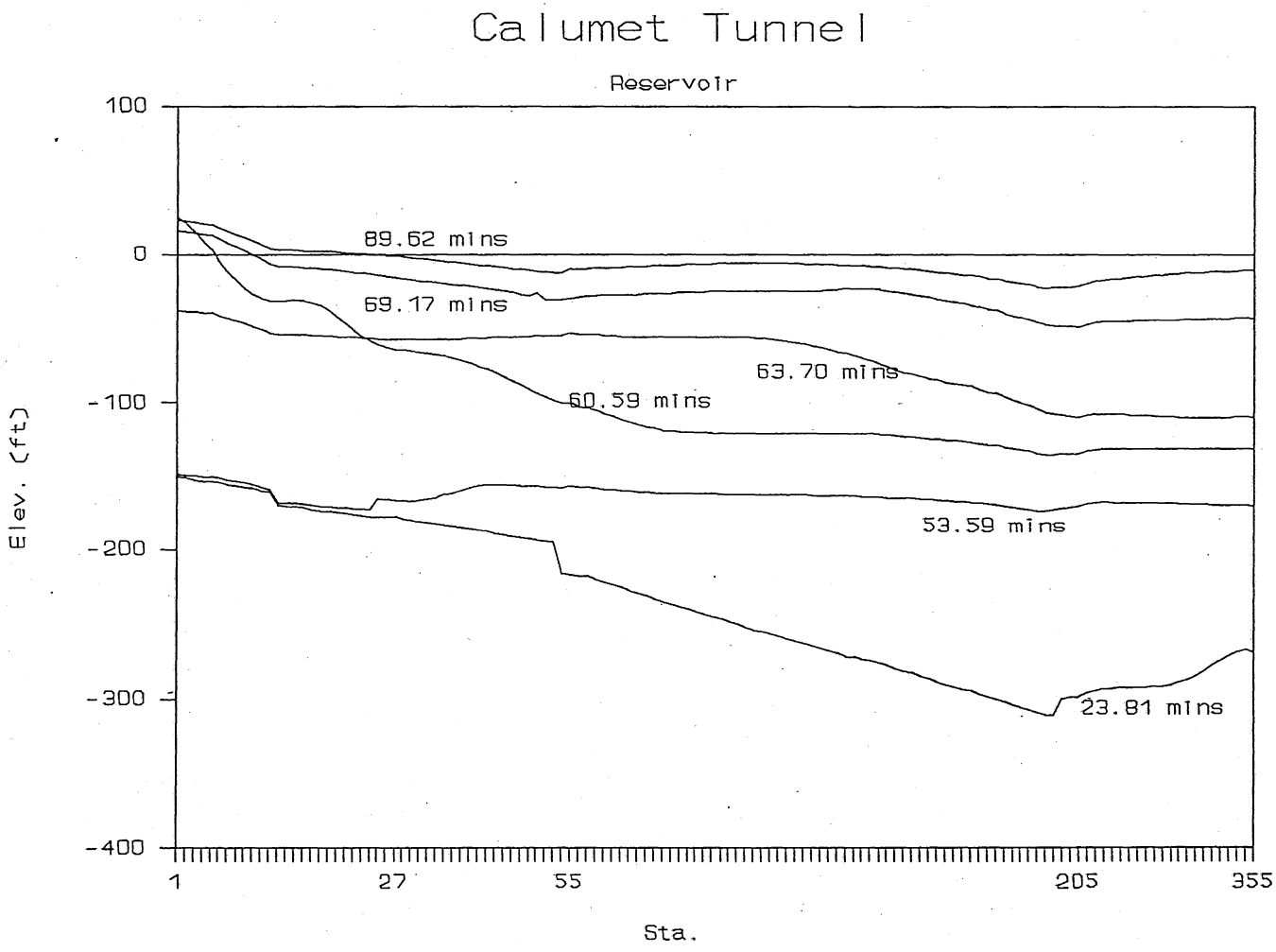

Fig. C-13, Instantaneous Hydraulic gradelines in main tunnel - System C-II.

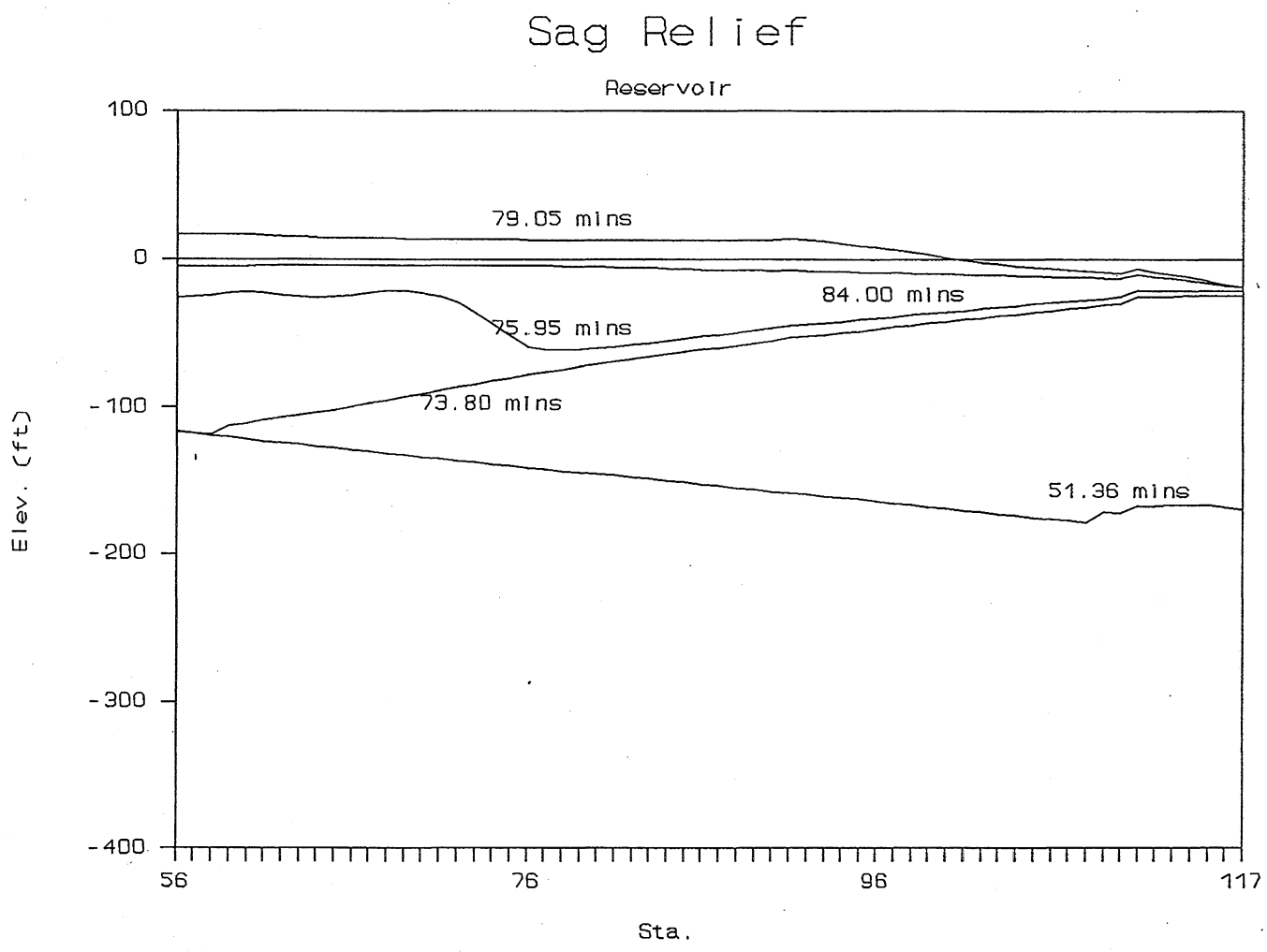

Fig. C-14, Instantaneous Hydraulic gradelines in Sag Relief tunnel - System C-II.

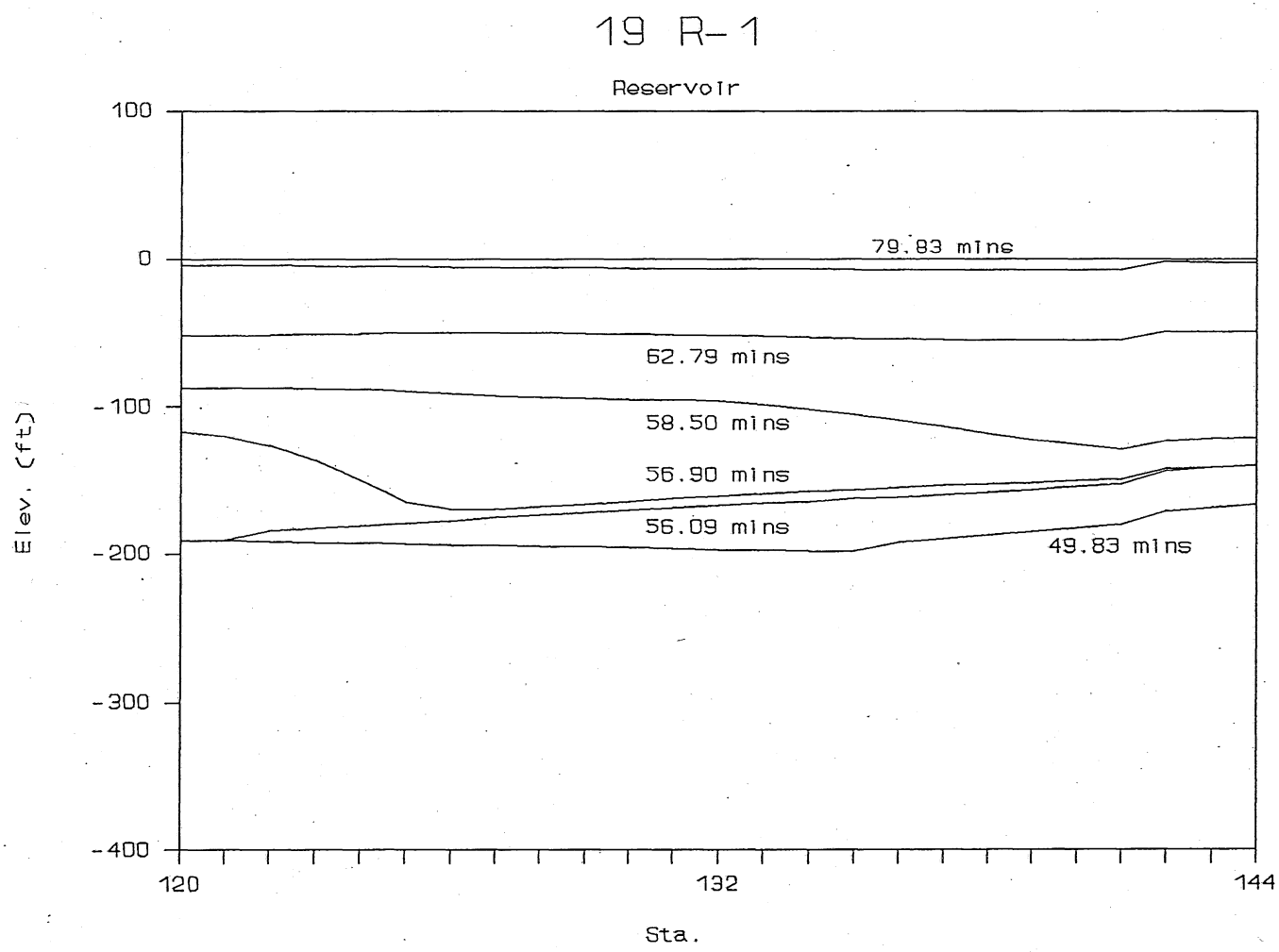

Fig. C-15, Instantaneous Hydraulic gradelines in 19R-1 tunnel - System C-II.

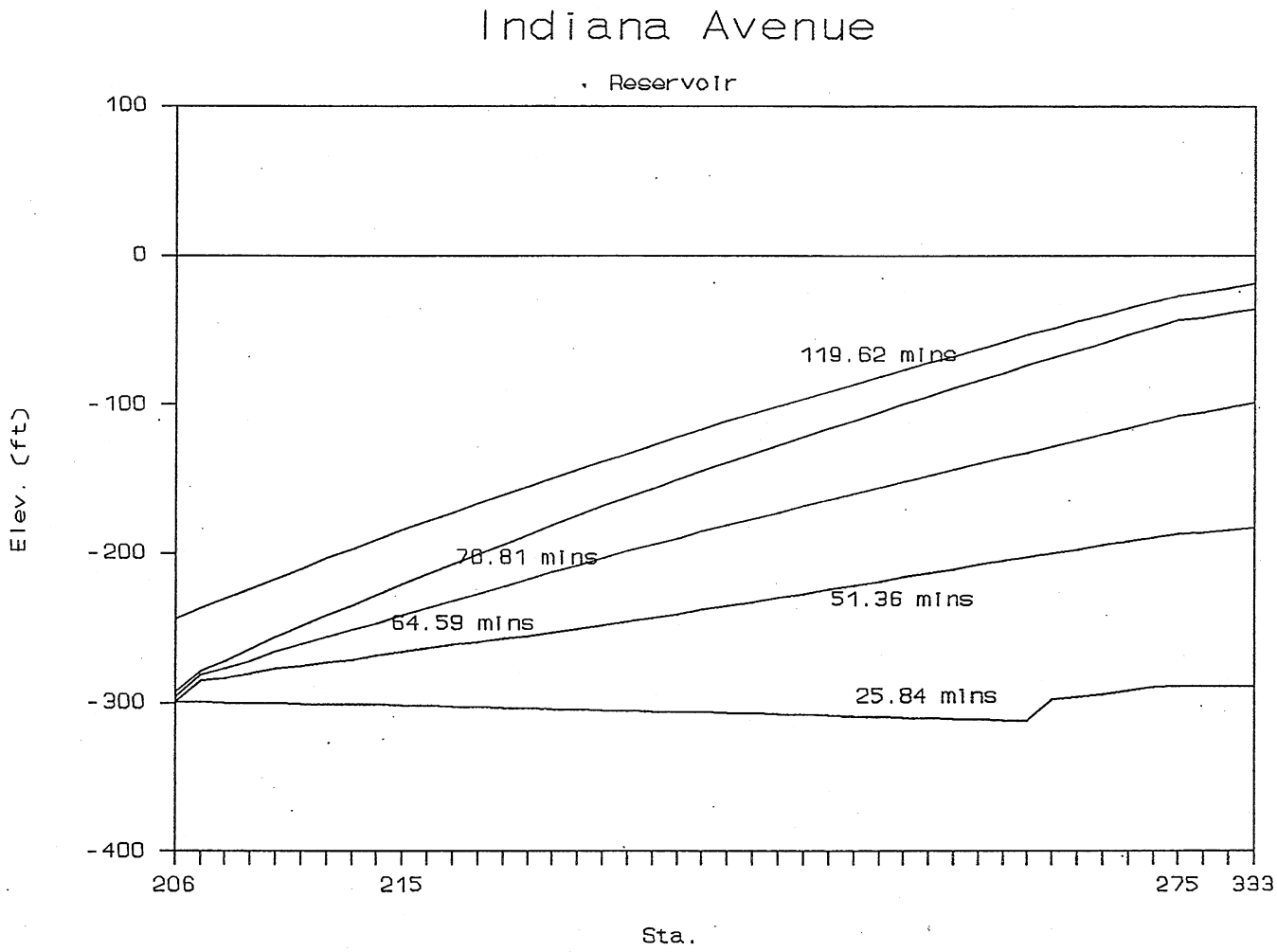

Fig. C-16, Instantaneous Hydraulic gradelines in Indiana Avenue tunnel - System C-II.

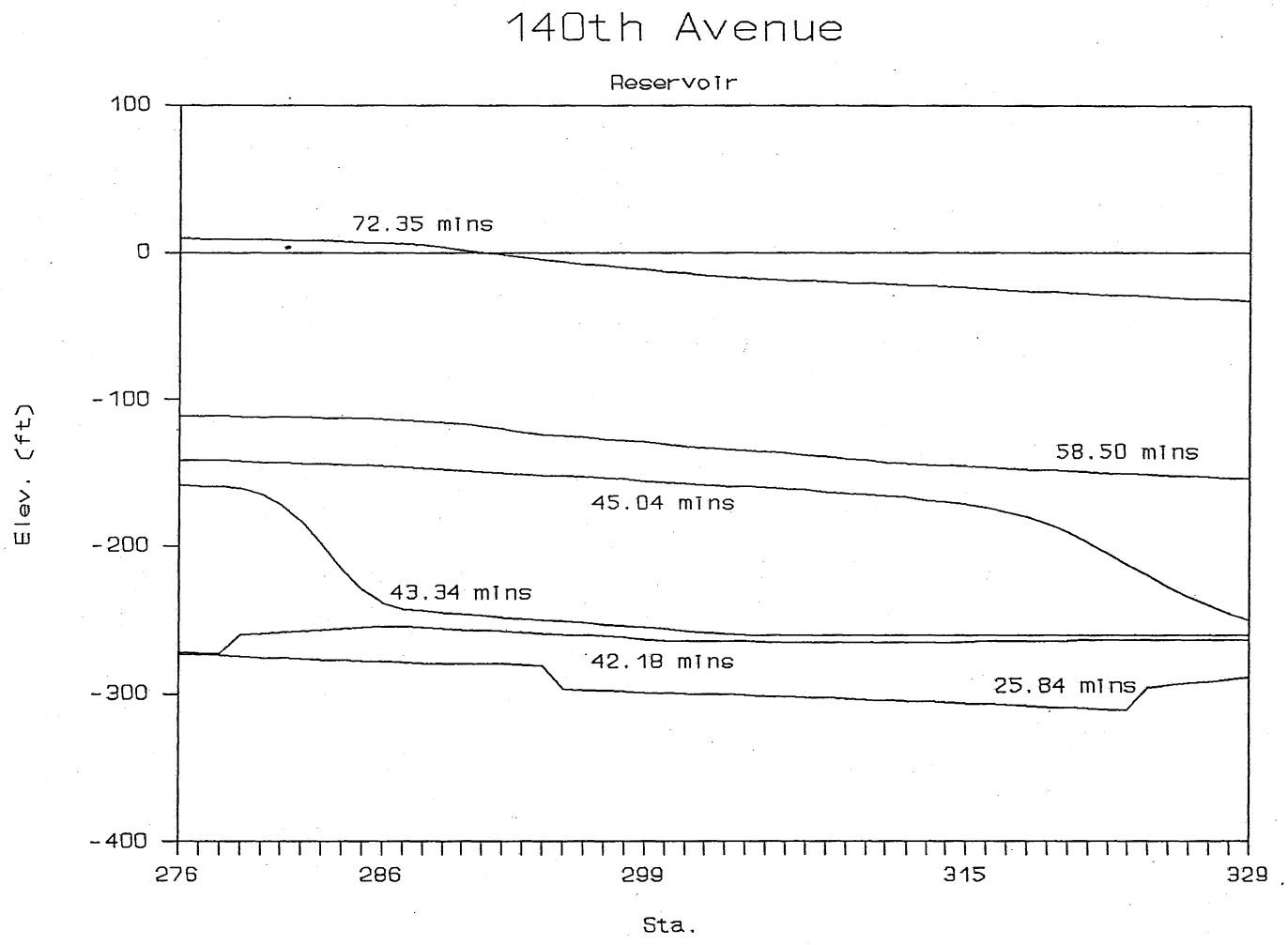

Fig. C-17, Instantaneous Hydraulic gradelines in 140th Avenue tunnel - System C-II.

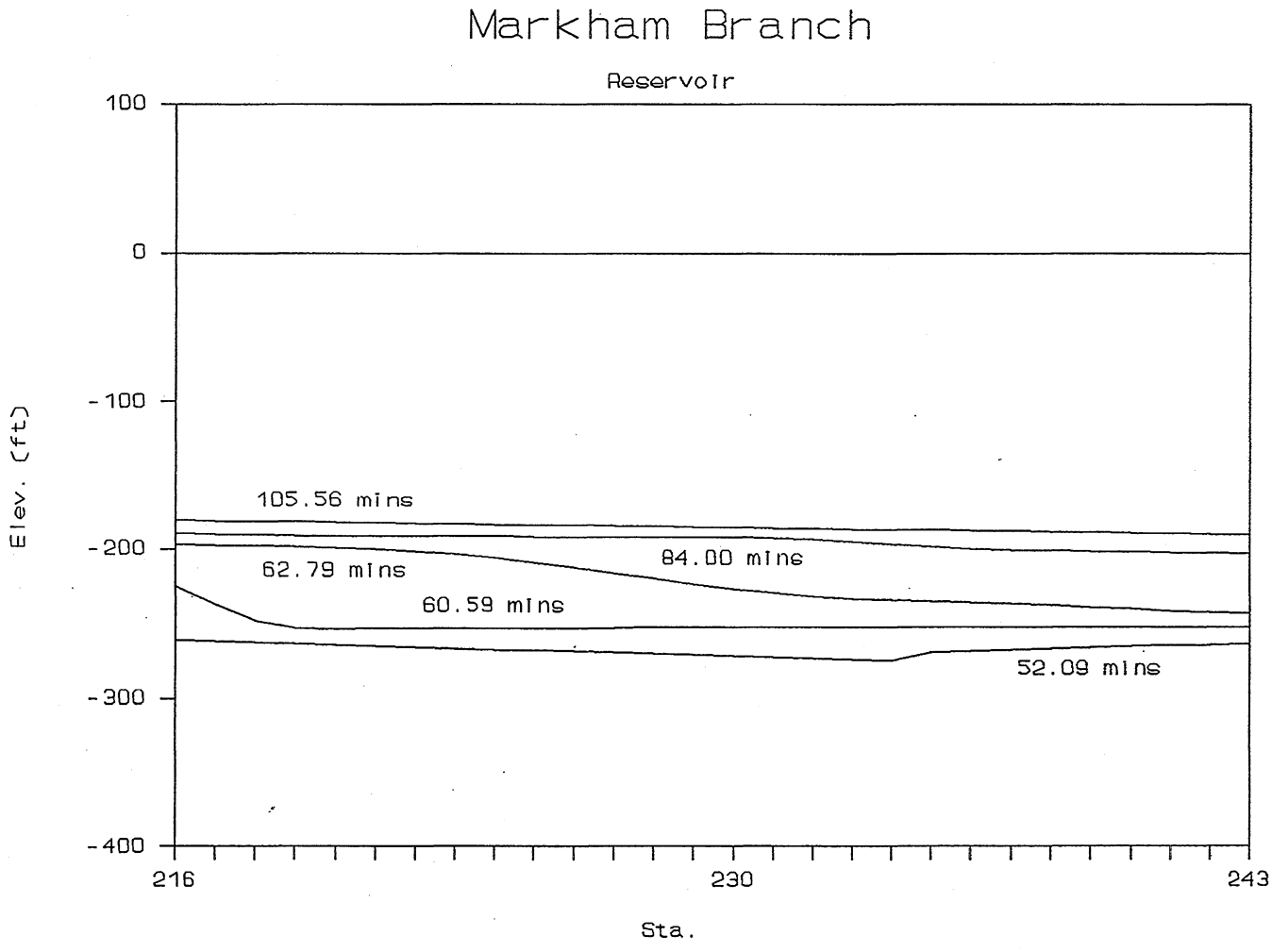

Fig. C-18, Instantaneous Hydraulic gradelines in Markham tunnel - System C-II.

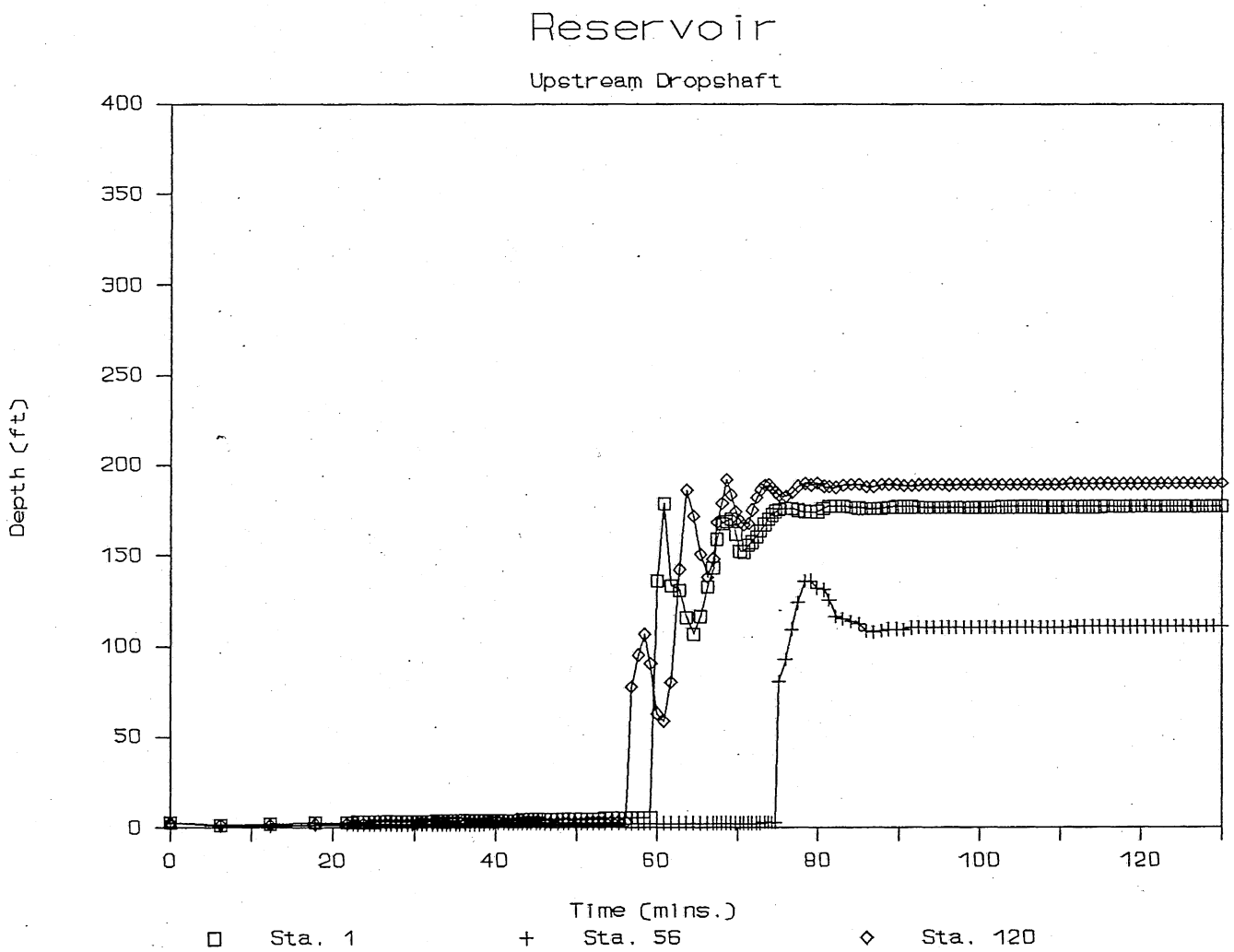

Fig. C-19, Time variation of water depth at 3 upstream ends, System C-II (Sta. 1, 56, 120).

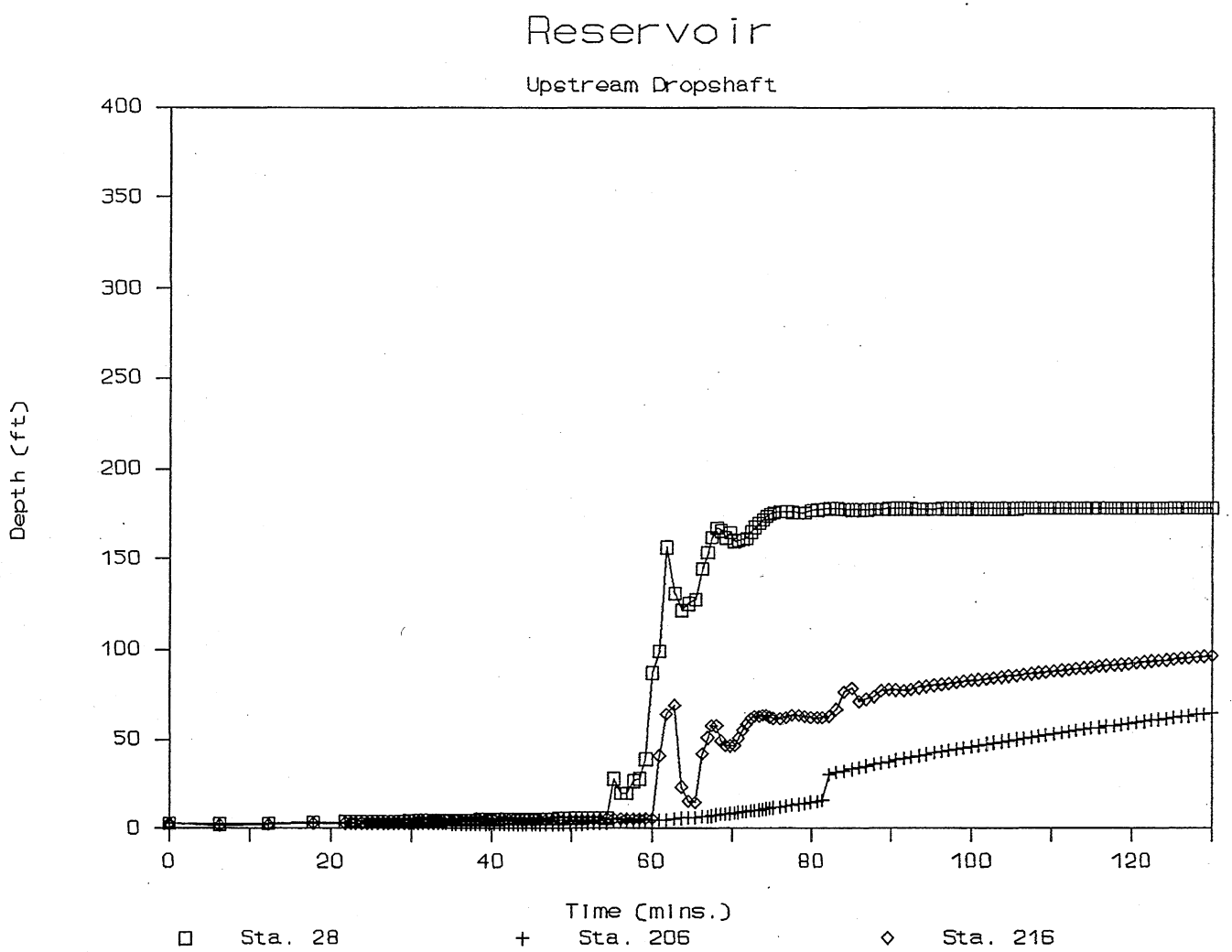

Fig. C-20, Time variation of water depth at 3 upstream ends, System C-II (Sta. 28, 206, 216).

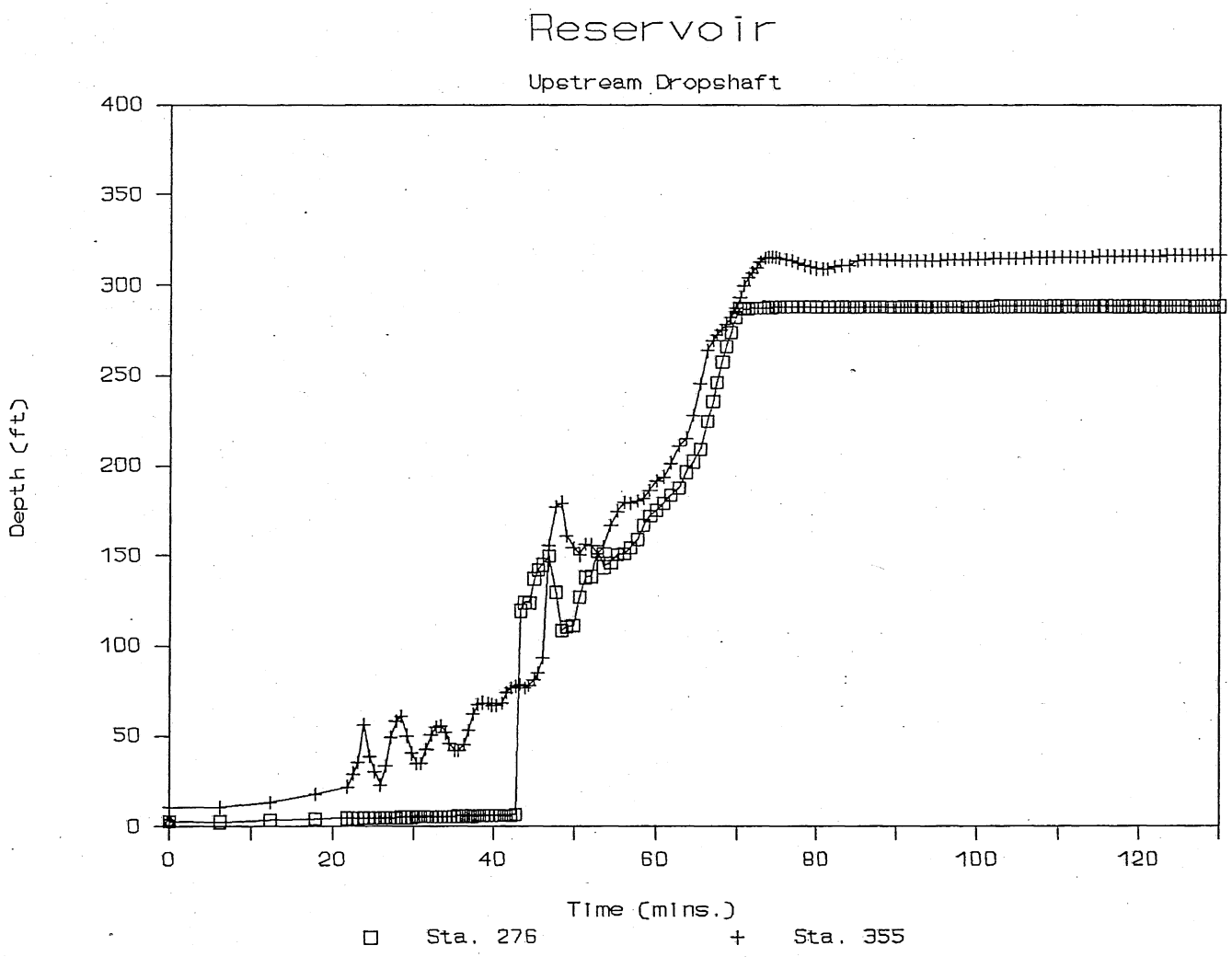

Fig. C-21, Time variation of water depth at 2 upstream ends, System C-II (Sta. 276, 355).

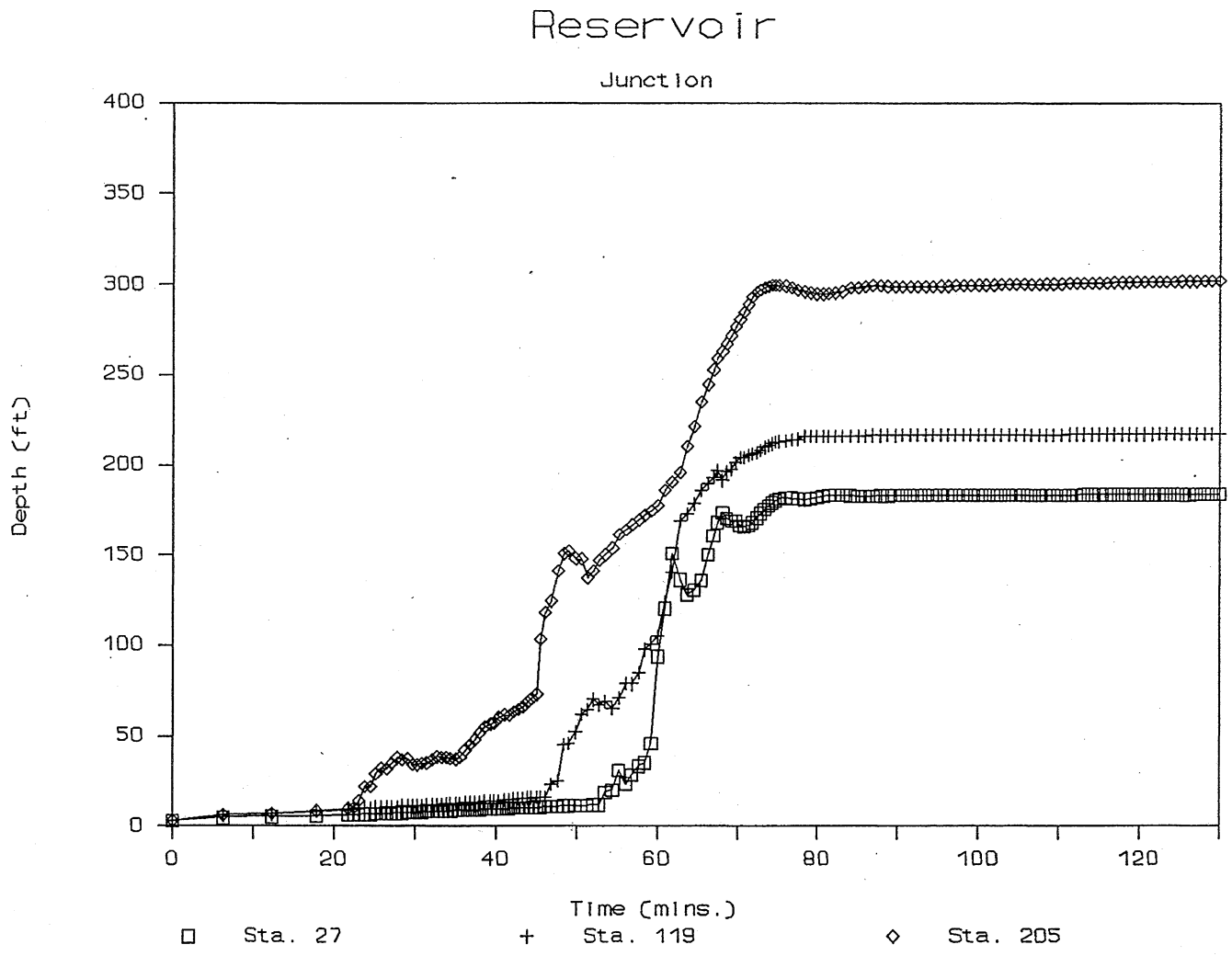

Fig. C-22, Time variation of water depth at junction points, System C-II(Sta. 27, 119, 205).

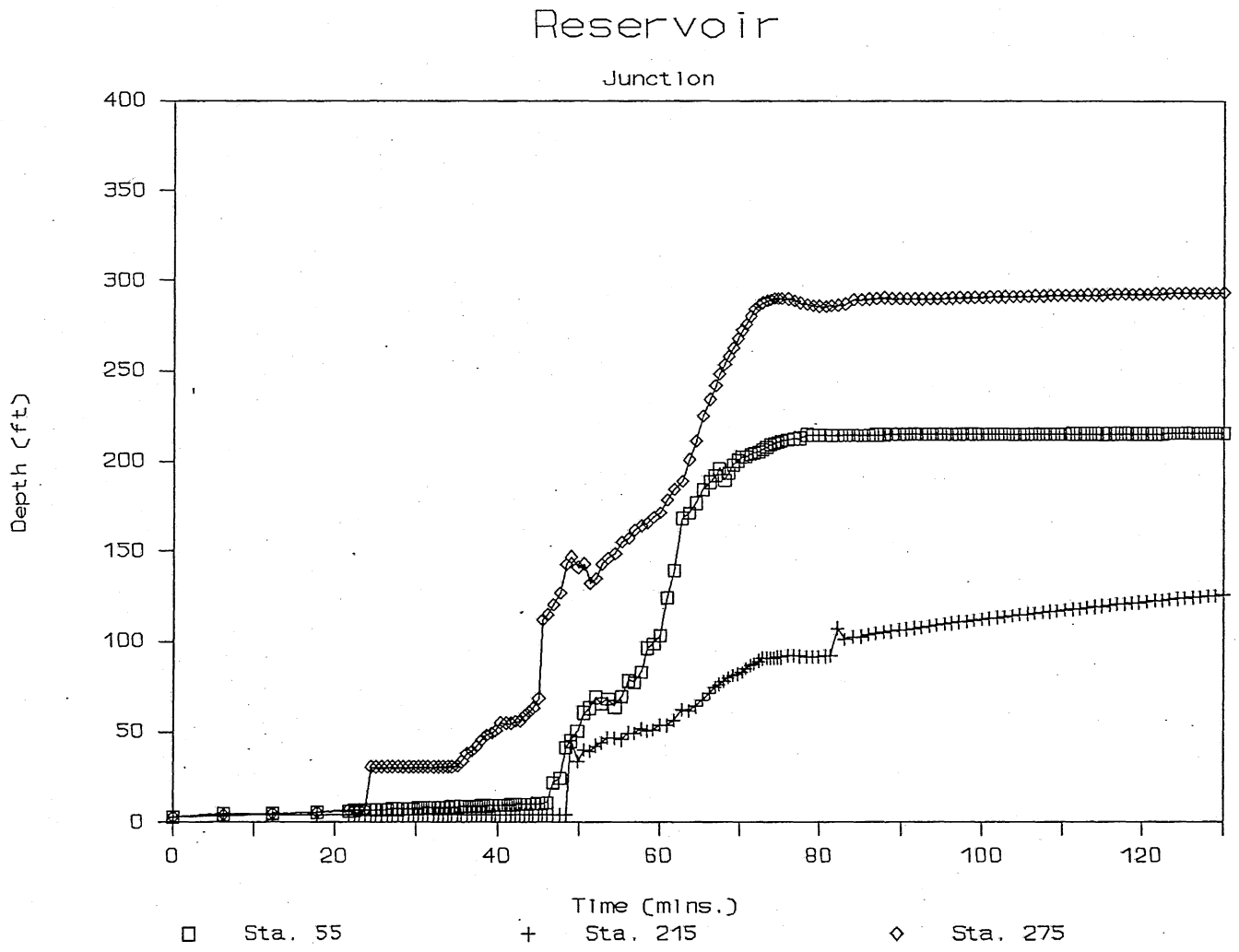

Fig. C-23, Time variation of water depth at junction points, System C-II (Sta. 55, 215, 275).

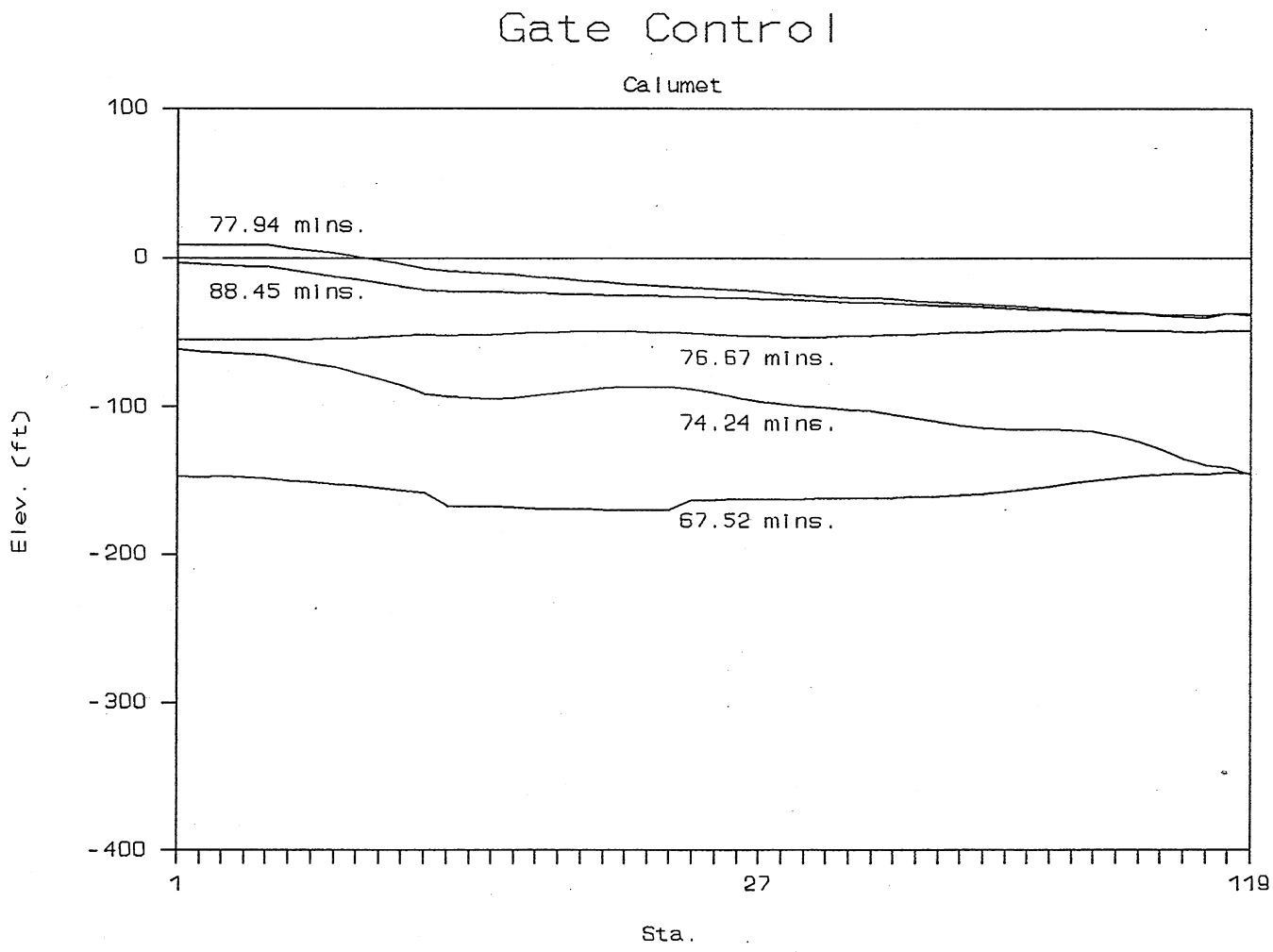

Fig. C-24, Instantaneous hydraulic gradelines upstream of roller gate, System C-III.

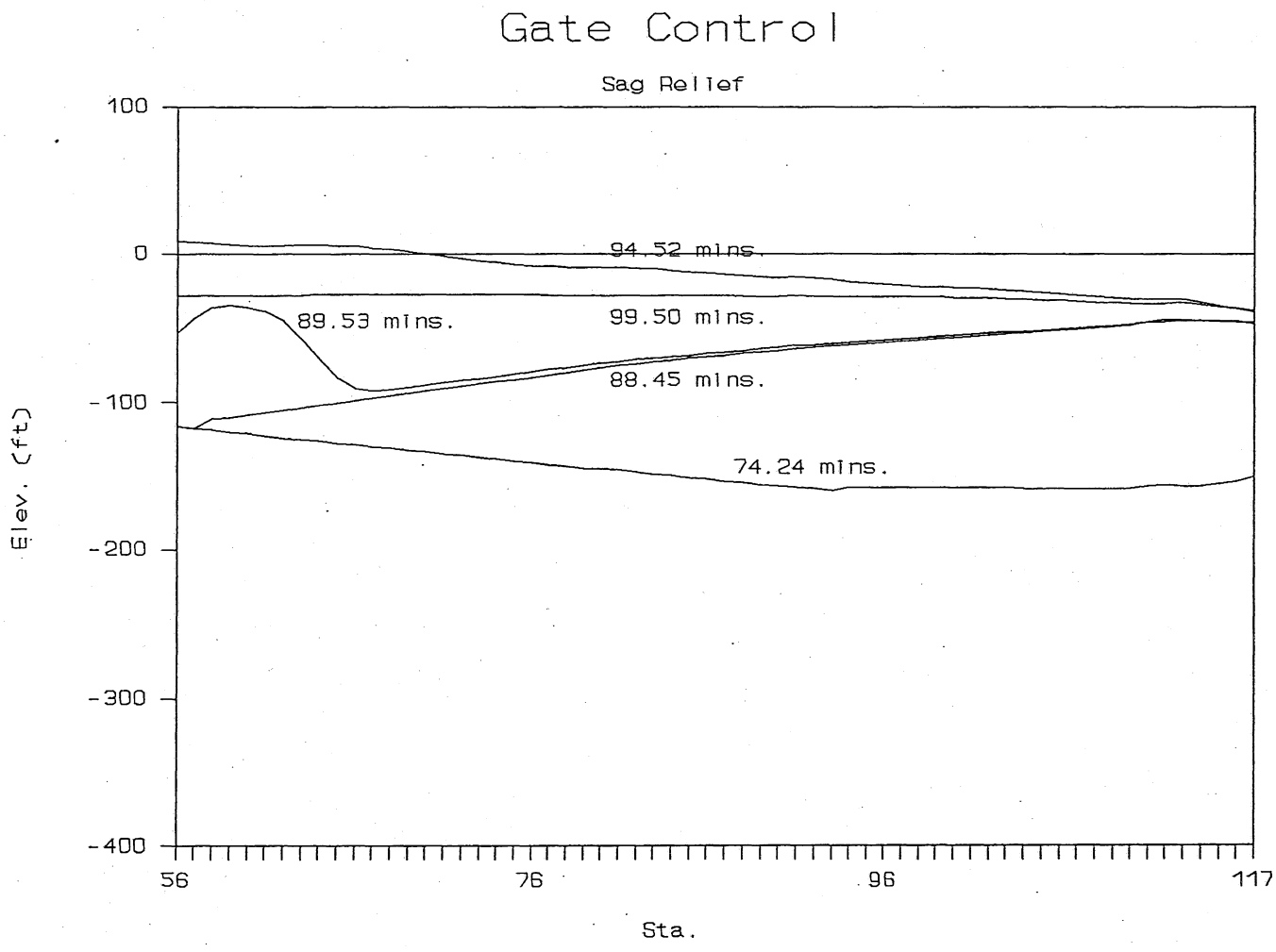

Fig. C-25, Instantaneous hydraulic gradelines in Sag Relief, System C-III.

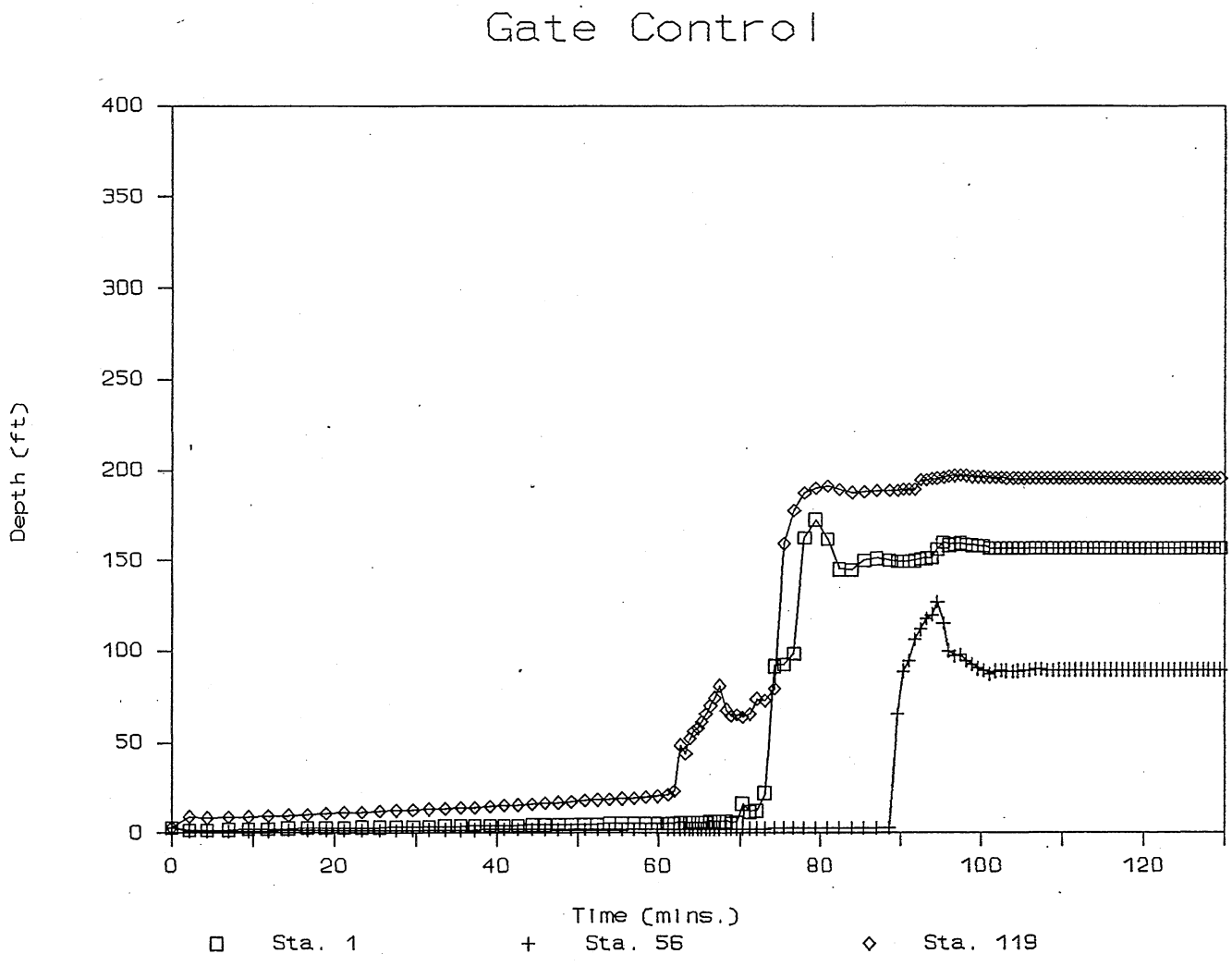

Fig. C-26, Time variation of water depth, System C-III (Sta. 1, 56, 119).

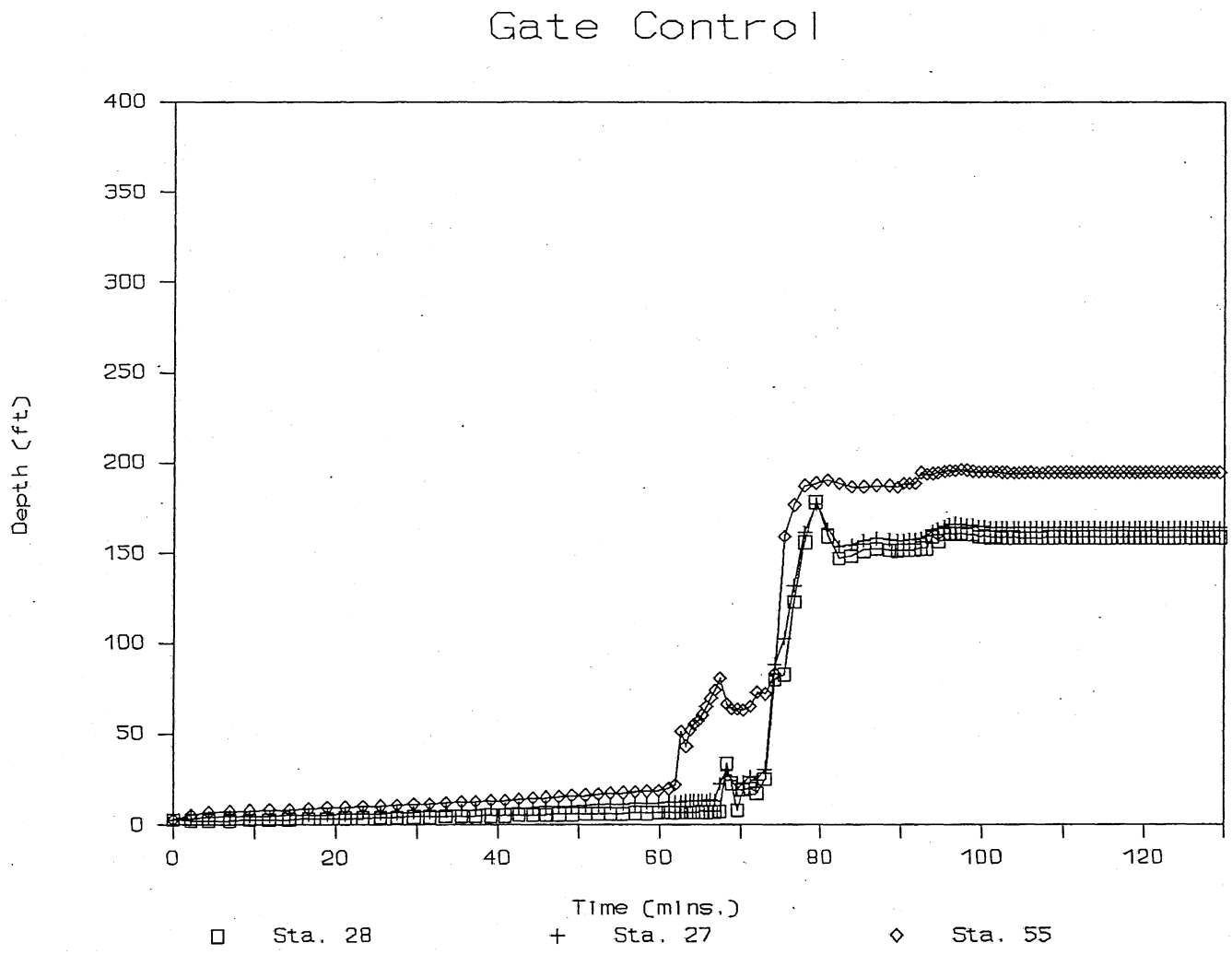

Fig. C-27, Time variation of water depth, System C-III (Sta. 28, 27, 55).

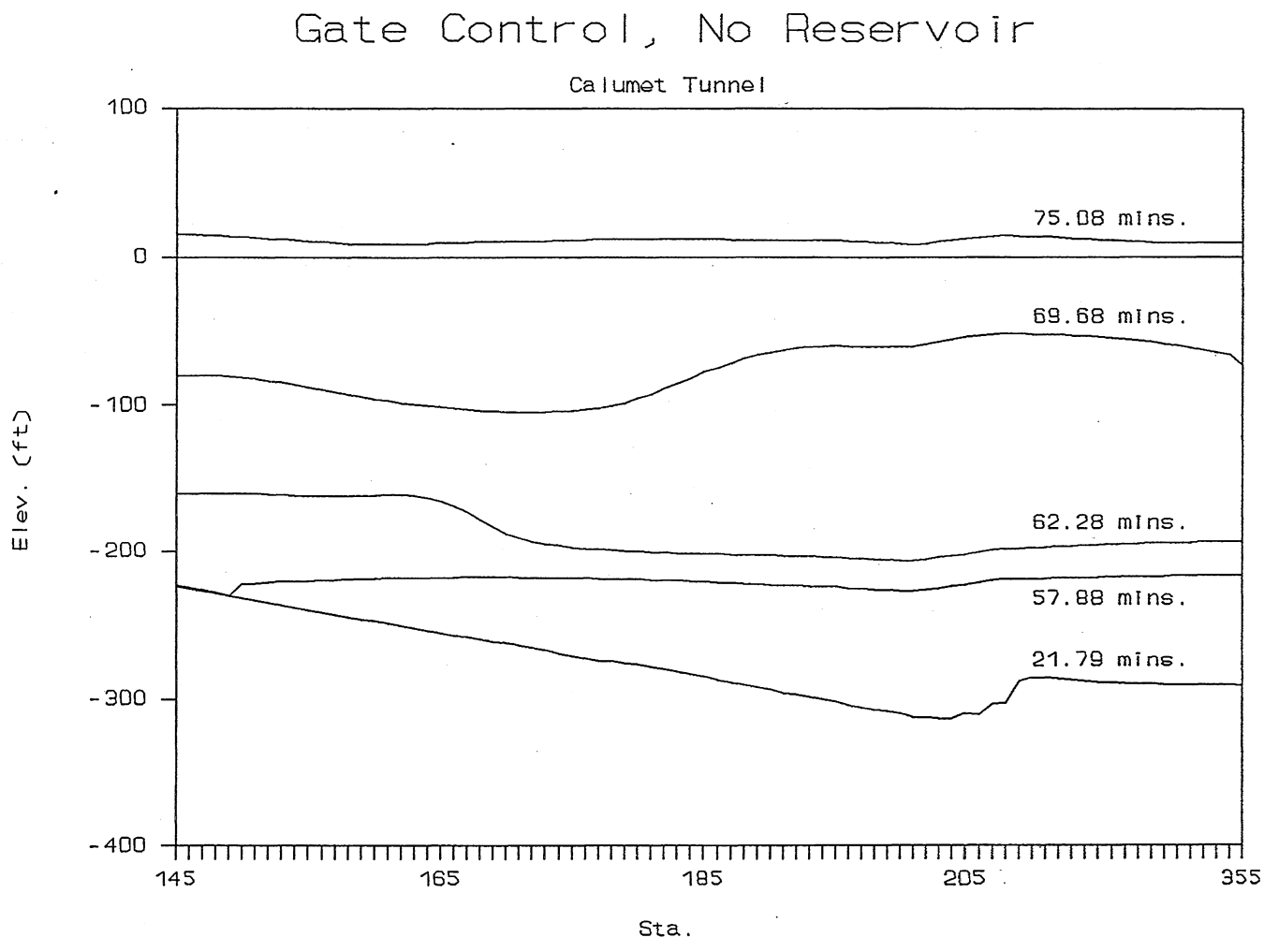

Fig. C-28, Instantaneous hydraulic gradelines downstream of roller gate, System C-III.

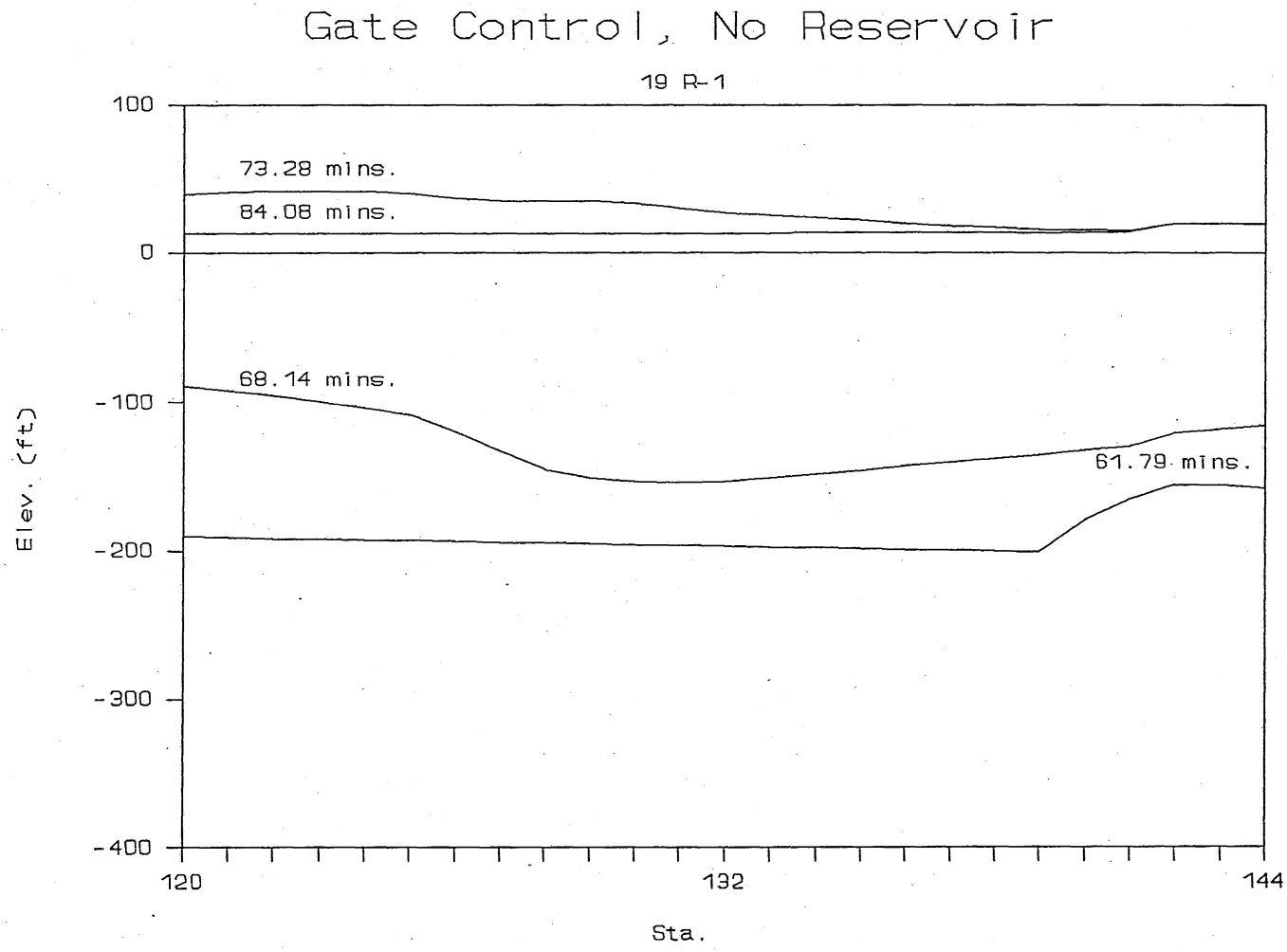

Fig. C-29, Instantaneous hydraulic gradelines downstream of roller gate in 19R-1 tunnel, System C-III.

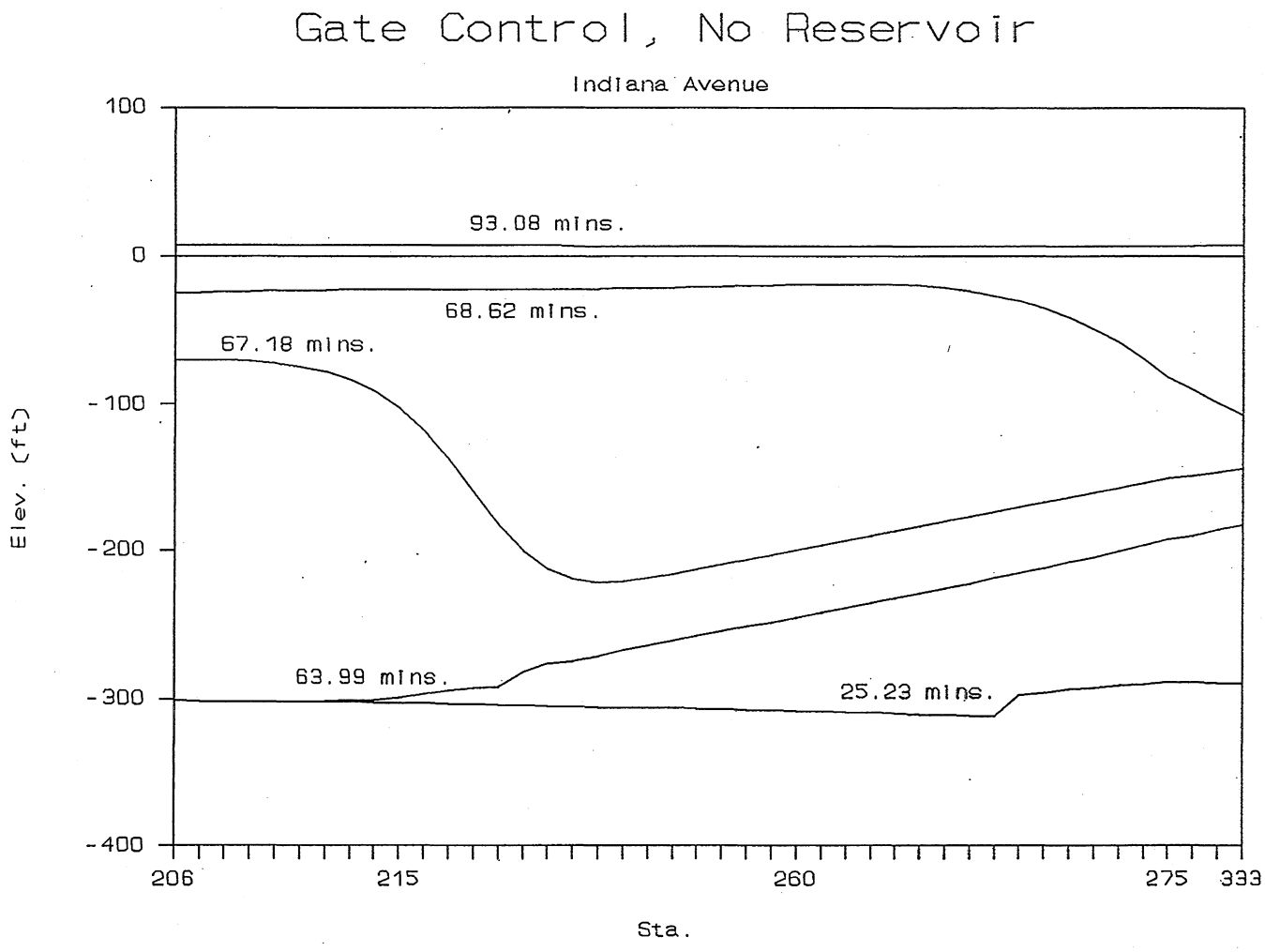

Fig. C-30, Instantaneous hydraulic gradelines downstream of roller gatein Indiana Avenue tunnel, System C-III.

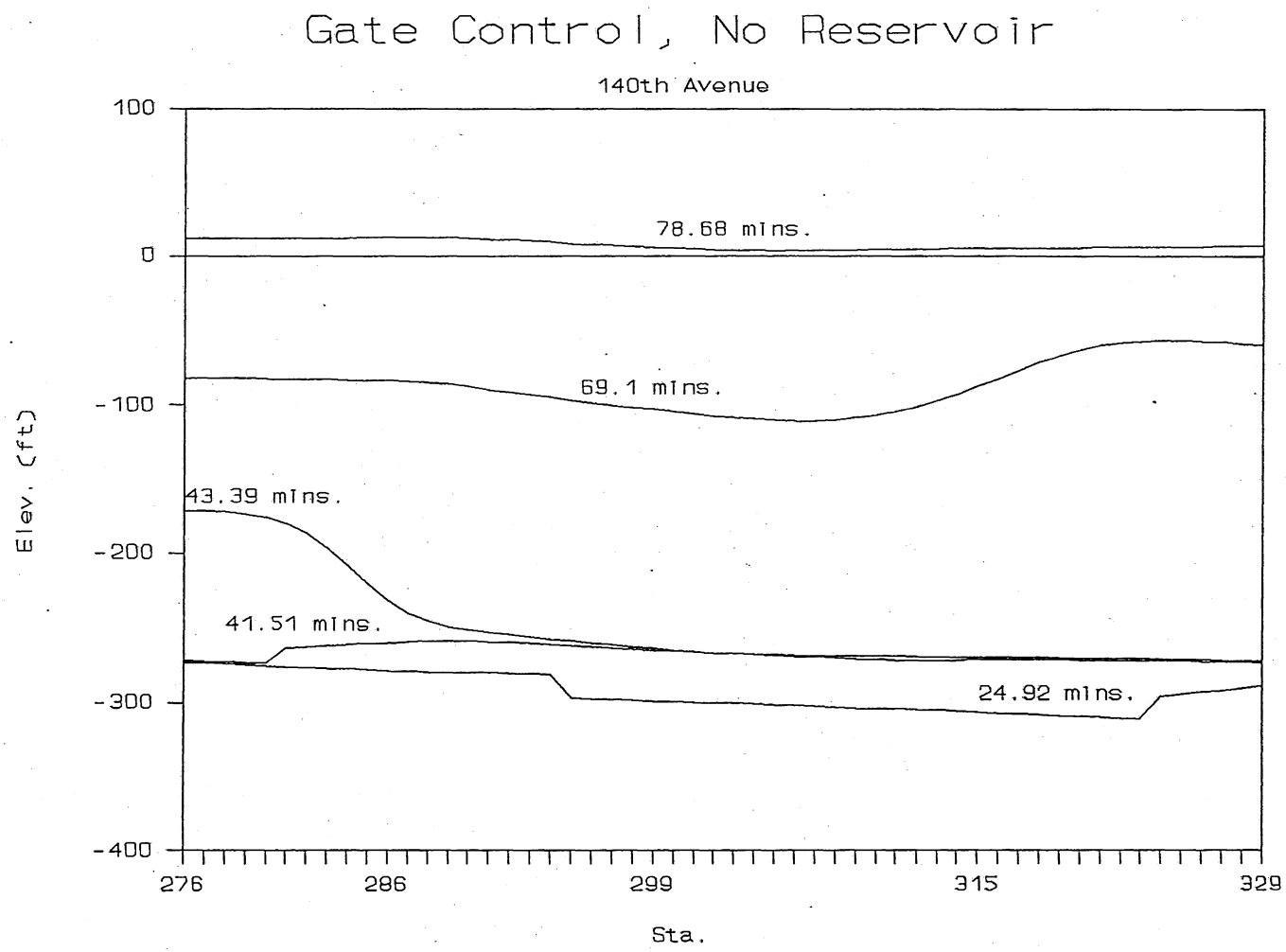

Fig. C-31, Instantaneous hydraulic gradelines downstream of roller gate in 140th Avenue tunnel, System C-III.

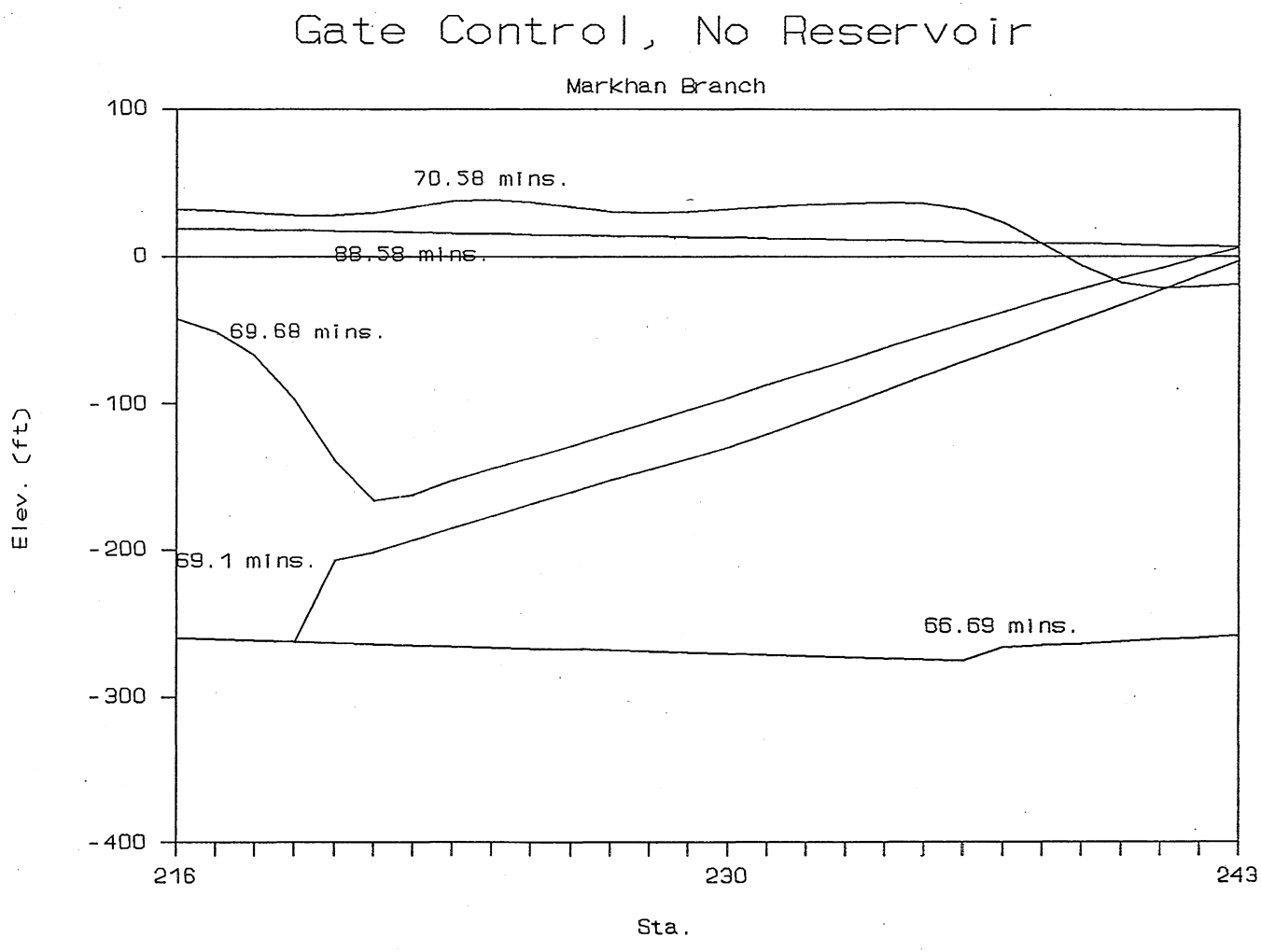

Fig. C-32, Instantaneous hydraulic gradelines downstream of roller gate in Markham tunnel, System C-III.

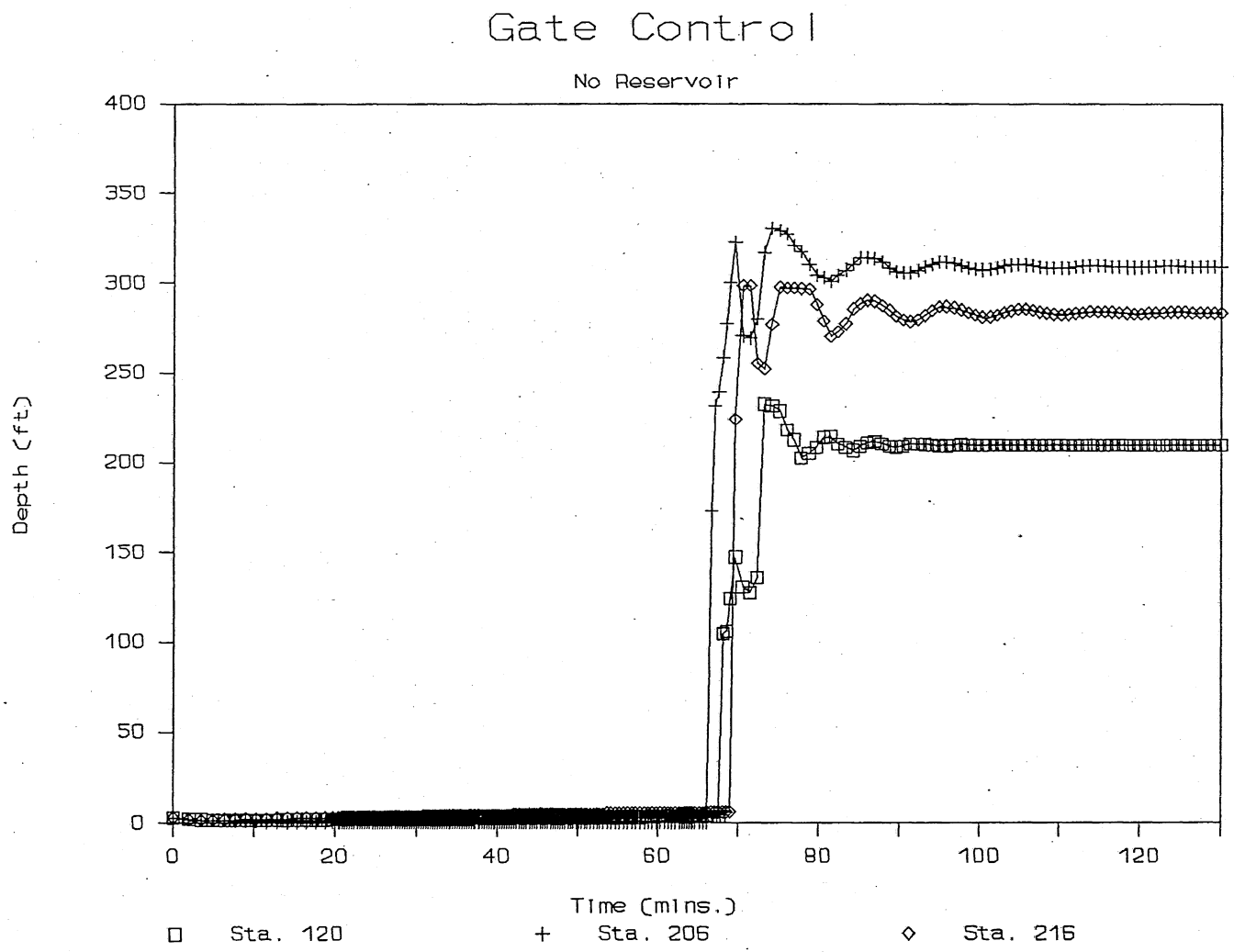

Fig. C-33, Time variation of water depth at some stations downstream of roller gate, System C-III (Sta. 120, 206, 216).

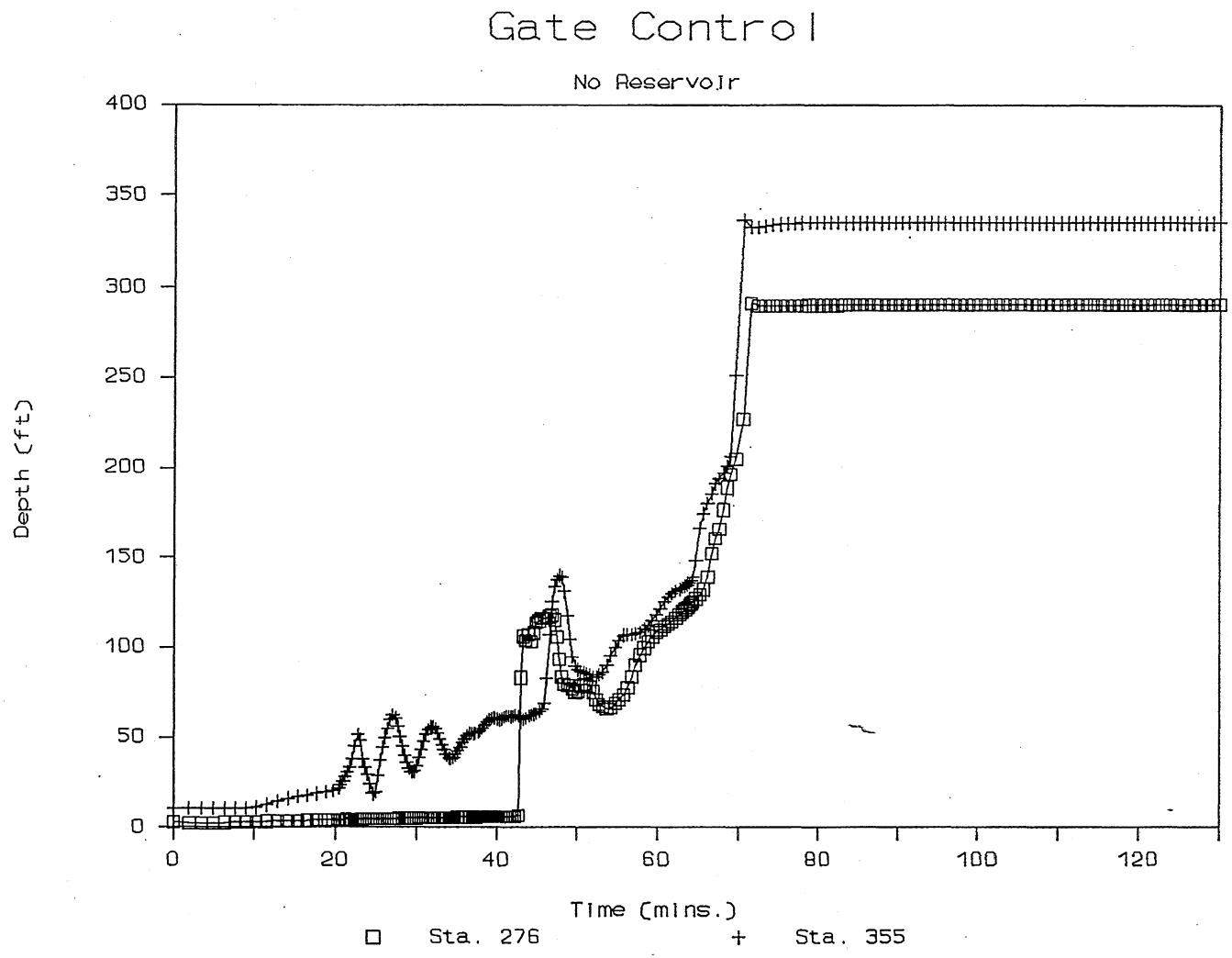

Fig. C-34, Time variation of water depth at some stations downstream of roller gate, System C-III (Sta. 276,355).

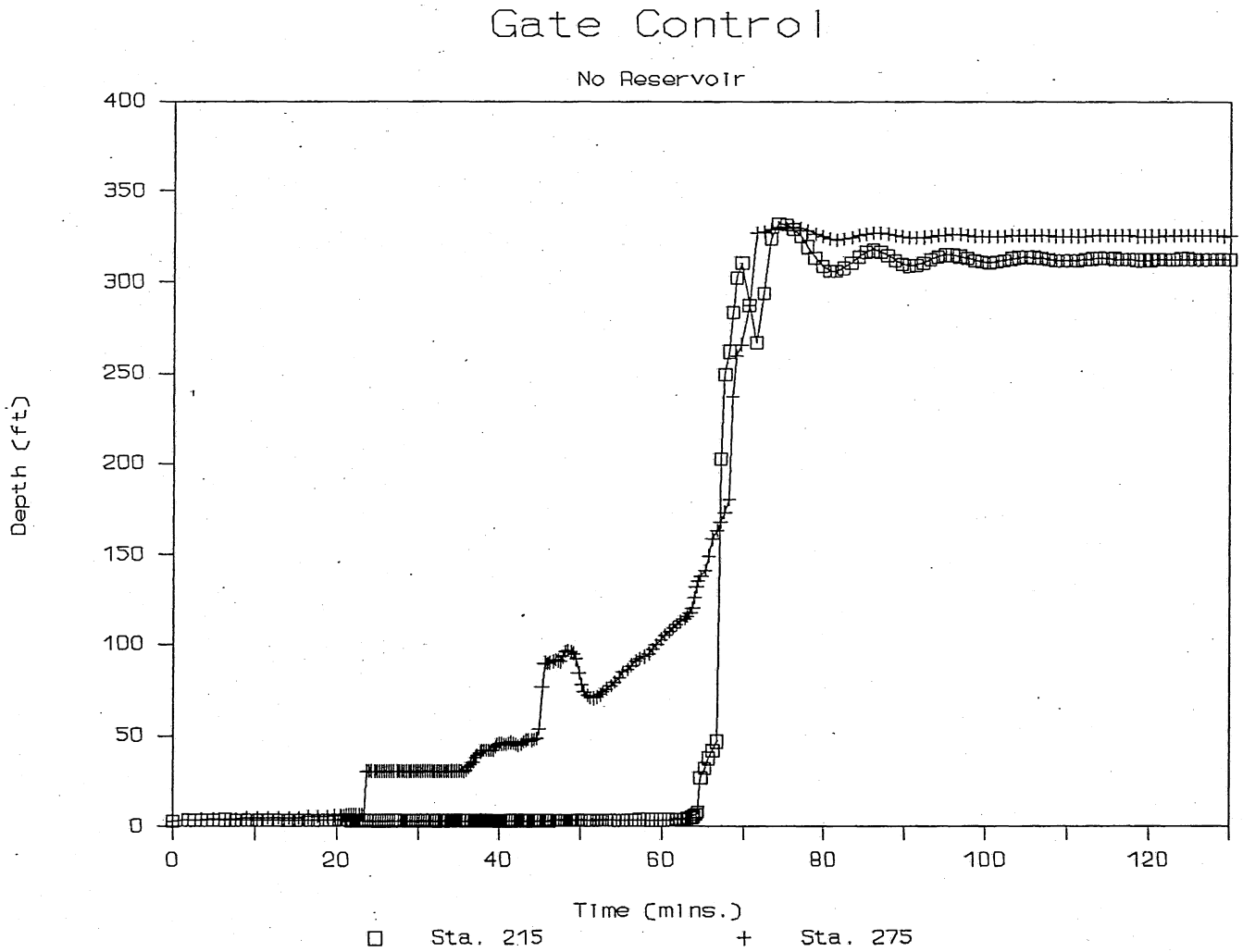

Fig. C-35, Time variation of water depth at some stations downstream of roller gate, System C-III (Sta. 119, 205).

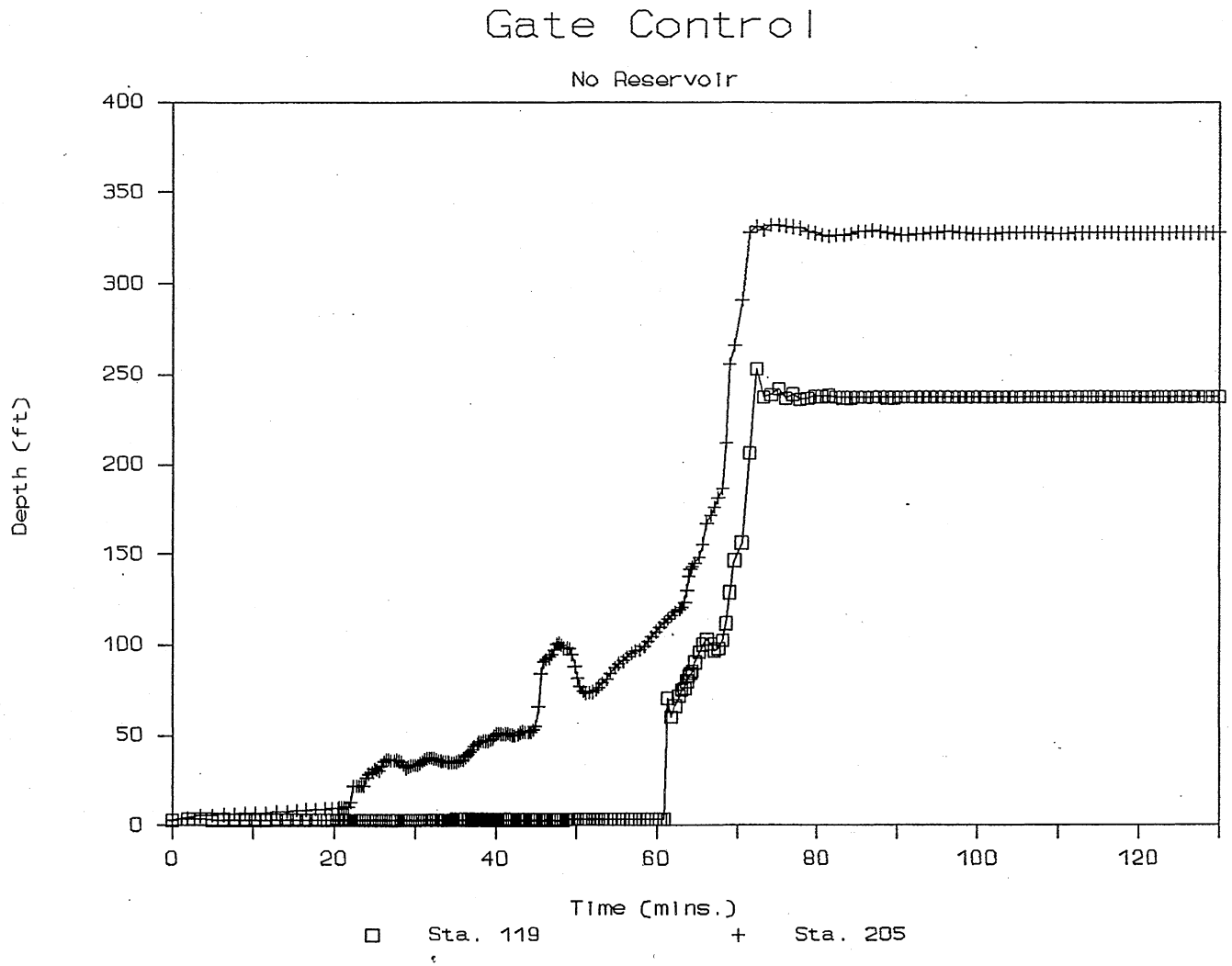

Fig. C-36, Time variation of water depth at some stations downstream of roller gate, System C-III (Sta. 215,275).

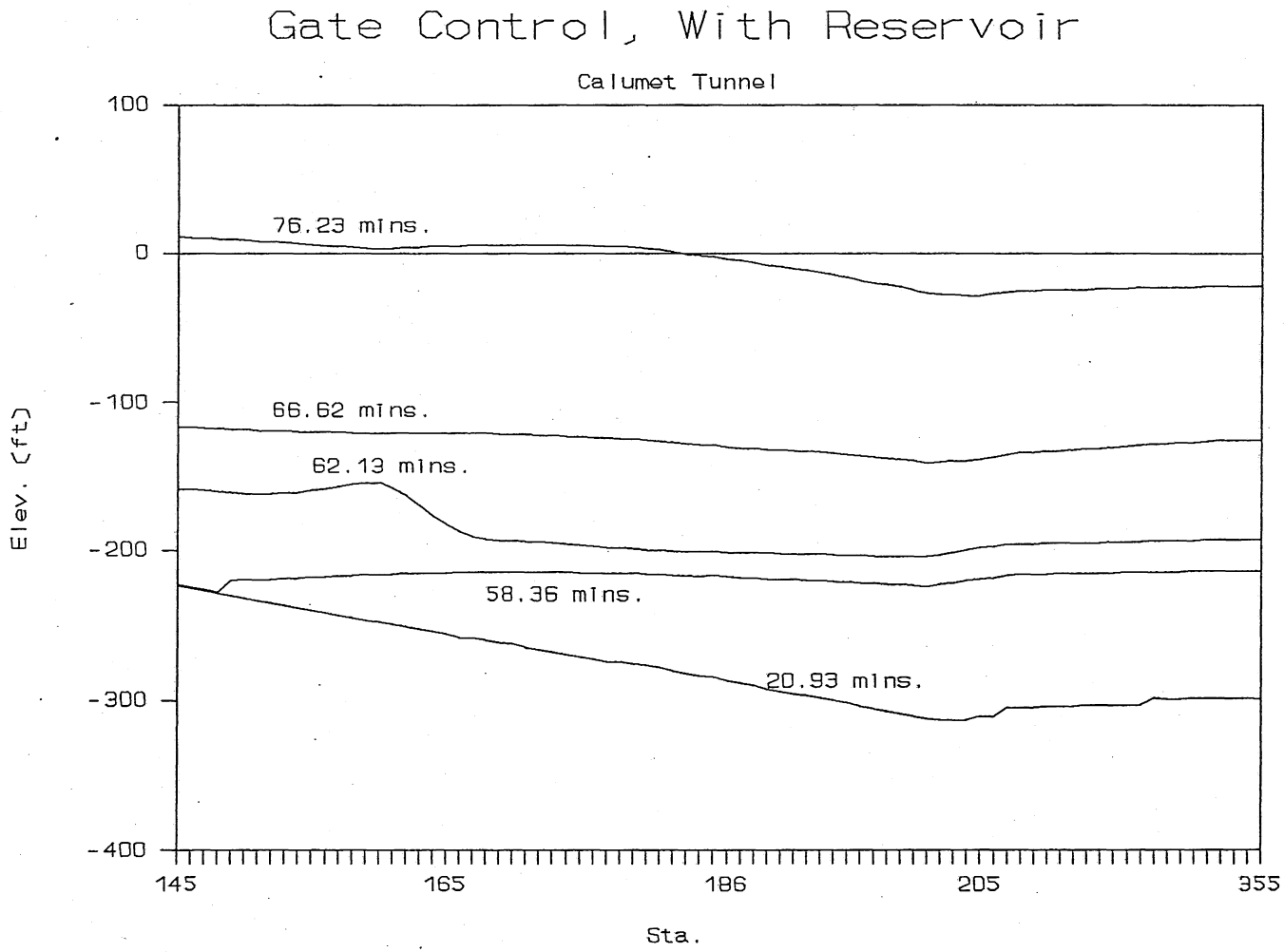

Fig. C-37, Instantaneous hydraulic gradeline downstream of roller gate, System C-IV.

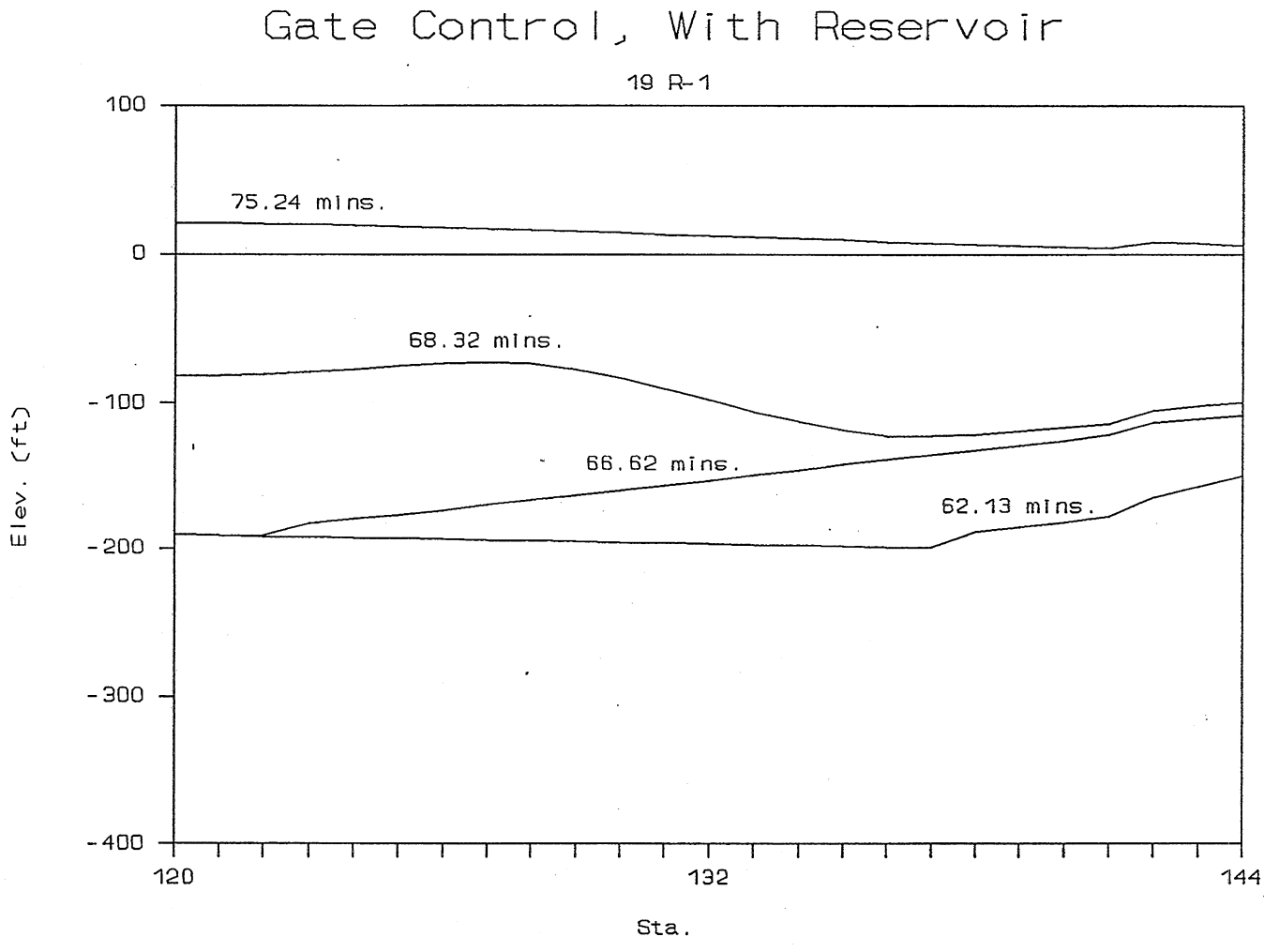

Fig. C-38, Instantaneous hydraulic gradeline downstream of roller gate in 19R-1 tunnel, System C-IV.

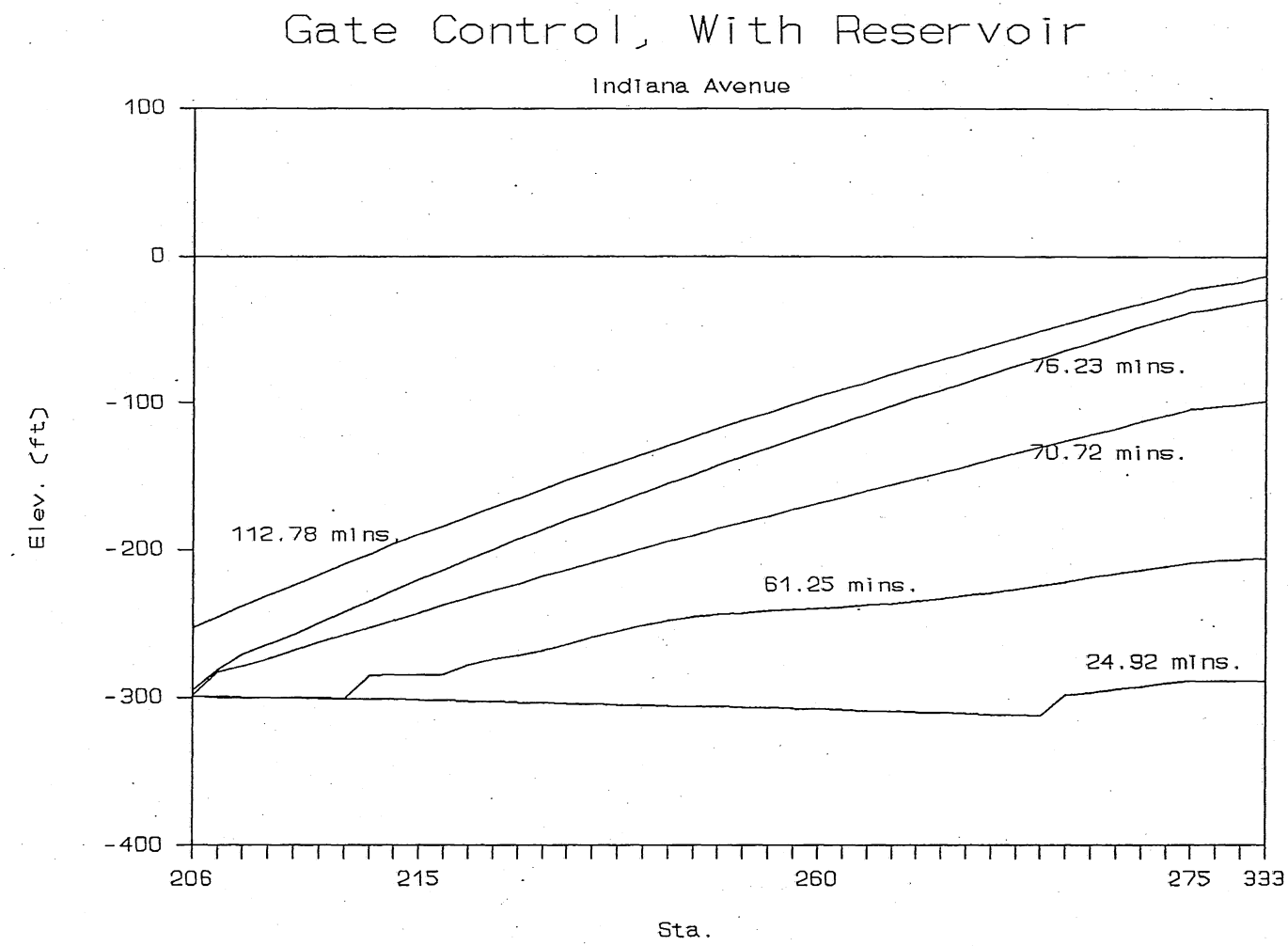

Fig. C-39, Instantaneous hydraulic gradeline downstream of roller gate in Indiana Avenue, System C-IV.

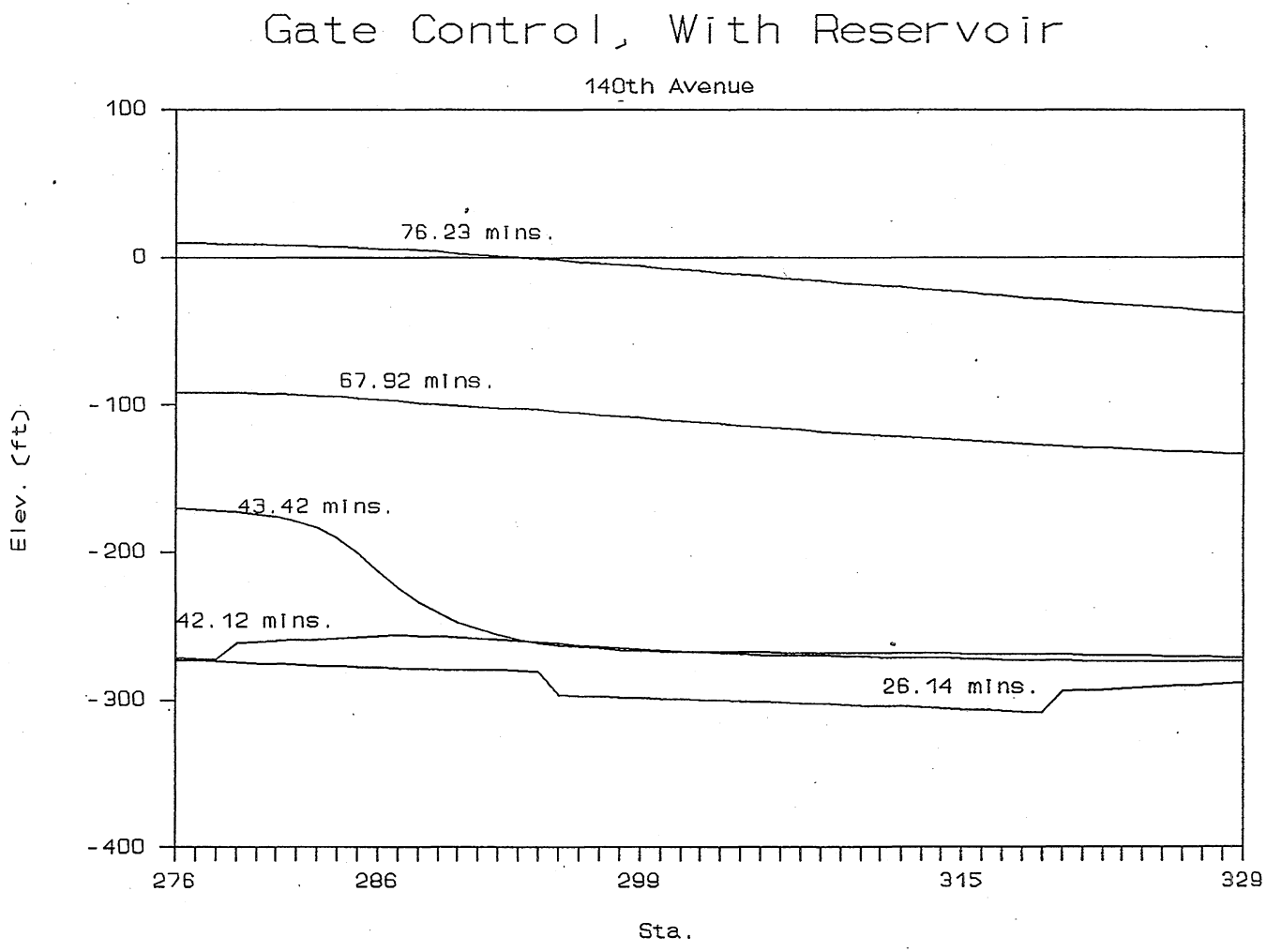

Fig. C-40, Instantaneous hydraulic gradeline downstream of roller gate in 140th Avenue., System C-IV.

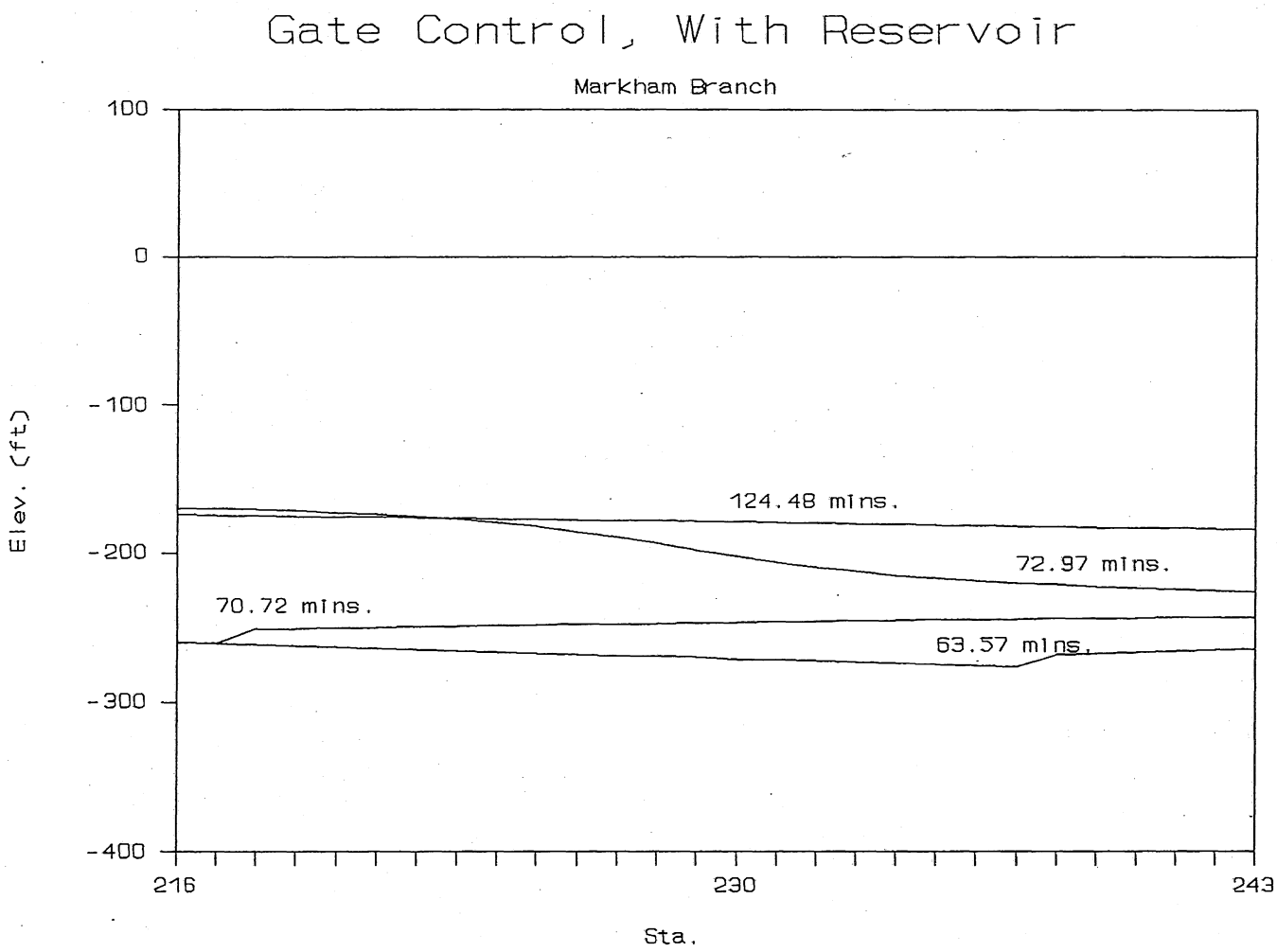

Fig. C-41, Instantaneous hydraulic gradeline downstream of roller gate in Markham tunnel, System C-IV.

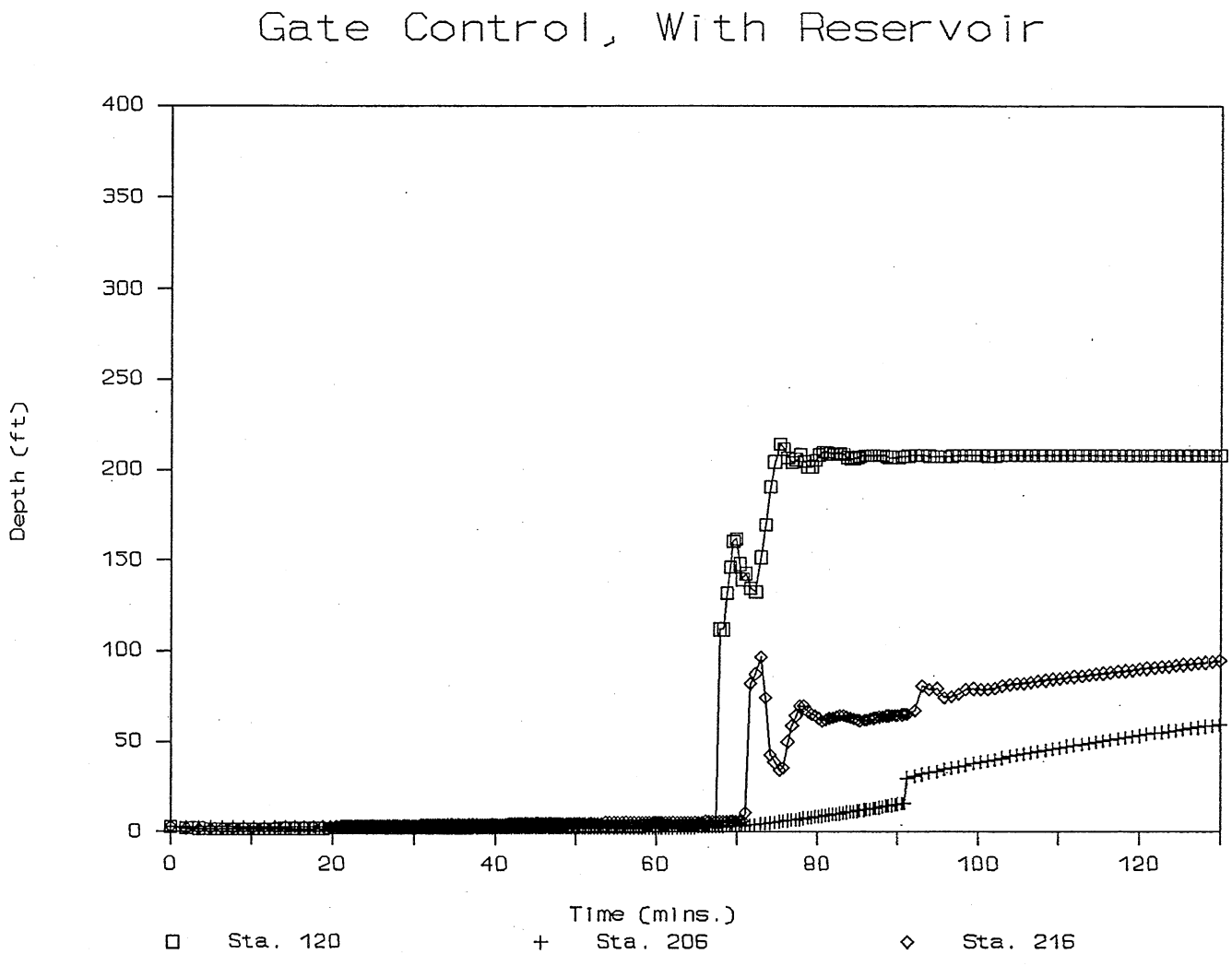

Fig. C-42, Time variation of water depth downstream of roller gate, System C-IV (Sta. 120, 206, 216).

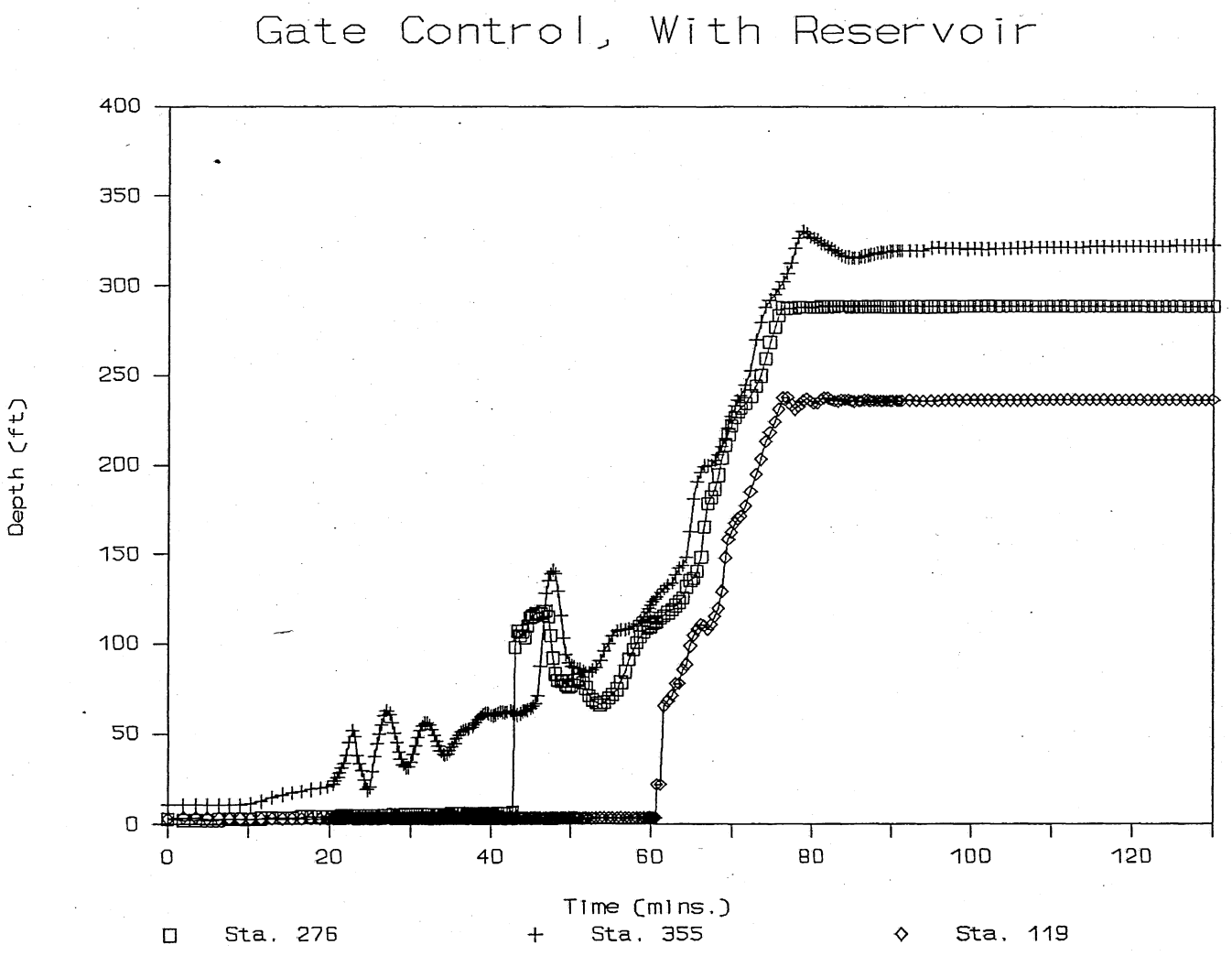

Fig. C-43, Time variation of water depth downstream of roller gate, System C-IV (Sta. 276, 355, 119).

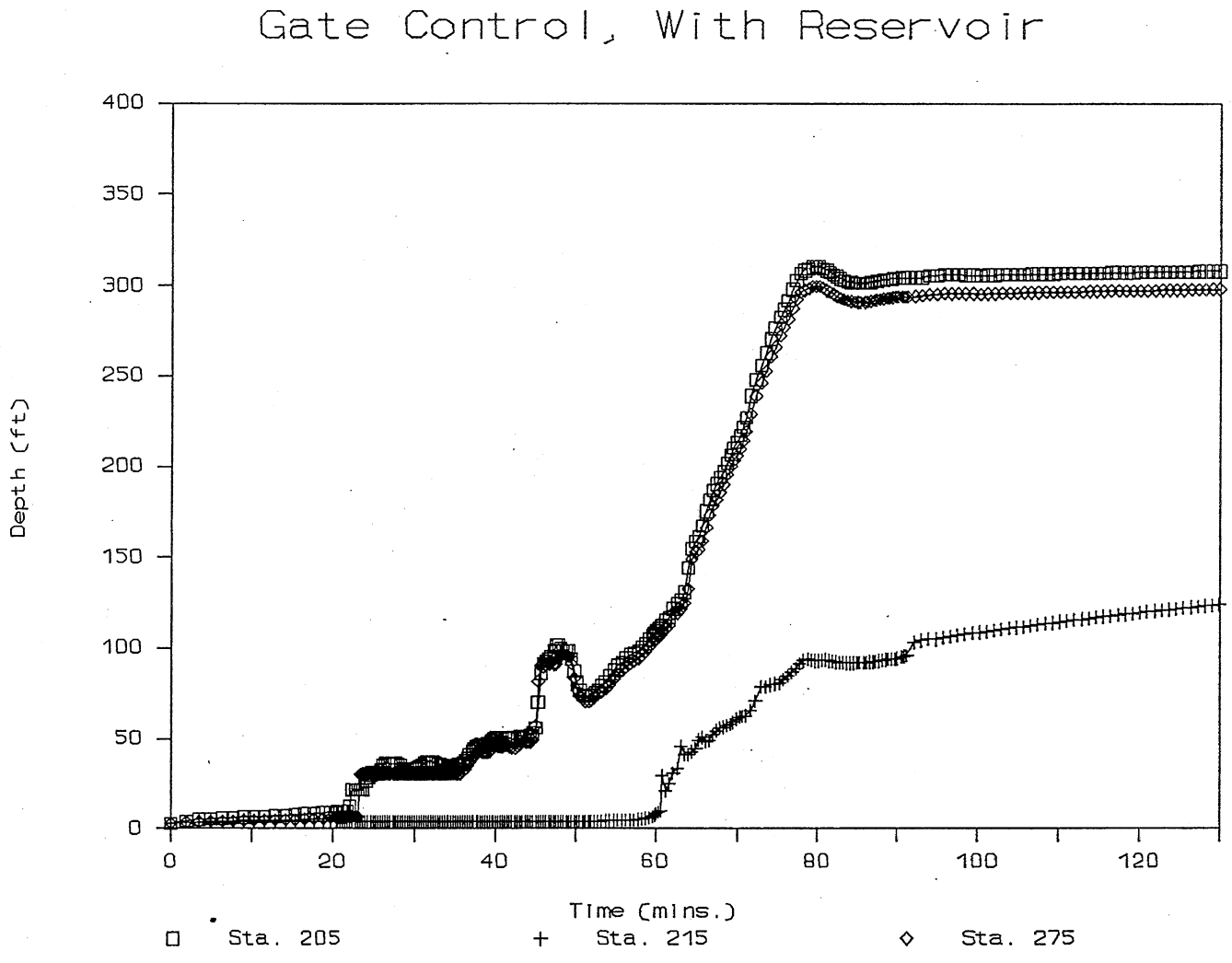

Fig. C-44, Time variation of water depth downstream of roller gate, System C-IV (Sta. 205, 215,275).

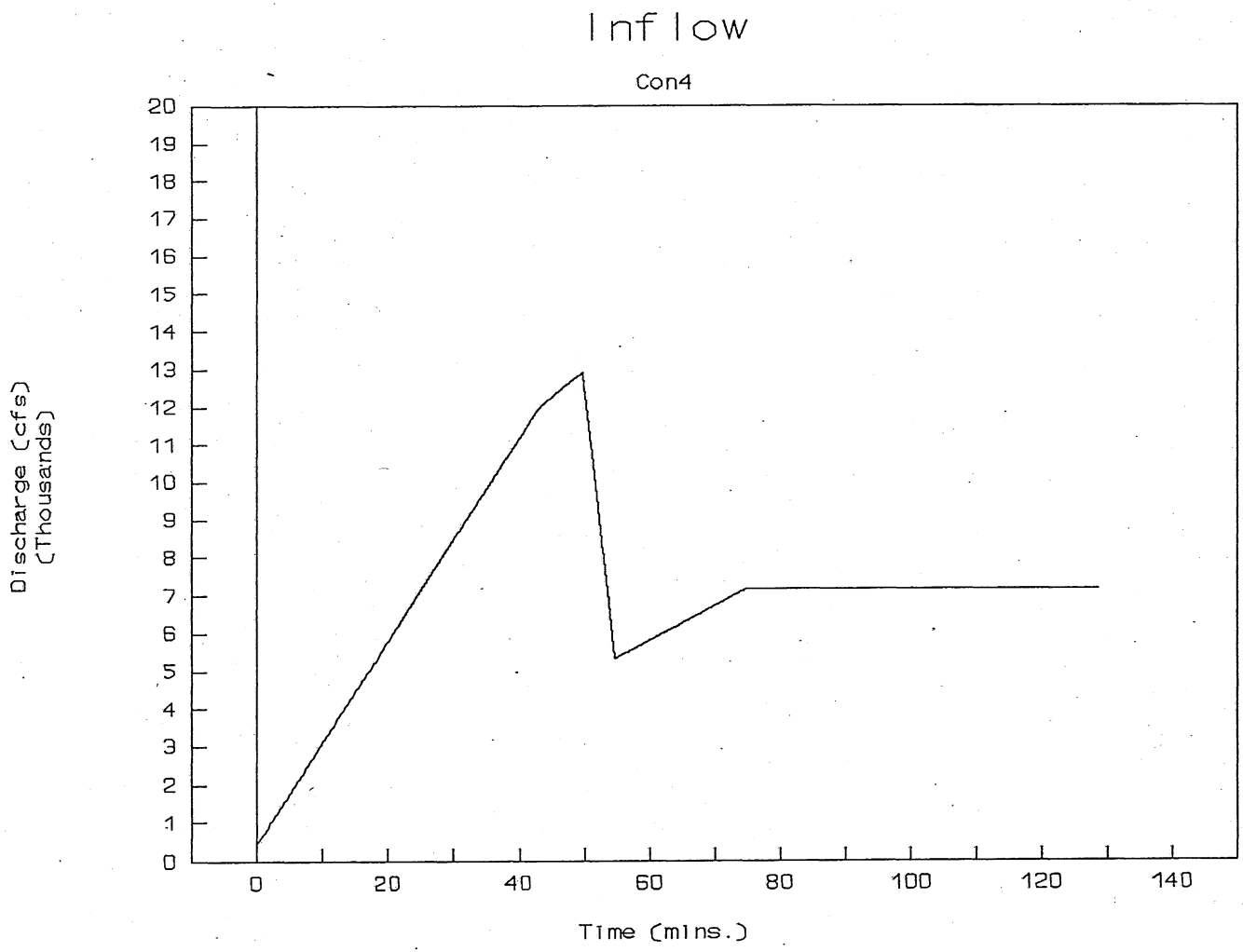

Fig. C-45, Total inflow hydrograph allowed for System C-I.

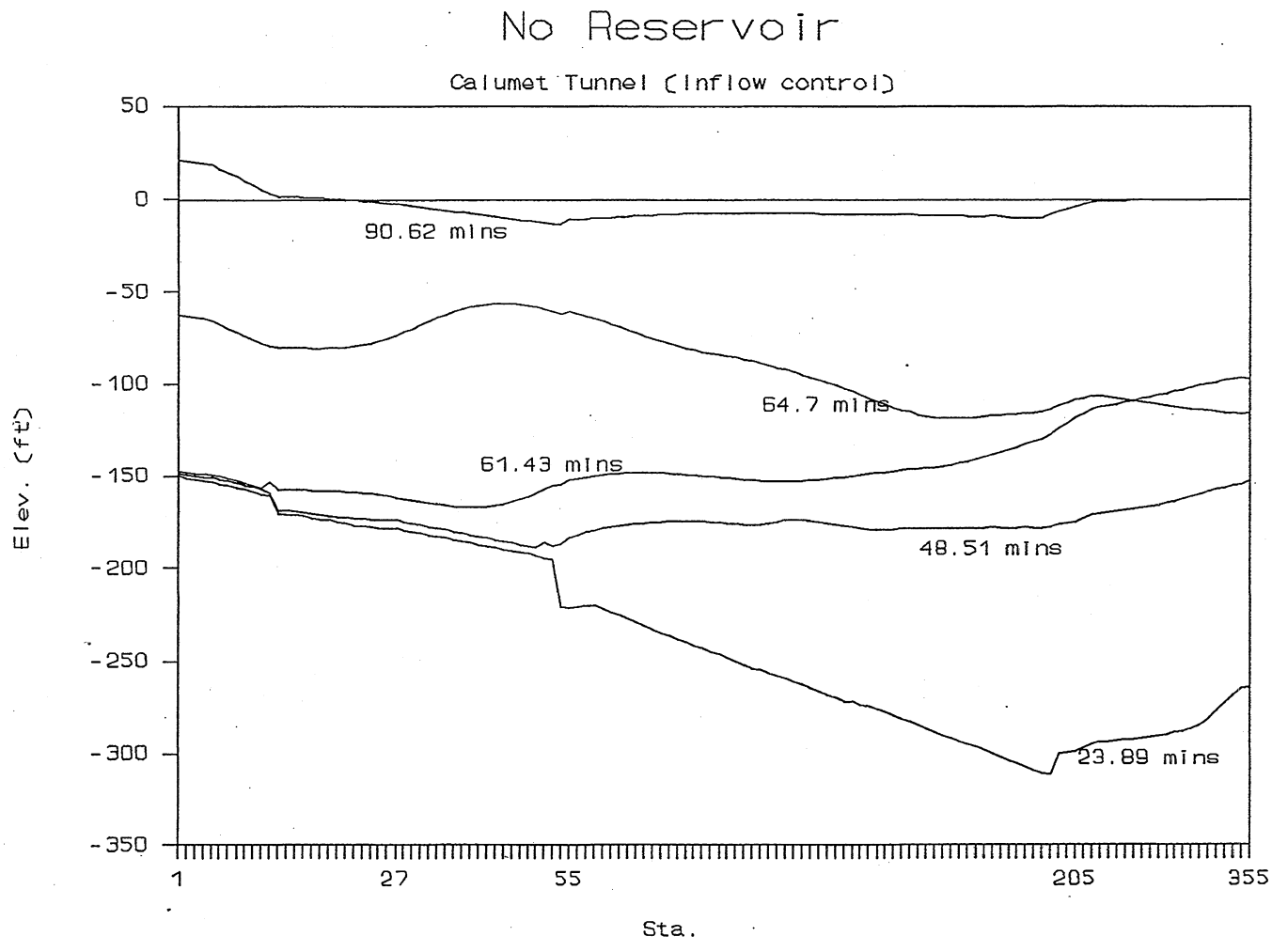

Fig. C-46, Instantaneous hydraulic gradelines in main tunnel of System C-I with inflow control.

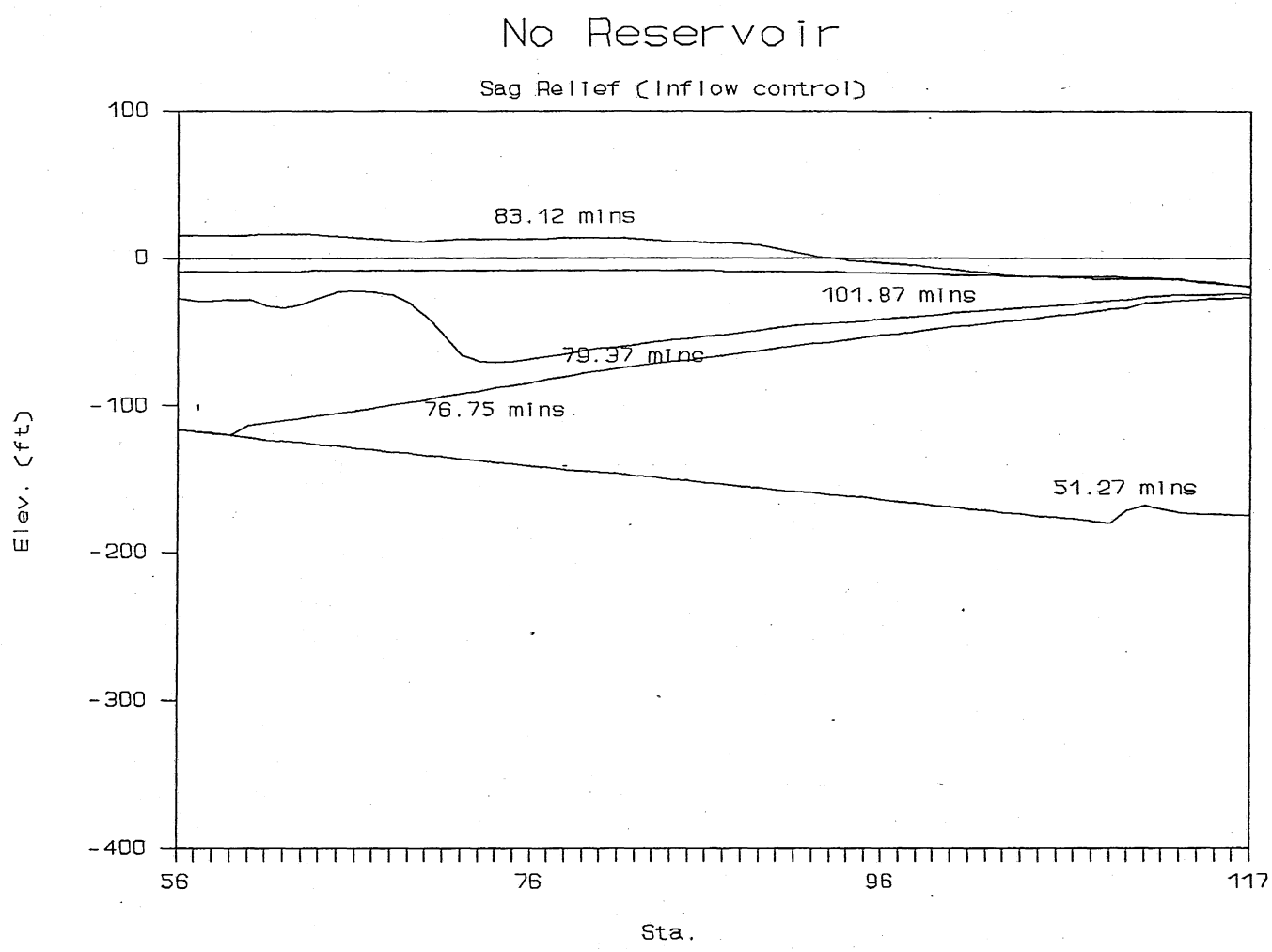

Fig. C-47, Instantaneous hydraulic gradelines in Sag Relief tunnel of System C-I with inflow control.

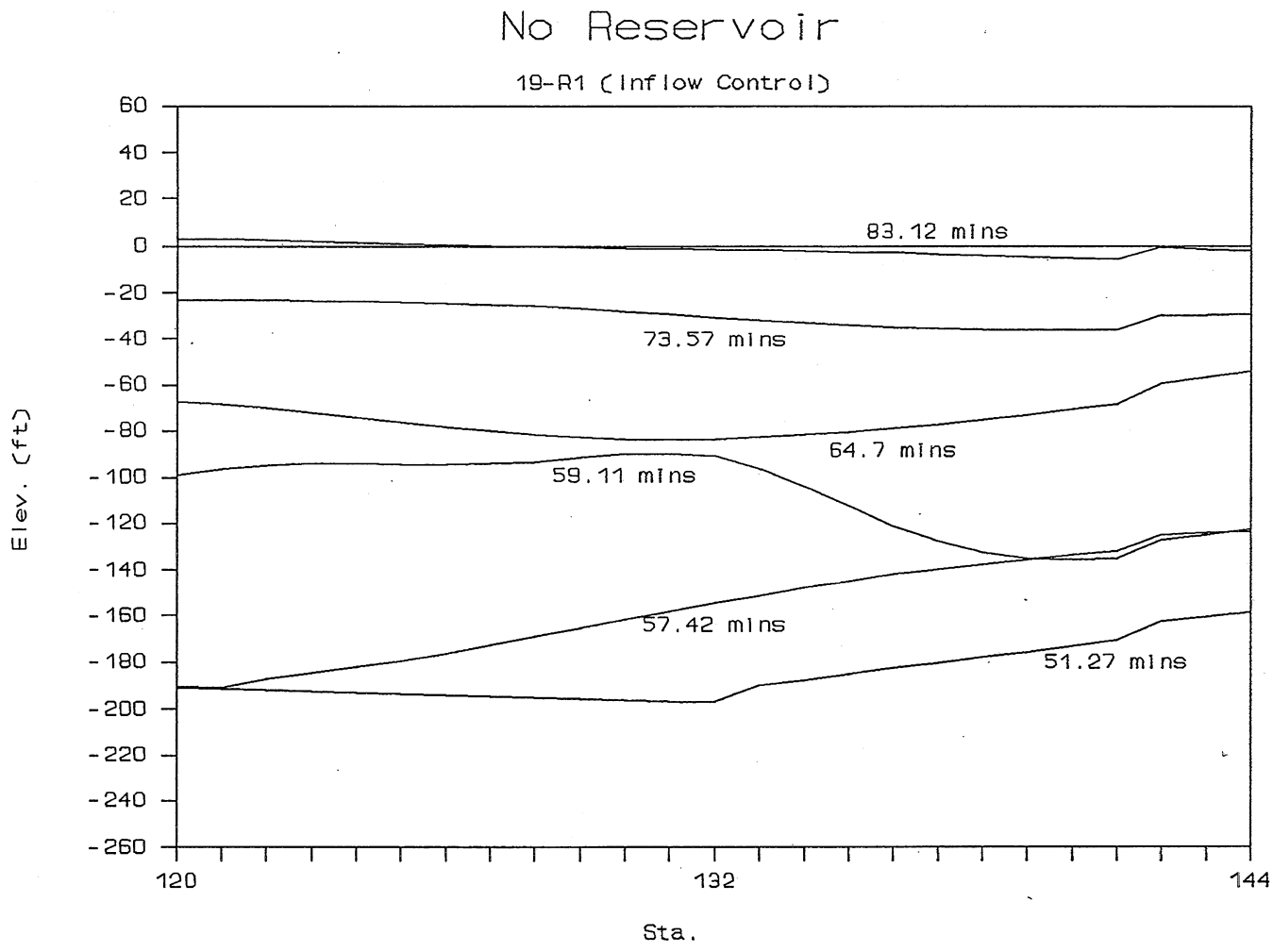

Fig. C-48, Instantaneous hydraulic gradelines in 19R-1 tunnel of System C-I with inflow control.

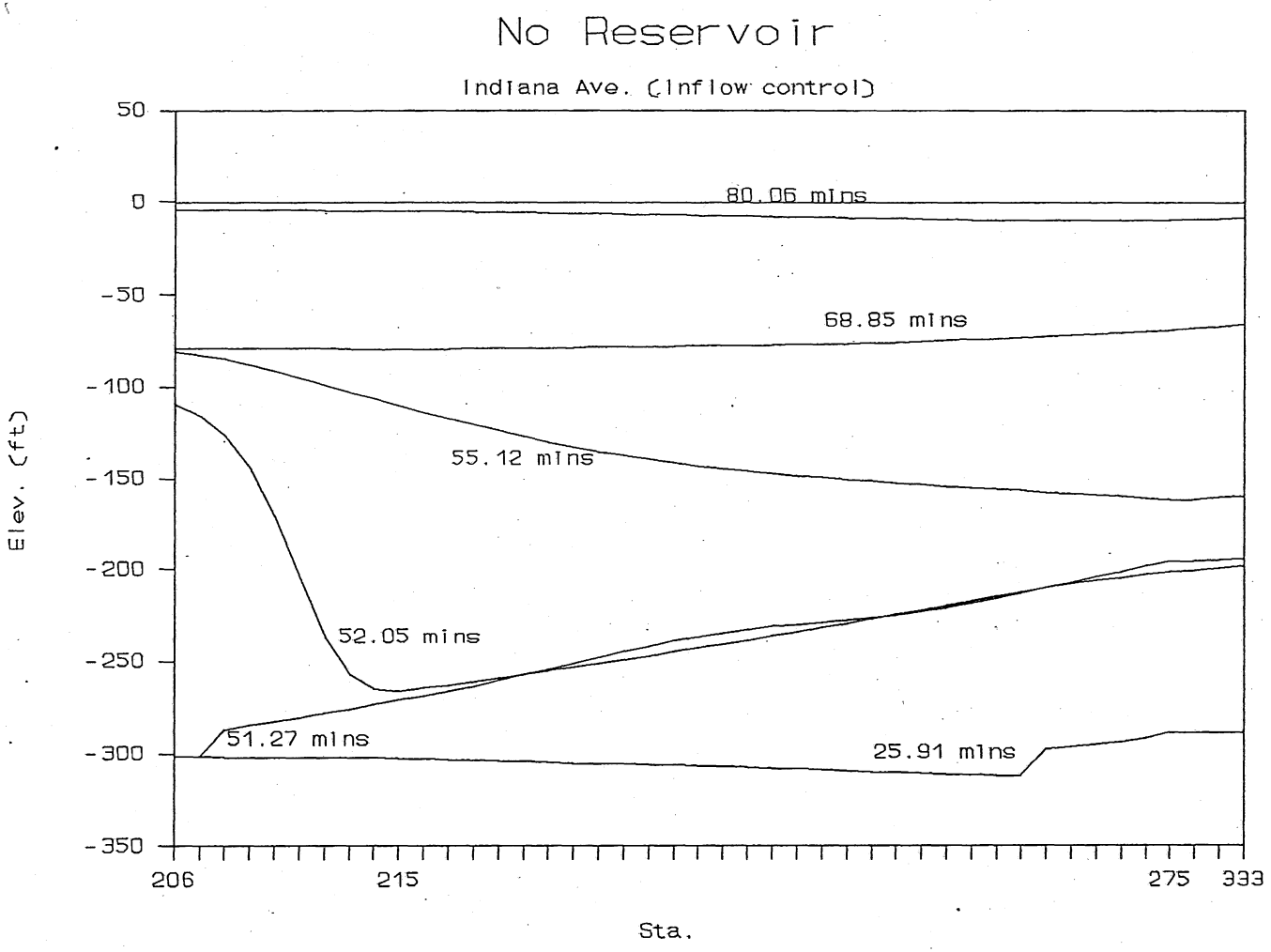

Fig. C-49, Instantaneous hydraulic gradelines in Indiana Avenue tunnel of System C-I with inflow control.

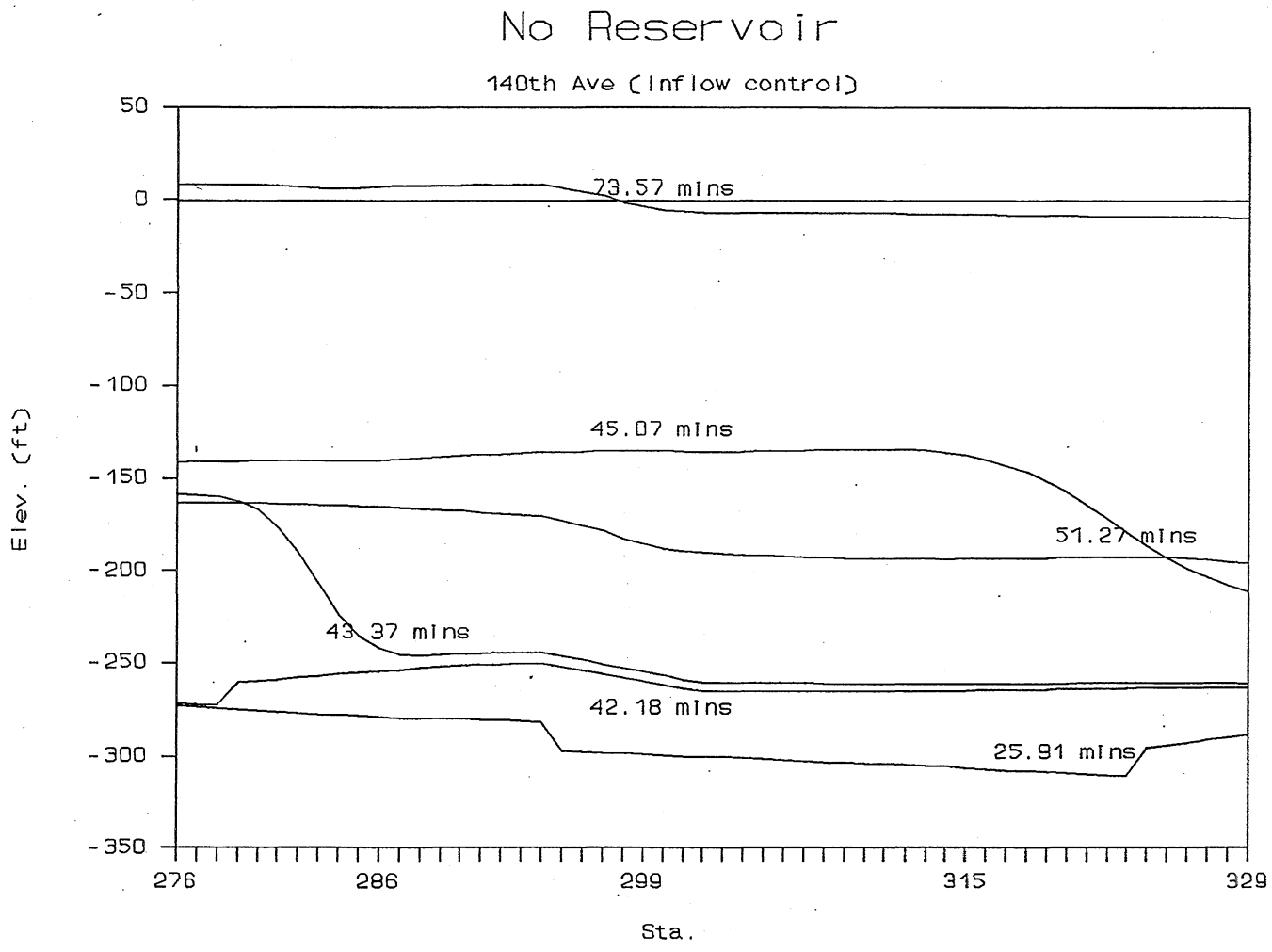

Fig. C-50, Instantaneous hydraulic gradelines in 140th Avenue tunnel of System C-I with inflow control.

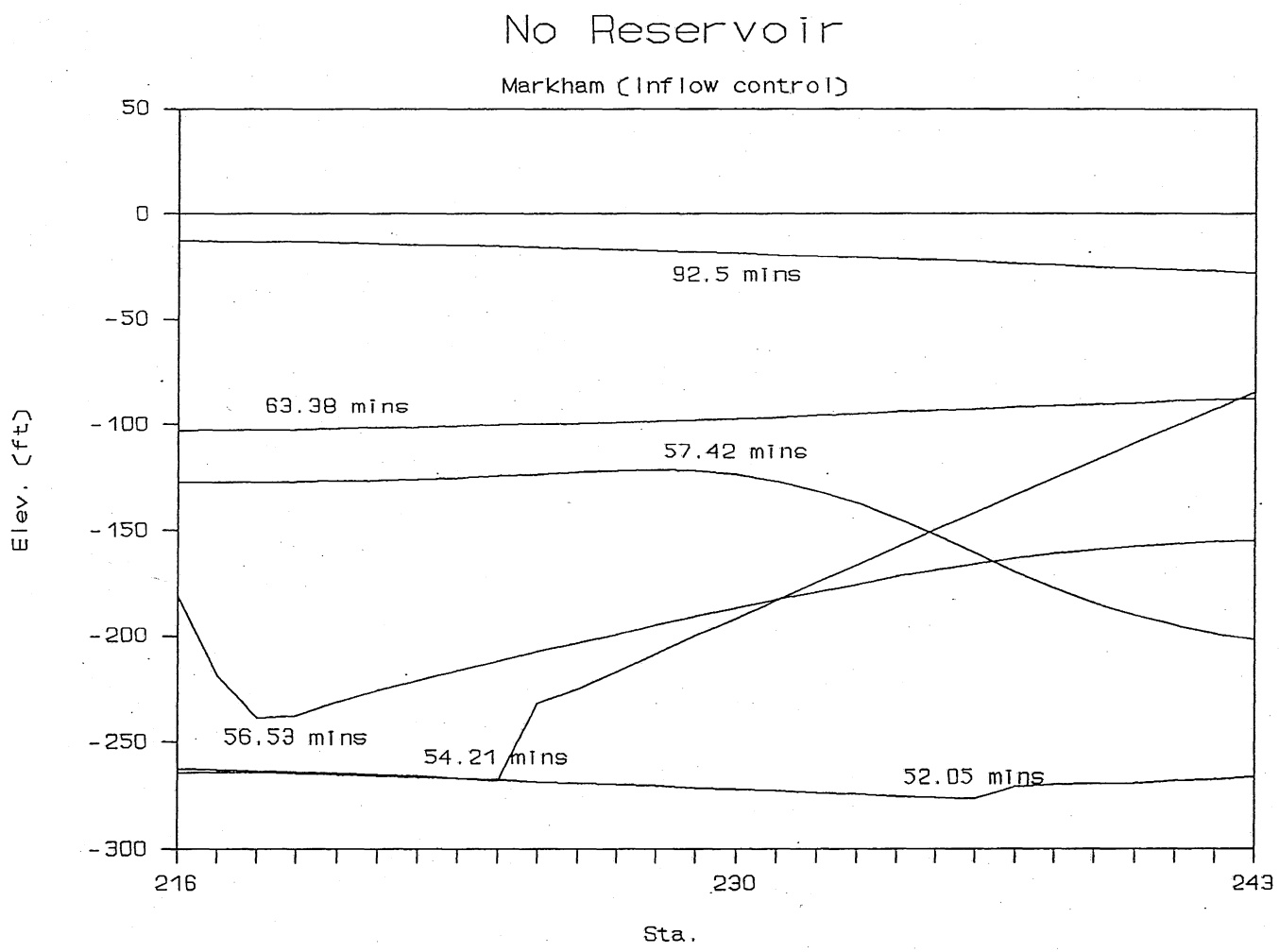

Fig. C-51, Instantaneous hydraulic gradelines in Markham tunnel of System C-I with inflow control.

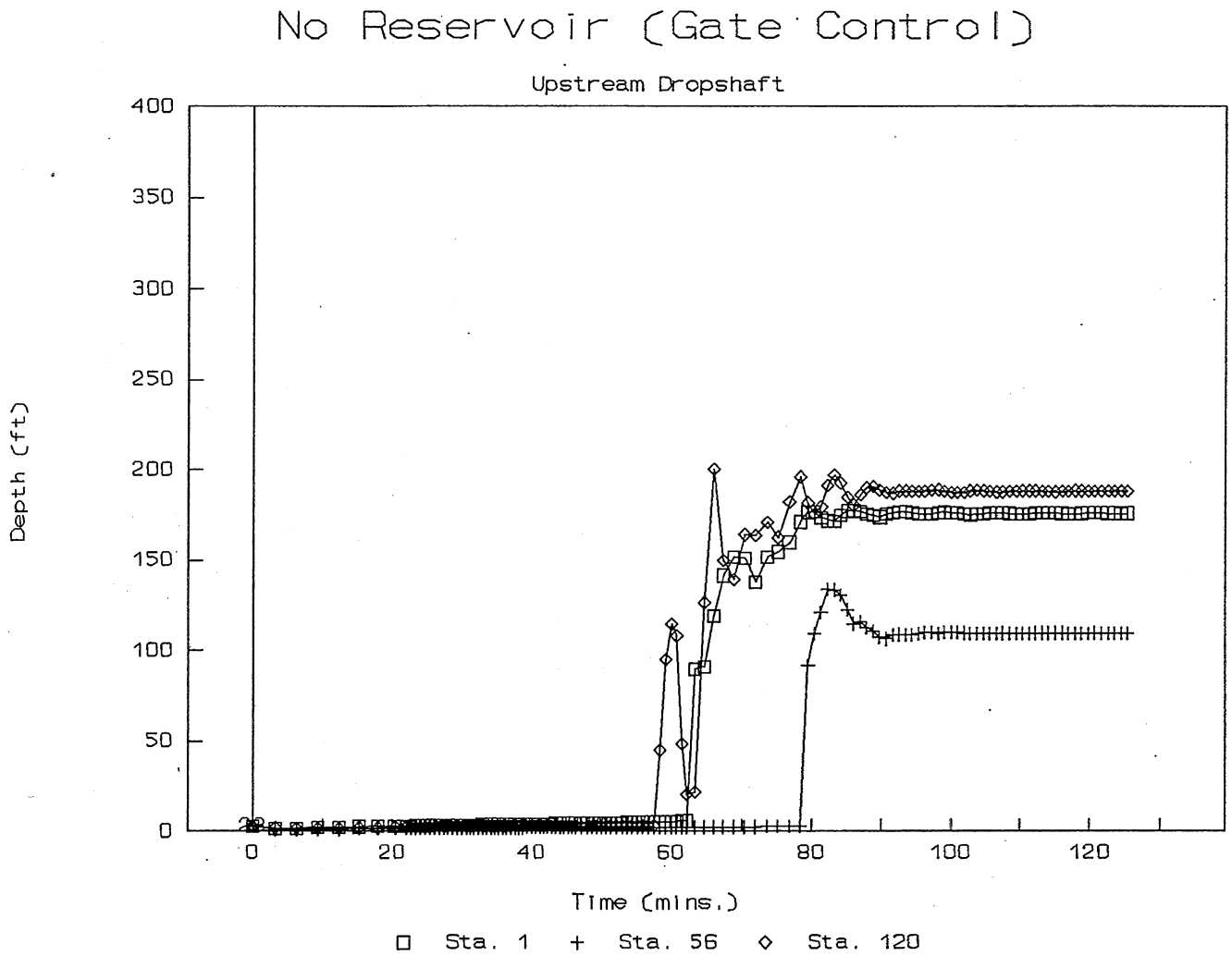

Fig. C-52, Time variation of water depth in system C-I with inflow control (Sta. 1, 56, 120).

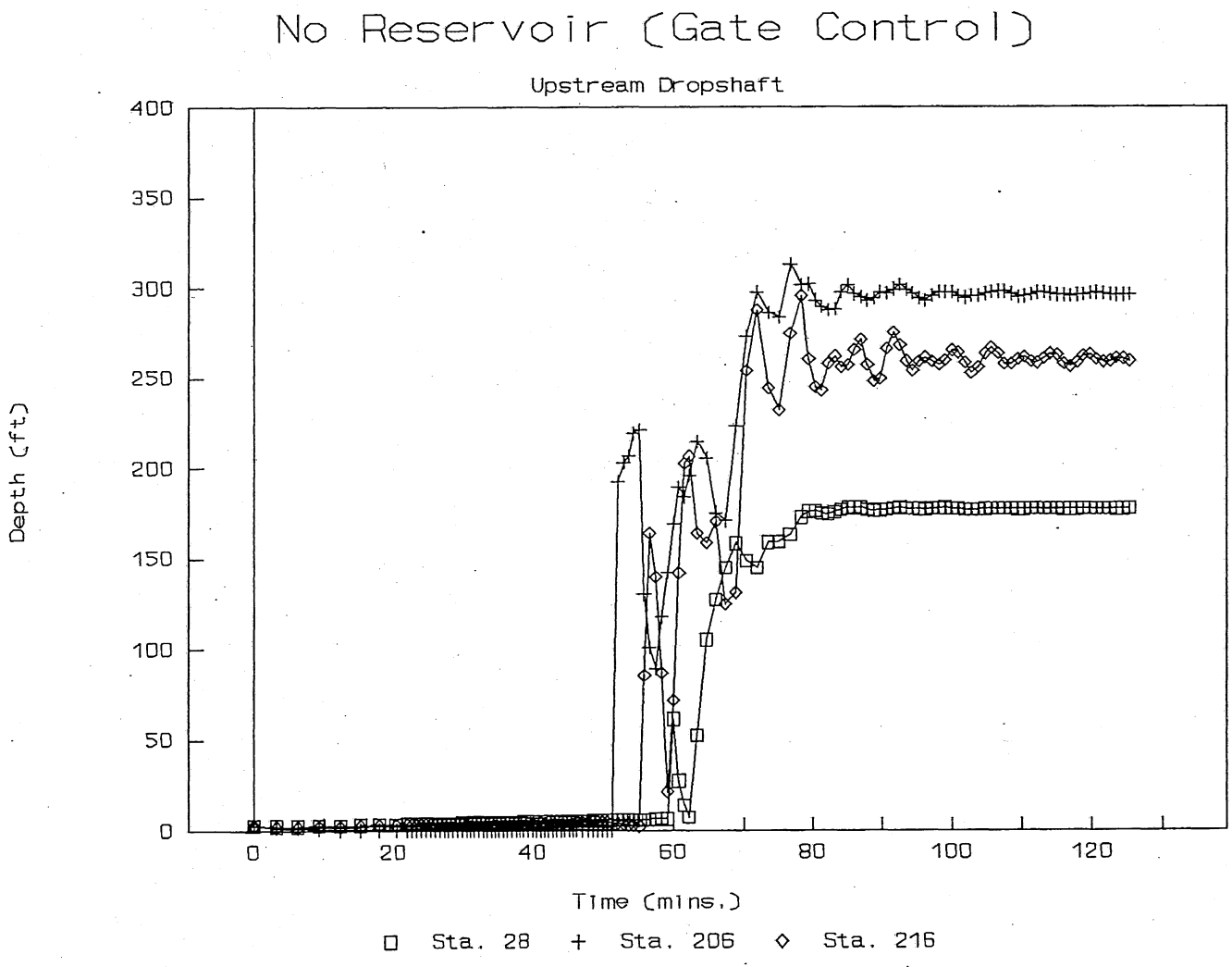

Fig. C-53, Time variation of water depth in system C-I with inflow control (Sta. 28, 206, 216).

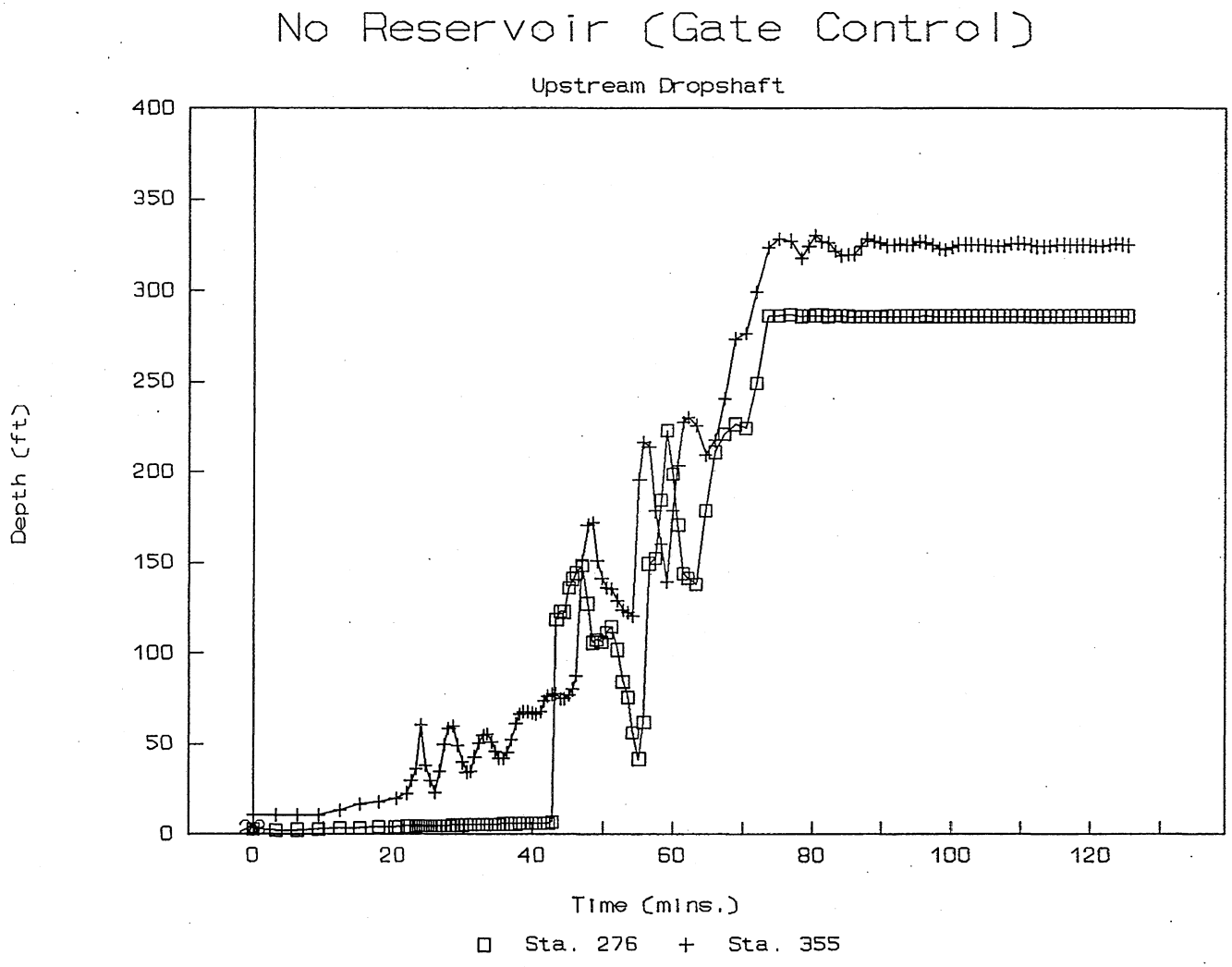

Fig. C-54, Time variation of water depth in system C-I with inflow control (Sta. 276, 355).

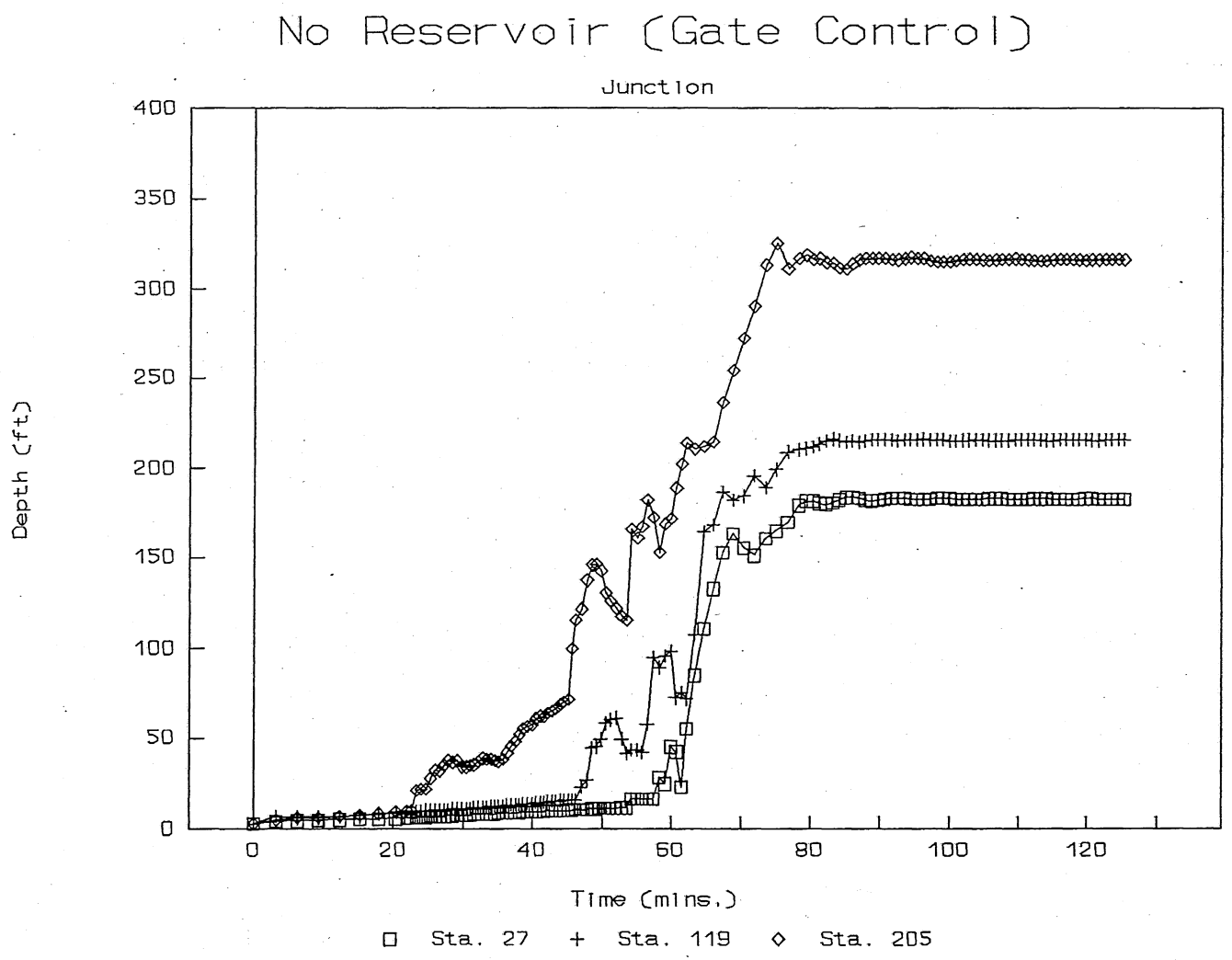

Fig. C-55, Time variation of water depth in system C-I with inflow control (Sta. 27, 119, 205).

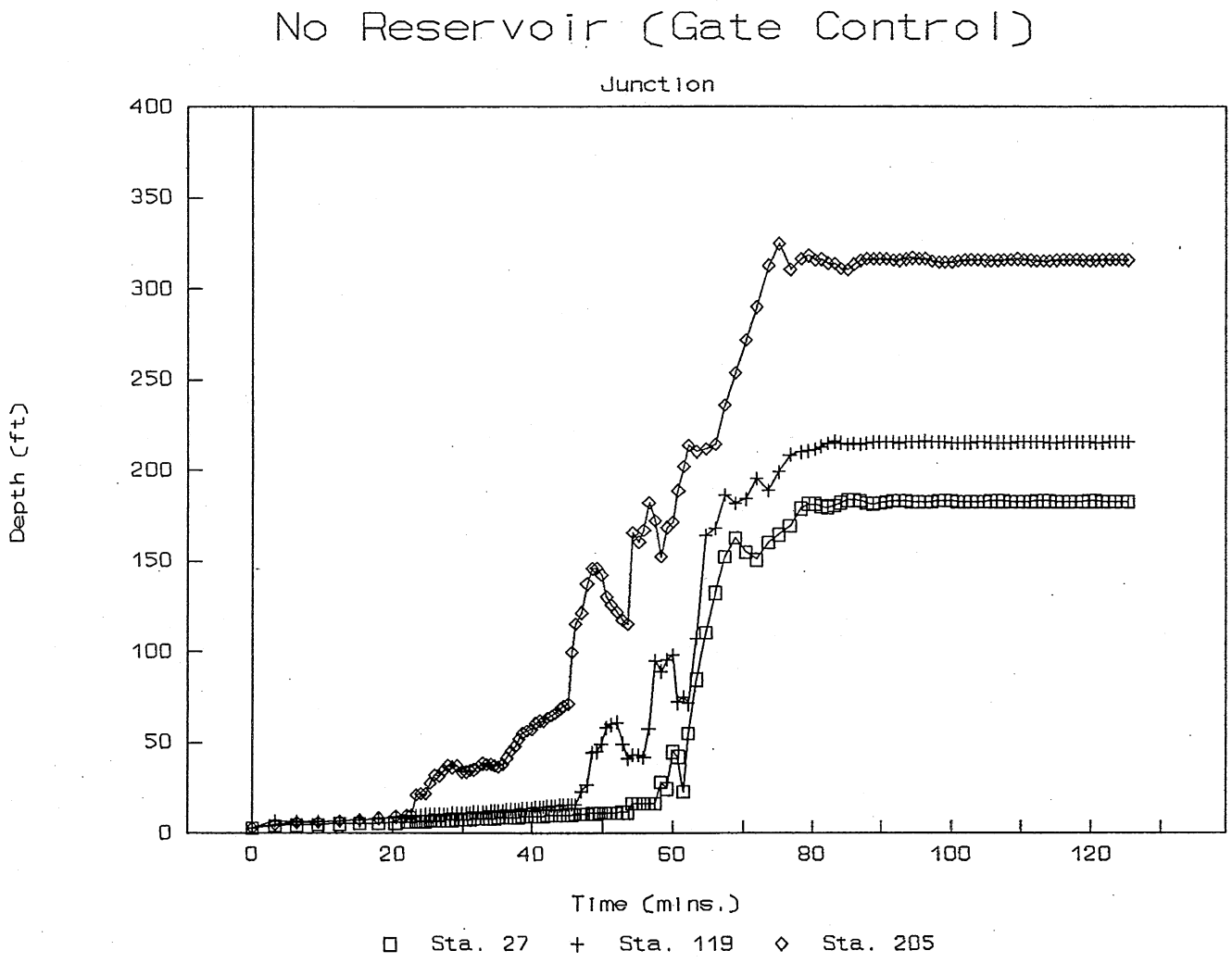

Fig. C-56, Time variation of water depth in system C-I with inflow control (Sta. 55, 215, 275).

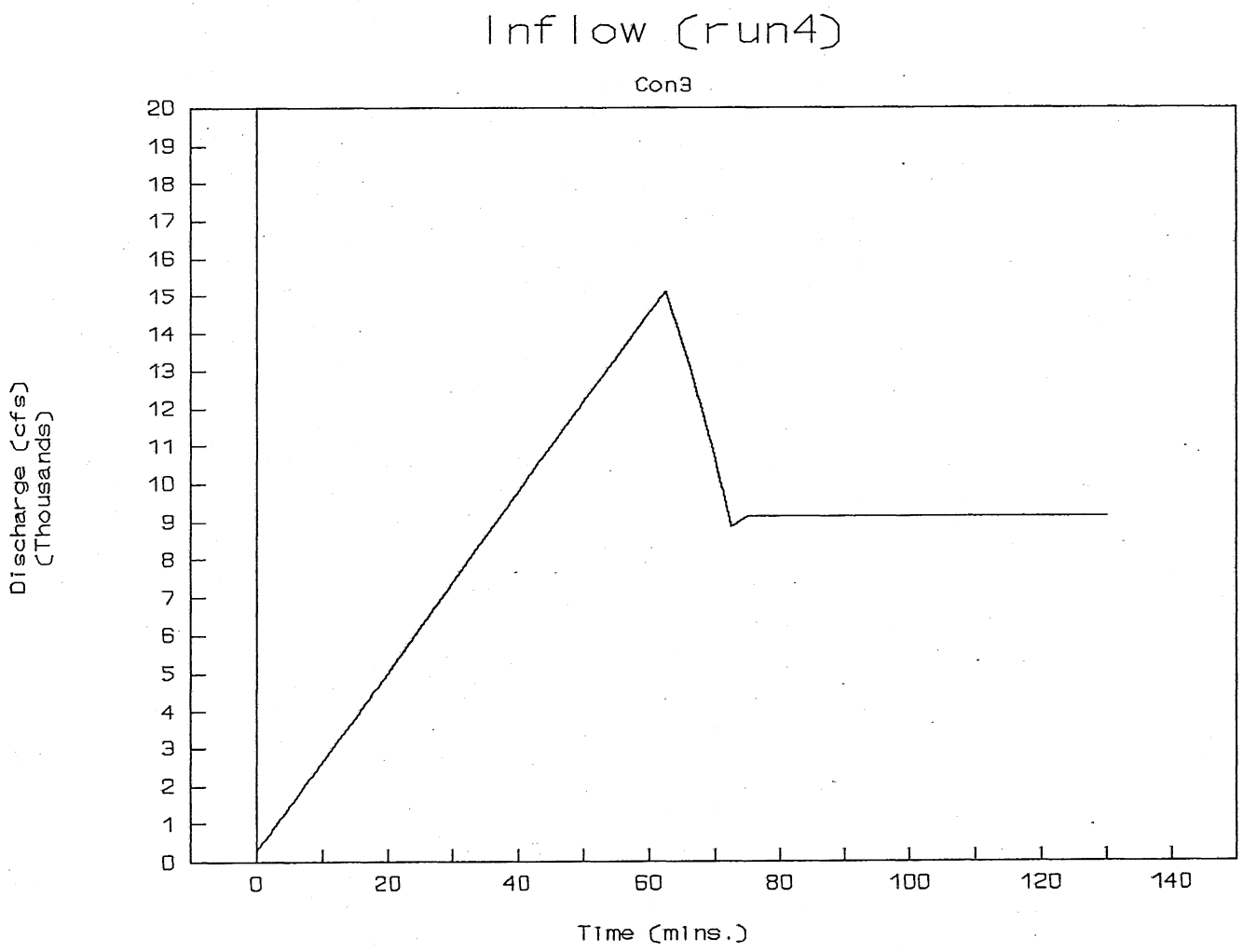

Fig. C-57, Total allowable inflow hydrograph, System C-III.

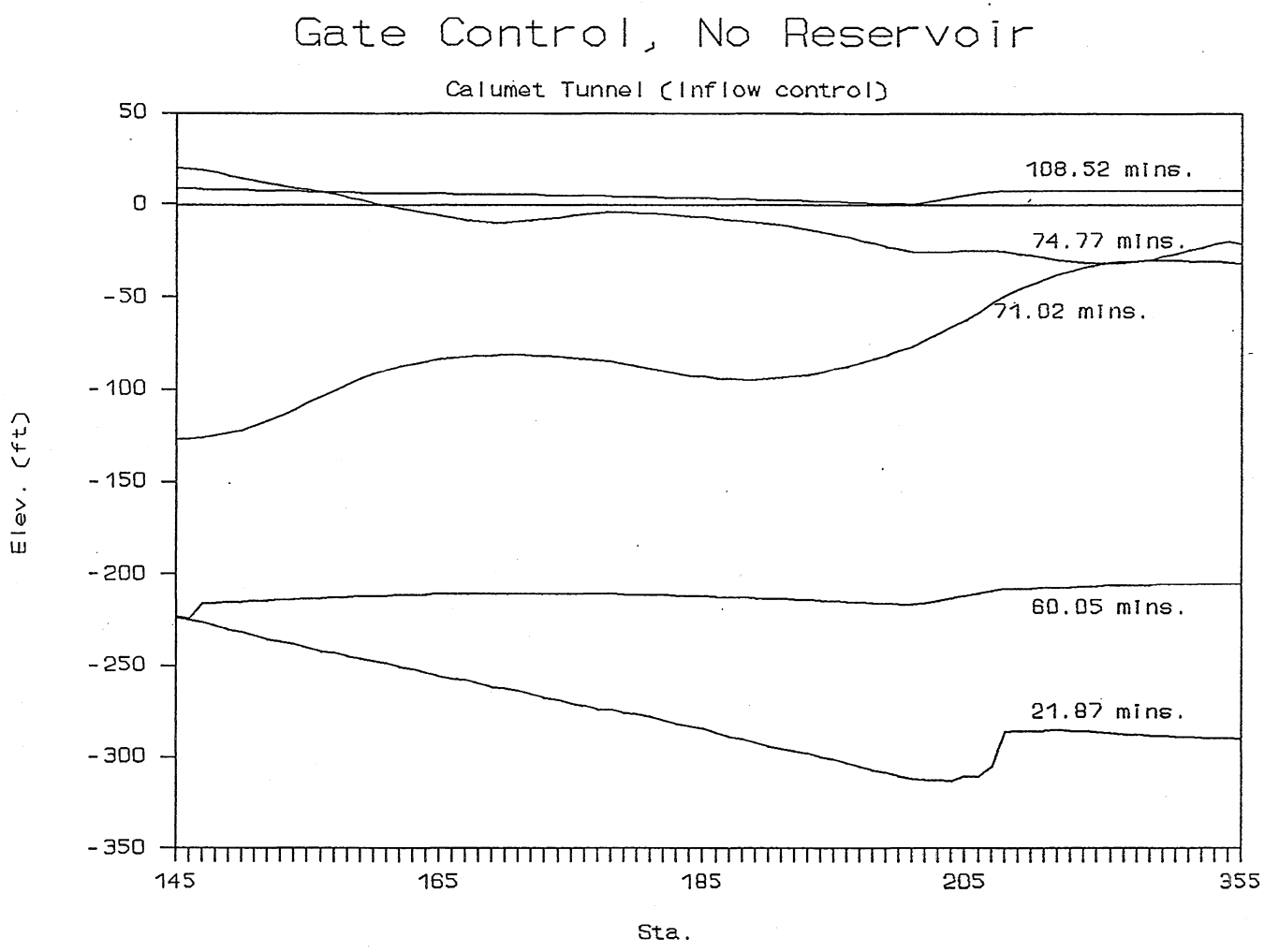

Fig. C-58, Instantaneous hydraulic grade lines in the main tunnel of System C-III with gate control.

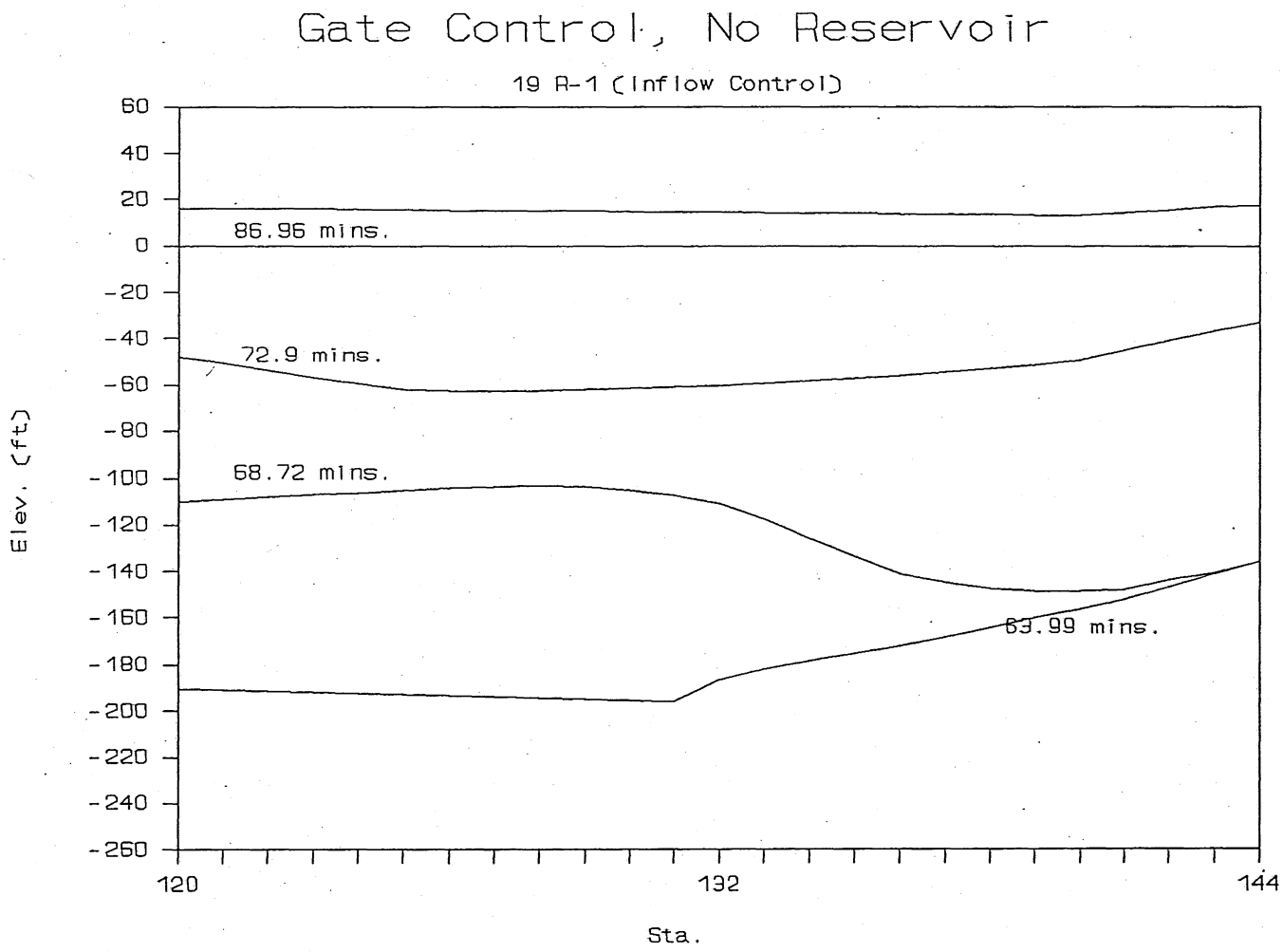

Fig. C-59, Instantaneous hydraulic gradelines in 19R-1 tunnel of System C-III with gate control

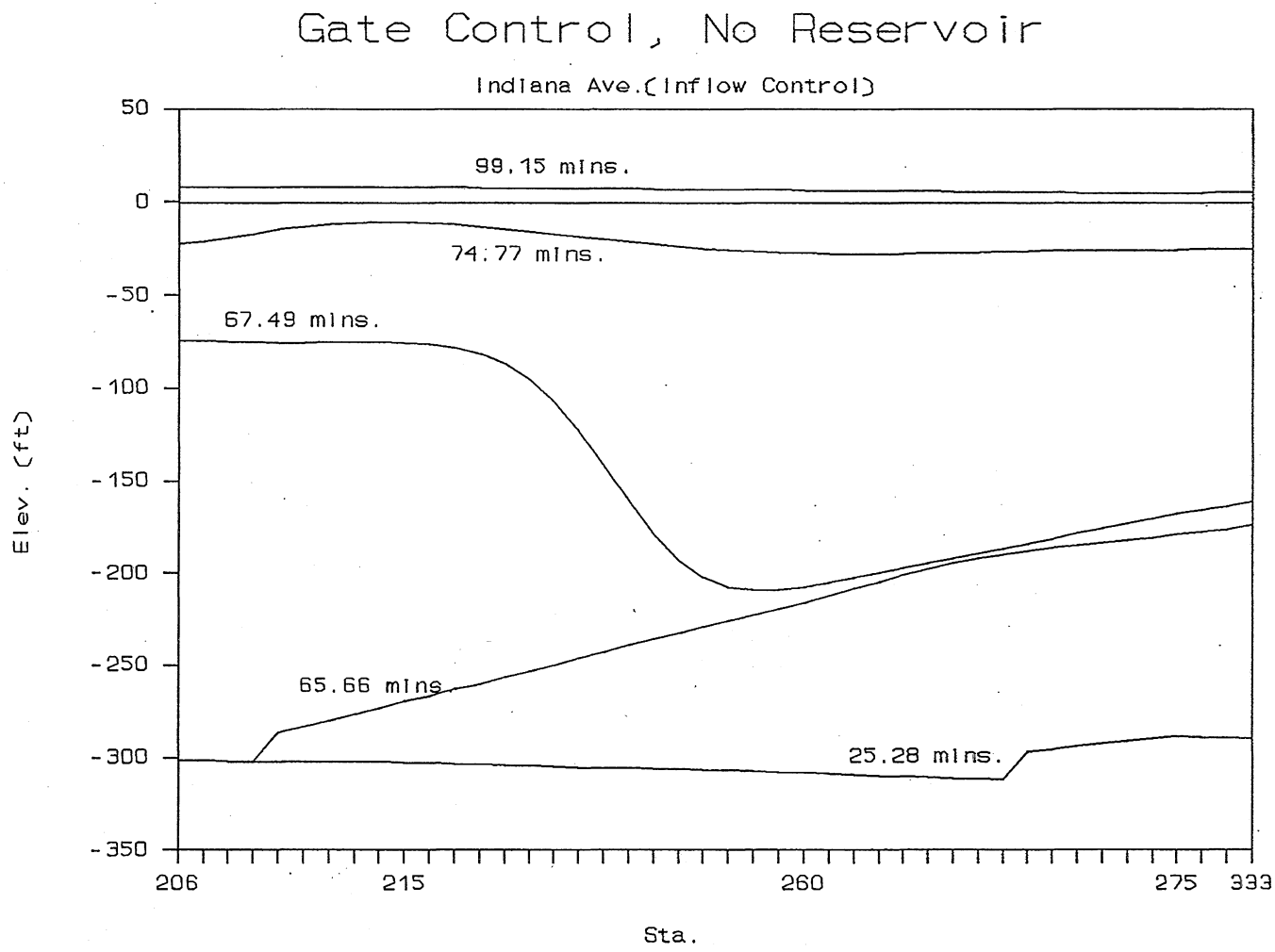

Fig. C-60, Instantaneous hydraulic gradelines in Indiana Avenue tunnel of System C-III with gate control.

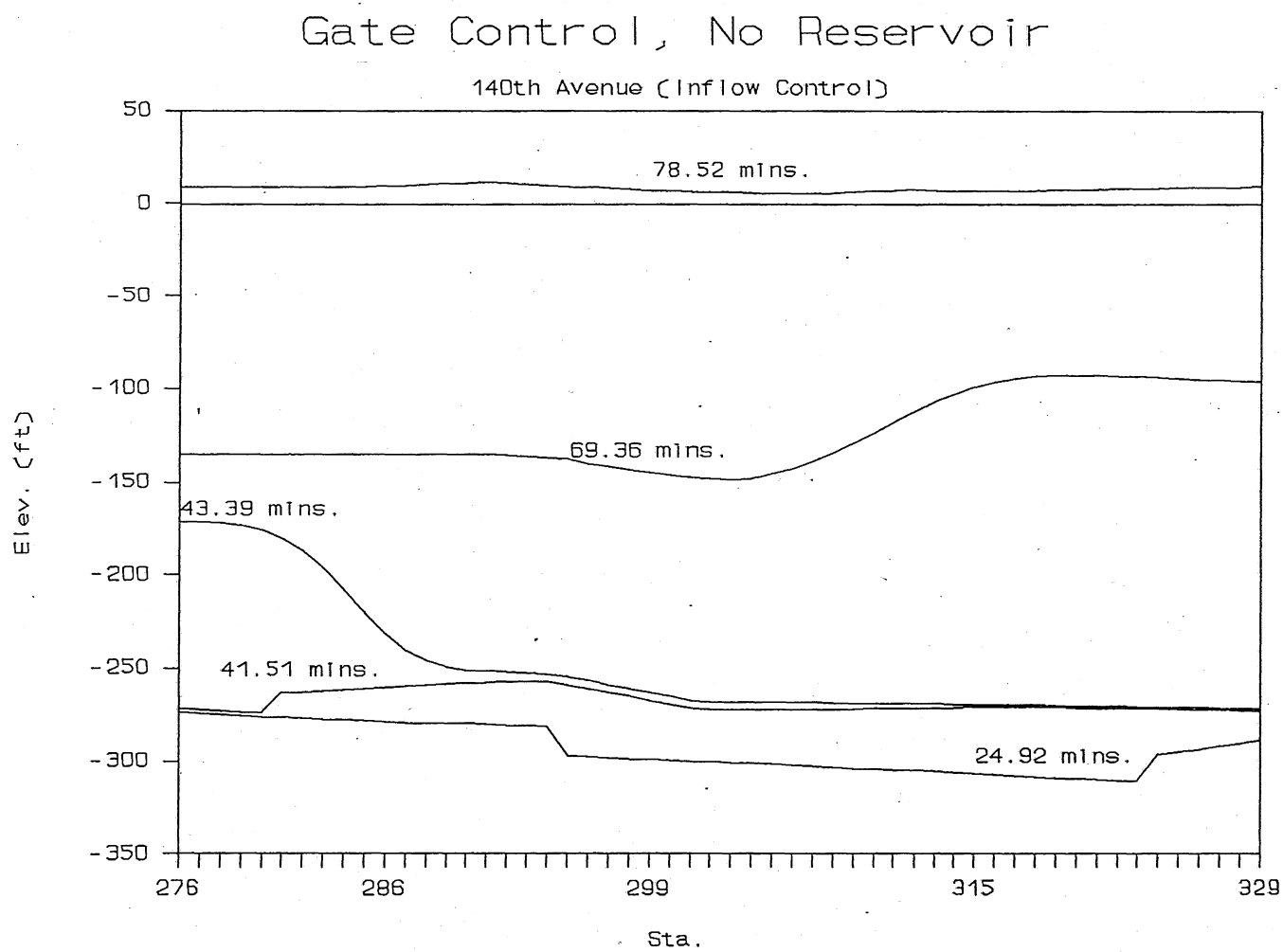

Fig. C-61, Instantaneous hydraulic grade lines in 140th Avenue tunnel of System C-III with gate control.

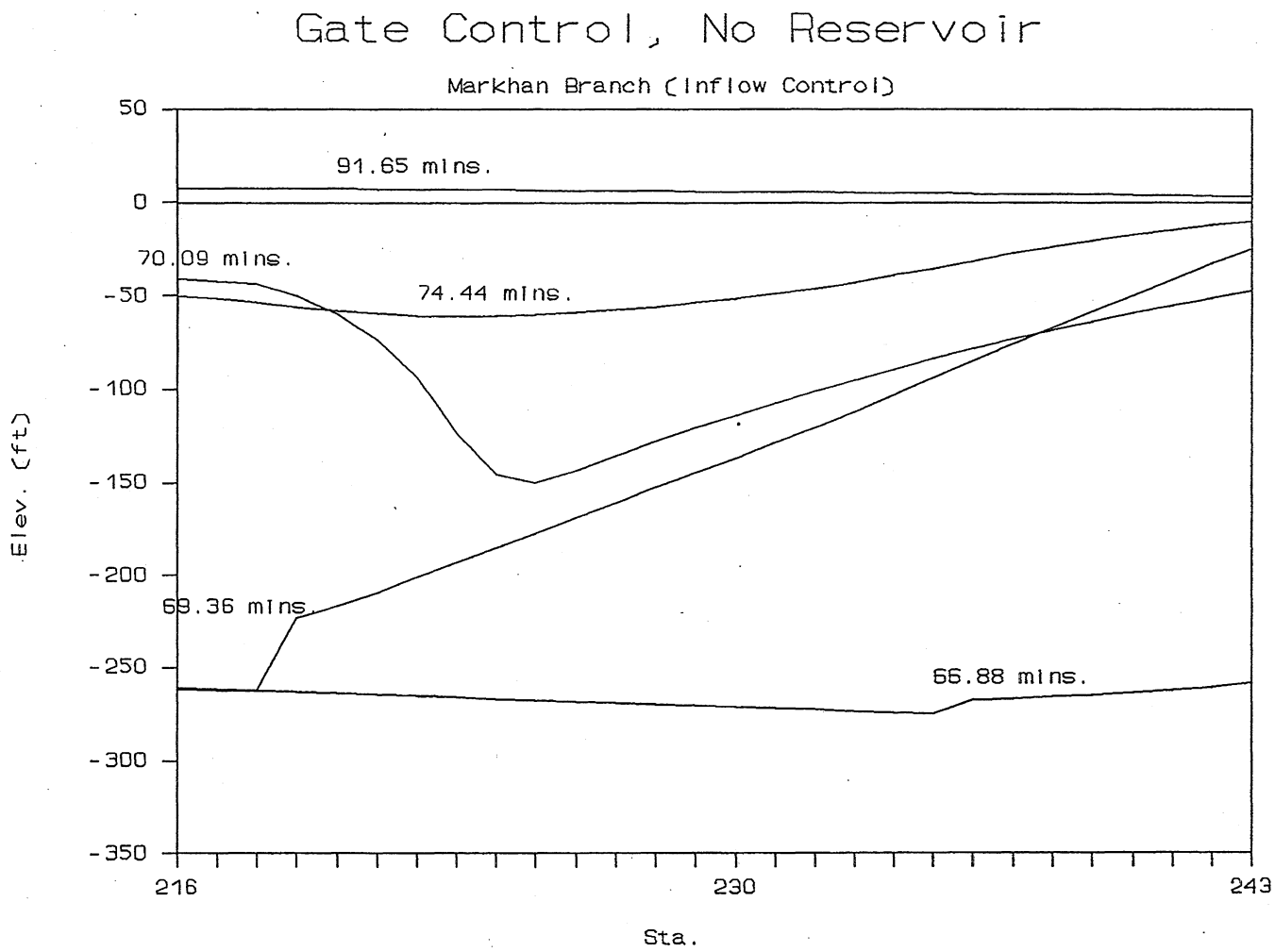

Fig. C-62, Instantaneous hydraulic gradelines in Markham tunnel of System C-III with gate control.

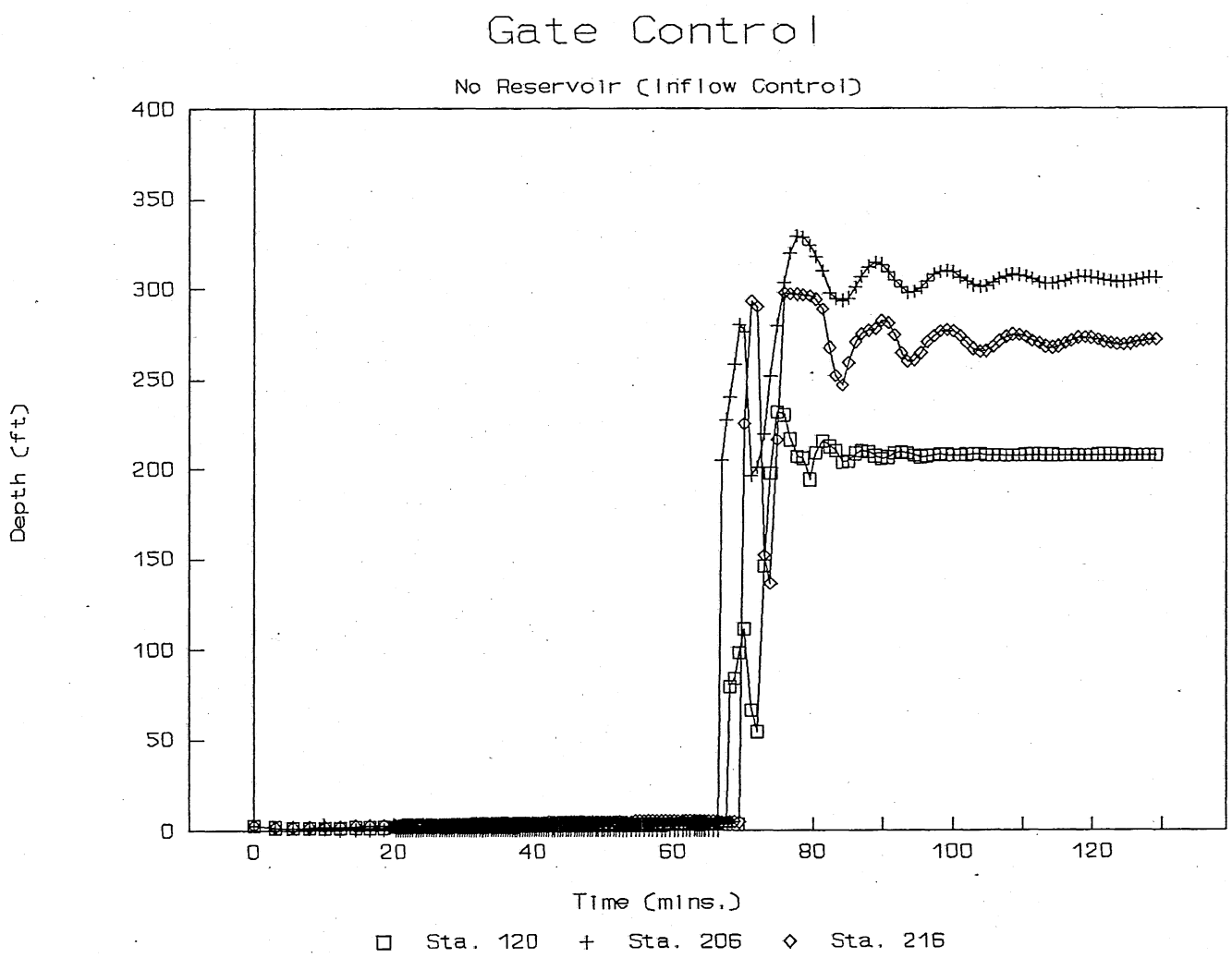

Fig. C-63, Time variation of water depth in System C-III with inflow control (Sta. 120, 206, 216).

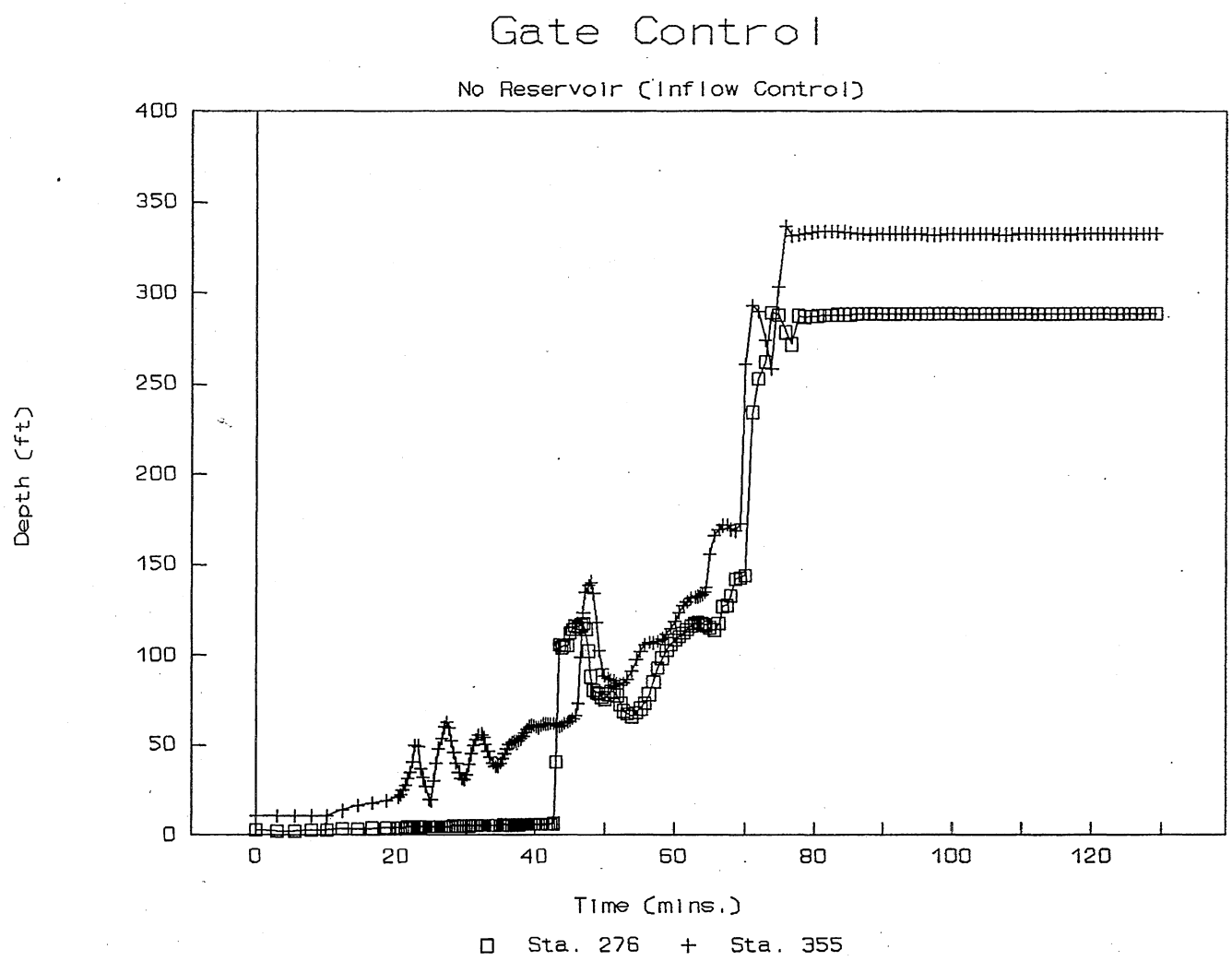

Fig. C-64, Time variation of water depth in System C-III with inflow control (Sta. 276, 355).

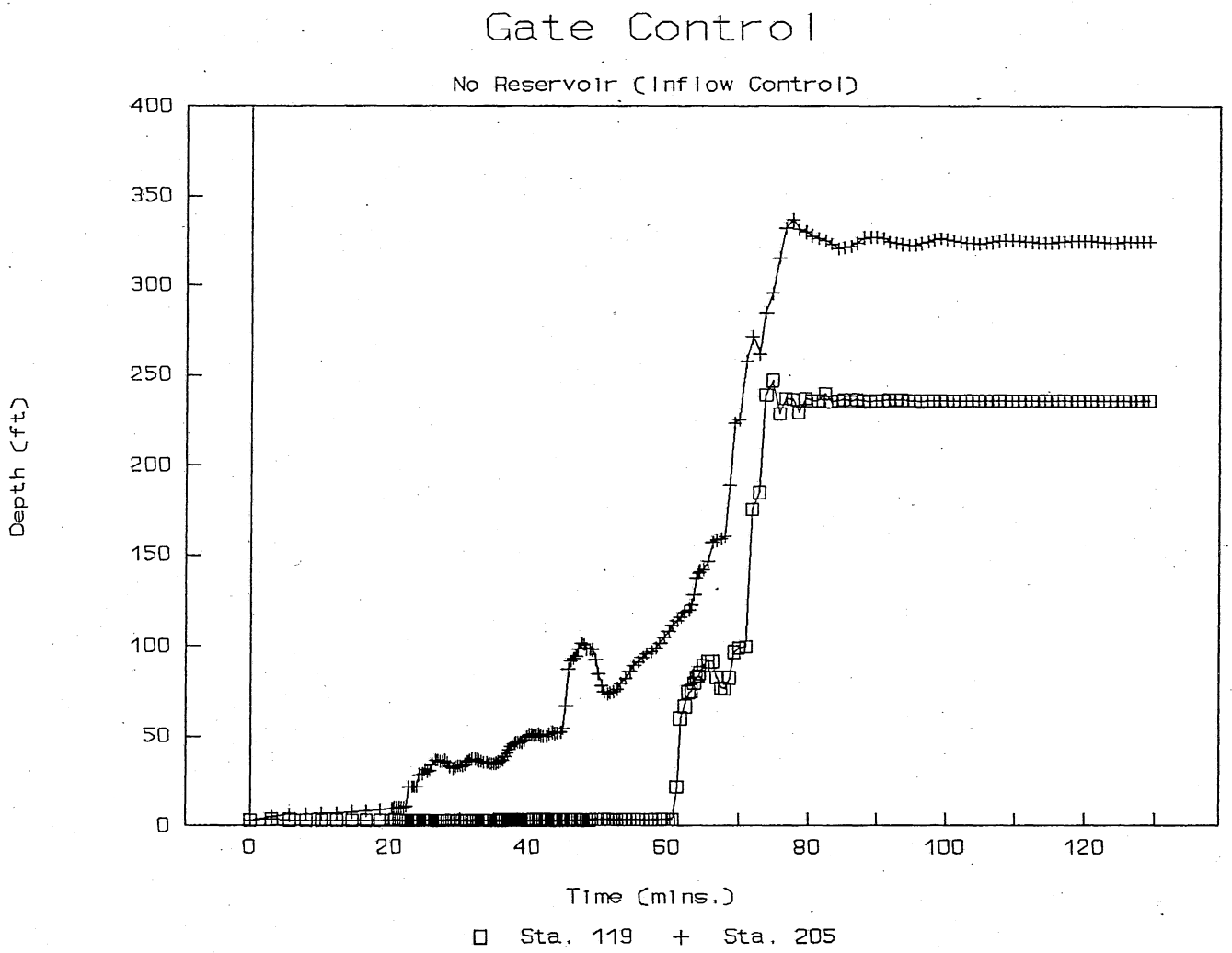

Fig. C-65, Time variation of water depth in System C-III with inflow control (Sta. 119, 205).

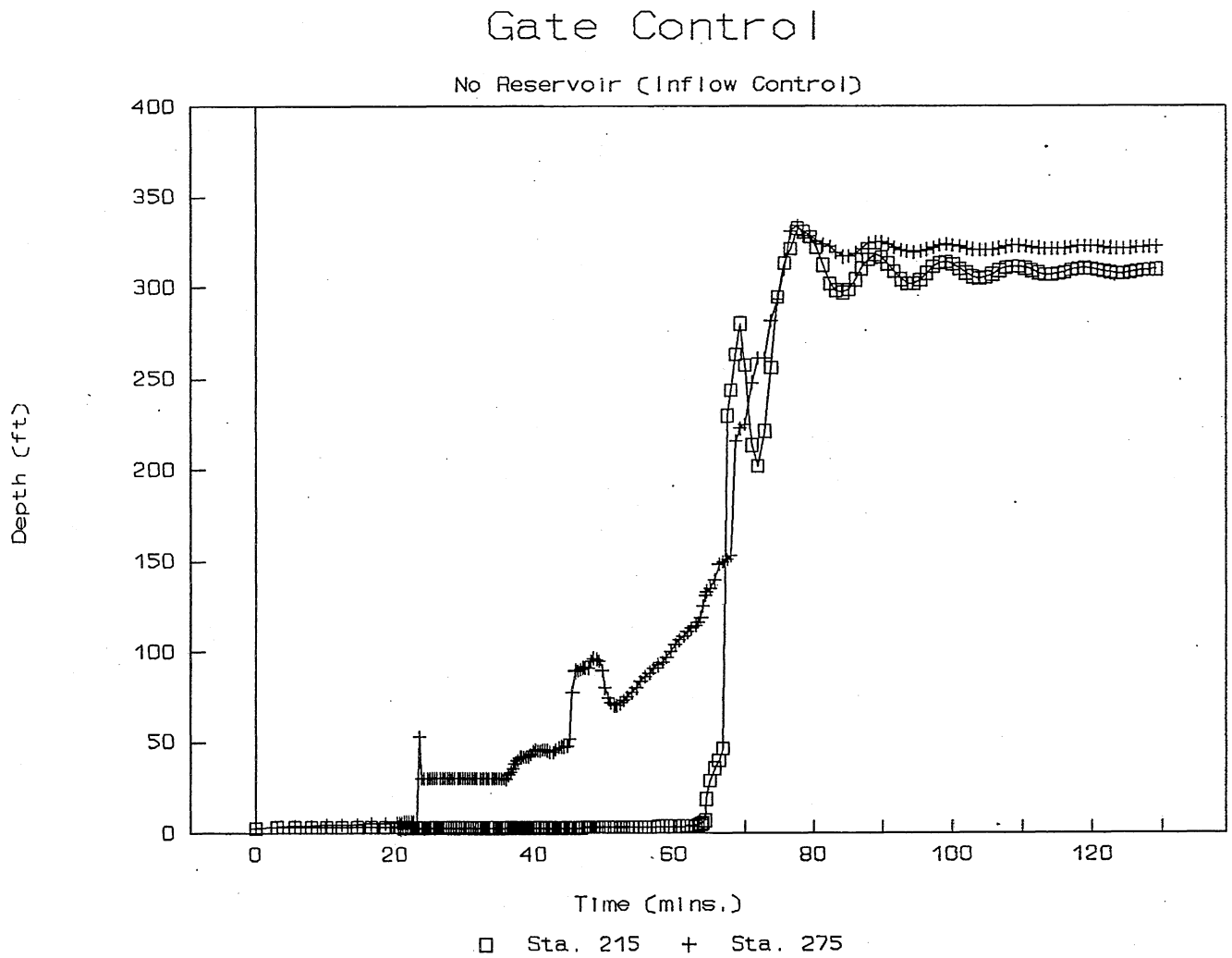

Fig. C-66, Time variation of water depth in System C-III with inflow control (Sta. 215, 275).

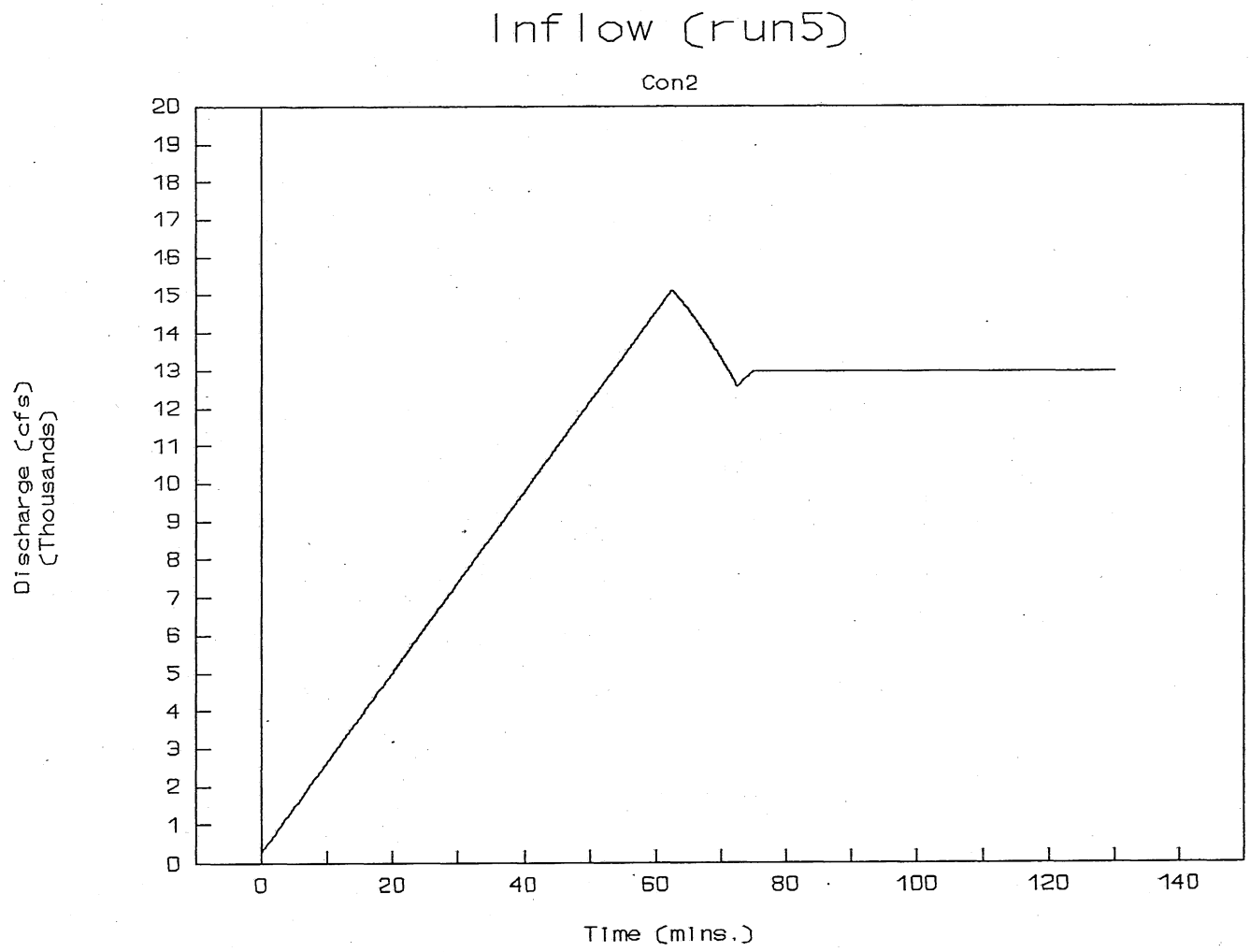

Fig. C-67, Total allowable inflow hydrograph for System C-IV.

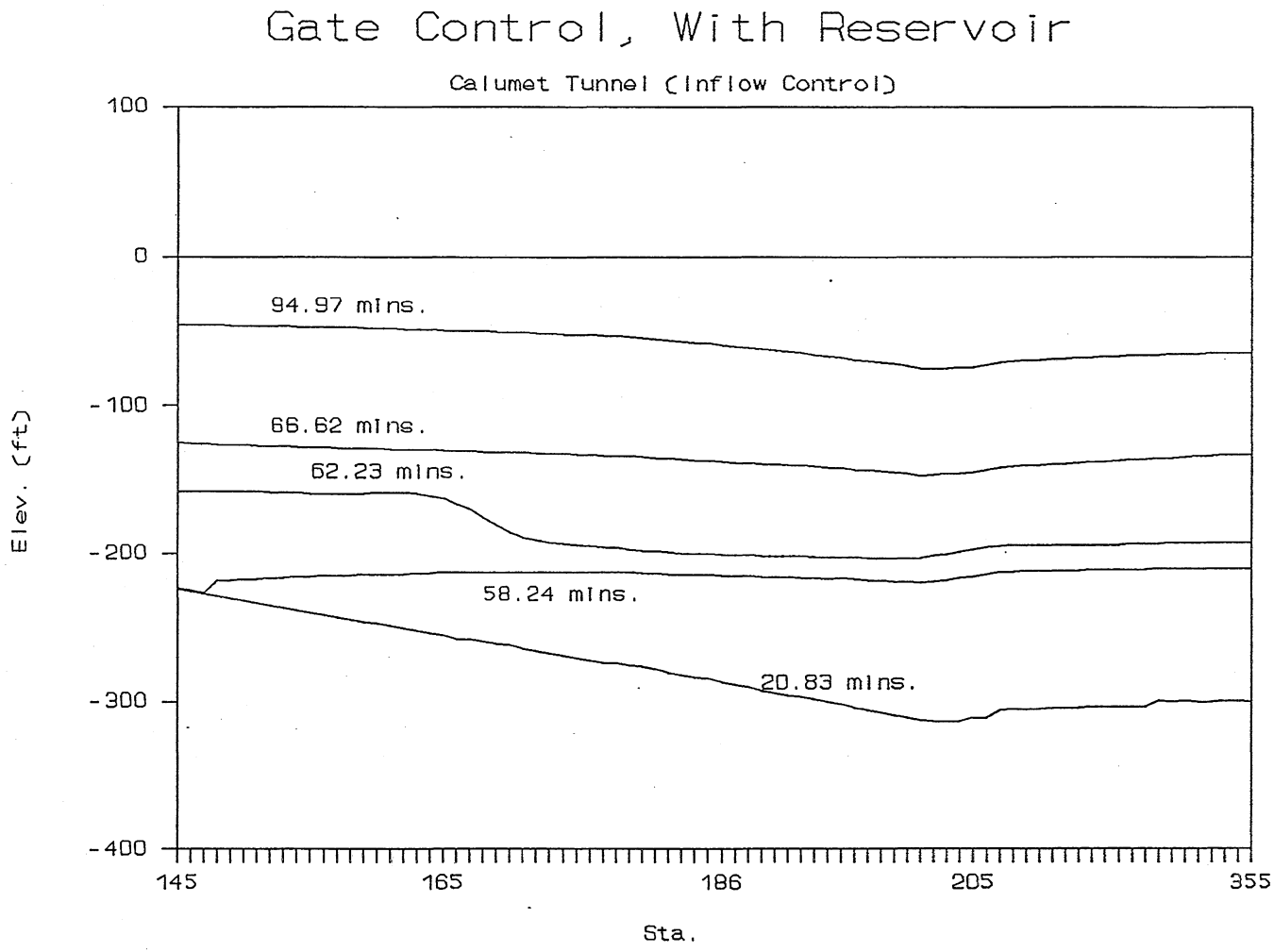

Fig. C-68, Instantaneous hydraulic gradelines in the main tunnel of System C-IV with inflow control.

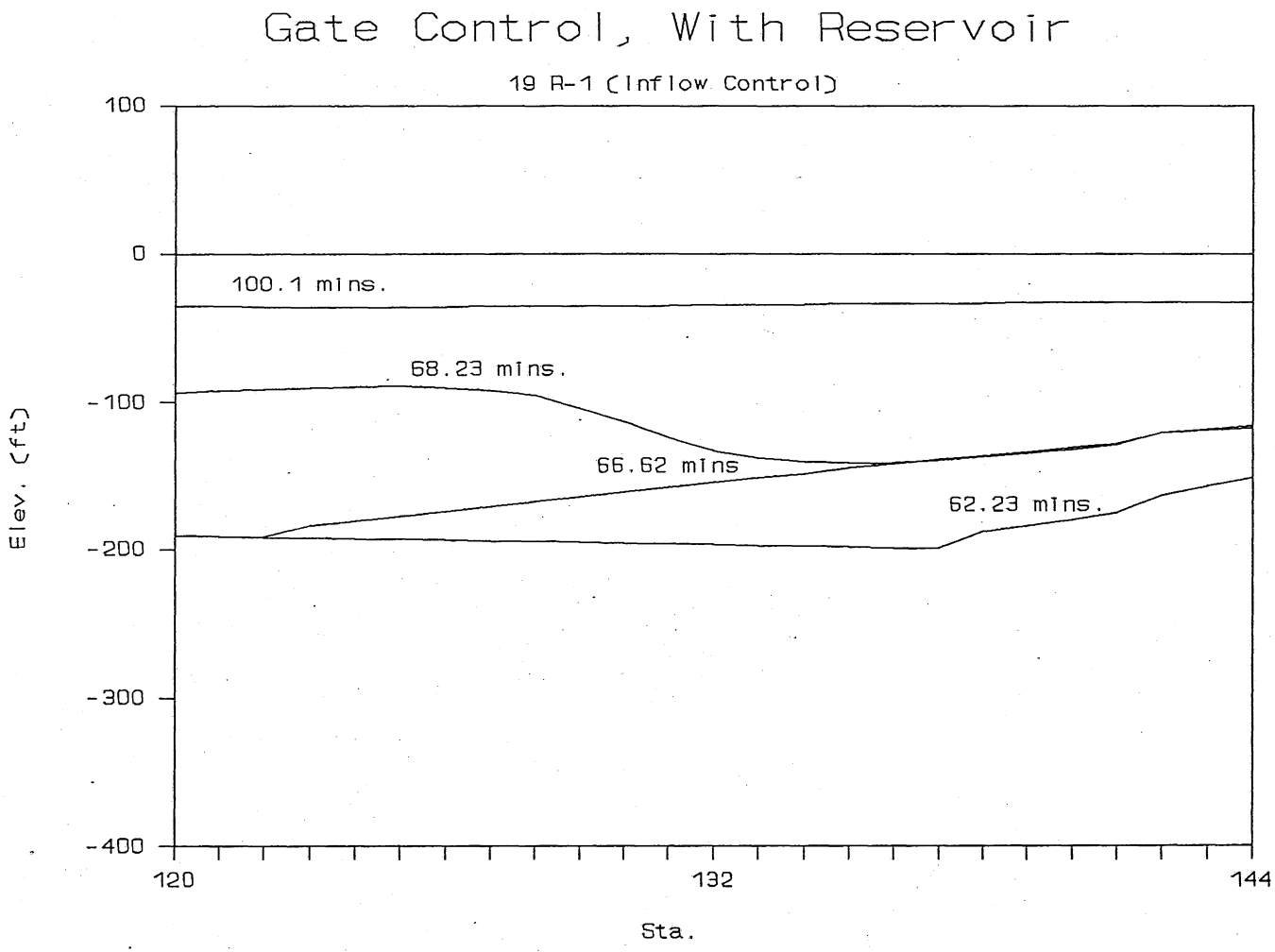

Fig. C-69, Instantaneous hydraulic gradelines in 19R-1 tunnel of System C-IV with inflow control.

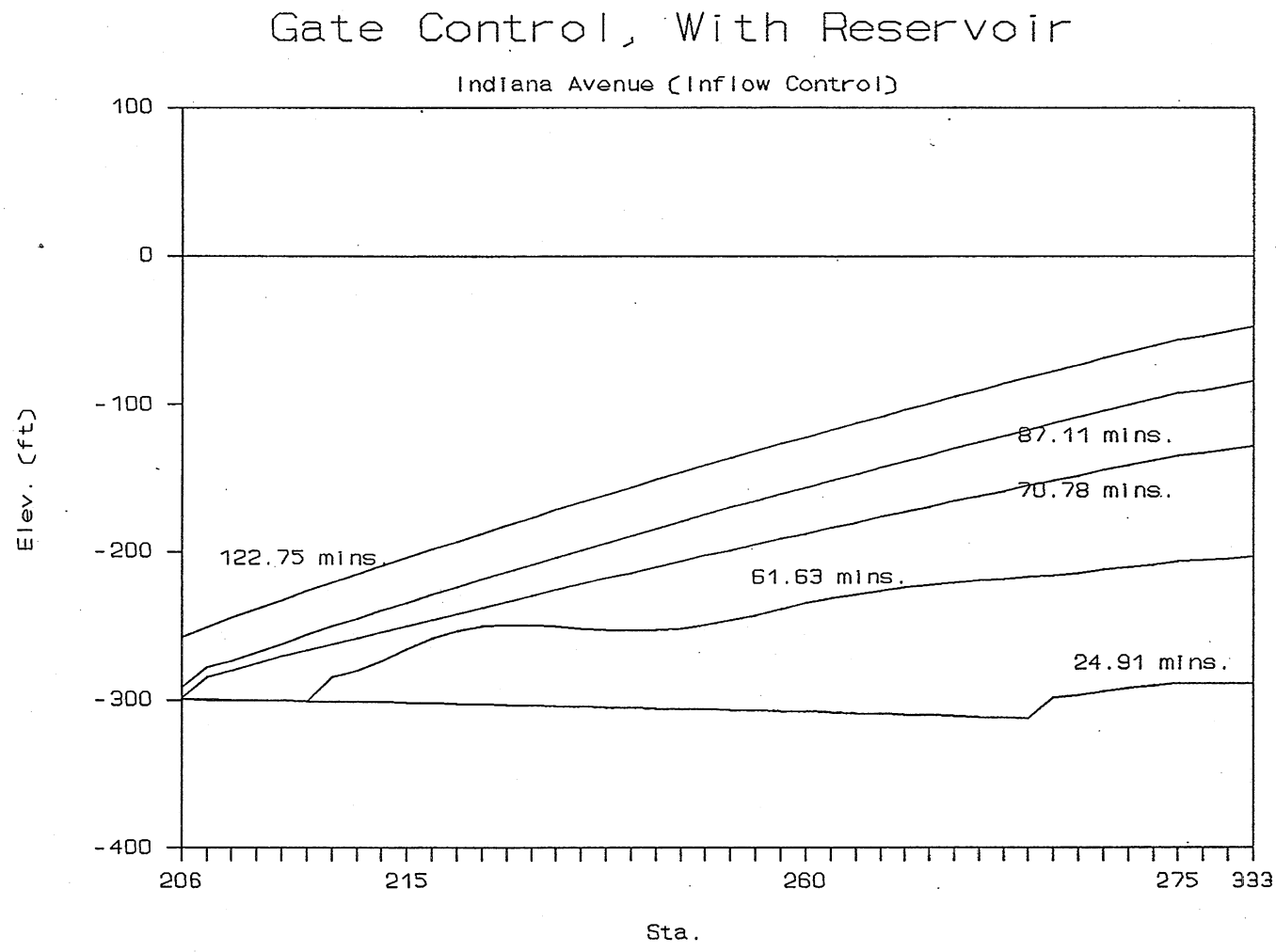

Fig. C-70, Instantaneous hydraulic gradelines in Indiana Avenue tunnel of System C-IV with inflow control.

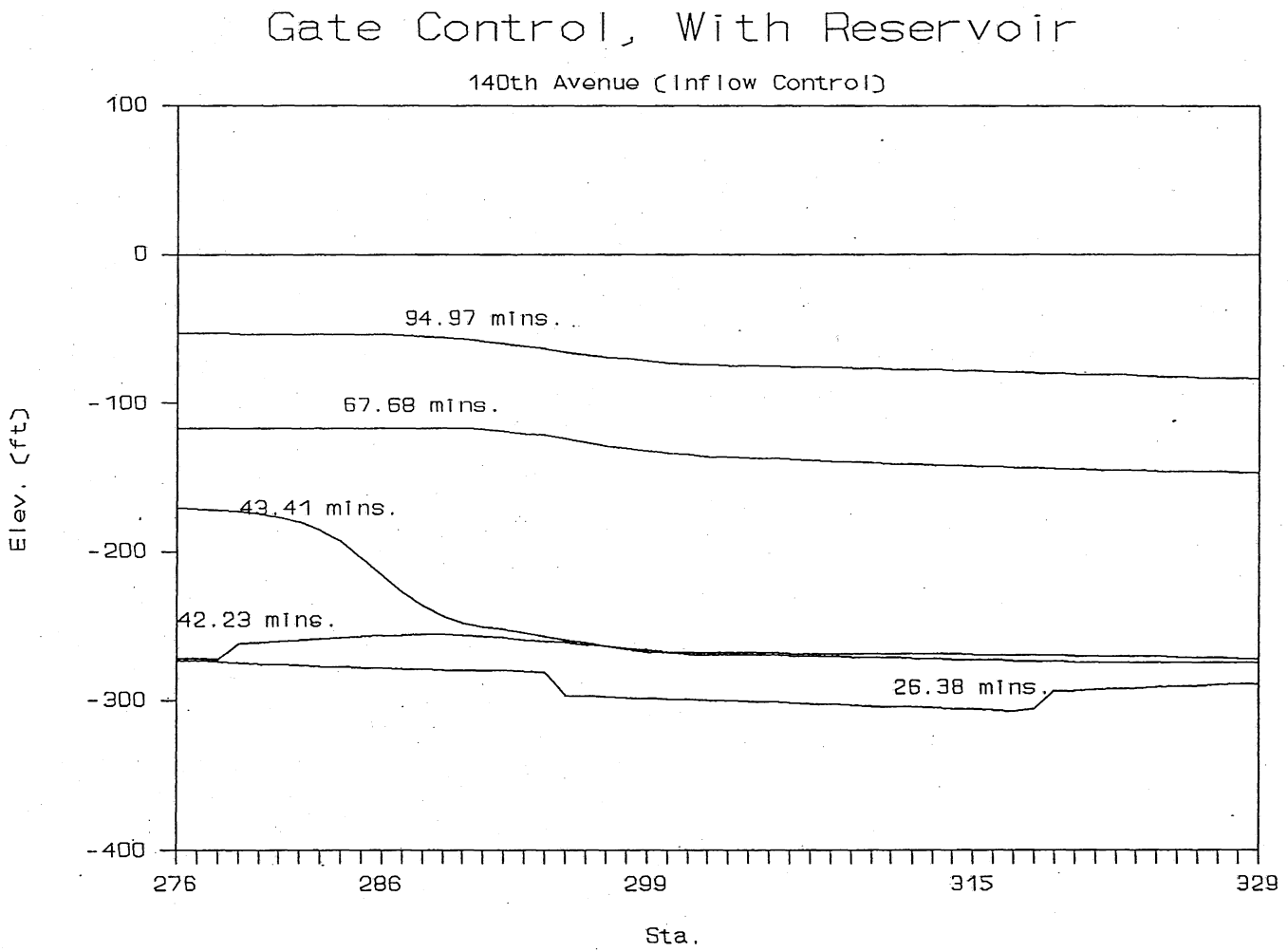

Fig. C-71, Instantaneous hydraulic gradelines in 140th Avenue tunnel of System C-IV with inflow control.

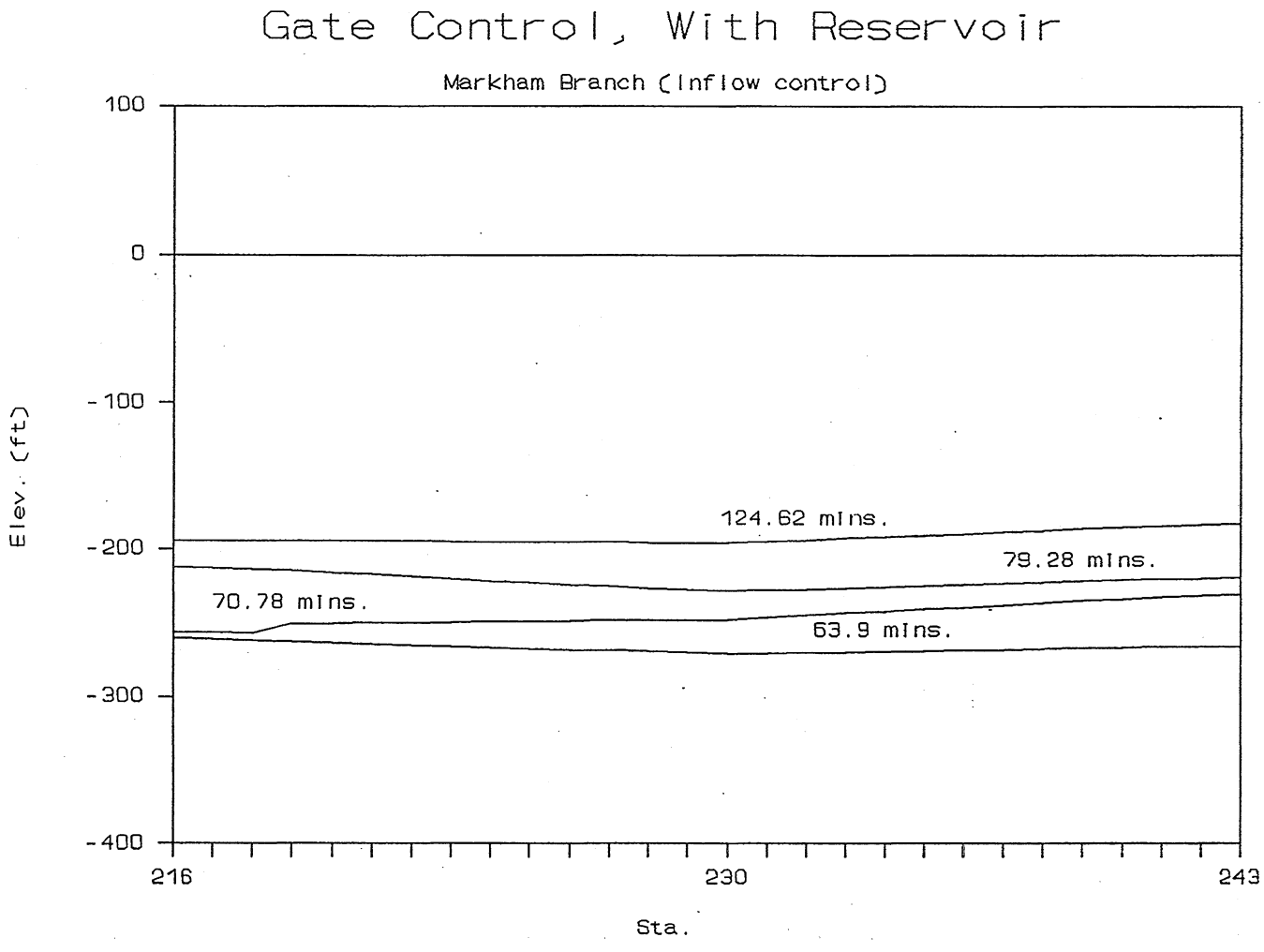

Fig. C-72, Instantaneous hydraulic gradelines in Markham tunnel of System C-IV with inflow control.

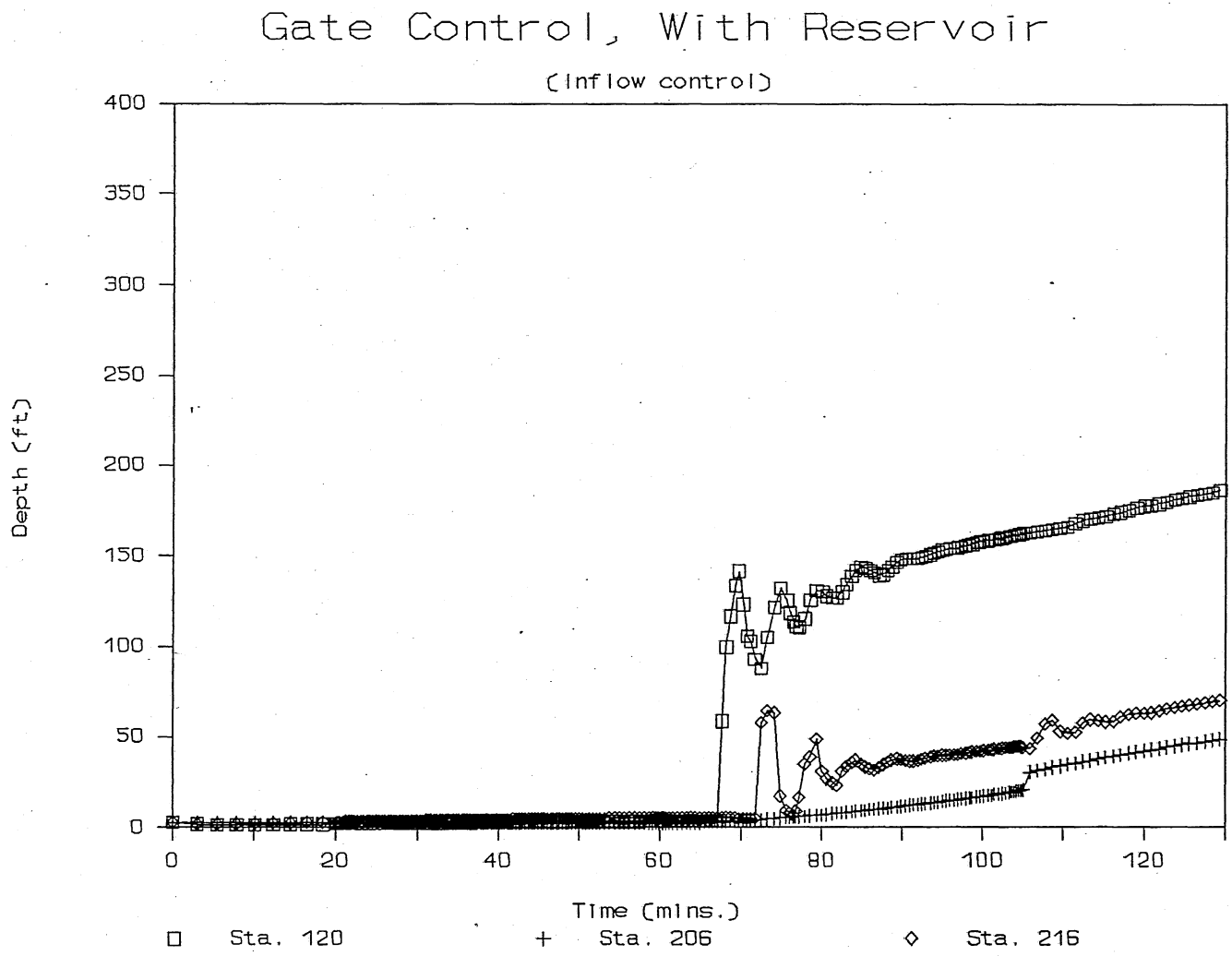

Fig. C-73, Time variation of water depth in System C-IV with inflow Control (Sta. 120, 206, 216).

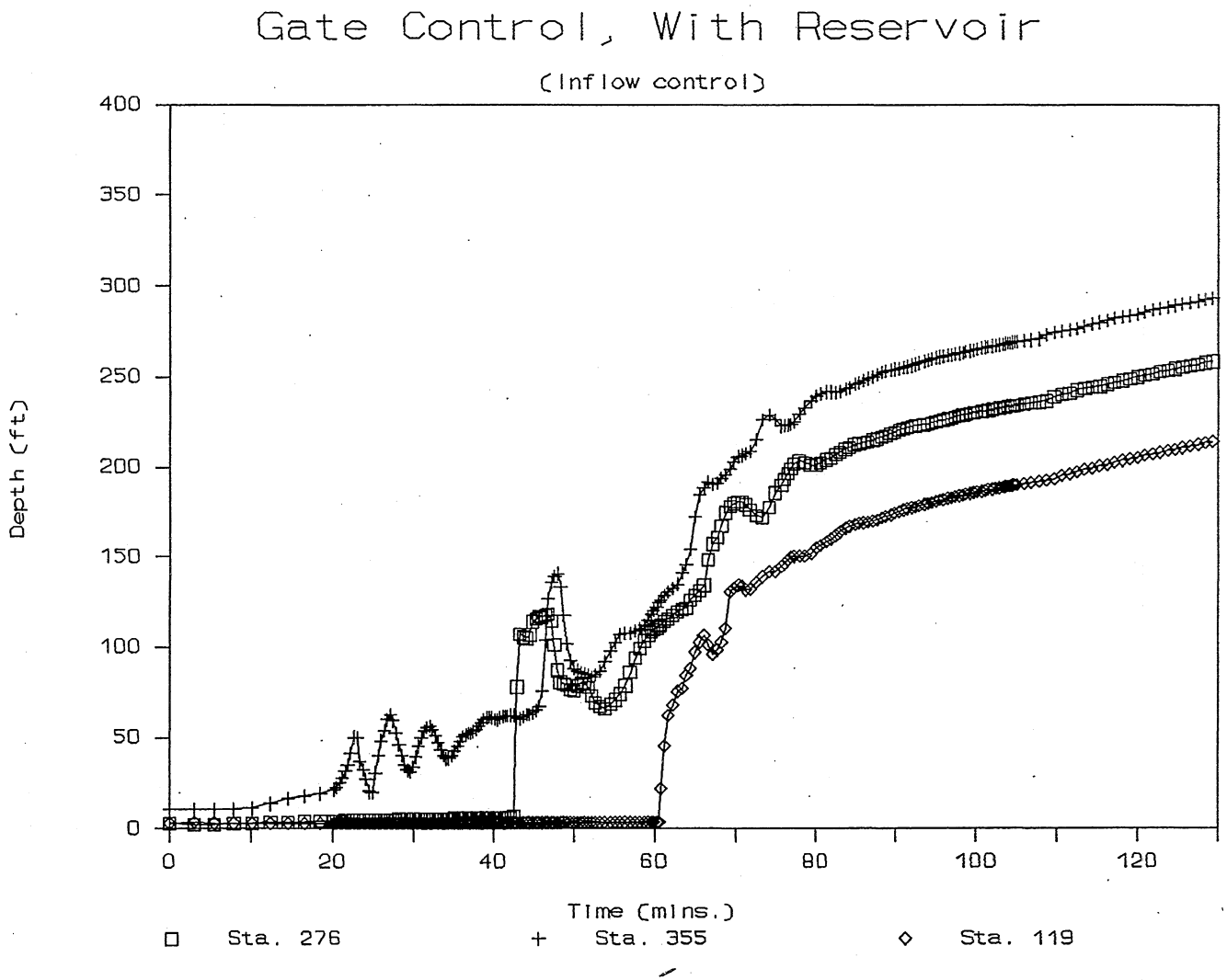

Fig. C-74, Time variation of water depth in System C-IV with inflow Control (Sta. 276, 355, 119).

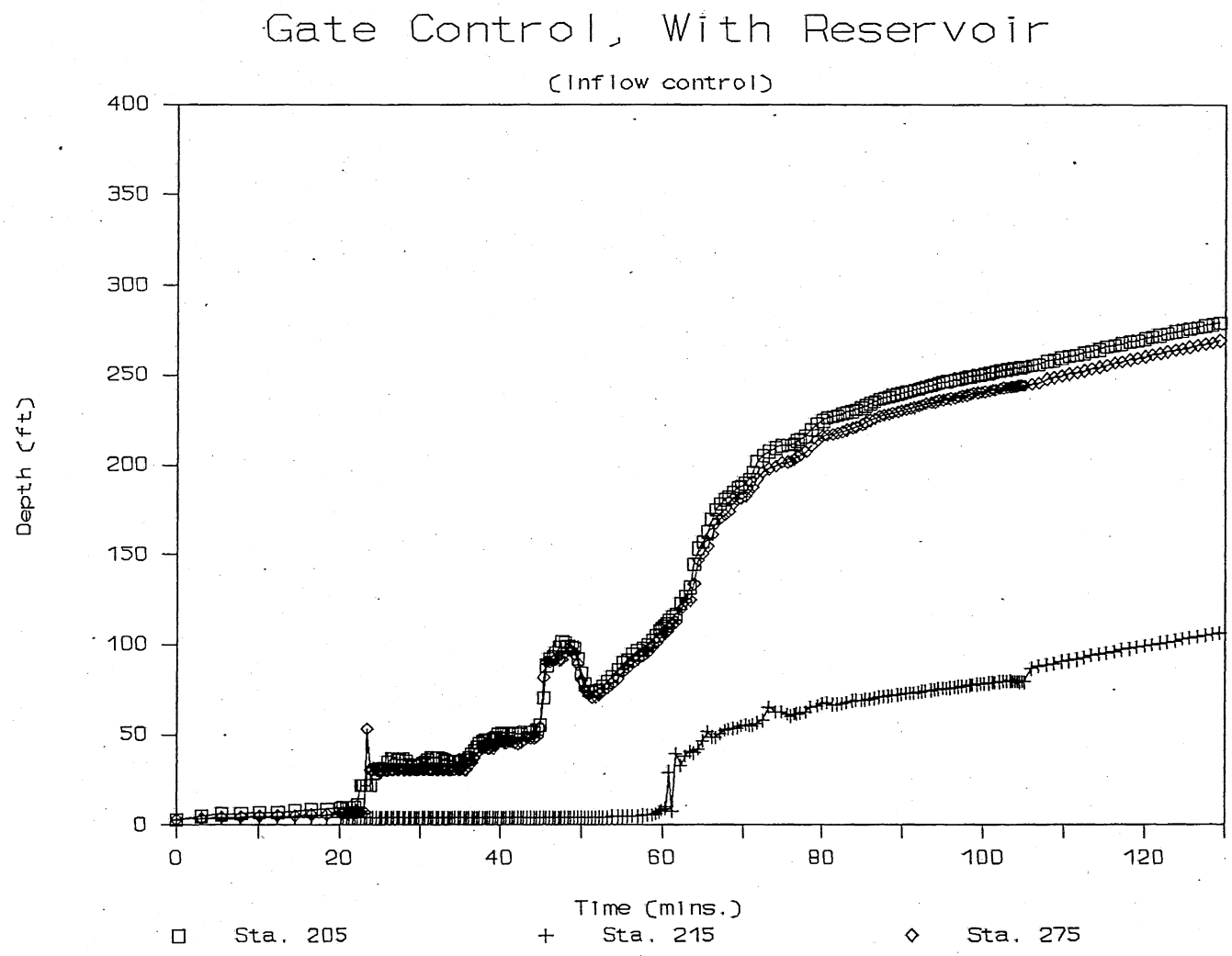

Fig. C-75, Time variation of water depth in System C-IV with inflow Control (Sta. 205, 215, 275).

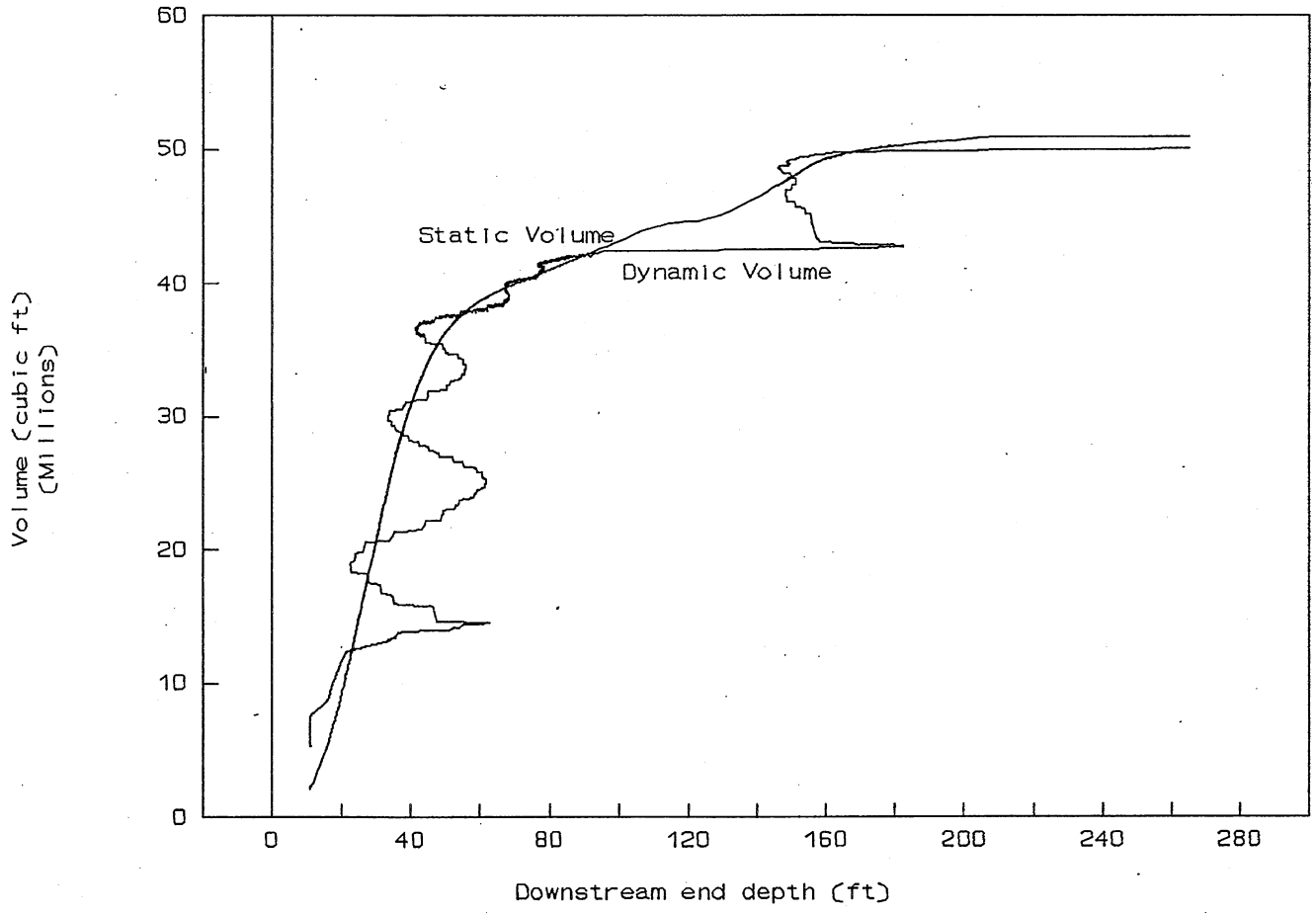

Fig. C-76. Statically and dynamically determined correlation between volume and depth at downstream end, Calumet System.

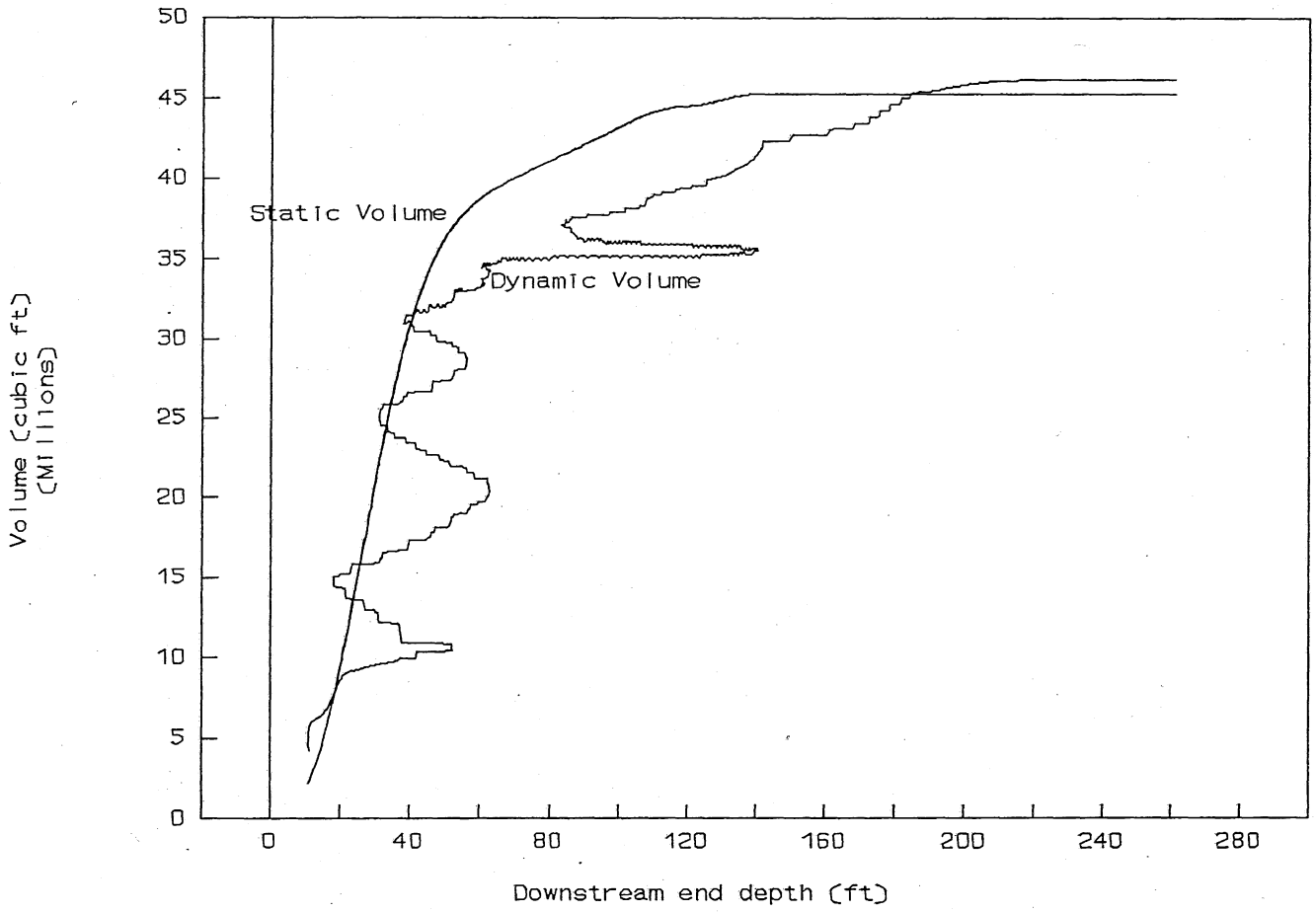

Fig. C-77, Statically and dynamically determined correlation between volume and depth at downstream end, Calumet System at downstream side of roller gate.